



HAL
open science

Innovative solutions for acoustic resonance characterization in metal halide lamps

Fang Lei

► **To cite this version:**

Fang Lei. Innovative solutions for acoustic resonance characterization in metal halide lamps. Acoustics [physics.class-ph]. Institut National Polytechnique de Toulouse - INPT, 2018. English. NNT : 2018INPT0041 . tel-04203145

HAL Id: tel-04203145

<https://theses.hal.science/tel-04203145v1>

Submitted on 11 Sep 2023

HAL is a multi-disciplinary open access archive for the deposit and dissemination of scientific research documents, whether they are published or not. The documents may come from teaching and research institutions in France or abroad, or from public or private research centers.

L'archive ouverte pluridisciplinaire **HAL**, est destinée au dépôt et à la diffusion de documents scientifiques de niveau recherche, publiés ou non, émanant des établissements d'enseignement et de recherche français ou étrangers, des laboratoires publics ou privés.



Université
de Toulouse

THÈSE

En vue de l'obtention du

DOCTORAT DE L'UNIVERSITÉ DE TOULOUSE

Délivré par :

Institut National Polytechnique de Toulouse (INP Toulouse)

Discipline ou spécialité :

Génie Électrique

Présentée et soutenue par :

Mme FANG LEI

le mercredi 24 janvier 2018

Titre :

Innovative Solutions for Acoustic Resonance Characterization in Metal
Halide Lamps

Ecole doctorale :

Génie Electrique, Electronique, Télécommunications (GEET)

Unité de recherche :

Laboratoire Plasma et Conversion d'Energie (LAPLACE)

Directeur(s) de Thèse :

M. PASCAL MAUSSION

M. GEORGES ZISSIS

Rapporteurs :

M. BABAK NAHID-MOBARAKEH, UNIVERSITÉ LORRAINE

M. MOUNSIF ECH CHERIF EL KETTANI, UNIVERSITE DU HAVRE

Membre(s) du jury :

Mme BETTY SEMAIL, UNIVERSITE LILLE 1, Président

M. GEORGES ZISSIS, UNIVERSITE TOULOUSE 3, Membre

M. PASCAL DUPUIS, UNIVERSITE TOULOUSE 3, Membre

M. PASCAL MAUSSION, INP TOULOUSE, Membre

Abstract

Metal halide lamp is one kind of the most compact high-performance light sources. Because of their good color rendering index and high luminous efficacy, these lamps are often preferred in locations where color and efficacy are important, such as supermarkets, gymnasiums, ice rinks and sporting arenas. Unfortunately, acoustic resonance phenomenon occurs in metal halide lamps and causes light flicker, lamp arc bending and rotation, lamp extinction and in the worst case, arc tube explosion, when the lamps are operated in high-frequency bands.

This thesis takes place in the context of developing electronic ballasts with robust acoustic resonance detection and avoidance mechanisms. To this end, several envelope detection methods such as the multiplier circuit, rectifier circuit, and lock-in amplifier, are proposed to characterize fluctuations of acoustic resonance. Furthermore, statistical criteria based on the standard deviation of these fluctuations are proposed to assess acoustic resonance occurrence and classify its severity.

The proposed criteria enable classifying between no acoustic resonance and acoustic resonance cases based upon either a two-dimensional plane, a histogram or a boxplot. These analyses are confirmed by the study of spectral variations (variations of the spectral irradiance and colorimetric parameters) as well. Standard deviations and relative standard deviations of these variations are also correlated with the presence of acoustic resonance. The results from this study show that whatever voltage envelope variations or spectral variations are significantly influenced by acoustic resonance phenomena.

A set of metal halide lamps from different manufacturers and with different powers are tested in our experiments. We concluded that our designed multiplier and rectifier circuits for acoustic resonance detection have the same sensitivity as the lock-in amplifier, paving the way for the implementation of this function directly into the ballast circuit board.

Keywords: Acoustic resonance, Envelope Detection, High-frequency Electronic Ballast, Metal Halide Lamps, Energy Efficiency, Real-time Dynamic Control, Electronics

Résumé

La lampe à iodure métallique est une des sources lumineuses de haute performance les plus compactes qui soit. En raison de leur bon indice de rendu des couleurs et de leur haute efficacité lumineuse, ces lampes sont souvent préférées dans les endroits où la couleur et l'efficacité sont importantes, comme les supermarchés, les gymnases, les patinoires et les arènes sportives. L'inconvénient majeur de ce type de lampe à iodure métallique vient d'un phénomène appelé « résonance acoustique ». Lorsqu'il se produit, la lumière scintille, l'arc au centre de la lampe se met à fléchir et à tourner. Cela peut aller jusqu'à l'extinction de la lampe et, dans le pire des cas, à l'explosion du tube lorsque les lampes fonctionnent dans certaines bandes de fréquence.

Cette thèse se situe dans le contexte du développement de ballasts électroniques incorporant des mécanismes robustes de détection et d'évitement de résonance acoustique. À cette fin, plusieurs méthodes de détection d'enveloppe telles que le circuit multiplicateur, le circuit redresseur et l'amplificateur à verrouillage de phase sont proposées pour caractériser les fluctuations de la résonance acoustique et mieux les détecter. Des critères statistiques basés sur l'écart-type de ces fluctuations ont été établis pour détecter la présence de résonances acoustiques et les classer suivant leur gravité.

Les critères proposés permettent de différencier les cas sans résonance acoustique et avec présence de résonance acoustique dans un plan bidimensionnel ou en utilisant des intervalles de confiance. Cette analyse temporelle est confirmée par l'étude des variations du spectre optique et des paramètres colorimétriques. Leurs écarts-types relatifs sont également corrélés à la présence de résonances acoustiques. Les résultats de cette étude montrent que les variations de l'enveloppe de tension ou les variations du spectre et des paramètres colorimétriques sont fortement influencées par les phénomènes de résonance acoustique

Un ensemble de lampes à iodure métallique de différents fabricants et avec des puissances différentes a été testé dans nos expériences. Nous avons conclu que les circuits à multiplicateurs et à redressement permettent de détecter les résonances acoustiques avec le même niveau de sensibilité que le système à verrouillage de phase, ouvrant la voie à l'implantation de cette fonction directement au niveau du circuit du ballast.

Mots Clés : Résonance acoustique, Détection d'enveloppe, Ballast électronique haute fréquence, Lampes à iodure métallique, efficacité énergétique, contrôle dynamique temps réel, électronique de puis

Acknowledgment

This work was developed in “Commande et Diagnostic des Systèmes Electriques (CODIASE)” and “Lumière et Matière (LM)” research groups of Laboratoire PLAsma et Conversion d’Energie (LAPLACE), Université de Fédérale Toulouse Midi-Pyrénées, Toulouse, France. The scholarship of Ph.D. for Fang LEI is supported by China Scholarship Council (CSC).

To achieve this thesis, except my efforts, I also got a lot of assistance, support and encouragement from so many people. I would like to thank all of them for their contributions to my work.

Firstly, I would like to express my sincere appreciation and gratitude to my supervisors, Prof. Pascal MAUSSION, Prof. Georges ZISSIS, and Dr. Pascal DUPUIS, for their guidance, encouragement, and support during my study. Their extensive knowledge, creative thinking, and rigorous science attitude influence me through my research and all my life.

I would like to thank the jury: Prof. Mounsif ECH CHERIF EL KETTANI (reviewer), Prof. Babak NAHIDMOBARAKEH (reviewer) and Prof. Betty SEMAIL (examiner). Thanks a lot for them reviewed and checked my thesis.

I would like to say thanks to all the members of my groups, such as Stéphane CAUX, Maurice FADEL, Antoine PICOT, Maria PIETRZAK-DAVID, David BUSO, Laurent CANALE, Manuel LOPES, etc. It is my pleasure to meet and work with them.

I would like to specially thanks to the technician Mr. Olivier DURRIEU. He gave me a lot of favorable guidance and professional suggestions on how to do the experiment and debug electrical circuits. Without his assistance and guidance, I could not finish my experiment well.

I would like to thank all dear my colleagues: Andrea VERDICCHIO, Benedikt BYRNE, Clément FILLEAU, Joseph FABRE, Kamil MROZEWSKI, Thomas GENEVE, Youssef DRIMZI, Lucille KUHNER, Kuljaree TANTAYAKUL, Tianyi LIU, Jingyi WANG, Wencong ZHANG, Feng TIAN, Qiankun SU. It is nice to meet them in this beautiful city, Toulouse. With them, I had a colorful and wonderful life during those three years.

I would like to thank CODIASE and LM groups of LAPLACE laboratory, Université de Fédérale Toulouse Midi-Pyrénées, which provided a wonderful academic environment to study and do research work.

Specially thanks to CSC, which gave a chance to study in France and offer me financial support.

Last but not least, I offer my deepest gratitude to my family, my parents, sisters, and brother, particularly to my parents and boyfriend for their trust, love, and support.

Toulouse, 23th November 2017

Fang LEI

Table of Contents

General Introduction	1
Chapter 1 State of the Art	5
1.1 Background	7
1.2 General summary of light source	7
1.2.1 Electromagnetic spectrum and light	7
1.2.1.1 Light sources metrics.....	9
1.2.2 Different types of light sources	16
1.2.2.1 Incandescent lamp	17
1.2.2.2 Gas discharge lamp.....	17
1.2.2.3 Solid state light source.....	22
1.2.2.4 Comparisons of different lamps	23
1.3 Ballast.....	24
1.3.1 Electromagnetic ballast	24
1.3.2 Electronic ballast.....	25
1.3.2.1 Low-frequency square-wave electronic ballast	25
1.3.2.2 High-frequency electronic ballast.....	26
1.3.3 Comparison between electromagnetic ballast and electronic ballast.....	27
1.4 Review of previous research about acoustic resonance.....	28
1.5 Thesis key points	31
References	34
Chapter 2 Acoustic Resonance in High-Intensity Discharge Lamps	39
2.1 Introduction.....	41
2.2 Phenomenon of acoustic resonance	41
2.3 Theory of acoustic resonance.....	42
2.3.1 Wave equations and their solutions.....	42
2.3.2 An example of AR frequency calculation	45
2.3.2.1 AR theoretical frequencies versus AR experimental frequencies	45
2.3.2.2 Simulation of three fundamental AR frequency modes	46
2.3.3 Power threshold in high-intensity discharge lamps	50
2.4 Methods for acoustic resonance detection	52
2.4.1 Electrical methods.....	52
2.4.1.1 Observed variations of electrical parameters.....	52
2.4.1.2 Low-frequency voltage fluctuations (Voltage envelope)	53
2.4.1.3 Changes of electrical parameters	54
2.4.1.4 FFT of lamp current fluctuation	55
2.4.2 Optical methods	56

2.4.2.1	Arc images.....	56
2.4.2.2	Arc motion and light flicker	57
2.4.2.3	Optogalvanic method.....	60
2.4.3	Sound spectrum.....	61
2.4.4	Temperature variations.....	62
2.4.5	Comparisons between different acoustic resonance detection methods	64
2.5	Methods for acoustic resonance avoidance.....	65
2.5.1	Changing lamp related parameters (AR-free frequency)	65
2.5.2	Operation supply of ballast.....	66
2.5.2.1	DC-type ballast.....	66
2.5.2.2	Low-frequency square wave electronic ballast	66
2.5.2.3	Extra-high frequency electronic ballast.....	66
2.5.3	Spread power spectrum.....	66
2.5.3.1	Frequency modulation	66
2.5.3.2	Injecting adjacent frequency.....	68
2.5.4	Comparisons of acoustic resonance avoidance methods	68
2.6	Advantages of acoustic resonance	69
2.6.1	Arc straightening	69
2.6.2	Color mixing for HID lamps operated vertically	69
2.6.3	Strength test of arc tube and outer bulb.....	70
2.7	Conclusions.....	70
	References	70

Chapter 3 Online Acoustic Resonance Detection and Electrical Modeling of Lamp Voltage in Metal Halide Lamps

3.1	Introduction.....	75
3.2	Circuit of the high-frequency electronic ballast.....	75
3.2.1	Main circuit	75
3.2.2	Ignition methods	76
3.2.2.1	Lamp ignited by a transformer	77
3.2.2.2	LCC circuit with frequency sweeping ignition for metal halide lamps in our experiment	77
3.3	Experimental set-up at Laplace N7	79
3.4	Online envelope detection for acoustic resonance.....	79
3.4.1	Principle of envelope detection	79
3.4.1.1	Synchronous envelope detection (Multiplier circuit)	80
3.4.1.2	Asynchronous full-wave envelope detection (Rectifier circuit).....	81
3.4.1.3	Synchronous complex envelope detection (Lock-in amplifier).....	82
3.4.2	Principle of synchronous voltage envelope detection.....	82
3.4.2.1	Mathematical model of amplitude modulation for synchronous envelope detection	83
3.4.3	Implemented methods	84

3.4.4	Multiplier envelope detection for acoustic resonance	85
3.4.4.1	Schematic of detection circuit and test bench	85
3.4.4.2	AR real-time detection with the proposed multiplier circuit	86
3.4.5	Rectifier envelope detection for acoustic resonance	89
3.4.5.1	Schematic of detection circuit	89
3.4.5.2	AR Real-time detection with proposed rectifier circuit.....	89
3.4.5.3	Characterizations of voltage envelope.....	91
3.5	Electrical modeling of lamp voltage in presence of acoustic resonance	92
3.5.1	Principle of lamp voltage modeling	92
3.5.1.1	Amplitude modulation.....	92
3.5.2	Electrical modelings of acoustic signals and acoustic resonance detection	93
3.5.2.1	Periodic acoustic signal with acoustic resonance	94
3.5.2.2	Stochastic acoustic signal with acoustic resonance.....	95
3.6	Lookup table of lamp voltage in the presence of acoustic resonance	96
3.7	Summary of acoustic resonance characterizations	97
3.8	Conclusions	99
	References	100

Chapter 4 Statistical Method for Acoustic Resonance Characterization in Metal Halide Lamps..... 103

4.1	Introduction	105
4.2	Experimental set-up at Laplace UPS	105
4.3	Statistical characterization of acoustic resonance using commercial devices	106
4.3.1	Data acquisition of voltage envelope and spectral variations	107
4.3.1.1	LabVIEW program in our experiment.....	107
4.3.1.2	Data acquisition of voltage envelope.....	108
4.3.1.3	Data acquisition of spectral variations (spectral irradiance and colorimetric parameters).....	108
4.3.1.4	Spectral variations and detection principle.....	109
4.3.2	Statistical analysis of voltage envelope detection	110
4.3.2.1	Two-dimensional plane of voltage envelope standard deviation versus average voltage envelope	110
4.3.2.2	Boxplot of voltage envelope and voltage envelope waveform.....	113
4.3.2.3	Histogram of voltage envelope.....	117
4.3.2.4	Analysis of variance of voltage envelope.....	119
4.3.2.5	Results Inter-comparison.....	123
4.3.2.6	Conclusions of voltage envelope using statistical analysis methods.....	124
4.3.3	Statistical analysis of spectral variation detection	124
4.3.3.1	Standard deviation and relative standard deviation in the spectral irradiance.....	125
4.3.3.2	Boxplot, standard deviation and relative standard deviation of colorimetric parameters.....	130

4.3.3.3	Comparisons between spectral variation detection methods	137
4.4	Correlation between voltage envelope detection and light spectral variation detection	137
4.4.1	Standard deviation of voltage envelope versus colorimetric parameters	137
4.5	Validations of our online detection methods with respect to the lock-in amplifier	139
4.5.1	Experimental result comparisons between different detection methods	139
4.5.2	Simulation results between different detection methods.....	140
4.5.3	Comparison between voltage envelope detection and spectral variation detection	145
4.6	Conclusions.....	146
	References	147
General Conclusion and Perspectives		149
	Conclusions	151
	Perspectives.....	152
Annexes		153
	List of Figures	155
	List of Tables	159
	List of Publications.....	161

Abbreviations

HID - High Intensity Discharge
MH - Metal Halide
HPS - High Pressure Sodium
HPM – High Pressure Mercury
CFL - Compact Fluorescent Lamp
LED - Light Emitting Diode
OLED - Organic Light Emitting Diode
CRI - Color Rendering Index
CCT - Correlated Color Temperature
LFSW - Low Frequency Square Wave
AR - Acoustic Resonance
STD - Standard Deviation
RSD - Relative Standard Deviations
ANOVA - Analysis of Variance
CIE - International Commission Illumination
UCS - Uniform Chromaticity Scale
SPD - Spectral Power Distribution
RFI - Radio Frequency Interference
EMI - Electromagnetic Interference
LCD - Liquid Crystal Display
FFT - Fast Fourier Transform
CCD - Charge Coupled Device
SNR - Signal to Noise Ratio

General Introduction

Metal halide (MH) discharge lamp is one of the most compact high-performance light sources with direct electrical-to-visible conversion efficiency up to 35%–55% [1]. As result of good color rendering index (CRI>90) and high luminous efficacy (up to 150 lm/W), MH lamps are widely used in locations where color and efficacy are important, such as retail stores, factories, gymnasiums, and sporting arenas. Furthermore, in situations requiring producing a large amount of lumen (scenery lighting, plant growth ...), LED-based luminaires are commercially available with similar characteristics but at a higher cost. Therefore, because of economic incentives, MH lamps will be kept as legacy devices for at least one decade.

Because of the negative impedance, MH discharge lamps are always supplied by ballasts to limit the current. High-frequency electronic ballasts with half-bridge inverter increase lamp-ballast efficiency, leading to increased energy efficiency and lower costs, compared to the low-frequency square-wave (LFSW) ballasts with full-bridge inverter [2], [3]. Additionally, high-frequency ballasts present a reduced hysteresis area [4].

A disadvantage of this ballast of high-frequency lamp operation is the occurrence of acoustic resonance (AR) for frequency bands above 1 kHz region [5]. AR can cause lamp arc distortion, rotation, extinction and in the worst case, lamp explosion [6], [7], [8]. Obviously, AR hinders the development of MH lamps and ballasts, and gives unknown risks or may increase the higher cost for lamps end-users' due to lamp destruction.

AR is excited when the lamp power frequency is close to the eigenfrequency of the arc tube and the excitation energy is over the threshold energy [9]. The common explanation for this phenomenon is that standing pressure waves are generated in the gas of the arc tube such as those which occur in organ pipes and other musical instruments [10], [11]. Another explanation is that acoustic streaming results in the occurrence of AR. An acoustic flow develops in the standing wave caused by an inhomogeneity of the acoustic field [12].

Since the 1960s, researchers have studied the AR phenomenon. However, AR is a multi-physic problem relevant to several disciplines: electrical, electronics, electromagnetic, chemical to mention a few. Up to now, AR understanding is far from complete. Nevertheless, there is an incentive in using high intensity discharge (HID) lamps at higher frequencies, as the plasma I-V behavior comes close to a pure resistance load, leading to a reduction of hysteresis losses and higher lamp efficiencies.

The first essential point for AR phenomenon is to use simple and online methods to detect it. Many methods already were developed by researchers, which can be categorized into three groups [13]: optically, electrically and other physical parameters such as sound emission and temperature profile. However, most of the methods are not online detection, and some of them are difficult to fulfill.

On the other hand, AR also affects the spectral irradiance and color properties of lamps. Nevertheless, there is no literature investigated how the AR phenomenon influences on the spectral irradiance and colorimetric parameters (spectral variations) in HID lamps.

Based on those reasons, this thesis will mainly focus on:

- 1) Online AR envelope detection methods with high sensitivity;
- 2) Voltage envelope characterizations of AR by using statistical analyses based on envelope detection results;
- 3) How AR does influence on spectral variations by using some statistical analyses.

Online detection methods are aiming at providing simple and high sensitivity AR detection in order to control AR phenomenon, contributing to design high-frequency electronic ballasts for energy savings. Statistical methods are used to analyze AR characterizations in order to understand this phenomenon further.

The dissertation is divided into the following four parts:

Chapter 1: The aim of this chapter is to introduce the framework about light sources, ballasts and AR phenomena and the relationships between them. The electromagnetic spectrum and light are defined first, and then different lamps and their emitting principles are presented as well, especially for HID lamps. Electromagnetic ballasts, low-frequency square wave electronic ballasts and high-frequency electronic ballasts are presented. We also compare the advantages and disadvantages of different ballasts. The previous researches about AR occurrence in HID lamps are reviewed. The key points and main work of this thesis are presented lastly.

Chapter 2: This chapter focuses on AR phenomena occurring in HID lamps. Different AR phenomena and the AR mechanism are reviewed. We then give an example of AR theoretical frequencies in one kind of our tested lamps, and the pressure variations in longitudinal, radial and azimuth modes are simulated in MATLAB as well. Although AR theoretical frequencies can be calculated, these frequencies depend on the tolerance of manufacture. Therefore, AR detection and avoidance methods are essential for HID lamps. We review different detection and avoidance methods, compare the methods presented in literature with our proposed methods, and give the advantages and disadvantages of each method. Finally, AR benefits are summarized as well.

Chapter 3: Our high-frequency electronic ballast is introduced. The simplified model of this ballast is described as well in order to analyze the lamp ignition. AR causes low-frequency fluctuations on plasma arc in HID lamps, resulting in fluctuations in the lamp voltage and current. The lamp voltage waveform with occurrence is similar to the signal with a double-sideband amplitude modulation. Different envelope detection methods and their implementation are analyzed in detail. Then, we propose two simple online envelope detection methods implemented by a multiplier circuit and a rectifier circuit. Those methods are easily embeddable into the ballast board at low cost and can fulfill the real-time detection. Lastly, the electrical modelings of the lamp voltage in the presence of AR are built in PSIM. Our proposed methods and simulations could help ballast designers to design ballasts with better performance for AR detection and avoidance.

Chapter 4: We propose two kinds of lab methods for physical measurements. A lock-in amplifier is applied to measure lamp voltage fluctuations. Then, different statistical methods are proposed to analyze AR characterizations and classify AR and no AR based on the standard deviation (STD) of the voltage envelope. The proposed criteria enabling to classify AR *versus* no AR cases use a two-dimensional plane plot, a boxplot, a histogram or an analysis of variance (ANOVA). In addition, the spectral variation detection (the variations of the spectral irradiance and colorimetric parameters) are presented as well. AR shifts the chemical balance in the arc tube, resulting in some variations in the spectral irradiance and colorimetric parameters, such as chromaticity coordinates and correlated color temperature. The STDs and the relative standard deviations (RSDs) of the spectral irradiance and colorimetric parameters are calculated to evaluate these variations. Finally, we analyze the correlation between lamp voltage variations and spectral variations. We also compare our online detection methods with the lab methods and give advantages and disadvantages of different detection methods.

This thesis will end with the general conclusion and perspectives. In this part, the conclusions are summarized in each chapter. At last, the future works are anticipated in this domain.

Chapter 1 State of the Art

1.1 Background

Nowadays, lighting consumption represents about 15% of annual world energy. In France, the overall electricity consumption of lighting is 56 TWh which accounts for 12% of French electricity consumption [14]. Although the global energy consumption is still rapidly growing [15], relative part of lighting consumption is slowly decreasing thanks to the wide LED adoption. Outdoor lighting, especially for roadways, is the main power consumption of public lighting and is also one of the most important areas particularly for safety. To meet the requirement of saving energy internationally, lighting research becomes more and more urgent to human society [16]. Thanks to much higher luminous efficacy, better color rendering index and longer lifetime than fluorescent lamps, high-intensity discharge (HID) lamps are used for commercial and industrial applications such as street lighting, plant growth, and stage lighting, etc.

HID lamps are a type of electrical gas-discharge lamp and produce light by striking an electric arc across tungsten electrodes housed inside a specially designed inner fused quartz or fused alumina tube [17]. This tube is filled with both gas and metals. The gas helps start the lamps. The metals produce the light once they are heated to a point of evaporation, forming a plasma.

Metal halide (MH) lamps regard as one kind of the most efficiency lamps in HID lamp family. The recent emergence of MH discharge lamps with ceramic arc tubes has led to a new generation of highly efficient light sources with higher color rendering index up to 93 that result in an improved perception. Like fluorescent lamps, MH lamps present the negative impedance characteristic and thus need auxiliary circuit namely “ballasts” to ensure steady lamp operation [18]. Compared to conventional magnetic ballasts, electronic ballasts have a smaller volume, lighter weight, higher efficiency and can dim lamps easily. Thus, they are widely used and developed.

There are mainly two kinds of electronic ballasts: low-frequency square wave ballast (LFSW) and high-frequency ballast. In the case of discharge lamps, half-bridge inverter ballasts increase system efficiency, leading to lower operating costs [19], [20]. Traditional LFSW ballasts with full-bridge inverter presents higher cost in this respect. However, acoustic resonance (AR) occurs in MH lamps operating at the high-frequency electronic ballast. The AR phenomenon that leads to lamp arc distortion, flickering and sometimes destruct the lamp’s tube [6]. The AR phenomenon brings the risk for lamps and hinders the development of ballasts and lamps. Therefore, it is essential to study the AR phenomenon, so as to avoid it.

The AR phenomenon is due to the development of standing acoustic wave in the lamp arc tube. However, the interaction between this acoustic wave and the arc is still poorly understood, particularly their impacts on the arc shape. Consequently, the mechanism of the AR phenomenon and AR characterizations need to be studied further.

To harness uncontrollable growth in energy demand of lighting system in the next years, developing high-frequency electronic ballast systems for MH lamps is a good choice. Developing these systems implies that we must solve AR phenomena first. Therefore, it is crucial to adopt innovative solutions and advanced diagnosis systems to track the operation state and AR characterizations in MH lamp.

1.2 General summary of light source

1.2.1 *Electromagnetic spectrum and light*

Light is a certain portion of the electromagnetic (EM) spectrum, which ranges from radio waves to gamma rays. The EM spectrum is the range of all types of EM radiation, as shown in Fig. 1-1. EM radiation can be described as a stream of photons, each traveling in a wave-like pattern, carrying energy and moving at the speed

of light. The difference between radio waves, visible light, and gamma rays is the energy of the photons. Radio waves have photons with the lowest energies. Gamma rays have the highest energies. The amount of energy a photon behaves like a wave, or more like a particle. This is called the “wave-particle duality” of light. Low energy photons (such as radio waves) behave more like waves, while higher energy photons (such as gamma rays) behave more like particles.

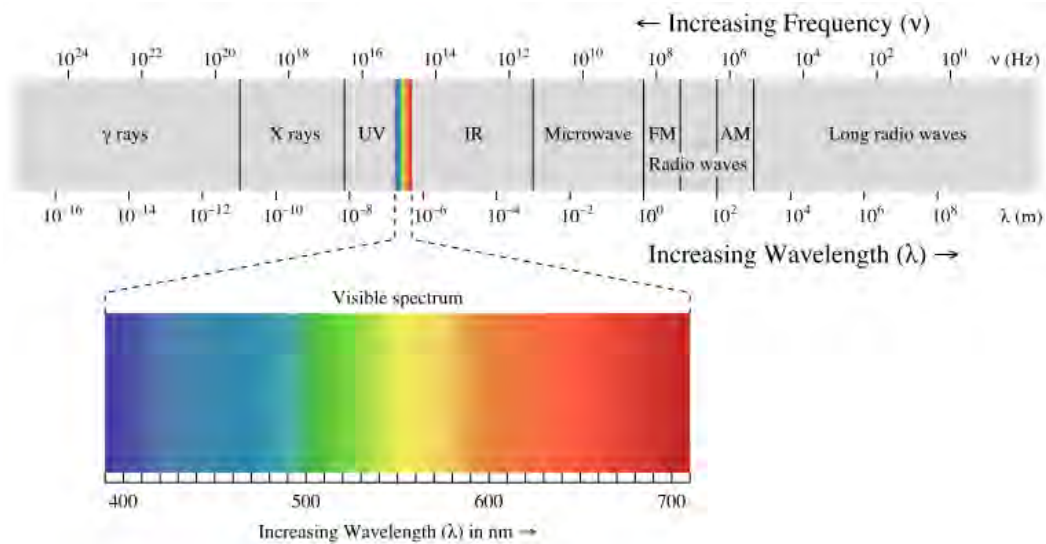


Fig. 1-1 Electromagnetic spectrum [22]

TABLE 1-1 EM radiation with respect to wavelength

Type of radiation	Wavelength (nm)
Gamma rays	< 0.01
X-rays	0.01 – 10
Ultraviolet	10 – 380
Visible light	380 – 780
Infrared	780 – 10^6
Microwave	10^6 – 10^9
Radio waves	10^9 – 10^{14}

Visible light is a just small part of the EM spectrum extended from the wavelengths of 380 to 780 nanometers (nm). More generally, visible light is defined as the wavelengths that are visible to most human eyes [21]. The eye looks like photoreceptor, is sensitive to only a narrow band of the electromagnetic spectrum, this band corresponding to “visible light”. Two different kinds of detectors exist in our eyes: the cones that perceive color and necessitate a minimum illumination level and the rods that perceive grey levels corresponding to brightness. Fig. 1-2 illustrates brightness relative sensitivity of human eyes under photopic and scotopic vision conditions.

The scotopic vision (dark-adapted response) corresponds to the eye response under low illumination level. The photopic vision (light-adapted response) represents the receptor’s sensitivity to high illumination level. The photopic vision is the only one concerning lighting design because eyes are “light-adapted” than “dark-adapted” under the most illumination levels produced by the manmade light.

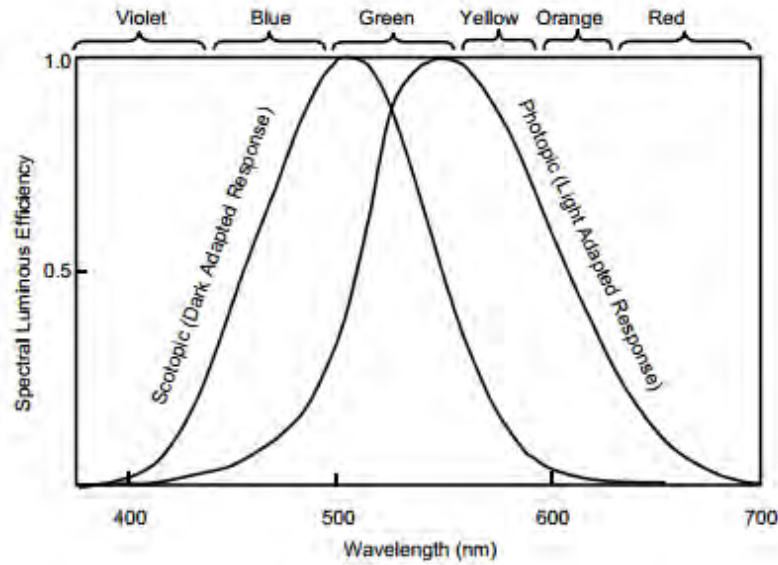


Fig. 1-2 Brightness relative sensitivity of human eyes under photopic and scotopic vision conditions [23] [24]

1.2.1.1 Light sources metrics

The basic parameters for measuring light are as follows:

A. Source efficiency and luminous efficacy

The efficiency of a source is defined as the percentage of electrical power converted into radiation, and the luminous efficacy is described as the percentage of power or energy converted to visible radiation. The efficacy is measured in lumens per watt, and the theoretical maximum is 683 lm/W if all the electricity is converted into radiation with a wavelength corresponding to the maximum sensitivity of the eye at 555 nm [25].

B. Luminous flux

The luminous flux (Φ) describes the quantity of light emitted per second from a light source and the unit is lumen. The lumen flux is usually measured in an integrating sphere, where the light is diffusely reflected by inner walls. Each unit surface of the sphere is illuminated proportionally to the flux of the light source, and a small window collects and measures the luminous flux.

The surface of a sphere is $4\pi r^2$, where r is the radius of the sphere, so the solid angle is:

$$\Omega = 4\pi(\text{sterad}) \quad (1-1)$$

The solid angle of a surface A is defined as:

$$\Omega = A / r^2 \quad (1-2)$$

The luminous efficiency is the ratio of the luminous flux to the electrical power consumed (lm/W). It is a measure of a light source's economic efficiency.

C. Luminous intensity

The luminous intensity (I) is defined as the flux of light emitted per second in a particular direction and its unit is the candela (cd=lm/sr). It is measured by a goniophotometer as follow:

$$I = \Delta\Phi / \Delta\Omega \quad (1-3)$$

where Φ is the luminous flux and Ω is the solid angle.

The luminous intensity of monochromatic light of wavelength λ is given by:

$$I = 683 \cdot \bar{y}(\lambda) \cdot I_e \quad (1-4)$$

I_e is the radiant intensity in watts per steradian (W/sr); $\bar{y}(\lambda)$ is the standard luminosity function.

If more than one wavelength is present), the luminous intensity is described as:

$$I = 683 \int_0^\infty \bar{y}(\lambda) \cdot \frac{dI_e(\lambda)}{d\lambda} d\lambda \quad (1-5)$$

D. Illuminance

Illuminance (E) is defined as the amount of light incident on a unit area and the unit of measurement is the lux ($lx=lm/m^2$). Illuminance is measured by photometers that convert light (photons) into current, applying the weighting of Fig. 1-2 (Lux meter).

$$E = \Phi / A \quad (1-6)$$

where A is the area of incidence.

E. Luminance

Luminance (L) is a photometric measure of the luminous intensity per unit of viewing area of light traveling in a given direction. It is defined as the amount of light that passes through, is emitted or reflected from a particular area, and falls within a given solid angle. The unit of luminance is candela per square meter (cd/m^2). Luminance is the only basic lighting parameter that is perceived by the eye. It describes a light source's impression of brightness on a surface and therefore depends to a large extent on the degree of reflection (color and surface). The luminance of a specified point of a light source, in a specified direction, is defined as:

$$L = \frac{d^2\Phi}{d\Sigma d\Omega_\Sigma \cos\theta_\Sigma} \quad (1-7)$$

where L is the luminance (cd/m^2); $d^2\Phi$ is the luminous flux (lm) in the area $d\Sigma$ in any direction contained inside the solid angle $d\Omega_\Sigma$; $d\Sigma$ is an area (m^2) of the source at specified point; $d\Omega_\Sigma$ is an solid angle (sr) at specified direction; θ_Σ is the angle between the normal n_Σ to the surface $d\Sigma$ in a specific direction. Fig. 1-3 illustrates the parameters for defining the luminance.

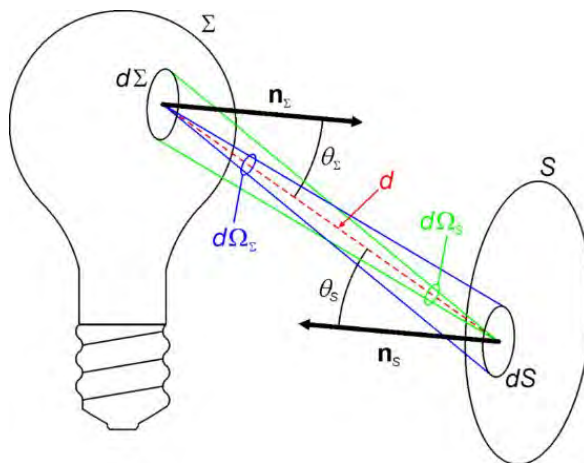


Fig. 1-3 Parameters for defining the luminance [26]

F. Colorimetric parameters

Color is used to describe the appearance of a visible stimulus within a certain spectral shape. The human eyes use three different kinds of cones to detect the color of blue, green and red of visible radiation. In this way, the spectral shape of visible stimulus is converted to three physiological signals. Some information is lost because a continuous spectral shape is described by only three numbers, defined as tristimulus values. Therefore, different spectra can be perceived as having the same color (metamerism). The tristimulus values can be calculated using color matching functions, which implicitly contain the relative sensitivity of the three cones in the human eye. To calculate the tristimulus values, the spectrum should be multiplied by the corresponding color-matching function, and then integrated over the whole wavelength range for visible radiation. When this theory was developed, the color of a spectrum was supposed to be independent of the intensity. Thus, the total value of the tristimulus values is normalized to unity. The result of this normalization is that the color of a spectrum can be expressed by two quantities: the chromaticity coordinates. A diagram containing these two chromaticity coordinates is called a chromaticity diagram. The most frequently used chromaticity diagram is the one defined by the international commission illumination (CIE) in 1931 [27]. The chromaticity coordinates are defined as x and y in this diagram. As explained latter, this approach was revised in 1960 and 1976. Nevertheless, to avoid losing inter-comparison with previous data, characterizations in another color space are always accompanied by measurements in this one.

a) Chromaticity coordinate

CIE 1931 chromaticity coordinates x and y are calculated from the spectral power distribution (SPD) of the light source and the CIE color-matching functions Fig. 1-4 (a). $\bar{x}(\lambda)$, $\bar{y}(\lambda)$, and $\bar{z}(\lambda)$ color-matching functions give the tristimulus value X , Y , and Z .

$$X = \int p\bar{x}(\lambda)d\lambda \quad (1-8)$$

$$Y = \int p\bar{y}(\lambda)d\lambda \quad (1-9)$$

$$Z = \int p\bar{z}(\lambda)d\lambda \quad (1-10)$$

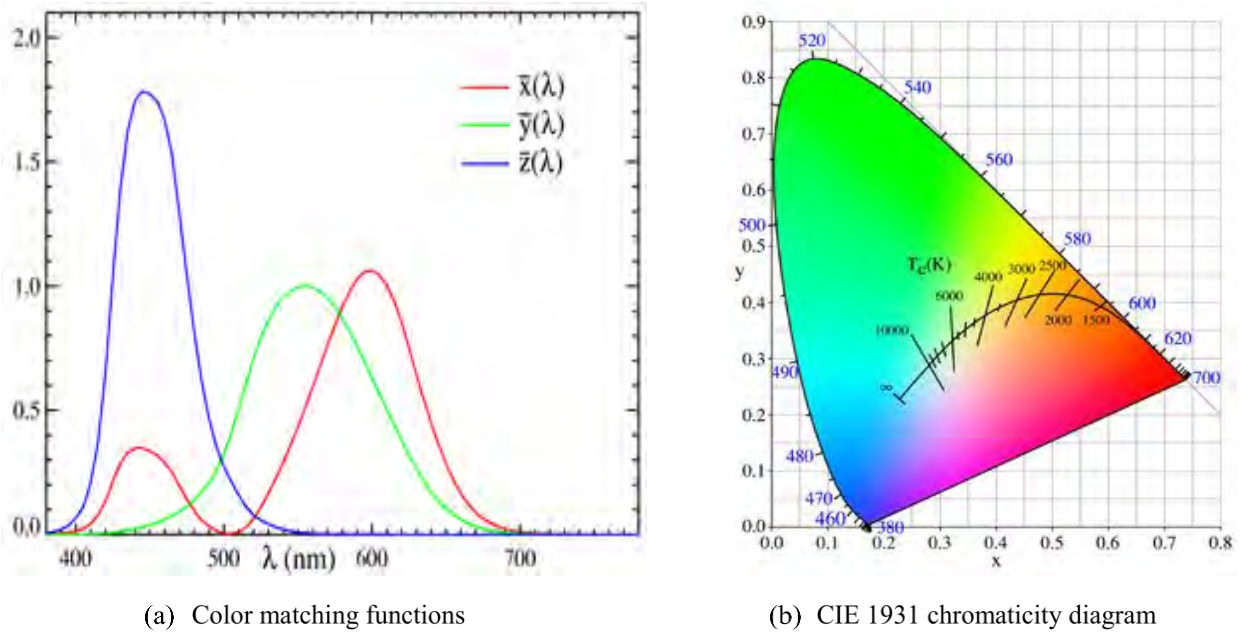
where p is the SPD of the light source. From X , Y , and Z , the chromaticity coordinates x , y , z can be obtained as follows:

$$x = \frac{X}{X + Y + Z} \quad (1-11)$$

$$y = \frac{Y}{X + Y + Z} \quad (1-12)$$

$$z = \frac{Z}{X + Y + Z} = 1 - x - y \quad (1-13)$$

Using x , y as the coordinates, a two-dimensional chromaticity diagram (the CIE 1931 color space diagram) can be plotted as shown Fig. 1-4 (b).



(a) Color matching functions

(b) CIE 1931 chromaticity diagram

Fig. 1-4 Standard color-matching functions and CIE 1931 chromaticity diagram [28]

In Fig. 1-4 (a), the color matching function $\bar{y}(\lambda)$ is equal to the overall sensitivity of the eye for visible radiations. In Fig. 1-4 (b), the x and y values of the monochromatic stimuli are plotted. The color of monochromatic stimuli and the color of the mixture of these stimuli are shown as well. The spectral locus, the boundary, and the blackbody locus comprise the chromaticity diagram.

The CIE 1976 uniform chromaticity scale (UCS) diagram was defined by the CIE in 1976, as illustrated in Fig. 1-5. It is intended to provide perceptually more uniform color spacing for colors at approximately the same luminance. The values of u' and v' can be calculated from the tristimulus values $X Y Z$ or from the chromaticity coordinates x, y according to the following formulas:

$$u' = \frac{4X}{X + 15Y + 3Z} = \frac{4x}{-2x + 12y + 3} \quad (1-14)$$

$$v' = \frac{9X}{X + 15Y + 3Z} = \frac{9x}{-2x + 12y + 3} \quad (1-15)$$

$$C_{uv} = \sqrt{(u')^2 + (v')^2} \quad (1-16)$$

where C_{uv} is the chroma; chroma is the colorfulness of an area judged as a proportion of the brightness of a similarly illuminated area that appears white or highly transmitting [29].

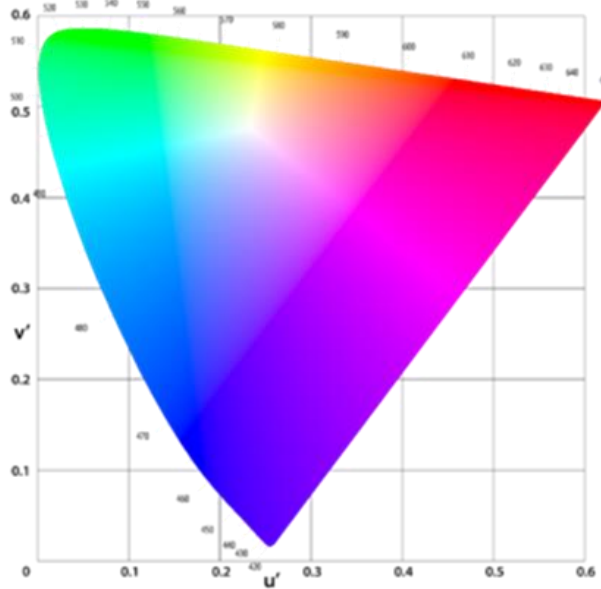


Fig. 1-5 CIE 1976 chromaticity diagram [30]

b) Color temperature or correlated color temperature

Planck's law describes the spectral density of electromagnetic radiation emitted by a black body in thermal equilibrium at a given temperature T . When the temperature of the blackbody is sufficiently high, it will start emitting visible light.

In the CIE 1931 chromaticity diagram, the blackbody emission appears as a parametric curve depending on temperature, as shown in Fig. 1-4 (b). When the color point of a lamp is close to the blackbody locus in the chromaticity diagram, the temperature of the proximal point on the locus is called correlated color temperature (CCT). The dominant color of a blackbody is called its hue, i.e. the monochromatic wavelength obtained at the intersection of a line starting from the radiometric neutral white (equal-energy) and passing by the lamp color point. The hue is a function of temperature as illustrated in Fig. 1-6. The blackbody distribution is used as reference white for temperatures up to 5000 K. Above 5000 K, daylight becomes the reference with an associated CCT. Fig. 1-6 (a) plots the hue appearing for most of the lighting devices. It ends at 6500 K, which is the reference white for computer display. Fig. 1-6 (b) starts at 6500 K and those values are generally not found in light sources.

A blackbody with CCT below 3300 K contains a lot of energy in the near infrared. When exposed to this kind of source, humans will feel a sensation of heating in their skin; this is why such sources are called “warm”. As CCT increase, the near infrared content drops; such sources are called “cold” for CCT above 5300 K. This explains the apparent discrepancy where low CCT are called “warm” and high CCT are described as cold.

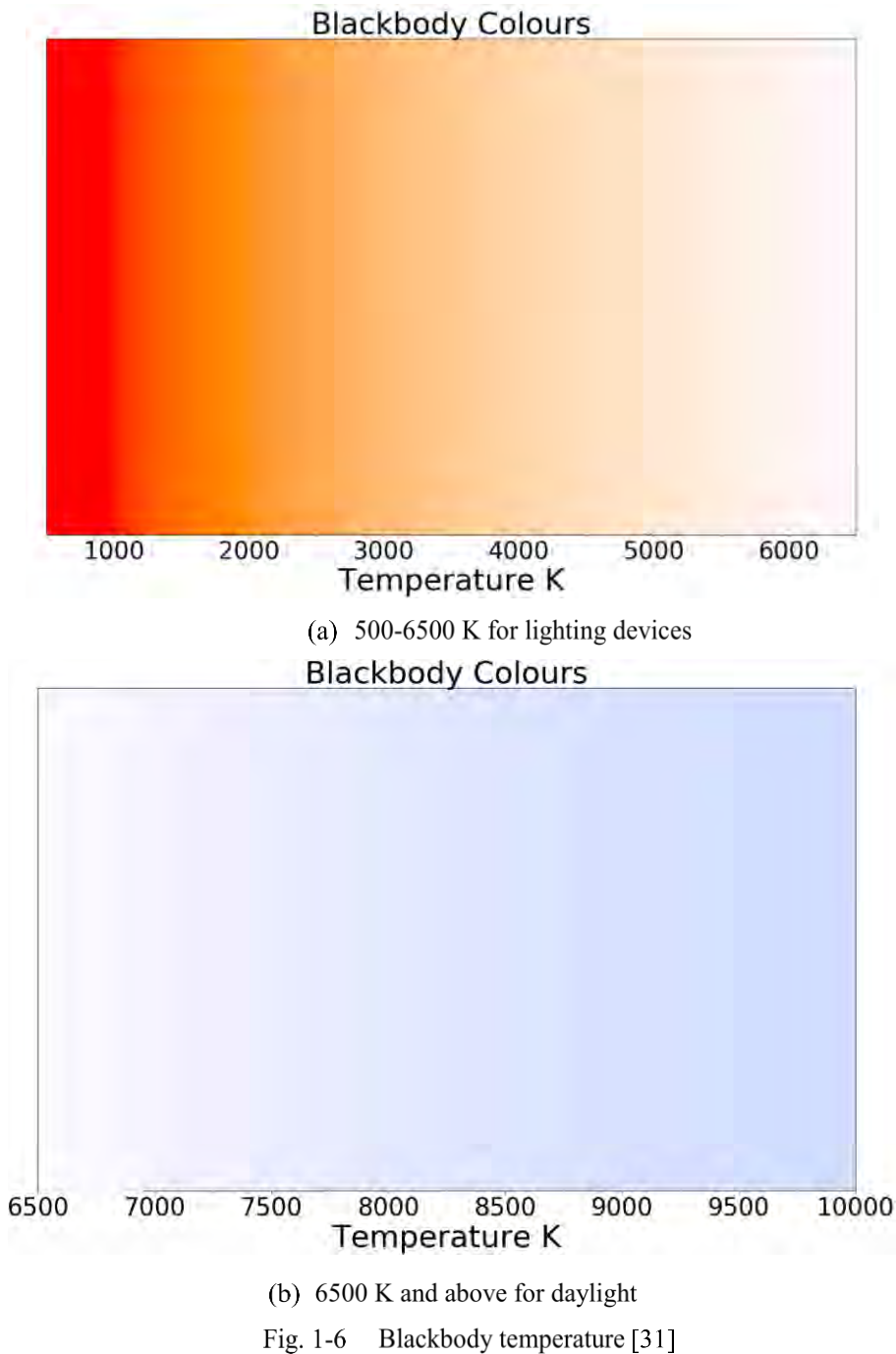


Fig. 1-6 Blackbody temperature [31]

c) Color rendering index

Color rendering index (CRI) is a measure of how accurately the light source reproduces the colors of an object in comparison to a reference light source. The CRI value of 100 means the sample light source reproduces the color as the reference light source does. Therefore, the higher the value of CRI, the more it resembles the reference light source. When evaluating CRI, the reference light source is chosen to have the same correlated color temperature as the sample light source.

Reference light source:

- 1) Lower than 5000 Kelvin: Planckian radiator;
- 2) 5000 Kelvin and higher: CIE daylight.

Ra is called average color rendering index or general color-rendering index as well as the special color-rendering indexes R1-R15. The color-rendering index Ra of the different light source is shown in TABLE 1-2.

TABLE 1-2 Average color rendering index Ra of different light source

Color rendering index Ra	≥90	80-89	70-79	60-69	40-59	20-39
Daylight	×					
Incandescent lamp	×	×				
Compact fluorescent lamp	×	×				
Fluorescent lamp	×	×	×	×	×	
Mercury vapor high-pressure lamp				×	×	
Metal halide lamp	×	×		×		
Sodium vapor high-pressure lamp		×		×	×	×

G. Spectral irradiance

The spectral irradiance is given as a function of wavelength λ and gives the power (energy per unit time) received by the surface for a particular wavelength of light [32]. The spectral irradiance can be expressed by:

$$F(\lambda) = \Phi(\lambda) * \frac{h \cdot c}{\lambda} \quad (1-17)$$

where $F(\lambda)$ is the spectral irradiance in $\text{Wm}^{-2}\mu\text{m}^{-1}$; Φ is the photon flux in $\text{m}^{-2}\text{sec}^{-1}$; h is Planck's constant; c the speed of light; λ is the wavelength of the given photon in meter. For commodity, the photon number is often expressed in "moles" ($1 \text{ mole} = 6.022 * 10^{23}$ particles). Hence, the spectral irradiance can be determined as the photon flux (the amount of photons) multiplies the energy of the photon, and divide by that wavelength.

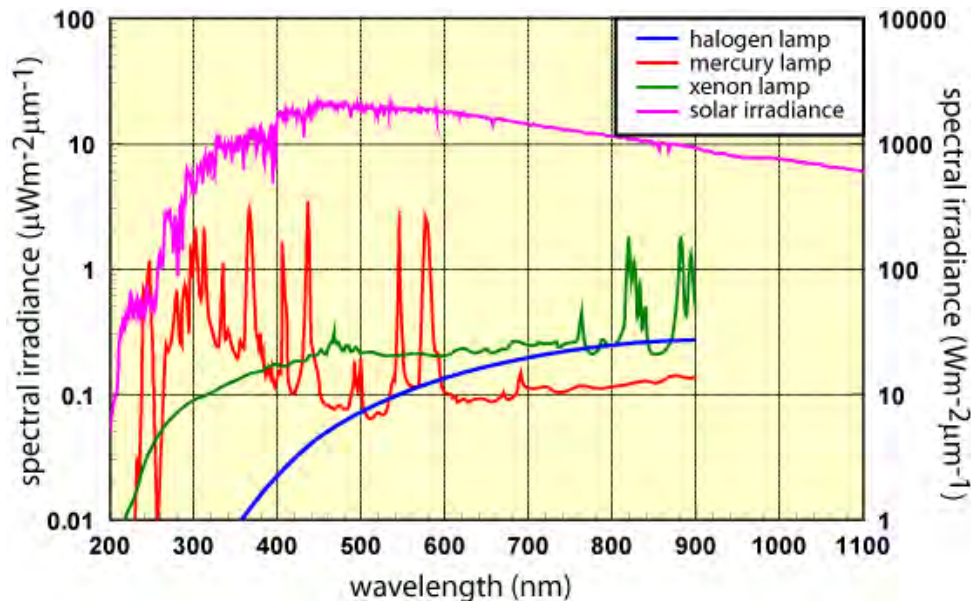


Fig. 1-7 Spectral irradiance for different light sources [32] (The axis of solar irradiance (on the right) and the axis of artificial light sources (on the left))

Fig. 1-7 shows the spectral irradiance for different light sources. The differences in spectra results from the differences in the light production mechanisms.

1.2.2 Different types of light sources

Light sources can be grouped into natural light sources and artificial light sources. The main artificial light sources are composed of thermal light sources (incandescent lamps), gas discharge lamps (Low-intensity and high-intensity discharge lamps) and semiconductor light sources (LED, OLED). Since Thomas Edison invented the first practical incandescent lamp in 1879, conveniences and advantages that were brought by the artificial light source are self-evident. It cannot be imaginable if our life does not have artificial light sources. Fig. 1-8 and Fig. 1-9 illustrate the families and the luminous efficiency of artificial light sources respectively.

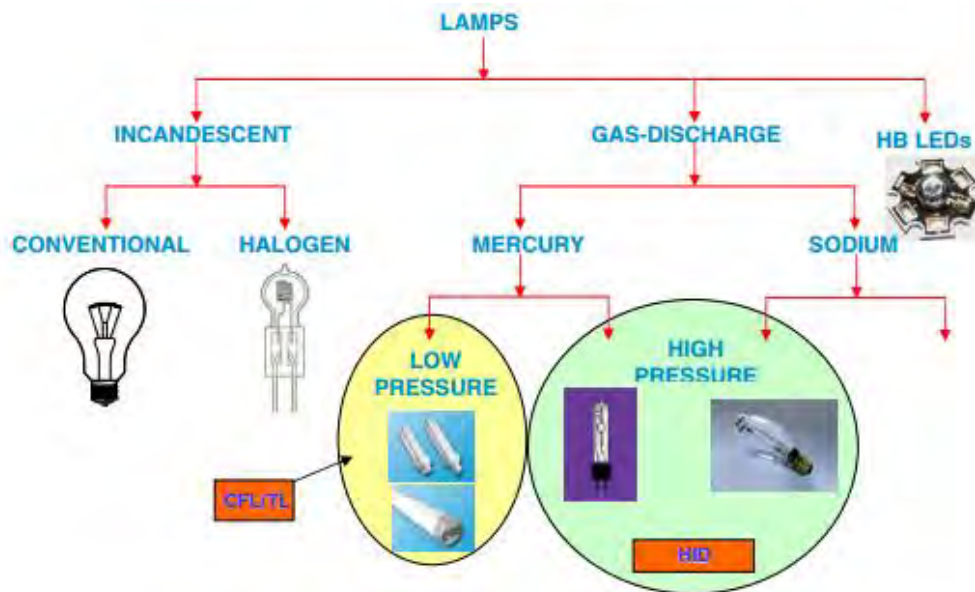


Fig. 1-8 Families of artificial light sources [33]

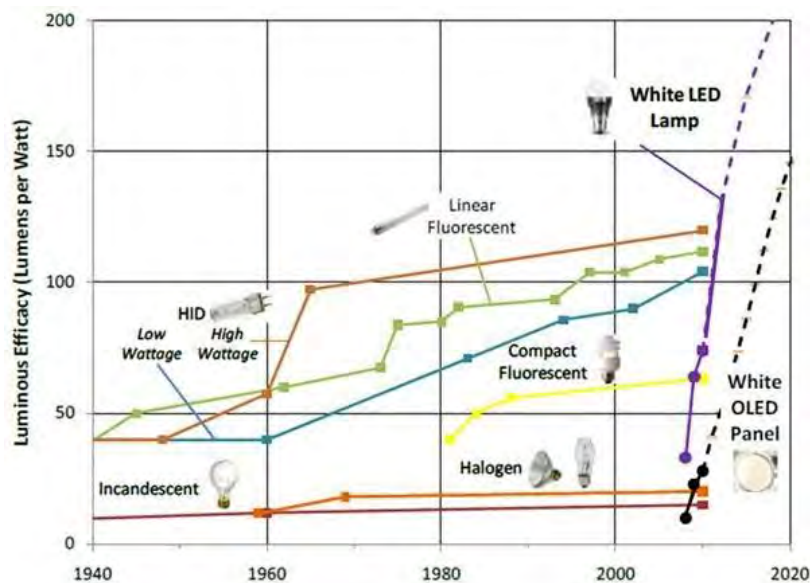
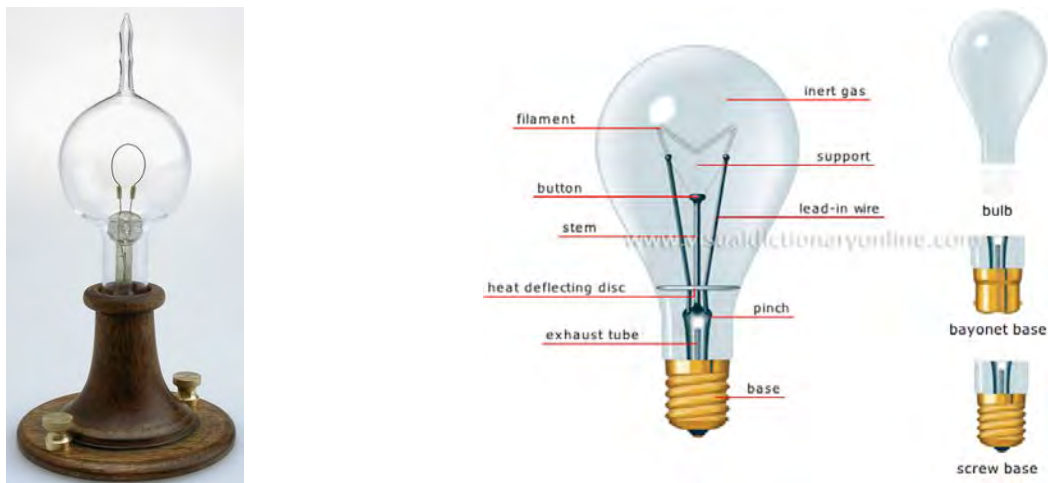


Fig. 1-9 Luminous efficiency of various lamps [33]

According to Fig. 1-9, we can see that HID lamps have higher luminous efficacy than incandescent and fluorescent lamps. Since 2009, white LED and OLED lamps are improved greatly and the luminous efficacy of these two kinds of lamps increases sharply, especially for LED lamps. This means that LED lamps are the development trend of light sources in the future. However, HID lamps take the main place in the market currently. Therefore, HID lamps still have research and use value.

1.2.2.1 Incandescent lamp

The incandescent light bulb or incandescent lamp is a thermal radiator. It is an electric light by heating a filament in the lamp to a high temperature so that it glows with visible light. The incandescent lamp is the second form of electric light to be developed for commercial use after carbon arc lamp. It is also the second most used lamp in the world except the fluorescent lamp. The incandescent lamp has good color rendering index (100), cheap price, and no quantity of toxic materials inside arc tube. However, it just can convert 10% of its energy to the visible light, 90% of the energy going to heat. Therefore, it is replaced by the fluorescent lamp. Fig. 1-10 shows the first incandescent light bulb and typical structure of the incandescent lamp.



(a) First incandescent lamp

(b) Typical structure of incandescent lamp

Fig. 1-10 Incandescent lamp [34] [35]

1.2.2.2 Gas discharge lamp

The gas discharge lamp is an artificial light source that produces light by creating an electrical discharge through an ionized gas, a plasma [36]. This kind of lamps uses a noble gas (argon, neon, krypton, and xenon) or a mixture of these gases. Some contain additional materials, such as mercury, sodium, and metal halides, which are vaporized during startup to become part of the gas mixture.

A. The V-I characteristics of gas discharge

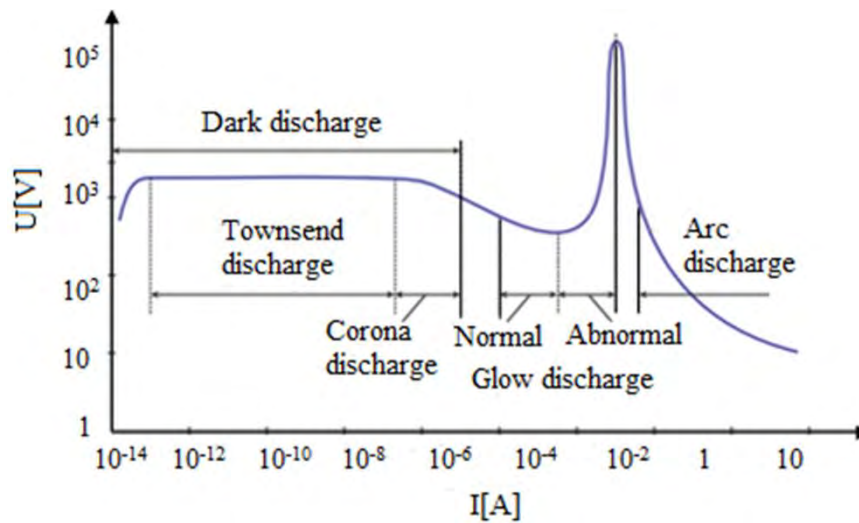


Fig. 1-11 The general V-I characteristics of self-sustained discharges [37]

Fig. 1-11 shows the V-I characteristics of self-sustained discharges. The V-I characteristics are composed of three regions: dark, glow and arc discharge. The dark discharge contains the Townsend and corona discharge. At this region, the low current is up to 10^{-4} A and voltage is over kilovolts. There is no significant luminance here.

The glow discharge includes normal and abnormal mode. It owes its name to the luminous glow of the plasma. Glow discharge is widely used as a source of light such as neon lights, fluorescent lamps, and plasma-screen televisions. The current is from 10^{-4} A to 10^{-1} A in the glow discharge.

The arc discharge can produce an ongoing electrical discharge. It is characterized by a lower voltage than the glow discharge and relies on thermionic emission of electrons from the electrodes sustaining the arc. Normally, the higher currents are over 10^{-1} A in a plasma during the arc discharge.

B. Types of gas discharge lamp

Gas discharge lamps can be categorized into two groups: low pressure and high-pressure discharge lamps. Low-pressure gas discharge lamps contain fluorescent lamps and low-pressure sodium lamps. High-pressure mercury lamps, metal halide lamps, and high-pressure sodium lamps are high-pressure gas discharge lamps, also called HID lamps. The term high-intensity discharge means a high-power density. For most of HID lamps, the arc tubes are enclosed in outer glass bulbs.

Compared to incandescent lamps, fluorescent lamps have much higher luminous efficacy (up to 100 lm/W) and they are widely used in the indoor environment. Because of much higher luminous efficacy (up to 140 lm/W), better color rendering index (up to 93), HID lamps are applied for the outdoor environment.

a) Fluorescent lamp

The fluorescent lamp or the fluorescent tube is a low-pressure mercury-vapor gas-discharge lamp that uses fluorescence to produce visible light. It is a cylindrical glass tube that is coated on the side with phosphors. It is composed of mercury and is filled with a small amount of argon, a combination of argon and neon or krypton gases. When it operates, some current passes through the lamp and the mercury is vaporized, producing ultraviolet light. Then the phosphor coating absorbs the ultraviolet light and radiates it as visible light. The fluorescent lamp needs starters and ballasts to start and limit current.

The compact fluorescent lamp (CFL) is a type of fluorescent lamp, also known as a compact fluorescent light or energy saving light. Compared to the incandescent lamp giving the same amount of visible light, the CFL uses less power and has a longer lifetime. For example, the incandescent bulb consumes anywhere from 4 to 8 times as much power to generate same amount light, and the lifetime is just 10% of the fluorescent lamp. Much of the wasted power in incandescent bulbs turns to heat. Fig. 1-12 shows two kinds of fluorescent lamps.



Fig. 1-12 Fluorescent lamps [38] [39]

The ballast is used to limit the current after lamp ignition. To start the lamp, there must be a high voltage spike to start the arc because of the high resistance of argon itself. To make the lamp work safely, preheat the lamp is figured out by using a starter switch. Recently, several approaches such as preheat, instant start, rapid start, semi-resonant start and programmed start are applied to start the lamps [40]. Fig. 1-13 shows the basic structure and operation principle of a fluorescent lamp.

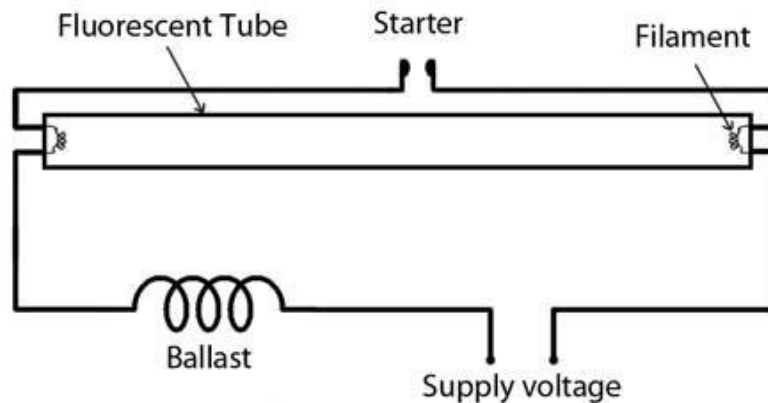


Fig. 1-13 The basic structure and operation principle of a fluorescent lamp [41]

b) High-pressure mercury lamp

High-pressure mercury lamps are gas discharge lamps which use an electric arc through vaporized mercury to produce light [42]. Fig. 1-14 shows the structure of a high-pressure mercury lamp.

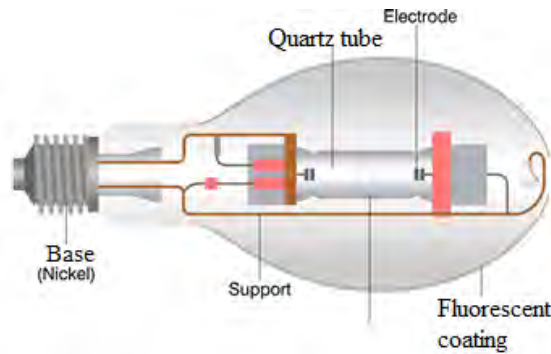


Fig. 1-14 High pressure mercury lamp [43]

In Fig. 1-14, an arc tube inside the lamp bulb is made of quartz, with two tungsten electrodes at the ends. The tube contains a few milligrams of mercury and about 25-50 torr of pure argon as a buffer gas [44]. An auxiliary starting electrode is mounted next to one of the main electrodes to help lamp ignition. Generally, the arc discharge is confined to a small fused quartz arc tube mounted within a larger glass bulb. The aim is to produce a bright white and bring a relatively long life.

Mercury vapor lamps produce white light with bluish-green because most chemicals inside arc tube are mercury. Thus, mercury lamps cannot be used in some applications which need high color rendering index properties such as shops, schools, hospitals and so on. In recent years, color rendering index of mercury lamps has been improved by using a phosphor inside of the outer bulb that emits better white light.

c) High pressure sodium lamp

High-pressure sodium (HPS) lamps produce light by an electric discharge through mixed vapors of mercury and sodium, with the sodium radiation dominating the spectral emission. The HPS lamp is one kind of HID lamps, which is used in industrial lighting especially in large manufacturing facilities and plant growth areas. It is also widely used for outdoor area lightings, such as highway roads, parking lots, and security areas. The HPS lamp is regarded as the most ubiquitous for street lighting on the planet because of good efficiency (up to 140 lm/W) and long lifetime (up to 40000 hours). The HPS lamp contains a narrow arc tube supported by a frame in a bulb. There is a higher pressure inside the arc tube to achieve a great efficiency. Sodium, mercury, and xenon are composed of the inside the arc tube. The arc tube is made of aluminum oxide ceramic which is resistant to the corrosion of alkalis like sodium. The HPS lamp starts an arc through xenon gas by a high voltage pulse via a ballast. Then the arc heats up the mercury. Finally, the sodium is vaporized (over 240 °C). The mercury helps produce a blue light which is added to the pure yellow of the sodium. The sodium is mixed with other impurities to achieve a nice white light.



Fig. 1-15 High pressure sodium lamp [45]

d) Metal halide lamp

Metal halide lamps are also one kind of HID lamps. Because their light-emitting materials of the inside arc tube are filled with several metal halide salts such as dysprosium iodide (DyI_3), thulium iodide (TmI_3), holmium

iodide (HoI_3), thallium iodide (TII), sodium iodide (NaI). Thus, they are called metal halide lamps. While the buffer gas and the starting rare gas are formed of mercury and argon. Gas discharge works through excitation of the metal halide salts and the mercury is excited by the current flow. The mixture of the visible radiation of the different elements results in the designed CCT and CRI for the lamps. Comparing with HPS lamps, MH lamps have excellent color rendering qualities. As one of the most efficient white light sources with higher CRI (up to 93), they are used for wide area overhead lighting of commercial, industrial and public spaces as well as residential security lighting and automotive headlamps. MH lamps consist of a fused quartz or ceramic arc tube that has the gases and the arc, enclosed inside a larger glass bulb that has a coating to filter out the ultraviolet light produced. They work at a high pressure between 4 and 20 atmospheres and need ballasts to start. Fig. 1-16 illustrates different arc tubes of MH lamps.



Fig. 1-16 Metal halide lamps [46] [47] [48]

e) *Electrodeless lamp*

Electrodeless lamps are also called induction lamps which are a kind of gas discharge lamps and there are no electrodes and light filament inside. Electrodeless lamps are based on a technology that is different from that of traditional light sources. They produce light by using an electromagnetic field to excite mercury particles mixed in a noble gas like argon or krypton [49]. The mercury creates a UV light and a phosphor on the inside of the tube filters the energy to visible light. This emitting principle is similar to fluorescent lamps. However, they do not consist of electrodes in the tube. These lamps have three parts: frequency generator (ballast), discharge tube and electromagnet. Fig. 1-17 illustrates the structure of an electrodeless lamp.

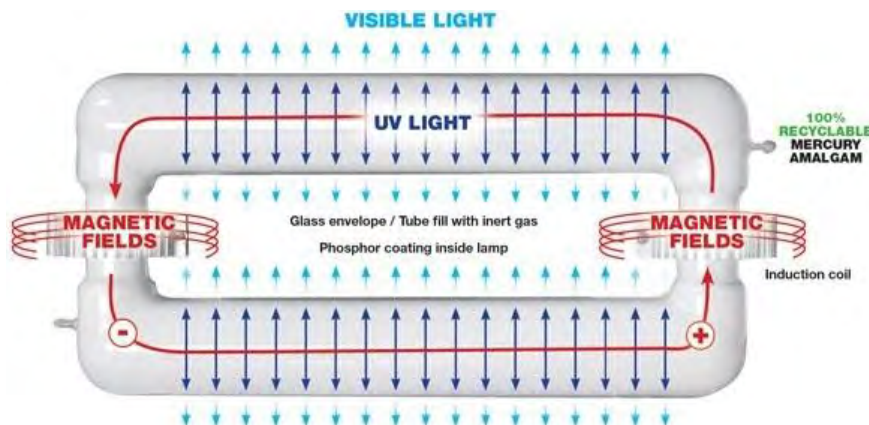


Fig. 1-17 Structure of the electrodeless lamp [51]

This kind of lamps has some advantages, such as long lifespan (25000 to 100000 hours) due to the lack of electrodes, high luminous efficacy 62 to 90 lm/W, and “Instant-on” and “hot re-strike” unlike most HID lamps. Electrodeless lamps also are environmentally friendly due to use of less energy and less mercury than the traditional lamps. Nevertheless, some of these lamps operated very high frequency, which can produce radio frequency interference (RFI) that interferes with radio communications in the area [50]. Due to intellectual property barriers, the makers of those lamps do not have access to HIGH-CRI fluorescent powders. Consequently, the CRI of commercial devices is currently in the range of 70 to 80.

1.2.2.3 Solid state light source

A. Light emitting diode

In some semiconductors, during the recombination process of electrons with holes at the junction of n-doped and p-doped semiconductors, energy is released in the form of light.

The light emitting diode (LED) is a monolithically integrated P-N semiconductor device that emits light when voltage is passed across its two terminals. A P-N junction can also convert absorbed light energy into a proportional electric current. The same process is reversed here (i.e. the P-N junction emits light when electrical energy is applied to it). This phenomenon is generally called electroluminescence, which can be defined as the emission of light from a semiconductor under the influence of an electric field. Fig. 1-18 shows the structure of the LED.



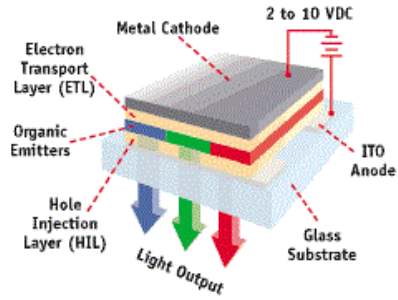
Fig. 1-18 Structure of the LED [52]

B. Organic light emitting diode

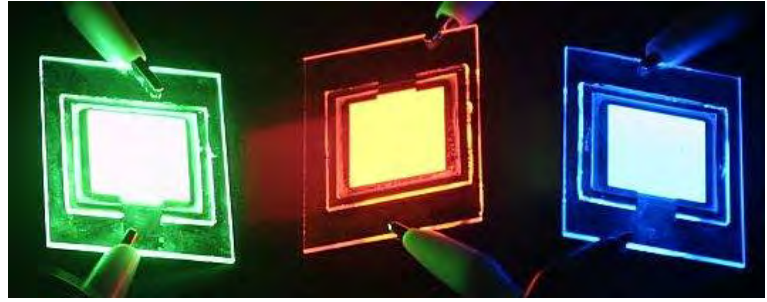
Organic light emitting diodes (OLEDs) are a relatively new technology for solid-state light sources. A typical OLED contains two organic layers: electron transport layer (ETL) and hole injection layer (HIL), embedded between two electrodes. The organic emitters are embedded between two organic layers. The top electrode is usually a metallic mirror with high reflectivity and the bottom electrode is a transparent indium tin oxide (ITO) layer on top of the glass substrate. Fig. 1-19 (a) illustrates the structure of the OLED.

OLEDs work in a similar way to LEDs, but instead of using layers of n-type and p-type semiconductors, they use organic molecules to create electrons and holes. When a voltage is added to the electrodes, the charges start moving in the device under the influence of the electric field. Then electrons leave the cathode and holes move from the anode in opposite direction. When these two charges meet, a brief burst of energy is released by in the form of a particle of light- a photon. Because this process happens many times, so OLEDs produces continuous light as long as the current keeps flowing.

OLEDs are the flat light emitting technology, which made by placing a series of organic thin films between two conductors. OLEDs are used to make digital displays and lighting. Because they can emit light, so they do not need a backlight. Comparing with liquid crystal display (LCD), OLEDs can display deep black levels and can be thinner and lighter. In a dark room, OLED screen can achieve a higher contrast ratio than LCD. Fig. 1-19 (b) shows the OLED displays.



(a) Structure of the OLED



(b) OLED displays

Fig. 1-19 OLEDs [53]

1.2.2.4 Comparisons of different lamps

TABLE 1-3 Comparisons of different lamps [54]

Name	Optical spectrum	Efficacy (lm/W)	Lifetime (MTTF) (hours)	Color temperature (Kelvin)	Dominant color	Color rendering index
Incandescent	Continuous	4–17	750-2000	2400–3400	Warm white (yellowish)	99
Fluorescent	Line spectrum + Phosphor	52–100 (white)	8000-20000	2700–5000	White (any color temperature)	60–95
High pressure mercury	Line spectrum	40-60	10000-20000	4000-7000	White with bluish green	40-69
High pressure sodium	Broadband (Pressure dependent)	55–140	10000-40000	1800–2200	Pinkish orange	0–70
Ceramic metal halide	Quasi-continuous	50–150	6000-24000	3000–4500	White and saturated colors available	80–93
Electrodeless	Line spectrum +Phosphor	70–90 (white)	80000–100000	2700-6000	Ditto	70–80 (white)
LED	Die(s) emission and phosphor (white LED only)	Up to 300 (Cree) [55]	35000–100000	2700-12000	Ditto	Up to 95 (white)
OLED	Broadband (RGB for white)	54-124	30000–100000	2300-9700	Ditto	74-90 (white)

According to the emitting principle, light sources can be categorized into three groups: thermal radiation, gas discharge, and solid-state lamps. Gas discharge light sources consist of low-pressure lamps and high-pressure lamps. Fluorescent lamps are one kind of low-pressure gas discharge lamps. Comparing with incandescent lamps, fluorescent lamps have much higher efficiency and better color properties. For a lot of outside lighting areas, HID lamps that consist of HPM, HPS and MH lamps surpass fluorescent lamps, no matter from efficacy and lifetime. TABLE 1-3 shows the characteristics of different lamps.

1.3 Ballast

Because of the negative impedance, discharge lamps need ballasts to stabilize them. The ballast is a device that is placed in line with the load in order to limit the amount of current in an electrical circuit. It can be viewed as a current source with finite impedance. For efficiency reasons, reactive devices are used to avoid supplemental power dissipation. Fig. 1-20 shows the impedance of discharge lamps.

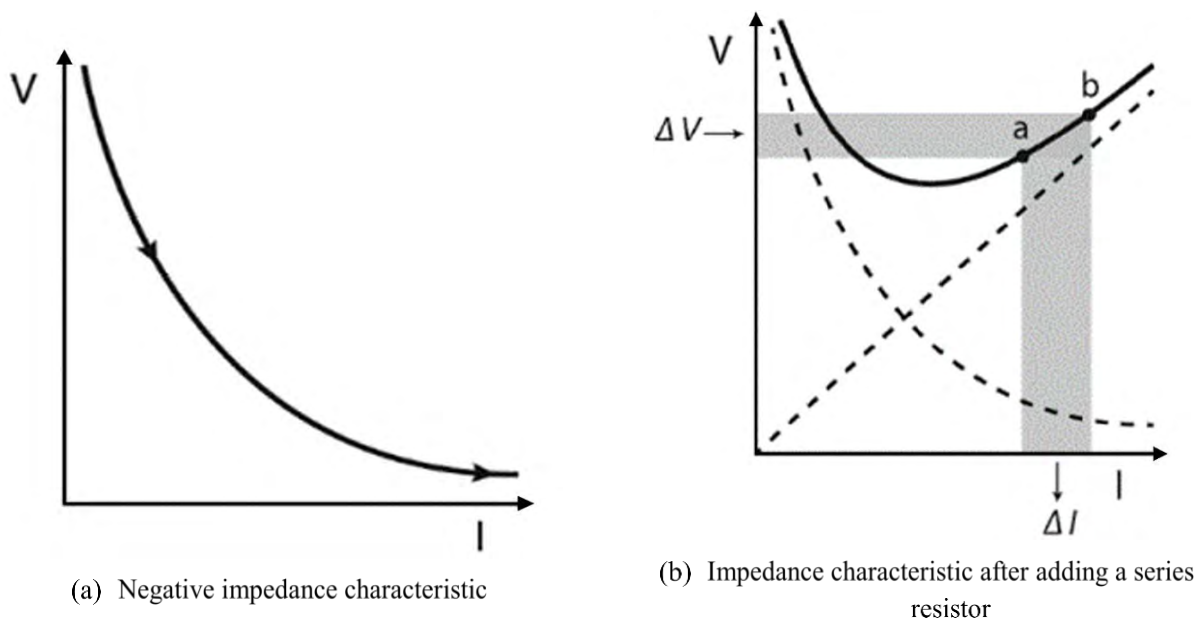


Fig. 1-20 The impedance of discharge lamp [57] [58]

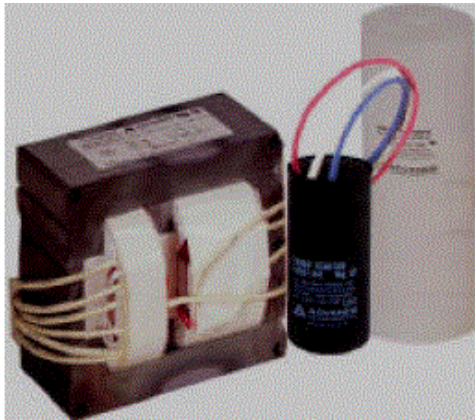
As can be seen from Fig. 1-20 (a), as the voltage decreases, the current increases. This means that unless something can prevent it, the current will increase uncontrollably. In Fig. 1-20 (b), the current is stabilized between points *a* and *b* after adding a resistor in the lamp circuit. The solid line is the result of adding the negative resistance of the ballast (dotted curve) to that of the series resistor (dotted straight line).

Ballasts of gas discharge lamps have two functions to perform: supplying high voltage to start the lamp and limiting the current after lamp ignition. There are mainly two kinds of ballasts: magnetic and electronic ballasts (low-frequency square wave and high-frequency electronic ballast).

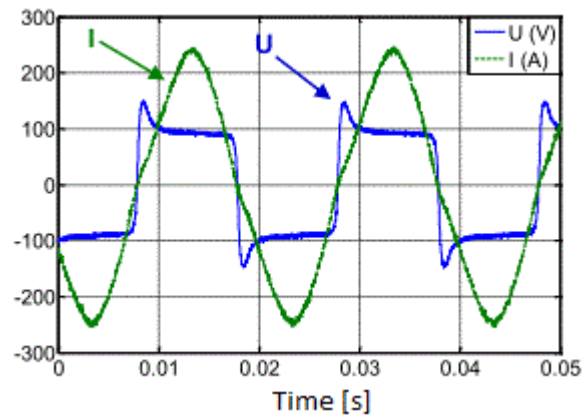
1.3.1 Electromagnetic ballast

Simple resistors can be used as current-limiting ballasts for gas discharge lamps, but they have many power losses. Inductive coils that have the same effect as a resistor can be used as ballast. These inductive ballasts are called “electromagnetic ballasts” because the electric and magnetic fields are generated by coils. Magnetic ballasts are “core-and-coil” electromagnetic ballasts wrapped with copper windings. They are heavier, bulkier,

less efficiency and lower power factor but cheaper comparing to the electronic ballast. Therefore, magnetic ballasts are gradually replaced by electronic ballasts. Fig. 1-21 shows the magnetic ballast and the lamp current and voltage supplying by the magnetic ballast.



(a) Magnetic ballast



(b) Waveforms of the lamp current and voltage at 50 Hz

Fig. 1-21 Magnetic ballast and waveforms of the lamp current and voltage [59]

In Fig. 1-21 (a), the magnetic ballast works accompanied by a starter. In Fig. 1-21 (b), the current waveform presents serious distortions. This characteristic causes a serious non-linear for the lamp I-V curve. Obviously, magnetic ballasts have a heavy weight, low efficiency, and low power factor.

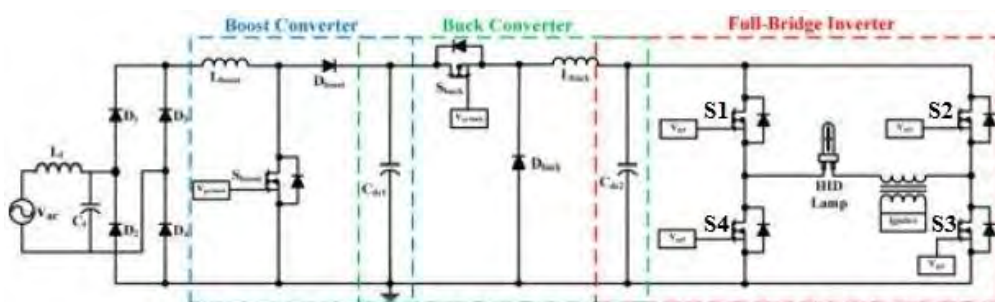
1.3.2 Electronic ballast

Electronic ballasts use solid-state electronic components to provide the proper starting and operating electrical conditions to power discharge lamps. They use integrated circuit (IC) chips and feedback to implement better controls and safety features into ballasts. Electronic ballasts have higher efficiency than similar electromagnetic ballasts. They also are small size, lightweight, improved lumen maintenance, fault mode protection and better power regulation, which results in better color consistency.

The most common electronic ballasts can be categorized into two types: low-frequency square-wave and high-frequency electronic ballasts.

1.3.2.1 Low-frequency square-wave electronic ballast

Most commercial electronic ballasts are low-frequency square wave ballasts that are reliable, and almost no AR occurrence for their supplying lamps. However, they are low efficiency due to complicated structures. Low-frequency square-wave electronic ballasts are shown in Fig. 1-22.



(a) Three stages of the low-frequency electronic ballast [60]

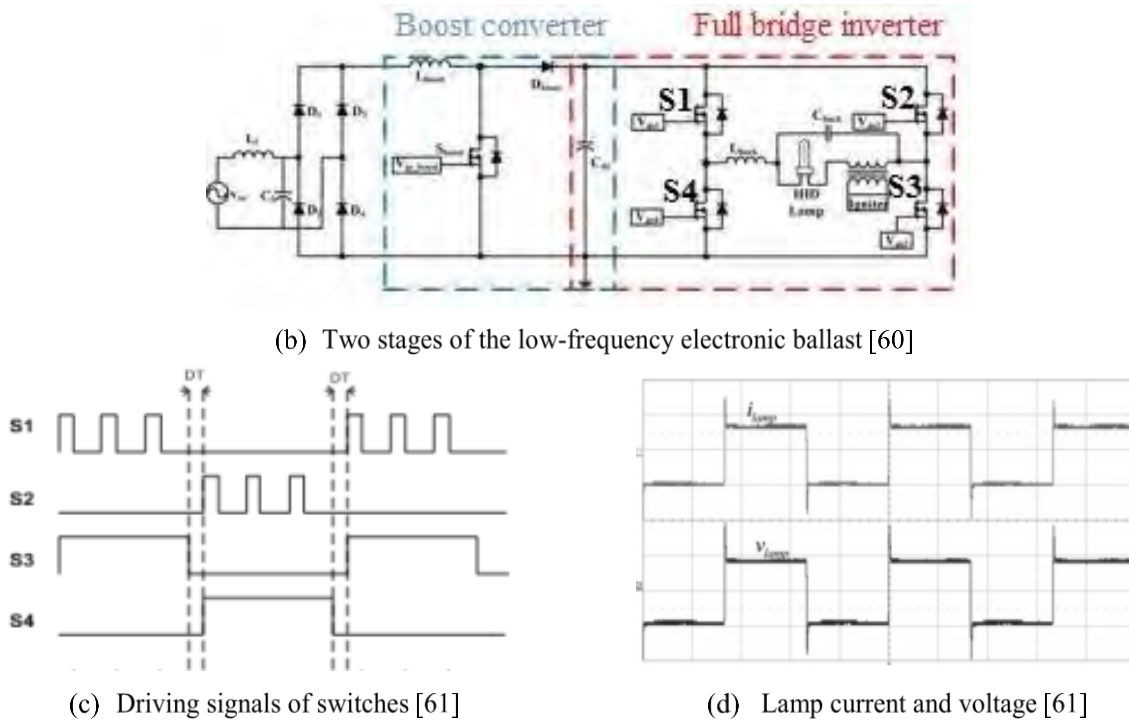


Fig. 1-22 Low-frequency square wave electronic ballast

In Fig. 1-22 (a), the commercial three-stage ballast consists of a PFC boost converter (an inductor L_{boost} , a switch S_{boost} , a diodes D_{boost} and a capacitor C_{dc1}), a buck converter (a switch S_{buck} , a diode D_{buck} and C_{dc2}) for regulating lamp power, and a full-bridge inverter (switches S_1 , S_2 , S_3 and S_4) for supplying low frequency square wave source. In Fig. 1-22 (b), the two-stage ballast consists of a PFC boost converter which is the same as the PFC boost converter in Fig. 1-22 (a), and a full-bridge inverter (an inductor L_{buck} , a capacitor C_{buck} and switches S_1 , S_2 , S_3 and S_4) for supplying low-frequency square wave source as well.

Fig. 1-22 (c) illustrates the driving signals of the ballasts; the switches S_1 and S_2 operate at high frequency, and the switches S_3 and S_4 operate at low frequency. When S_1 and S_3 are on, S_2 and S_4 are off, and *vice versa*. The waveform for the lamp current and voltage are low-frequency square waveforms, as shown in Fig. 1-22 (d). The common low frequencies are 60 Hz, 120 Hz, and 400 Hz.

1.3.2.2 High-frequency electronic ballast

HID electronic lighting has now become a practical alternative to traditional magnetic-based technology. In particular, high-frequency electronic ballasts for HID lamps have proven to be technologically feasible and economically justifiable, while generating significant energy savings. Fig. 1-23 illustrates the schematic of the high-frequency electronic ballast, the waveforms of driving signals, and the lamp voltage and current.

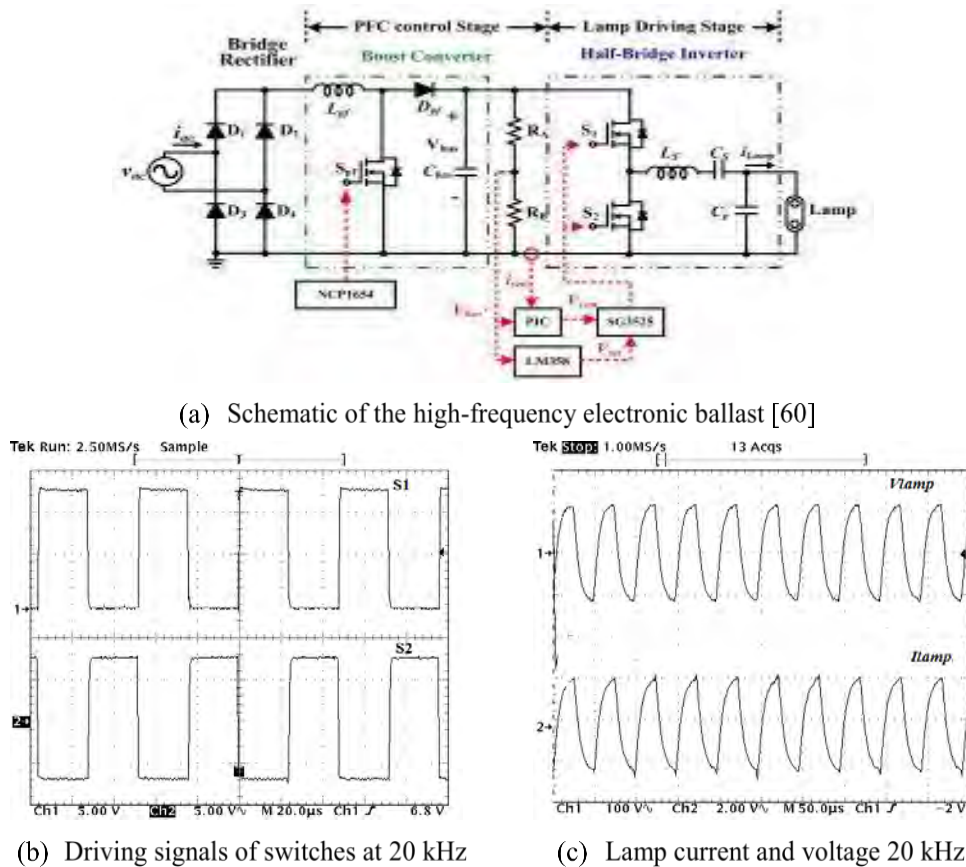


Fig. 1-23 High-frequency electronic ballast

As can be seen from Fig. 1-23 (a), the high-frequency electronic ballast has the simpler structure and the inverter is half-bridge inverter just contained two switches. Thus, it has better system efficiency and lower cost. The high-frequency electronic ballast also increases luminous efficacy by almost 10% when the lamp is driven at frequencies in excess of 2 kHz in an improved compact, lightweight package [62]. Nevertheless, AR may occur when HID lamps are operated at frequencies from several kHz to a few hundred kHz. The AR spectrum, unfortunately, always covers the frequency band suitable for the high-frequency electronic ballasts. AR can reduce the lamps' lifetime and damage the ballasts or lamps. Therefore, the high-frequency ballasts must have the AR control circuit.

1.3.3 Comparison between electromagnetic ballast and electronic ballast

While magnetic ballasts are simple and easy to design, the more sophisticated electronic ballasts have too many advantages. In addition to not causing light flicker and noise like magnetic ballasts, electronic ballasts are preferred because they are smaller in size and weigh less. They are also great for the environment because of their higher energy efficiency. Additionally, electronic ballasts can be used in lamps that are in parallel and series mode. This means that if one of the lamps goes out, this will not affect the other lamps even though all the lamps are using the same ballast. TABLE 1-4 shows the comparison between the electromagnetic ballast and the electronic ballast.

TABLE 1-4 Electromagnetic ballast *versus* electronic ballast

Type	Electromagnetic ballast	Electronic ballast
Electric energy consumption	100	Reduced from 10 to 15%
Lamp lifetime	100	Increased up to 30% depending on the light sources
Ignition time	From 90 to 60 seconds to reach 90% of the nominal luminous flux	50% quicker
Heat	More	Less
Noise	Humming noise 100 Hz (magnetic constriction)	No noise
Light fluctuations	no perceived flickering but reported health effects	No flickering
Size and weight	Heavy and large size	Lightweight and compact
Power factor	0.5-0.7	>0.95

1.4 Review of previous research about acoustic resonance

The phenomenon of AR was first reported by Campbell [63]. The research achievements about AR can be grouped into several categories as follows:

b) AR characterization

AR not only causes arc fluctuations, deformations, and light flicker but also changes chromaticity coordinates, and color temperature significantly [64]. As presented in the paper [6], AR can change electrical parameters, increasing the lamp voltage and decreasing the current. In the paper [65], AR can cause noisy sounds in arc tube of HID lamps. Overall, there is no doubt that AR hampers the development of HID lamps and reduces lamps' lifetime. Fig. 1-24 and Fig. 1-25 show arc distortions in different kinds of HID lamps.

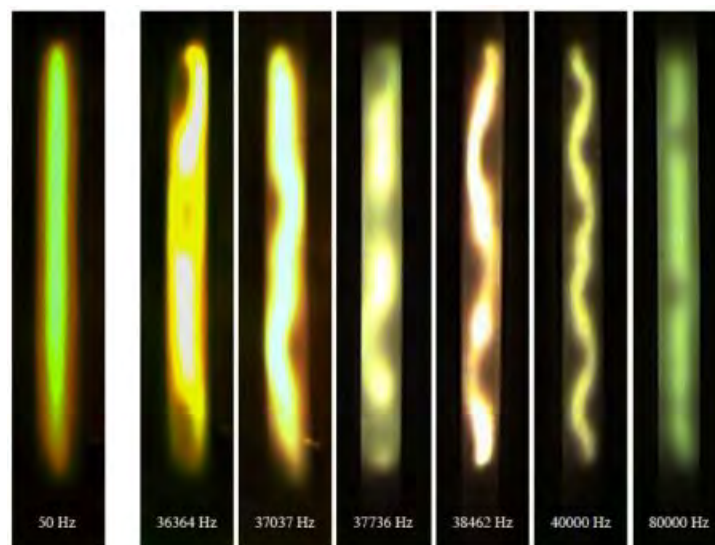


Fig. 1-24 Arc distortions in an HPS lamp [66]

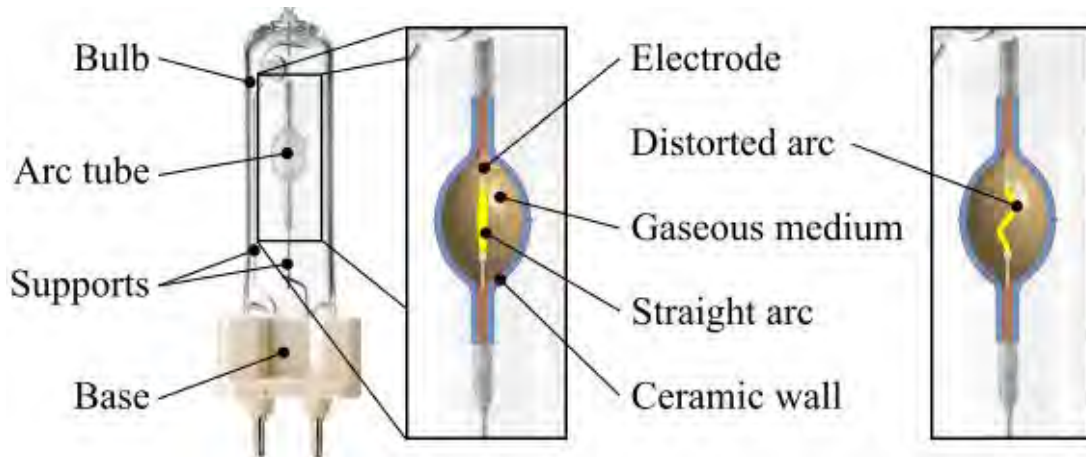


Fig. 1-25 Arc distortion in an MH lamps [67]

c) *AR mechanism and theoretical frequencies*

In the paper [12], the AR mechanism has been defined. Alternating electric current represents a periodic heat source in the arc tube. The resulting temperature fluctuations cause pressure oscillations. The ballasts operating at the eigenfrequency of the arc tube produces standing pressure waves, which affect the velocity field of the plasma and cause arc flicker. The other explanation of AR occurrence can be attributed to acoustic streaming.

According to the solution of the simplified acoustic wave equation, three kinds of AR frequency modes can be calculated in HID lamps: the longitudinal mode, the radial mode and the azimuth mode [68].

d) *AR Detection*

AR detection methods can be classified depending on how the AR is detected: measuring lamp electrical parameters (voltage, current, or relative impedance) [6], [8], [69], or observing other lamp physical parameters (sound emission, thermal parameters, or optical parameters) [2], [65], [70].

e) *AR avoidance*

The main effect of AR excitation in the arc tube of HID lamps is the changes of the chemical and physical balance of filling materials. This basic phenomenon leads to fluctuations of electrical parameters, light instability, and light flickering.

Although certain free AR windows exist in HID lamps, due to the production tolerance or aging time of lamps, these free windows are unpredicted. In order to avoid AR in HID lamps, several methods are applied, such as square wave supply [13], pulse operation [71], extra-high frequency [72], frequency modulation [11], amplitude modulation, injection of fundamental and the third harmonic [73], and injection of several adjacent frequency signals [74]. The main ideas are to reduce the power harmonic below the AR excitation threshold.

f) **Model of acoustic streaming**

In recent years, acoustic streaming in HID lamps becomes a research hot point. The numerical model including acoustic streaming using 2-D axisymmetric geometry was implemented in an HID lamp [8], [75], as shown in Fig. 1-26.

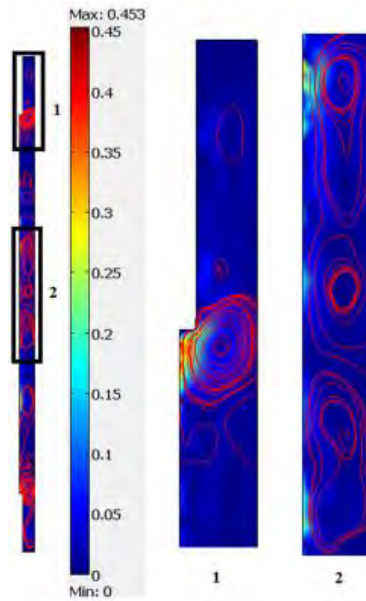


Fig. 1-26 Convection velocity including the influence of the acoustic streaming in an HPS lamp and corresponding to the frequency equal to 10.8 kHz (the streamlines correspond to the velocity) [8]

In Fig. 1-26, several velocity fluxes are generated by the acoustic streaming force. Except for these fluxes, the amplitude of the velocity increases from 0.1 cm/s (without AR) to 4.5 cm/s (with AR). The rise of the velocity and the generation of the velocity fluxes can explain the instabilities in the arc tube and the displacement of the electrical arc.

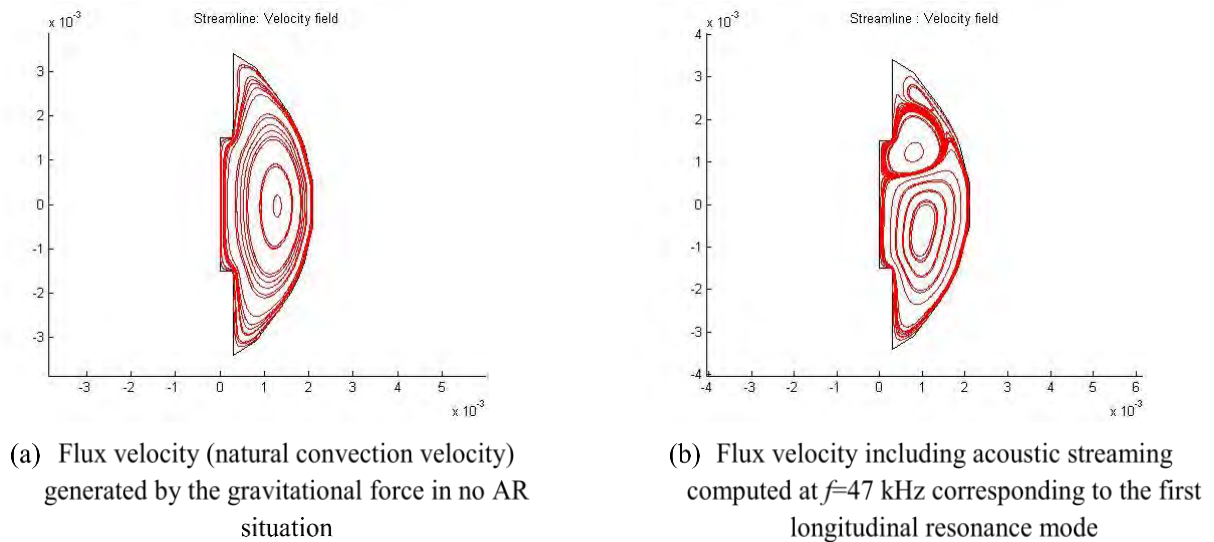


Fig. 1-27 The flux velocity in an HID lamp [75]

In Fig. 1-27 (a), the flux velocity is generated because of the gravitational force, when AR does not occur in the HID lamp. Fig. 1-27(b), several fluxes are generated due to the acoustic streaming force. In addition, the streamline is divided into several irregular parts.

3D multi-physics mode of high-intensity discharge mode has been set up to calculate the acoustic streaming velocity field inside the arc tube of HID lamps [76], [67]. In the paper [77], a 3D finite element model was

presented to determine the influence of acoustic streaming on the temperature field near an acoustic eigenfrequency. The results show that acoustic streaming affects voltage drop, temperature field, and flow field. Furthermore, it has recently been discovered that the acoustic streaming phenomenon is the link between the high-frequency resonances and the low-frequency light flicker. The high-frequency sound wave causes a low-frequency movement of the plasma arc that is visible as light flicker. As presented in the paper [78], there are low frequencies (8-15Hz) of discharge arc flicker and arc fluctuations due to the excitation of AR in MH lamp. The reason of low-frequency flicker with AR can be identified as acoustic streaming effects.

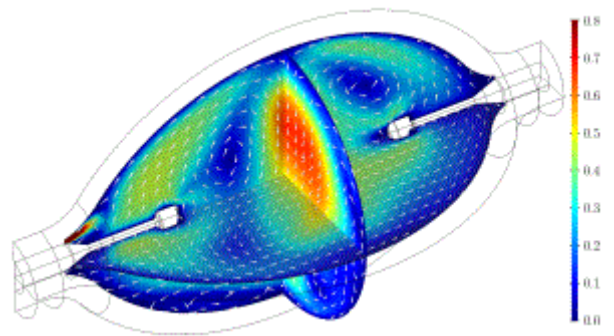


Fig. 1-28 Acoustic streaming velocity field (velocity in m/s) [67]

In the paper [67], acoustic streaming is assumed to be responsible for light flicker caused by AR. According to Fig. 1-28, the maximal streaming velocity is about 0.8 m/s near an AR frequency. For the diameter of an arc tube 6 mm, this velocity is very large, so it is not surprising that the streaming field can disturb the plasma arc.

1.5 Thesis key points

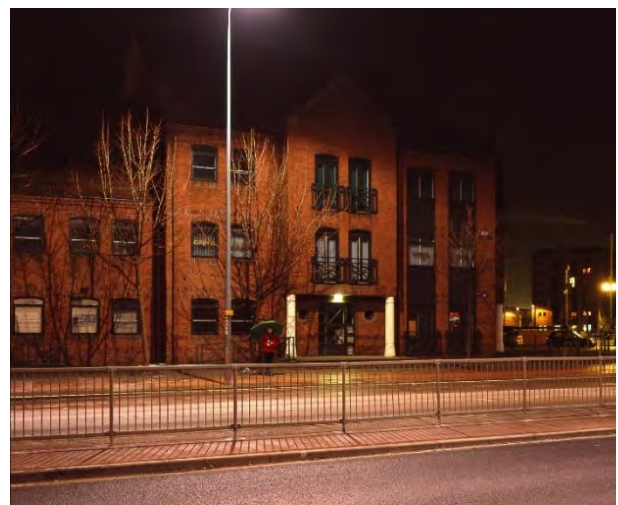
Base on the current research achievements studied by others, our work focuses on several parts as follows:

a) Why we choose MH lamps, not HPS lamps?

MH lamps have quasi-continuous spectrum, higher CCT, and better color rendering index. In addition, MH lamps produce white light, comparing to HPS lamps producing yellow light. MH lamps can be used for somewhere needs high color qualities. Fig. 1-29 shows HPS and MH lamps using in different streets.



(a) HPS lamps in street 1



(b) MH lamps in street 1



(c) HPS lamps in street 2



(d) MH lamps in street 2

Fig. 1-29 High pressure sodium lamp versus metal halide lamp (Taken by GEL UK for NumeLiTe consortium)

As can be seen from Fig. 1-29, the difference between HPS lamps and MH lamps are obvious. MH lamps have better color rendering index. The other reason we choose MH lamps is that many researchers study the AR phenomenon in HPS lamps, whereas just few study AR in MH lamps. In addition, according to McKinsey's report "Lighting the way" [78], although HID lamps are increasingly replaced by light-emitting diodes (LEDs), they will be still used and needed in several years due to the higher cost of LEDs. Based on these reasons, we study the characterizations of MH lamps in this thesis.

b) Why we study high-frequency electronic ballast?

As presented in section 1.3.2, high-frequency electronic ballasts have simpler structures, resulting in higher power efficiency, smaller size, lighter weight, and lower costs compared the low-frequency square wave electronic ballasts. In addition, the luminous efficacy can increase 10%, when the lamp operating frequency is higher than 2 kHz [62]. More importantly, the high-frequency electronic ballast can dim lamps as low as 35% of their rated power. In order to save energy, dimming control of lamps becomes more and more important. For example, the required light output is different in the street during the night and the morning. During the night 10-12 pm, there are many people and cars, thus streets need more light output. During the morning 4-6 am, streets do not need many light outputs. If the ballasts can dim light feasibly, much more energy can be saved. Although AR occurs in the lamps, this problem can be solved totally with better control. Therefore, developing high-frequency electronic ballast is the trend in the future. TABLE 1-5 shows the comparison between the low-frequency electronic ballast and the high-frequency electronic ballast.

TABLE 1-5 Low-frequency square wave *versus* high-frequency electronic ballast

Type	Low-frequency square wave electronic ballast	High-frequency electronic ballast
Operating frequency	100-400 Hz	>1 kHz
Energy consumption	10% of lamp energy	5% of lamp energy
Lumen maintenance	Lower	Improved lumen maintenance
Size and weight	Larger components (Coil and capacitor)	smaller components
Luminous efficiency	100	Increased 10%
Dimming control	DC level dimming	Frequency dimming at constant DC level
Acoustic resonance occurrence	high frequency ripple on the square wave susceptible to trigger AR	Susceptible to AR generation

c) Importance of online methods for AR detection

AR occurs in HID lamps operated at the frequency higher than 1 kHz. This problematic phenomenon may reduce the lamps' lifespan, and sometimes destroy the lamps, resulting in higher cost for lamps' users. It is essential to use some simple and online methods to detect this phenomenon. So many methods already were developed by other researchers. However, most of the methods are not online detection, and some of them are difficult to fulfill. In fact, AR phenomenon is a dynamic process. AR detection methods must have a very good sensitivity and diagnostic this abnormal phenomenon quickly. Thus, we emphasize the importance of the sensitivity and online detection in this thesis. Low-frequency fluctuations appear on the lamp voltage envelope when AR occurs in MH lamps. In this case, we propose two kinds of online envelope evaluation methods: a multiplier circuit and a rectifier circuit to classify between AR and no AR cases in MH lamps.

d) Electrical modelings of lamp voltage in the presence of AR for the high-frequency electronic ballast

AR cause the lamp arc rotation, and bending, resulting in fluctuations in the lamp voltage and current. The lamp voltage waveform with AR occurrence is similar to the double side amplitude modulation. In addition, the periodic and the stochastic signals are observed from the lamp voltage in the presence of AR. Based on these interesting observations, we built the modelings of the lamp voltage in AR case. In fact, it is helpful to build the numerical models of the lamp voltage for the high-frequency electronic ballast. These numerical simulations can help the ballast circuit designer to develop some methods for AR detection and avoidance, and save experimental costs as well.

e) AR Detection by using statistical methods of voltage envelope characterization in MH lamps

Based on our literature reviews, there are no objective approaches to classify AR severity. Most people identify AR severity by human eyes. Our purpose is to build objective criteria to classify AR severity. To our knowledge, the statistical methods developed in this thesis are reported for the first time in this context.

Our online detection methods show the voltage envelope detection is a good method to classify between AR and no AR cases. Therefore, we continue to measure the lamp voltage envelope, but a commercial device: the lock-in amplifier SR830. Furthermore, statistical methods are used to analyze the characterizations of the voltage envelope in MH lamps. The objective criterion is proposed by a 2-D plane plot, a boxplot, a histogram or an ANOVA plot. By using statistic methods, we conclude that AR has both short-term and long-term signatures.

AR significantly influences the voltage envelope. In addition, our measurement and analysis methods also can be as indicators to detect the lifetime of lamps.

f) How does the AR phenomenon influence the spectral variations of MH lamps? (validation of electrical methods)

AR can shift the balance inside arc tube of the MH lamp, resulting in some variations in the spectral irradiance and colorimetric parameters such as chromaticity coordinates, CCT, and CRI. Nevertheless, no literatures reported how the AR phenomenon influences these variations of MH lamps. The variations of the spectral irradiance and colorimetric parameters are called light spectral variations in this thesis. We measure these variations by using a spectrophotometer. The interesting results are found that the spectral variations are able to distinguish AR and no AR cases thanks to some statistical analyses.

References

- [1] K. Stockwald, H. Kaestle, H. Ernst, "Highly efficient metal halide HID systems with acoustically stabilized convection," in *IEEE Trans. Industry Applications*, vol. 50, no. 1, pp. 94-103, Feb. 2014.
- [2] J. Schwieger, B. Baumann, M. Wolff, "Arc Shape of High-Intensity Discharge Lamps: Simulation and Experiments," *International Journal of Thermophysics*, vol. 36, no. 5-6, pp. 1327-1335, Jun. 2015.
- [3] F. T. Wakabayashi, C. A. Canesin, "An improved design procedure for LCC resonant filter of dimmable electronic ballasts for fluorescent lamps, based on lamp model," in *IEEE Trans. on Power Electronics*, vol. 20, no. 5, pp. 1186-1196, Sept. 2005.
- [4] S. Ben-Yaakov, M. Shvartsas, S. Glozman, "Statics and dynamics of fluorescent lamps operating at high frequency: modeling and simulation," in *IEEE Trans. on Industry Applications*, vol. 38, no. 6, pp. 1486-1492, Nov/Dec 2002.
- [5] W. Kaiser, R. P. Marques, A. F. Correa, "An Alternative Optical Method for Acoustic Resonance Detection in HID Lamps," in *Proc. IEEE IAS Annual Meeting*, pp. 1-6, Oct. 2009.
- [6] L. Chhun, P. Maussion, S. Bhosle, G. Zissis, "Characterization of Acoustic Resonance in a High-Pressure Sodium Lamp," *IEEE Trans. Industry Applications*, vol. 4, no. 2, pp. 1071-1076, Dec. 2010.
- [7] H. Peng, S. Ratanapanachote, P. Enjeti, L. Laskai, I. Pitel, "Evaluation of acoustic resonance in metal halide (MH) lamps and an approach to detect Its occurrence," in *Proc. IEEE IAS Annual Meeting*, vol. 3, pp. 2276-2283, Oct 1997.
- [8] A. Burgio, D. Menniti, "HID lamp acoustic resonance detection: A simple current-based method using sample-and-hold circuits," in *Proc. Environment and Electrical Engineering Conference (EEEIC)*, pp. 1-4, May 2011.
- [9] A. Toumi, L. Chhun, S. Bhosle, G. Zissis, P. Maussion, B. Baumann, M. Wolff, "Acoustic Resonance Characterization and Numerical Model Including Acoustic Streaming in an HPS Lamp," in *IEEE Trans. on Industry Applications*, vol. 49, no. 3, pp. 1154-1160, May. -Jun. 2013.
- [10] H. L. Witting, "Acoustic resonances in cylindrical high-pressure arc discharges," *Journal of Applied Physics*, 1978, vol. 49, no 5, p. 2680-2683.
- [11] J. Correa, M. Ponce, J. Arau, M. Sanchez, J. M. Alonso, "Evaluation of frequency modulation techniques to avoid acoustic resonances in electronic ballast for HID lamps: analysis and methodology," in *Proc. IEEE Power Electronics*, vol. 10, pp. 245-250, 17-22 Oct. 2004.
- [12] F. Afshar, "The theory of acoustic resonance and acoustic instability in HID lamps," *LEUKOS: The Journal of the Illuminating Engineering Society of North America*, vol. 5, no. 1, pp. 27-38, Sep. 2008.

- [13] F. Afshar, "Allowed level of the power ripple in low-frequency square wave ballast of metal halide lamps," LEUKOS: The Journal of the Illuminating Engineering Society of North America, vol. 3, no. 2, pp. 143-157, Oct. 2006.
- [14] <http://www.clusterlumiere.com/opus-light-4/>
- [15] J. Garcia, A. J. Calleja, E. L. Corominas, D. Gacio, J. Vina and D. G. Llera, "Interleaved Inverter for HF Ripple Cancellation in Metal Halide Lamps," IECON Proceedings (Industrial Electronics Conference), Nov. 2010, pp. 2584-2588.
- [16] T. D. Baenziger, "Energy management in lighting systems," The 35th IAS Annual Meeting and World Conference on Industrial Applications of Electrical Energy, vol. 5, pp. 3452-3459, Oct. 2000.
- [17] https://en.wikipedia.org/wiki/High-intensity_discharge_lamp
- [18] W. B. Cheng, Y. R. Zhong and S. Jin, "Suppressing acoustic resonance in HID lamp with combined frequency modulation," The 37th IEEE Power Electronics Specialists Conference, pp.1002-1006, Jun. 2006.
- [19] R. Redl and J. D. Paul, "A new high-frequency and high-efficiency electronic ballast for HID lamps: topology, analysis, design, and experimental results," Applied Power Electronics Conference and Exposition, vol. 1, pp. 486-492 vol.1, Mar. 1999.
- [20] R. L. Steigerwald, "A comparison of half-bridge resonant converter topologies," in IEEE Trans. on Power Electronics, vol. 3, no. 2, pp. 174-182, Apr 1988.
- [21] <http://www.livescience.com/38169-electromagnetism.html>
- [22] <https://www.kullabs.com/classes/subjects/units/lessons/notes/note-detail/1823>
- [23] M. A. Cayless and A. M. Marsden, Lamps and lighting. Baltimore, MD: Edward Arnold Ltd., London, 1983.
- [24] G. Zissis and J. J. Damelinourt, "Electrical discharge light sources: a challenge for the future," High temperature material processes: an international quarterly of high-technology plasma processes, 15(3), 2011.
- [25] S. Kitsinelis, "Light sources: technologies and applications," CRC Press, Apr. 2016.
- [26] <https://en.wikipedia.org/wiki/Luminance>
- [27] Commission Internationale de l'Eclairage, Colorimetry (Official Recommendations of the International Commission on Illumination), CIE Publ. No 15 (E-1.3.1), Bureau Central de la CIE, Paris (1971).
- [28] https://en.wikipedia.org/wiki/CIE_1931_color_space
- [29] Schanda, János (2007), Colorimetry: Understanding the CIE System, Wiley Interscience.
- [30] <https://en.wikipedia.org/wiki/CIELUV>
- [31] <https://zenodo.org/record/821825#.WhQLxPnhAdU>
- [32] <http://www.pveducation.org/pvcdrom/properties-of-sunlight/spectral-irradiance>
- [33] http://www.st.com/resource/en/application_note/cd00192161.pdf.
- [34] <https://fr.pinterest.com/pin/326440672960555003/>
- [35] <http://smartsleep.e-monsite.com/pages/les-ampoules-a-incandescence.html>
- [36] http://www.pcbheaven.com/wikipages/How_Gas_Discharging_Lamps_work/
- [37] Raizer Y 1991 Gas Discharge Physics (Berlin: Springer) pp. 172-4
- [38] <https://powerplantmen.wordpress.com/tag/fluorescent-lamp/>
- [39] <http://www.ledandcflsupplier.com/compact-fluorescent-lamp.html#high-efficiency-compact-fluorescent-lamp>
- [40] <https://unvlt.com/literature/literature-finder/articles-and-tech-papers/programmed-start-the-new-way-to-start-a-fluorescent-lamp.html>
- [41] <http://www.circuitstune.com/2012/01/fluorescent-light-wiring-diagram-tube-light-circuit.html>
- [42] https://en.wikipedia.org/wiki/Mercury-vapor_lamp
- [43] <https://www.energieplus-lesite.be/index.php?id=10686#c5615>
- [44] <http://www.lamptech.co.uk/Documents/M1%20Introduction.htm>
- [45] <http://catalogus.electrocirkel.com/en/electrocirkel/product/552112>

- [46] <http://www.cp-lighting.co.uk/Sylvania-CMI-TT-70W-830-E27-Warm-White-Clear>
- [47] <http://www.schrack.com/shop/hit-ce-150w-830-g12-metal-halide-lamps-li5x783949.html>
- [48] <http://www.crossfold.co.uk/shop/view/-17528>
- [49] <http://www.edisontechcenter.org/InductionLamps.html>
- [50] https://en.wikipedia.org/wiki/Electrodeless_lamp
- [51] <http://stanprols.aimledlamps.com/induction-faq-en.html>
- [52] https://ftp.utcluj.ro/pub/users/cemil/dwdm/dwdm_Intro/6_5311732.pdf
- [53] <https://www.iapp.de/organische-elektronik.de/en/?OLEDs>
- [54] https://en.wikipedia.org/wiki/Luminous_efficacy
- [55] <http://www.cree.com/news-media/news/article/cree-first-to-break-300-lumens-per-watt-barrier>
- [56] M. Bagher, "A Detailed Review on Types of lamps and their applications", *Journal of Physical and Chemical Sciences*, vol. 4, no. 1, pp. 1-5, 2016.
- [57] E. Deng and S. Cuk, "Negative incremental impedance and stability of fluorescent lamps," *Proceedings of APEC 97 - Applied Power Electronics Conference*, Atlanta, vol. 2, pp. 1050-1056, 1997.
- [58] E. E. Deng, "I. Negative incremental impedance of fluorescent lamps. II. Simple high-power factor lamp ballasts," Ph.D. thesis, California Institute of Technology, 1996.
- [59] L. Chhun, "Modes d'Alimentation et de Commande des lampes sodium haute pression en vue d'éviter les résonances acoustiques," PhD thesis, Institut National Polytechnique de Toulouse, 2010.
- [60] C. A. Cheng, H. L. Cheng, C. W. Ku and T. Y. Chung, "Design and implementation of a single-stage acoustic-resonance-free HID lamp ballast with PFC," *IEEE Trans. on Power Electronics*, vol. 29, no. 4, pp. 1966-1976, Apr. 2014.
- [61] H. L. Cheng, C. A. Cheng, Y. N. Chang and K. M. Tsai, "Analysis and implementation of an integrated electronic ballast for high-intensity-discharge lamps featuring high-power factor," in *IET Power Electronics*, vol. 6, no. 5, pp. 1010-1018, May 2013.
- [62] <http://www.lampstech.co.uk/Documents/FL%20Frequency.htm>
- [63] J. H. Campbell, "Initial characteristics of high-intensity discharge lamps on high-frequency power," *IES Transaction*, vol. 64, no. 12, pp 713-722, Dec. 1969.
- [64] F. Lei, P. Dupuis, G. Zissis and P. Maussion, "Spectral variations of metal halide lamps during acoustic resonance," 2016 *IEEE International Conference on Plasma Science (ICOPS)*, pp. 1-1, Jun. 2016.
- [65] R. Schäfer, H. P. Stormberg, "Investigations on the fundamental longitudinal acoustic resonance of high pressure discharge lamps," *Journal of Applied Physics*, 1982, vol. 53, no 5, p. 3476-3480.
- [66] Sylvain Epron, "Etudes et effets des oscillations acoustiques dans les lampes à décharge haute pression", thèse doctorat en génie électrique en 1999, université Paul Sabatier, Toulouse, France.
- [67] B. Baumann, J. Schwieger, M. Wolff, F. Manders, and J. Suijker. "3D Acoustic Streaming Field in High-Intensity Discharge Lamps," In *Annual Comsol Conf.*, Cambridge. 2014.
- [68] M. A. Dalla Costa, J. M. Alonso, J. Garcia, J. Cardesin and M. Rico-Secades, "Acoustic Resonance Characterization of Low-Wattage Metal-Halide Lamps Under Low-Frequency Square-Waveform Operation," in *IEEE Transactions on Power Electronics*, vol. 22, no. 3, pp. 735-743, May 2007.
- [69] B. Siessegger, K. Guenther, H. Gueldner and G. Hirschmann, "Characterization of acoustic resonances in HID lamps based on relative impedance difference with an automated measuring station," 2008 *IEEE Power Electronics Specialists Conference*, pp. 1898-1904, Jun. 2008.
- [70] J. C. A. Anton, C. Blanco, F.J. Ferrero, J. C. Viera, N. Bordel, A. Martin, G. Zissis, "An Acoustic Resonance Band Detection Workbench for HID Lamps," *IEEE Trans. Industry Applications*, vol. 43, no.5, pp. 1191-1198, Mar. 2011.
- [71] J. A. Vilela and A. J. Perin, "Pulse operation of HPS lamp in high-frequency modulation," *Power Electronics and Applications*, European Conference on, pp. 9 pp.-P.9, Sept. 2005.

- [72] M. H. Ohsato, Q. Mao, H. Ohguchi, T. Shimizu, G. Kimura and H. Takagi, "Megahertz operation of voltage-fed inverter for HID lamps using distributed constant line," in IEEE Trans. on Industry Applications, vol. 34, no. 4, pp. 747-751, Aug 1998.
- [73] L. M. F. Morais, P. F. Donoso-Garcia, S. I. Seleme, P. C. Cortizo and F. N. A. Silva, "Acoustic Resonance Rejection via Voltage Modulation Method for HPS Lamps," IEEE International Symposium on Industrial Electronics, pp. 2996-3001, Jun. 2007.
- [74] L. Chhun, P. Maussion and G. Zissis, "HPS lamp control with adjacent frequency signal injection for acoustic resonance avoidance," IECON Annual Conference on IEEE Industrial Electronics Society, Glendale, pp. 2571-2577, Dec. 2010.
- [75] A. Toumi, J. Hirsch, B. Baumann, M. Wolff, S. Bhosle, G. Zissis, "convection velocity in HID lamp including acoustic resonance," Proc. 12th int. Symposium on the science and technology of light sources, pp. 473-474, Jul. 2010.
- [76] B. Baumann, J. Schwieger, M. Wolff, B. Baumann, F. Manders, J. Suijker, "Numerical investigation of symmetry breaking and critical behavior of the acoustic streaming field in high-intensity discharge lamps," Journal of Physics D: Applied Physics, vol. 48, no. 25, pp. 1-10, Jun. 2015.
- [77] J. Schwieger, B. Baumann, M. Wolff, F. Manders, and J. Suijker, "Backcoupling of acoustic streaming on the temperature field inside high-intensity discharge lamps," In Journal of Physics: Conference Series, vol. 655, no. 1, IOP Publishing, 2015.
- [78] C. S. Moo, C. K. Huang, C. Y. Yang, "Acoustic-Resonance-Free High-Frequency Electronic Ballast for Metal Halide Lamps," IEEE Trans. Industrial Electronics, vol. 55, no. 10, pp. 3653-3660, Apr. 2008.
- [79] McKinsey & Company, "Lighting the way: Perspectives on the global lighting market," 2012.

**Chapter 2 Acoustic Resonance
in High-Intensity Discharge Lamps**

2.1 Introduction

The aim of this chapter is to provide a detailed analysis of scientific literatures over acoustic resonance (AR) phenomena. AR occurs in high-intensity discharge (HID) lamps operating at high frequency, which can cause lamp arc distortion, extinction, and in the worst situation, lamp explosion [64]. In addition to cause visual effects on lamps, AR also can affect lamps' electrical parameters, even producing acoustic noise in the lamp arc tube.

Although AR frequencies can be calculated according to the wave equation, these frequencies depend on the tolerance of manufactures. Consequently, AR frequencies are different from lamp to lamp, even for the same manufacture' lamps [2]. Moreover, AR is a dynamic process that changes over time. This problematic phenomenon gives unpredicted risks to lamps and ballasts. It is essential to understand AR mechanism, characterize, detect and at least control it. However, until now AR phenomenon still is not completely understood. Therefore, the mechanism of AR is analyzed firstly in this chapter. We then give an example of AR theoretical frequencies calculated in our tested MH lamps. The associated pressure variations in three fundamental frequencies: longitudinal, radial and azimuth modes have been simulated in MATLAB.

Additionally, different AR detection methods are reviewed. AR can be detected by measuring lamp electrical parameters [3] or observing optical parameters [4], or detecting lamp physical parameters [5] such as sound emission, thermal parameters. Several AR avoidance methods are reviewed as well. They are based on the following conditions: either adjusting the operation frequency or spreading the excitation energy. Except for the mentioned deleterious effects, AR may bring some advantages to lamps, for example, making the arc of the lamp in horizontal position straightly or testing whether arc tubes of lamps have enough strength.

2.2 Phenomenon of acoustic resonance

Different kinds of arc shapes are observed in different HID lamps when AR occurs. Fig. 2-1 and Fig. 2-2 show arc distortions in high-pressure sodium (HPS) and metal halide (MH) lamps respectively.

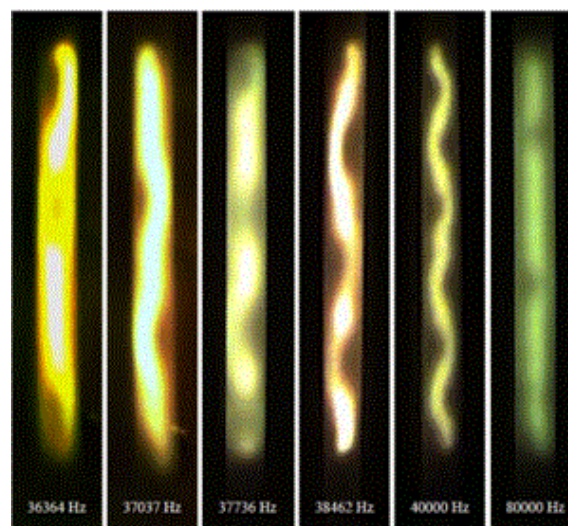


Fig. 2-1 Plasma arc with AR in an HPS lamp [64]

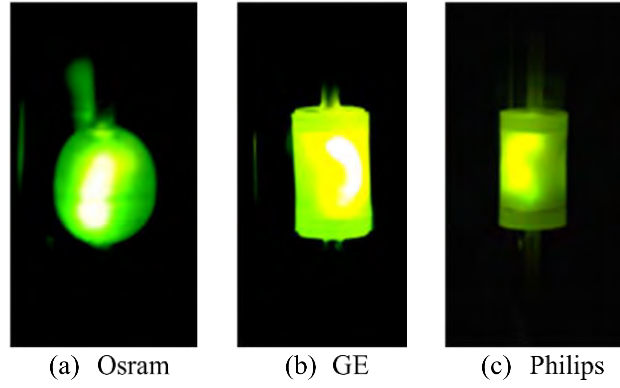


Fig. 2-2 Plasma arc with acoustic resonance in MH lamps (Taken in Laplace laboratory)

As can be seen from Fig. 2-1, when AR occurs in HPS lamps, different arc shapes are observed at different frequencies, such as sausage and snake shaped. In our experiment, AR phenomena are observed in three kinds of MH lamps from three manufacturers: Osram, GE, and Philips. Fig. 2-2 shows plasma arcs with AR situations in different MH lamps operating at different frequencies. In Fig. 2-2, the plasma arc bends and there are arc fluctuations, light flicker and sometimes lamps extinguish and explode in the presence of AR.

2.3 Theory of acoustic resonance

AR can be explained by the fact that the periodic power input from the discharge current causes pressure fluctuations in the gas volume of the lamp. If the power frequency is close to one eigenfrequency of the lamp arc tube, traveling pressure waves will appear. These waves travel toward and reflect on the discharge tube wall, resulting in standing pressure waves (acoustic resonances) [2], [6]. Therefore, the associated resonance frequencies can be easily estimated at least in a cylindrical arc tube.

The theoretical developments of this section mainly summarize the work of Sylvain Epron [64] as follows:

2.3.1 Wave equations and their solutions

Thermodynamics explains that the excitation of AR in an adiabatic gas volume can be described by the wave equation as follow [7], [8], [64]:

$$\frac{\partial^2 p}{\partial t^2} + \Gamma \frac{\partial p}{\partial t} - C_s^2 \nabla^2 p = (\gamma - 1) \frac{\partial N}{\partial t} \quad (2-1)$$

Where p is the local pressure fluctuation, Γ the damping coefficient accounting for acoustic losses, c the sound velocity, $\gamma = C_p / C_v$ the specific heat ratio, N the local acoustic power and t is the time variable.

For an ideal gas, the sound velocity can be written as:

$$C_s = \sqrt{\frac{C_p}{C_v} \frac{R_g T}{M_g}} = \sqrt{\gamma \frac{R_g T}{M_g}} \quad (2-2)$$

Where C_p and C_v are specific heat capacities for monatomic at constant pressure and volume respectively; R_g is the molar gas constant; M_g is the molar mass of the gas; T is the temperature.

N can be written as: $N = P - P_{rad} - P_{cond}$, where P is the high frequency input electrical power, P_{rad} is the irradiative loss and P_{cond} the conduction loss all per unit volume.

By assuming that the input power and losses are sinusoidal time-dependent, the solution in the frequency domain is:

$$p(\omega) = \frac{j\omega(\gamma - 1)N(\omega)}{\omega^2 - \omega_0^2 + j\omega\Gamma} \quad (2-3)$$

where ω is the operating frequency of the lamp power supply and ω_0 describes the eigenfrequency of the lamp's arc tube. Therefore, the amplitude of the pressure at the eigenfrequency reaches the maximum value:

$$p(\omega_0) = \frac{(\gamma - 1)N(\omega_0)}{\Gamma} \quad (2-4)$$

As can be seen from Eq. 2-4, the local acoustic power, the specific heat ratio and the damping coefficient affect the amplitude of the pressure.

By assuming an isotropic compressible perfect fluid, without damping and source term, the wave equation in Eq. 2-1 can be simplified as follow:

$$\nabla^2 p = \frac{1}{C_s^2} \frac{\partial^2 p}{\partial t^2} \quad (2-5)$$

The boundary condition follows from the requirement that the particle velocity perpendicular to the wall v_n must be zero at wall.

$$v_n = grad_n p = 0 \quad (2-6)$$

The term $\nabla^2 p$ in Eq. 2-1 and Eq. 2-5 is defined as $\nabla^2 p = div(grad_n p)$, where p is the pressure and ∇^2 is the Laplacian or Laplace-operator.

According to Eq. 2-2, the sound velocity is proportional to the square root of T . The temperature T of the arc tube is dependent on the position inside the tube.

In the specific tested MH lamps, the radius of the tube is about equal to the distance between two electrodes. Therefore, the temperature inside the arc tube can be treated as uniform. The average temperature over the discharge volume is used, which is named "effective temperature". The sound velocity is also treated to be independent of curvilinear coordinates. The simplified wave equation is a linear equation and can be solved analytically.

Hence, the appropriate solution of the simplified wave equation in cylindrical coordinates r , φ , and z is expressed as:

$$p(r, \varphi, z, t) = p_A J_n\left(\frac{\omega_{nm} r}{C_s}\right) \cos(n\varphi) \cos\left(\frac{\omega_l z}{C_s}\right) \exp(-i\omega_{nm} t) \quad (2-7)$$

where J_n are Bessel functions, ω_{nm} is transverse angular frequency and ω_l is the longitudinal angular frequency. In any acoustic mode, the oscillation angular frequency is described as:

$$\omega^2 = \omega_{nm}^2 + \omega_l^2 \quad (2-8)$$

In Eq. 2-7, the term “ l ” determines the periodicity along the direction parallel to $[O, z]$; the term “ n ” determines the repetition periodicity when the radius vector rotates around $[O, z]$; the term “ m ” determines the number of nodal circles. The various oscillations which exist inside the cylindrical cavity are determined by the set of numbers (n, m, l) . Fig. 2-3 show examples of acoustic modes in a cylindrical cavity ($l=2, n=2, m=2$) and ($l=3, n=3, m=3$).

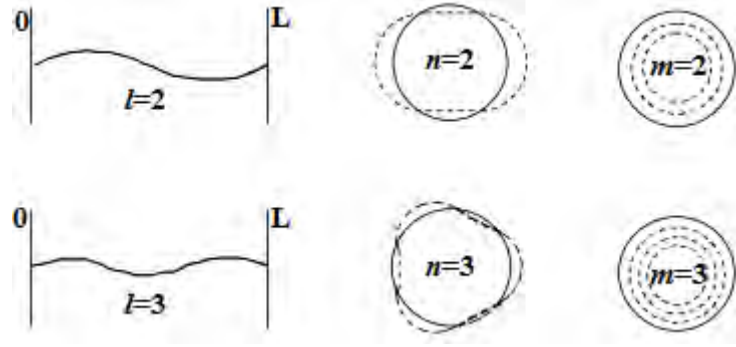


Fig. 2-3 Acoustic modes in a cylindrical cavity [64]

Applying the boundary condition, the derivative of p with respect to z is zero at $z = 0$, and $z = L$. The derivative is zero at $z = 0$ for the cosine function and at $z = L$, $\omega_l L / C = l\pi$ ($l=0, 1, 2, \dots$). Hence, the longitudinal frequency is expressed by:

$$f_l = \frac{\omega_l}{2\pi} = \frac{lC_s}{2L} \quad (2-9)$$

The radial particle velocity is zero at the cylinder walls, when $(dJ_n / dr) = 0$ at $r = R$. Thus, $(\omega_{nm} R / C) = \pi\alpha_{nm}$, where α_{nm} is a solution of the equation $\left[dJ_n \left(\frac{\pi\alpha}{d\alpha} \right) \right] = 0$. Thus, the transverse frequency is given as:

$$f_{nm} = \frac{\omega_{nm}}{2\pi} = \frac{\alpha_{nm} C_s}{2R} \quad (2-10)$$

By combining equation (2-8) and (2-9), the acoustic resonance frequency can be expressed as follows:

$$f_{nml} = \sqrt{f_{nm}^2 + f_l^2} = \sqrt{\left(\frac{\alpha_{nm} C_s}{2\pi R} \right)^2 + \left(\frac{l C_s}{2L} \right)^2} \quad (2-11)$$

Hence, the fundamental longitudinal frequency ($n=m=0, l=1$):

$$f_{001} = \frac{C_s}{2L} \quad (2-12)$$

The fundamental azimuthal frequency $n=1, m=l=0$:

$$f_{100} = \frac{\alpha_{10} C_s}{2\pi R} \quad (2-13)$$

The fundamental radial frequency ($n=l=0, m=1$):

$$f_{010} = \frac{\alpha_{01} C_s}{2\pi R} \quad (2-14)$$

2.3.2 An example of AR frequency calculation

According to Eq.2-11, AR frequencies can be calculated and different AR modes (longitudinal, radial and azimuth) are presented by using a MATLAB program. At fundamental resonant frequencies, a minimum input energy can excite arc instabilities inside the arc tube. In addition to the fundamental AR frequencies, the higher modes can occur as well. Nevertheless, higher order resonance mode needs more energy to be excited. According to Eq.2-9, the effective sound velocity needs to be determined first. For lamps' manufacturer, they do not disclose the gas composition. Therefore, it is difficult to get the molar mass of the gas M_g . Normally, the effective sound velocity is estimated at 500 m/s [2].

In our experiment, several 150 W MH lamps from three manufacturers are tested, e.g. Osram Powerball HCI-TT, GE Constant Color CMH, and Philips Master City White CDO-TT. GE and Philips MH lamps have similar dimensions and structures, and both are cylindrical arc tubes. The arc tube shape of tested Osram MH lamps is spherical. AR frequencies are difficult to calculate for spherical arc tube. Therefore, we do not calculate AR frequencies here.

The tested Philips and GE MH lamps in our experiment, the radius of the arc tube is $R=6$ mm and the length is $L=21.2$ mm. TABLE 2-1 shows AR theoretical frequencies between 11-100 kHz for 150 W Philips and GE MH lamps.

TABLE 2-1 AR theoretical frequencies for 150 W Philips/GE MH lamps

Modes	f_{nml} (kHz)	Modes	f_{nml} (kHz)	Modes	f_{nml} (kHz)	Modes	f_{nml} (kHz)	Modes	f_{nml} (kHz)
0.0.1	11.79	0.1.0	50.82	0.1.4	69.34	2.0.6	81.53	0.2.0	93.05
0.0.2	23.56	0.1.1	52.17	4.0.0	70.52	0.0.7	82.55	0.2.1	93.79
1.0.0	24.42	1.0.4	53.12	1.1.0	70.71	1.1.4	85.00	0.0.8	94.34
1.0.1	27.12	2.0.3	53.78	0.0.6	70.75	5.0.0	85.09	0.1.7	96.94
1.0.2	31.95	3.0.0	55.72	4.0.1	71.50	5.0.1	85.90	1.0.8	97.45
0.0.3	35.38	0.1.2	56.03	2.0.5	71.54	1.0.7	86.08	6.0.0	99.50
2.0.0	40.51	3.0.1	56.95	1.1.1	71.69	0.1.6	87.11	1.1.6	100.03
2.0.1	42.19	0.0.5	58.96	1.1.2	74.54	2.1.0	88.94		
1.0.3	42.99	0.1.3	61.92	1.0.6	74.85	2.1.1	89.72		
2.0.2	46.87	2.0.4	62.18	0.1.5	77.84	2.0.7	91.95		
0.0.4	47.17	1.0.5	63.82	1.1.3	79.07	1.1.5	92.07		

In TABLE 2-1, three fundamental AR frequencies are emphasized in bold. AR frequency bands are wide in our tested MH lamps. Therefore, it is difficult to find some AR-free frequency bands are absolute safe.

2.3.2.1 AR theoretical frequencies versus AR experimental frequencies

AR occurs when the eigenfrequency of the arc tube is equal or close to the power frequency of the lamp. In our case, the lamp current and voltage are quasi sinusoidal waveforms. The lamp power frequency is always 2 times to the current frequency ($2f_{current} = f_{power}$). TABLE 2-2 shows the comparison between theoretical AR frequencies and experimental AR frequencies.

TABLE 2-2 AR theoretical frequencies vs. AR experimental frequencies in our tested MH lamps

Type	Theoretical AR frequency	Tested current frequency bands ($2f_{current}=f_{power}$)
150 W GE MH lamps (Constant Color CMH)	$f_{100}=24.42$ kHz $f_{102}=31.95$ kHz	Around 12 kHz e.g. 12.7 and 12.8 kHz Around 15 kHz e.g. 15.5 and 15.6 kHz
150 W Philips MH lamps (Master City White CDO-TT)	$f_{100}=24.42$ kHz $f_{102}=31.95$ kHz	Around 12 kHz e.g. 12.4 and 12.5 kHz Around 15 kHz e.g. 15.3 and 15.4 kHz

According to TABLE 2-2, theoretical AR frequencies are consistent with experimental AR frequencies. The fundamental azimuthal frequency f_{100} is 24.42 kHz for our tested lamps. At fundamental eigenfrequency areas, a minimum input energy is sufficient to trigger an arc instability and AR phenomena are very serious. That is why several lamps have exploded with a lamp current frequency of about 12 kHz. At higher order modes, AR needs more energy to be triggered. When the lamp current frequency is about 15 kHz, this frequency is around the eigenfrequency 31.95 kHz. At this frequency, we did not get lamp explosion.

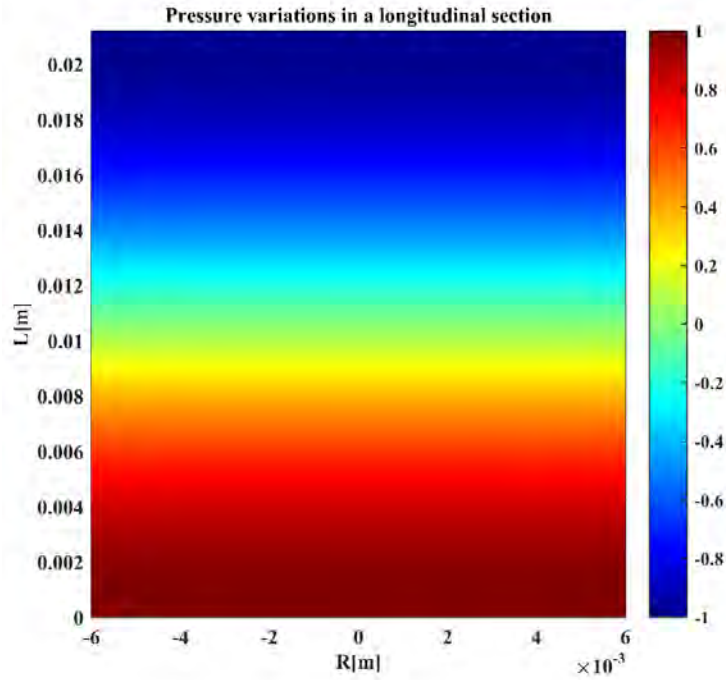
2.3.2.2 Simulation of three fundamental AR frequency modes

According to Eq. 2-7, the pressure variations of different acoustic modes can be simulated by using our MATLAB program. The input data are the numbers n , m and l , the radius R , length L and the sound velocity C_s of the lamp. we arbitrarily choose the amplitude of the sound pressure p_A equal to 10 Pa. The pressure distributions of the discharge tube are simulated in a longitudinal section and in a radial section. For example, the functions can be expressed in the longitudinal section $\varphi = 0$ and in a radial section $z = 0$ respectively:

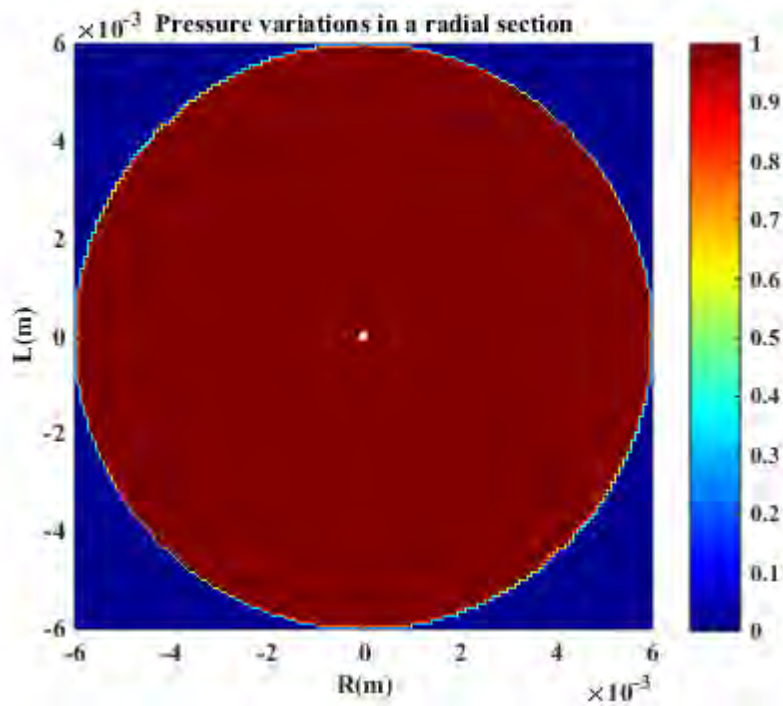
$$p(r, z) = p_A J_n\left(\frac{\omega_{nm} r}{C_s}\right) \cos\left(\frac{\omega_l z}{C_s}\right) \quad (2-15)$$

$$p(r, \varphi) = p_A J_n\left(\frac{\omega_{nm} r}{C_s}\right) \cos(n\varphi) \quad (2-16)$$

Fig. 2-4, Fig. 2-6 and Fig. 2-5 show the simulation results of pressure variations in the fundamental longitudinal, radial and azimuth modes.



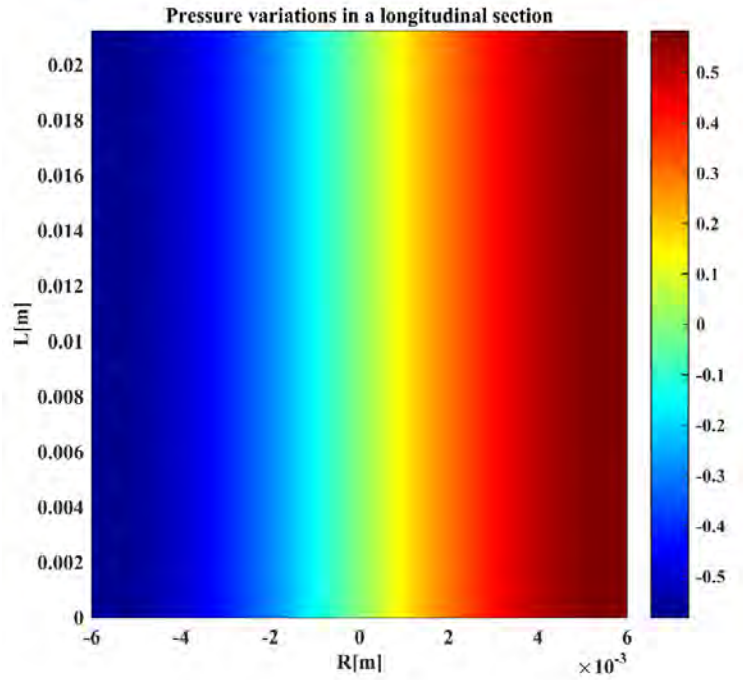
(a) Pressure variations in a longitudinal section



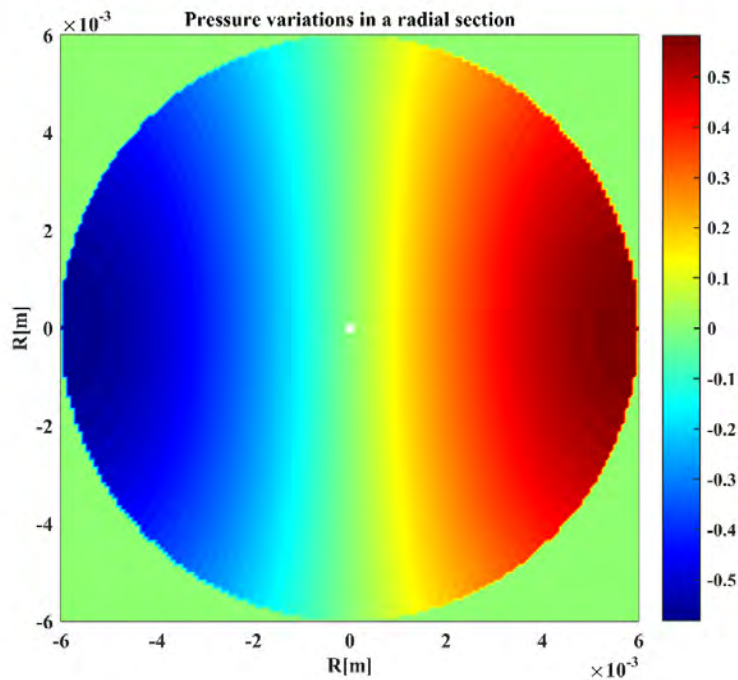
(b) Pressure variations in a radial section

Fig. 2-4 Pressure variations at the fundamental longitudinal mode $(0\ 0\ 1)$ $f=11.79$ kHz

As can be seen from Fig. 2-4, when AR occurs at the fundamental longitudinal frequency, the pressure in the longitudinal section varies from -10 Pa to 10 Pa. The maximum pressure takes place at the end of the arc tube near the electrode. We may conclude that if the lamp works in this mode, the electrode could be damaged first, reducing the lifetime of the lamps.



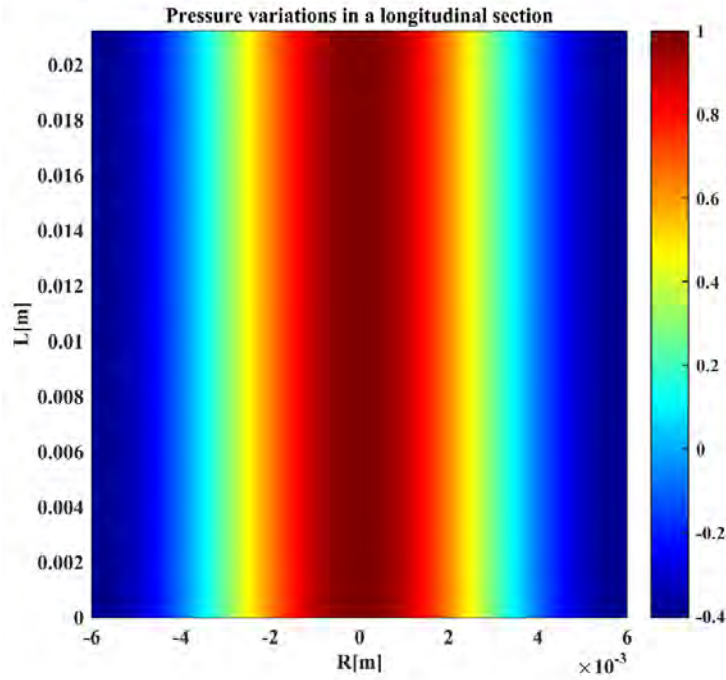
(a) Pressure variations in a longitudinal section



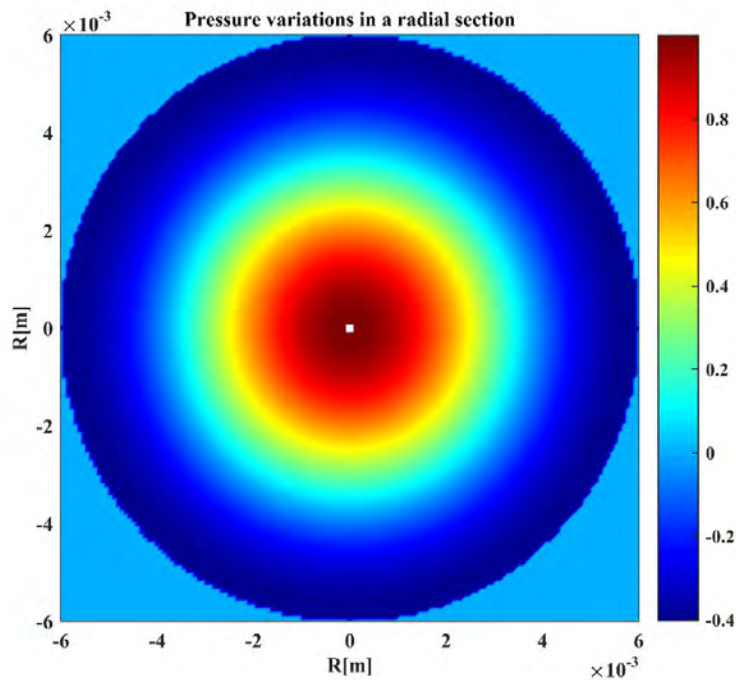
(b) Pressure variations in a radial section

Fig. 2-5 Pressure variations at the fundamental azimuth mode (1 0 0), $f=24.42$ kHz

In Fig. 2-5, at the fundamental azimuth frequency, the maximum pressure appears on the wall of the arc tube whatever in a longitudinal or a radial section. At this frequency mode, the wall of the arc tube will be damaged by AR, resulting in lamp explosion. This also can explain why several MH lamps are exploded in our experiment when the lamp power frequencies are around 24 kHz.



(a) Pressure variations in a longitudinal section



(b) Pressure variations in a radial section

Fig. 2-6 Pressure variations at the fundamental radial mode (0 1 0) $f=50.82$ kHz

In Fig. 2-6, the maximum pressure appears in the center of the arc tube at the fundamental radial frequency. Comparing Fig. 2-4 with Fig. 2-6 and Fig. 2-5, at the fundamental longitudinal frequency, the arc tube around either one electrode stands the maximum pressure. At the fundamental azimuth mode, the maximum pressure is just a half of at the fundamental longitudinal mode, but the maximum pressure is near the wall of the arc tube.

In conclusion, this simulation describes the pressure distribution in a simplified case for the lamp arc tube when AR occurs in MH lamps. It can explain why the lamps are damaged and how AR influence on lamps.

2.3.3 Power threshold in high-intensity discharge lamps

AR occurs when the lamp power frequency is close to the eigenfrequency of the lamp arc tube and at this frequency, the excitation energy is over the threshold energy. The eigenfrequency of the lamp arc tube was calculated and analyzed in section 2.3.2. For the lamp, the input energy is power. Here according to previous literatures [64], [9], we analyze the power threshold or the threshold energy in a HPS lamps.

The power threshold can be determined by supplying the lamp with a square wave power source that supplies the lamp at its nominal power, and superimposing a sinusoidal voltage source with a variable amplitude and frequency to excite AR [64], [10]. Fig. 2-7 shows the acoustic resonance excitation circuit and Fig. 2-8 show its corresponding lamp voltage waveform.

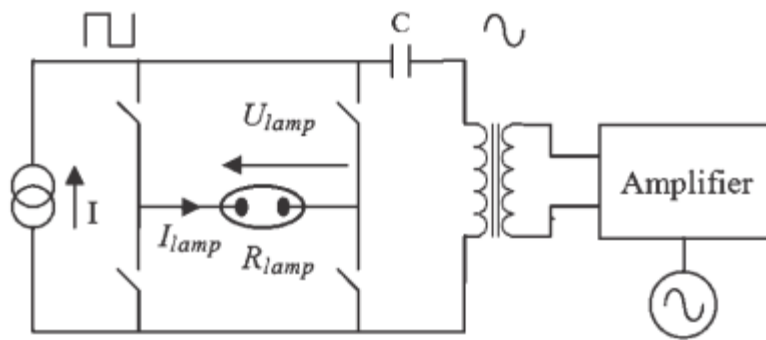


Fig. 2-7 Acoustic resonance excitation circuit [9]

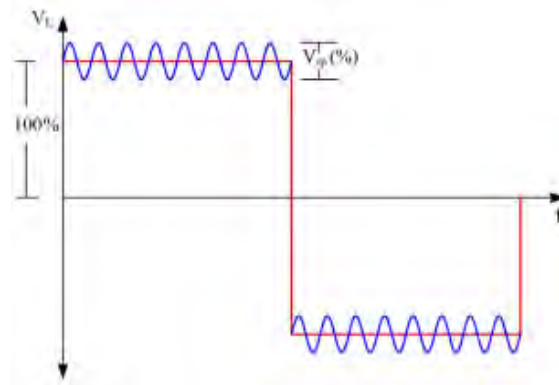


Fig. 2-8 Typical lamp voltage waveform [10]

In Fig. 2-7, the lamp is supplied with a low-frequency square waveform on which a high-frequency sinusoidal ripple waveform is superposed. In Fig. 2-8, injection of voltage ripple is used to control AR.

In order to define the power threshold of an HPS lamp, the DC source and sinusoidal source are supplied as presented in Fig. 2-7, leading to the expression:

$$\begin{aligned}
 P_{lamp}(t) &= U_{lamp}(t)I_{lamp} \\
 &= (U_c + U_{sin} \cos \omega t)(I_c + I_{sin} \cos \omega t) \\
 &= (U_c I_c + \frac{U_{sin} I_{sin}}{2}) + (U_c I_{sin} + U_{sin} I_c) \cos \omega t + \frac{U_{sin} I_{sin}}{2} \cos 2\omega \\
 &= P_0 + P_{thr} \cos \omega t + P_2 \cos 2\omega
 \end{aligned} \tag{2-17}$$

U_c and I_c are the voltage and current amplitude of the square wave supply respectively. U_{sin} and I_{sin} are the voltage and current amplitude of the sinusoidal supply respectively. Hence, the lamp power contains a DC component P_0 , the fundamental harmonic component P_{thr} , and the second harmonic component P_2 .

Chhun and others [9] measured the power threshold in a high-pressure sodium lamp, as shown in Fig. 2-9.

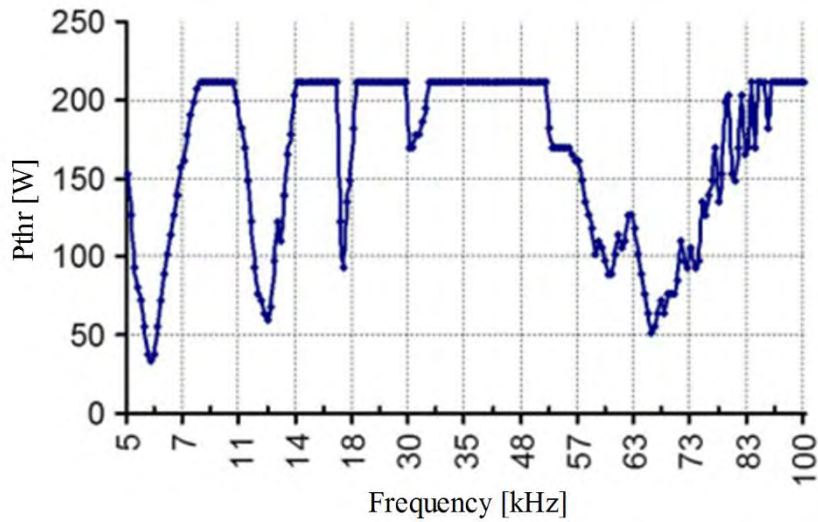


Fig. 2-9 Power threshold of acoustic resonance in a 150W HPS lamp [9]

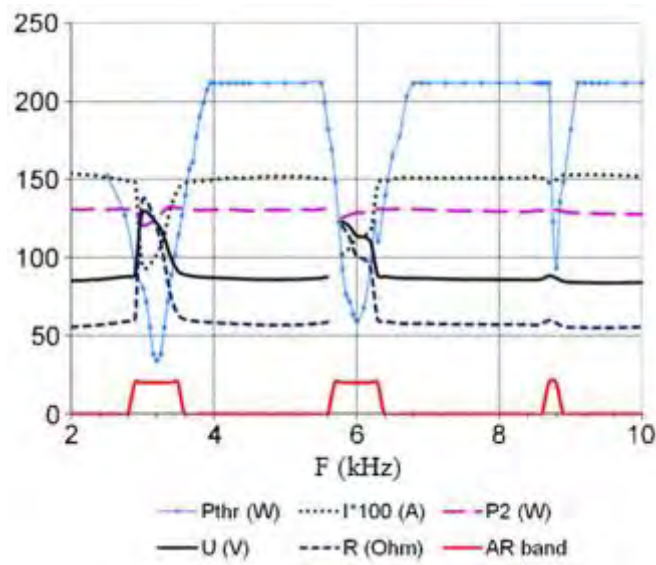


Fig. 2-10 Variations of the threshold power, current, harmonic power, voltage, equivalent resistance in a 150 W HPS lamp [9]

Fig. 2-10 shows the variations of the threshold power, current, harmonic power, voltage, equivalent resistance in a 150 W HPS lamp with the supply frequency. The discontinuous line refers to lamp arc extinction. As can be seen from Fig. 2-10, when the harmonic power P_2 is higher than the threshold power P_{thr} , AR occurs.

2.4 Methods for acoustic resonance detection

As it was mentioned in previous researches, AR changes the chemical and physical balance of the filling elements in the arc tube of HID lamps. This phenomenon could result in some variations of electrical parameters, light flicker and sound emission. Thus, the methods for AR detection are established based on these effects. Basically, the methods for AR detection can be categorized into several groups: electrically, optically and physically (sound-based and temperature profile). Fig. 2-11 illustrates different AR detection methods.

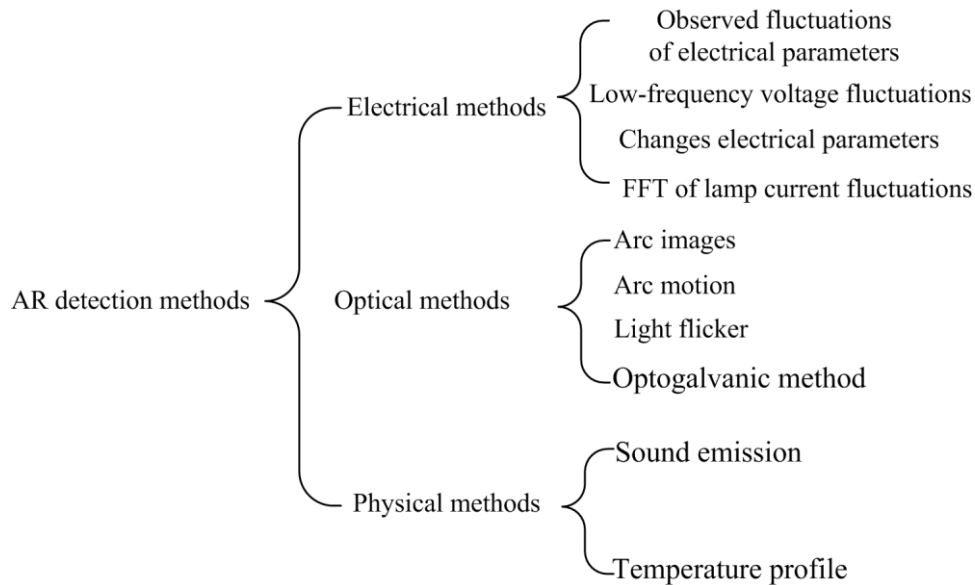


Fig. 2-11 Different AR detection methods

2.4.1 Electrical methods

The occurrence of AR results in arc instabilities. The arc instabilities are accompanied by arc deformations and then the length and thickness of the arc are changed. These changes influence on the electrical parameters of the lamp, such as the voltage, current, and impedance. This means that variations of the lamp electrical parameters are indicators of AR occurrence.

2.4.1.1 Observed variations of electrical parameters

In the paper [3], lamp electrical parameters were proposed to detect the occurrence of AR. Several 70 W MH lamps from different manufacturers were tested and the lamps worked in a wide frequency band from 20 kHz to 60 kHz. The relevant waveforms were observed on a digital oscilloscope. TABLE 2-3 shows the fluctuations of the electrical parameters in a GE MH lamp.

TABLE 2-3 The fluctuations of electrical parameters in a GE MH lamp [3]

f (kHz)	V (V)	I (A)	R (Ω)	$\Delta V/V$ (%)	$\Delta I/I$ (%)	$\Delta R/R$ (%)	AR	P (W)
20.6	78.5~87.2	0.72~0.88	89.2~121	9.5	22.2	25.0	Y	70
23.7	79.9~85.3	0.65~0.82	97.4~131.2	5.9	23.6	26.6	Y	70
25.4	78.4~86.2	0.63~0.79	99.2~136.8	8.5	22.2	29.5	Y	70
27.4	91.5	0.72	127	0	0	0	0	70
29.6	89.4~93.2	0.72~0.86	104~129.4	4.1	19.4	20.1	Y	70
30.9	87.4~94.6	0.68~0.89	98.2~139.1	7.7	28.0	32.2	Y	70
36.6	93.2	0.74	126	0	0	0	0	70
38.8	93.6	0.75	124.8	0	0	0	0	70
40.9	91.3~99.5	0.58~0.72	126.8~171.6	8.8	18.6	35.9	Y	70
43.5	88.2~96.8	0.62~0.79	111.7~156.1	9.2	22.6	35.6	Y	70

Both theoretical analysis and experimental results showed that the change $|\Delta R/R|$ is larger than the change in $|\Delta V/V|$ and $|\Delta I/I|$. The percentage change of lamp impedance $|\Delta R/R|$ presents the best sensitivity. Thus, $|\Delta R/R|$ was verified as an indicator for the occurrence of AR in their experiment. This method is simple and the variations of $|\Delta R/R|$ have a high signal to noise ratio. However, this method need to calculate the variations of the impedance first and it cannot evaluate AR directly.

2.4.1.2 Low-frequency voltage fluctuations (Voltage envelope)

Moo [11] observed that low-frequency fluctuations occurs in the lamp voltage and current waveform in MH lamps. The lamp voltage relative fluctuations are greater than those present in the lamp current. In order to measure the lamp voltage fluctuations, an AR detection circuit was proposed in Fig. 2-12. The lamp was supplied by a high-frequency electronic ballast with sinusoidal waveform.

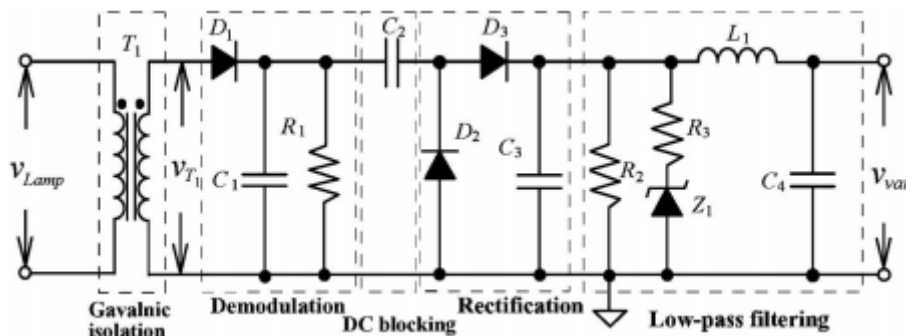


Fig. 2-12 AR detection circuit [11]

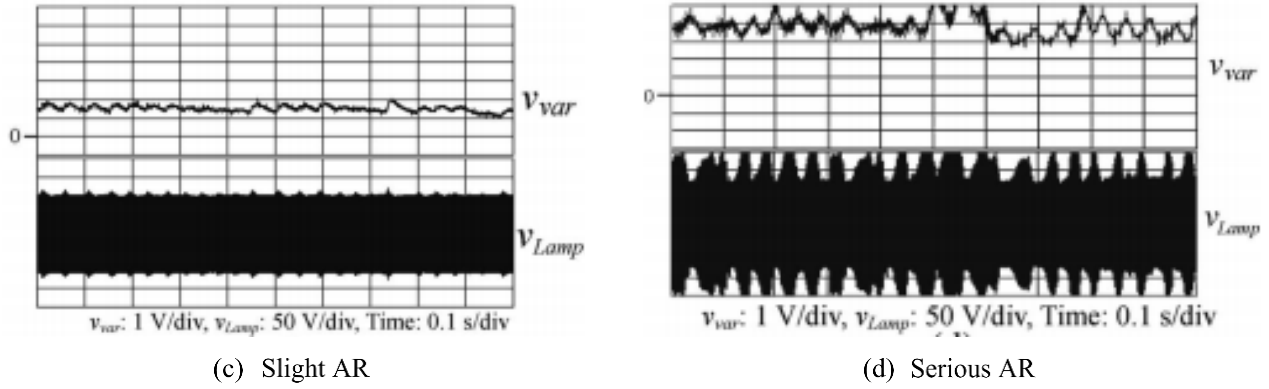


Fig. 2-13 Lamp voltage waveforms and their voltage envelopes [11]

In Fig. 2-12, the circuit looks like “simple and low-cost”, it is composed of a transform, 3 diodes, one Zener, 4 capacitors, 3 resistors and one inductor. According to the results in Fig. 2-13, this circuit can detect AR occurrence. However, it used a peak detector and diodes to demodulate the input signals, resulting in non-linearities and a low sensitivity to AR. Moreover, the thresholding applied on the output stage define a lower limit under which no detection occurs.

2.4.1.3 Changes of electrical parameters

Early experimental results have showed that electrical parameters are influenced by disturbances of the AR. Chhun and others [12] proposed to measure the lamp current, voltage in order to evaluate the occurrence of AR. In their experiment, the lamp was supplied by the high-frequency sinusoidal waveform. The set-up is composed of a function generator, an amplifier, a transformer, and a blocking capacitor C_b in series with a resistance R_b , as shown in Fig. 2-14. Fig. 2-15 shows the variations of the lamp current and the lamp voltage in an HPS lamp.

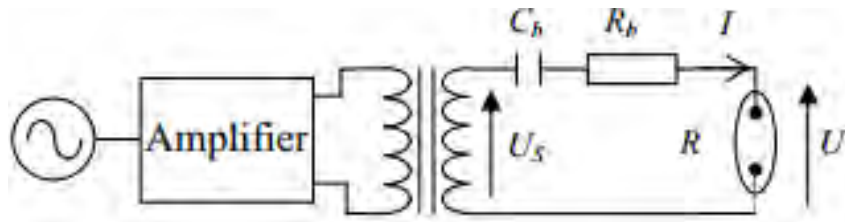


Fig. 2-14 Sinusoidal supply for an HPS lamp [12]

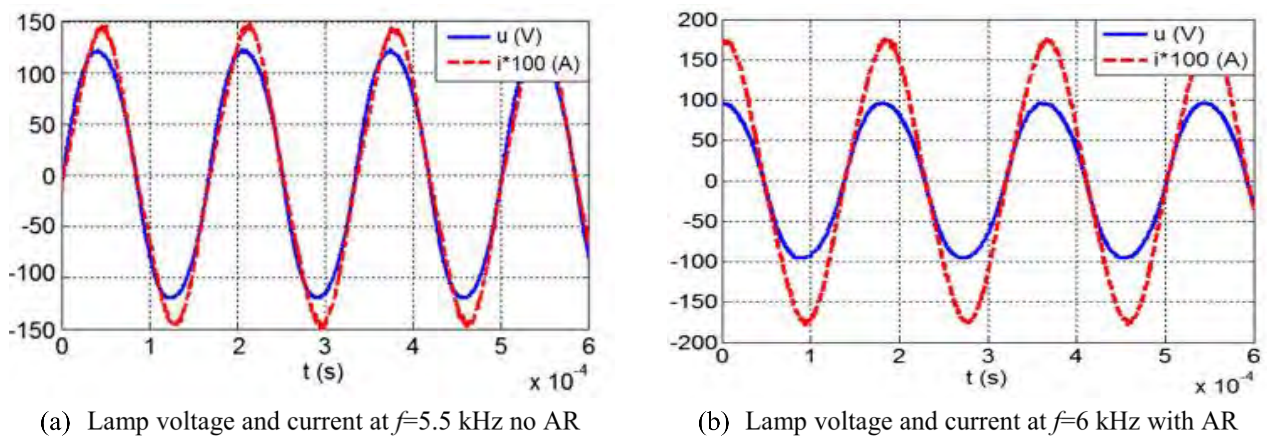


Fig. 2-15 Lamp voltage and current in no AR and AR situations in an HPS lamp [12]

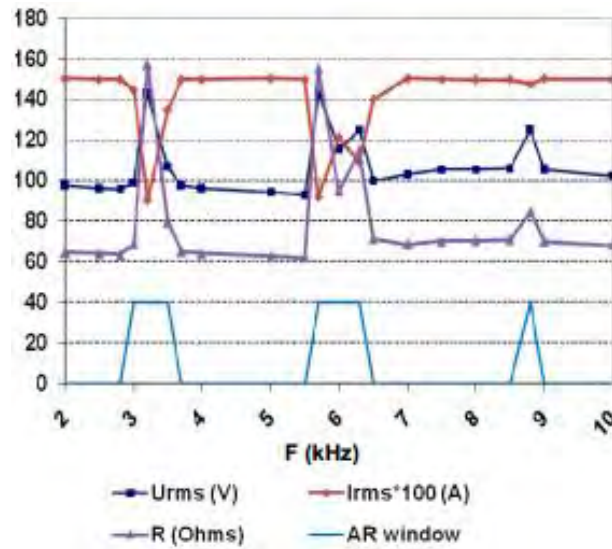


Fig. 2-16 Variations of electrical parameters and AR windows Vs. the supplying frequency [12]

Comparing Fig. 2-15 (a) with Fig. 2-15 (b), it can be seen that the lamp voltage increases and the current decreases at $f=6$ kHz in AR situation. Accordingly, the equivalent resistance of the lamp increases as well. In addition, Fig. 2-16 not only shows this trend of the electrical variations, but also the lamp resistance presents the most significant variations.

2.4.1.4 FFT of lamp current fluctuation

There is a low frequency (about 5-20Hz) ripple in the lamp current when AR occurs. Based on this observation, Jiang [13] proposed a method to detect this low frequency ripple in MH lamps. The operating frequency of tested lamps are from 30 kHz to 40 kHz. The proposed supply circuit is illustrated in Fig. 2-17.

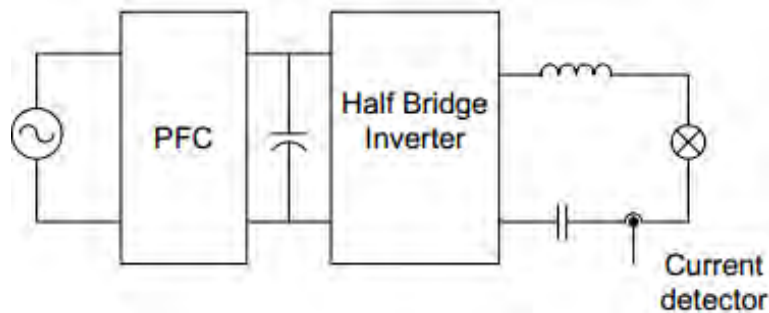


Fig. 2-17 Proposed circuit for MH lamps [13]

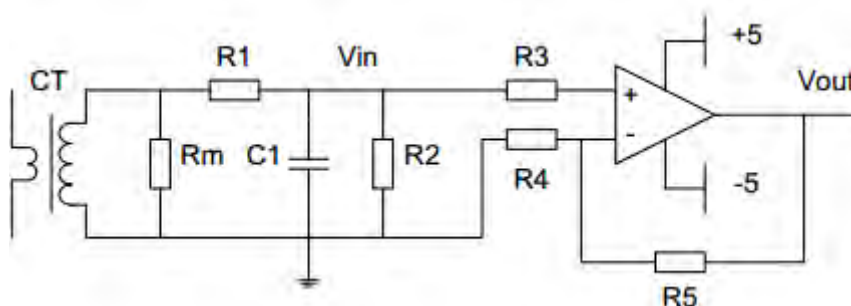


Fig. 2-18 Current detector for AR detection [13]

In Fig. 2-18, the lamp current is measured by a current transformer CT, then the signal is filtered to eliminate the switching frequency element and amplified. After that, the amplified current is sampled and analyzed by FFT in an MCU. The sampling frequency and sampling points of data are 200 Hz, 64 respectively, in order to detect the low frequency ripple in the lamp current. Therefore, the frequency resolution is about 3 Hz. To determine whether AR occurs, the part of the results of FFT is considered:

$$V_a = \sum_{n=2}^6 X(n) \quad (2-18)$$

where $X(n)$ is the result of FFT and V_a is the sum of low frequency elements of the lamp current. To validate the occurrence of AR, the threshold voltage V_{th} must be defined as the reference signal first, according to the experience. If the V_a is greater than V_{th} , this means that AR occurs in the lamps. This method is simple, but it needs more time to calculate V_a . On the other hand, the threshold voltage is needed to choose first.

2.4.2 Optical methods

2.4.2.1 Arc images

An automatic workbench was proposed to detect AR phenomenon in an HID lamp, as presented in [3]. AR was detected by analyzing arc distortions inside arc tube of HID lamps. The acquisition system of arc distortions is composed of a closed box, two projection lenses, a flat screen, a mirror, fiber optics ends and photodiodes. The arc image acquisition system is shown in Fig. 2-19.

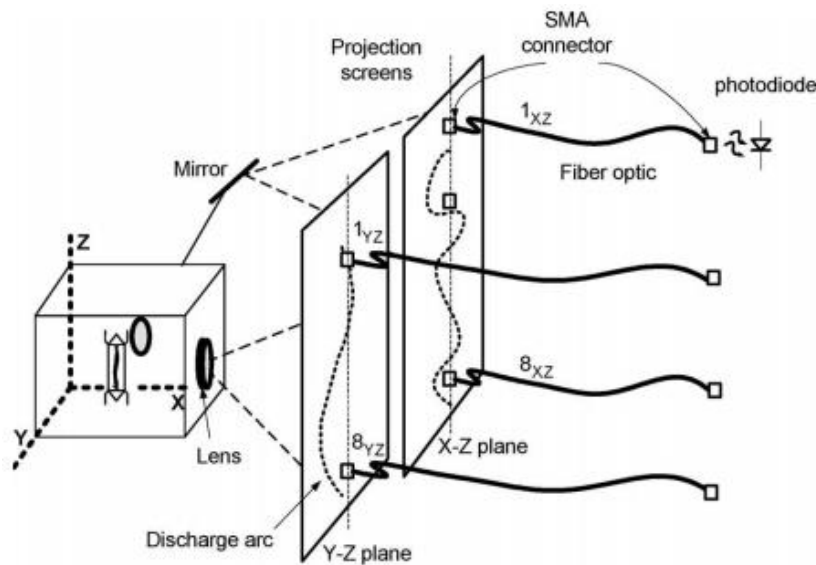


Fig. 2-19 Arc images acquisition system [3]

In this experiment, the lamp is supplied by sinusoidal waveforms. The waveform frequency ranges from 40 kHz to 95 kHz and is adjusted by a function generator which is controlled by a computer. This can be easily adjusted the lamp operating in AR and no AR situations. An HPS lamp is placed inside a closed box with two projection lenses. The lenses project the lamp arc on two perpendicular planes to get a three-dimensional view of the arc image. The discharge arc images then are projected on a flat screen with the help of a mirror.

There are two columns of 8 optical fiber ends placed on the screen. The arc is projected over an optical fiber end. Each fiber end collects light at specific point of the discharge arc projection corresponding to a specific point of the lamp discharge tube. Fiber optics transmit arc discharge light to two sets of 8 photodiode detectors. If there is no AR occurrence, all fibers transmit a similar amount of light. The arc shape will be a straight line

and its projection is aligned with the fiber optic ends placed on the screen. The straight line in absence of AR can be taken as reference and it will be compared with the distorted line in AR situation.

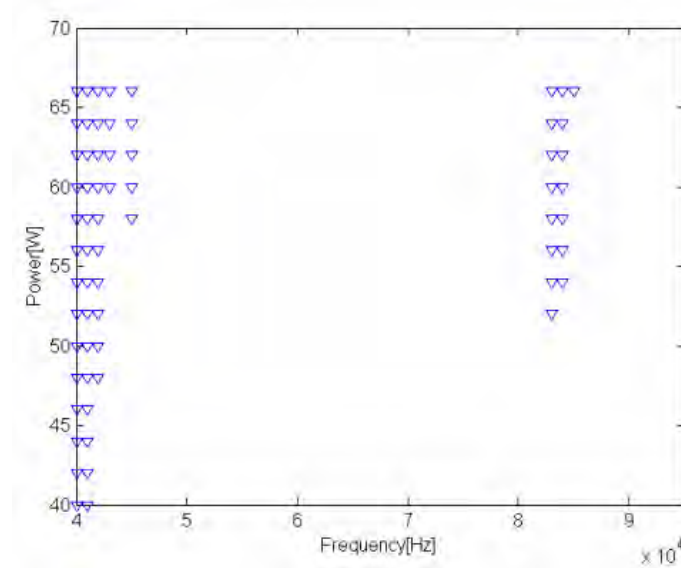


Fig. 2-20 AR map in a 70 W HPS lamp [3]

Fig. 2-20 illustrates AR detection results in a 70W HPS lamp. According to this AR map, two AR frequency bands (marked in ∇) at 40 kHz and 85 kHz are observed at different delivered power.

This detection method is based on an array of phot liquid crystal display (LCD)-detectors with the ability to identify arc distortions. Relative intensity measurements at different points of projections are made and analyzed to detect AR. This is an accurate method to detect AR phenomenon. However, due to maladjustments of the projection system or differences of photodiode sensitivity, it is difficult to choose the reference measurement of the system. Moreover, the structure of this detection system is complicated, and it is also impossible to embed this system to a ballast.

2.4.2.2 Arc motion and light flicker

AR causes some light fluctuations, light flickers, distortions in discharge arc, and arc deflection. Thus, there were some literatures studied the light flickers and arc deflection in HID lamps. As presented in the paper [14], the brightness fluctuations of discharge arc flicker were measured by a high-speed photodiode. This means that the photodiode converts the incident light into a current. After this, this current signal was measured by an oscilloscope and analyzed by the fast Fourier transform (FFT). The resulting frequency is named flicker frequency. Meanwhile, a fast camera was recorded the brightness distribution of the discharge arc to measure the time-dependent arc deflection. The arc deflection in the center of the arc tube is named arc motion. This time signal then was split into 5-s segments and analyze by FFT. This frequency is called motion frequency.

In their experiment, an HID lamp was operated at a square waveform superimposing with a sinusoidal voltage with an adjustable frequency. The frequency of the sinusoidal signal is called excitation frequency in order to excite AR phenomenon and its frequency is called excitation frequency. The first acoustic eigenfrequency for the used HID lamp is about 41.5 kHz. Therefore, the range of the excitation frequency in this experiment was set $41.5\text{kHz} \pm 2.5\text{ kHz}$. Fig. 2-21 illustrates arc deflections at an excitation frequency of 41.0 kHz with a modulation depth 15%. (The modulation depth is defined that the amplitude of the sinusoidal signal is expressed relative to the amplitude of the square-wave voltage.)

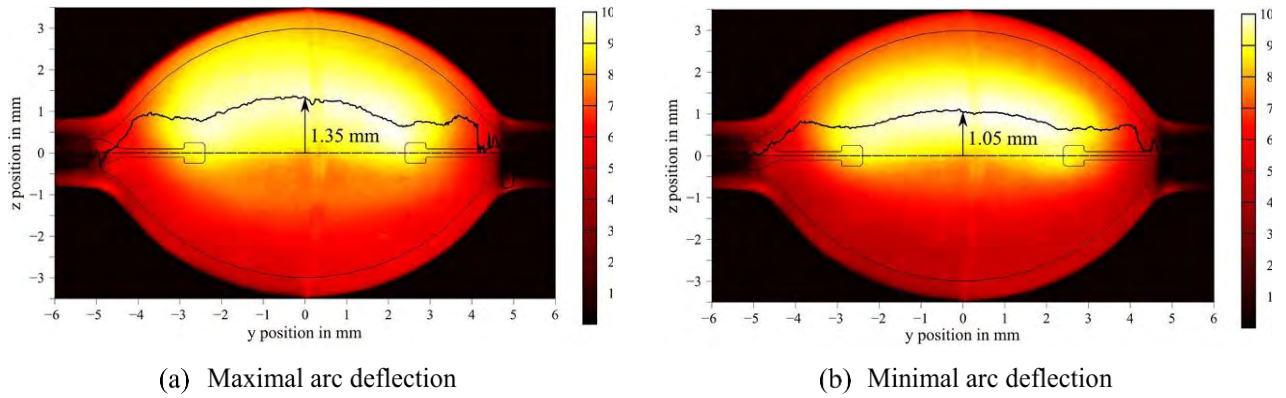
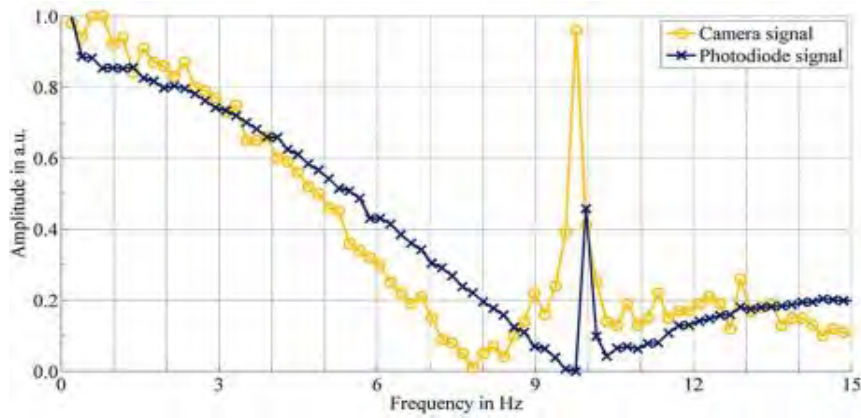
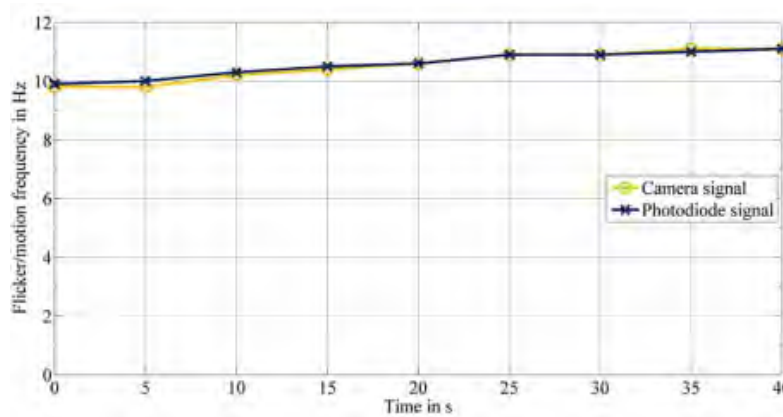


Fig. 2-21 Light intensity distribution at an excitation frequency 41.0 kHz [14]

In Fig. 2-21 (a) and (b), a maximal arc deflection and a minimal arc deflection are shown respectively. In the figures, black lines mean the maximal brightness. The arc deflection is defined as the distance between the black line and the horizontal symmetry line. Additionally, Fig. 2-22 shows the results of arc motion frequency and arc flicker frequency.



(a) arc motion frequency and arc flicker frequency in frequency domain



(b) arc motion frequency and arc flicker frequency in time domain

Fig. 2-22 Results of arc motion frequency and arc flicker frequency in an HID lamp [14]

In Fig. 2-22 (a), the arc motion frequency observed by the camera is 9.8 Hz and the arc flicker frequency detected by the photodiode is 10 Hz. Fig. 2-22 (b), the photodiode signal exactly follows the camera signal from

10 Hz to 11 Hz during 0-40 s. The results show that the arc motion frequency and the arc flicker frequency have good agreement whatever in frequency domain or time domain. Furthermore, they also studied that how the excitation frequency and modulation depth influenced the arc flicker, as presented Fig. 2-23.

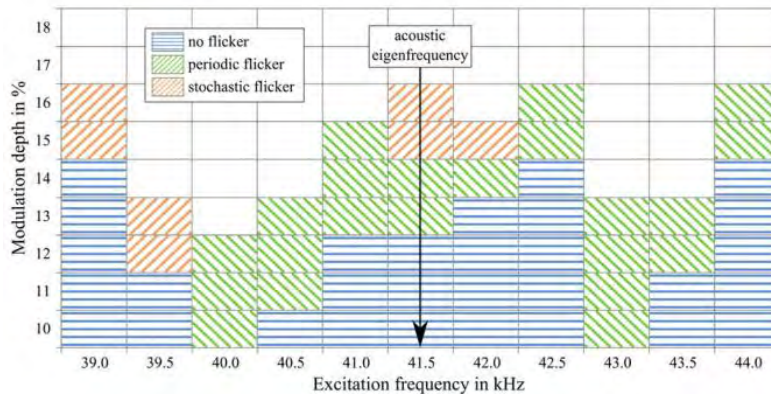


Fig. 2-23 Flicker as function of excitation frequency and modulation depth [14]

In Fig. 2-23, the characterization of the arc flicker and arc motion changed significantly near the acoustic eigenfrequency. The excitation frequency was tuned from 39 to 44 kHz with a 500 Hz step and the modulation depth changed from 10% to 16% with a 1% step. Both periodic flicker and stochastic flicker were observed in their experiment. The absolute value of arc deflection increased with the modulation depth. At some certain frequencies, the periodic flicker can change to stochastic flicker with the rise of the modulation depth. In conclusion, the results shown in the paper [14] are interesting. Using the photodiode to detect arc flicker is simple. But the method for arc motion detecting by a camera is not recommended. This cannot be implemented into an online detection. Moreover, the camera is a high-cost instrument.

Another result using the light flicker to detect AR was presented by Dalla Costa and others [10]. In their experiment, a photodiode was used to detect visible light first. Then, an 8th order Butterworth low pass filter was used to get low-frequency fluctuations of light flicker. A flicker parameter was defined as the ratio between the ac peak-to-peak output voltage of the sensor circuit in the presence of AR, to the output voltage of the sensor circuit in the absence of AR at nominal lamp power. The test lamps were supplied with a low frequency square waveform on which a high-frequency sinusoidal ripple waveform was superposed. The frequency of the high-frequency waveform is from 20 kHz to 200 kHz Fig. 2-24 shows the supply system for the lamps.

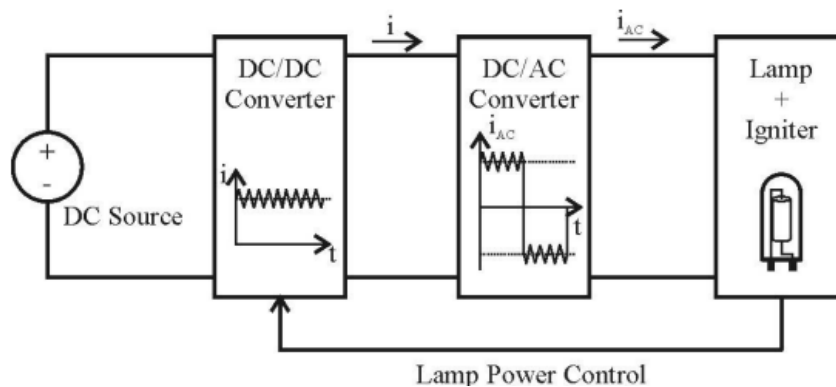
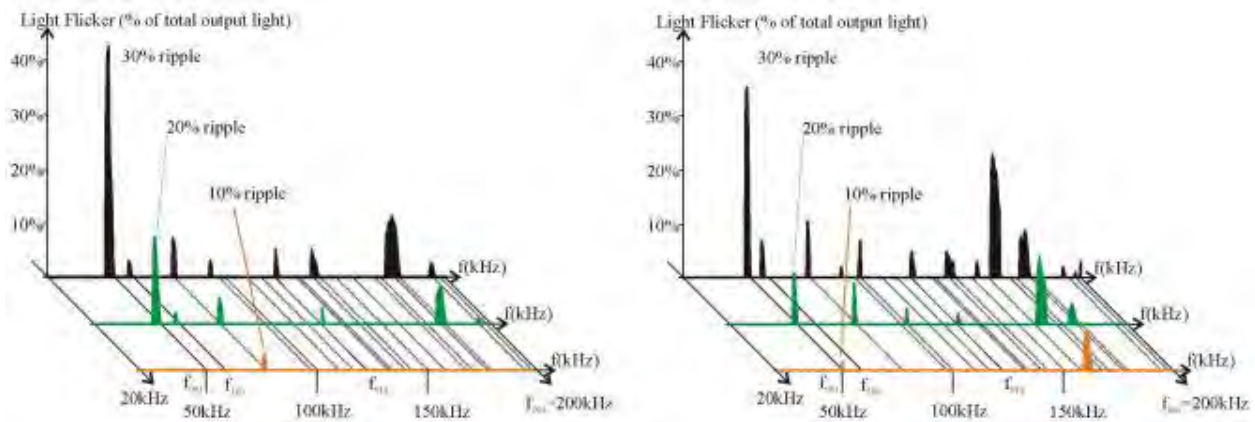
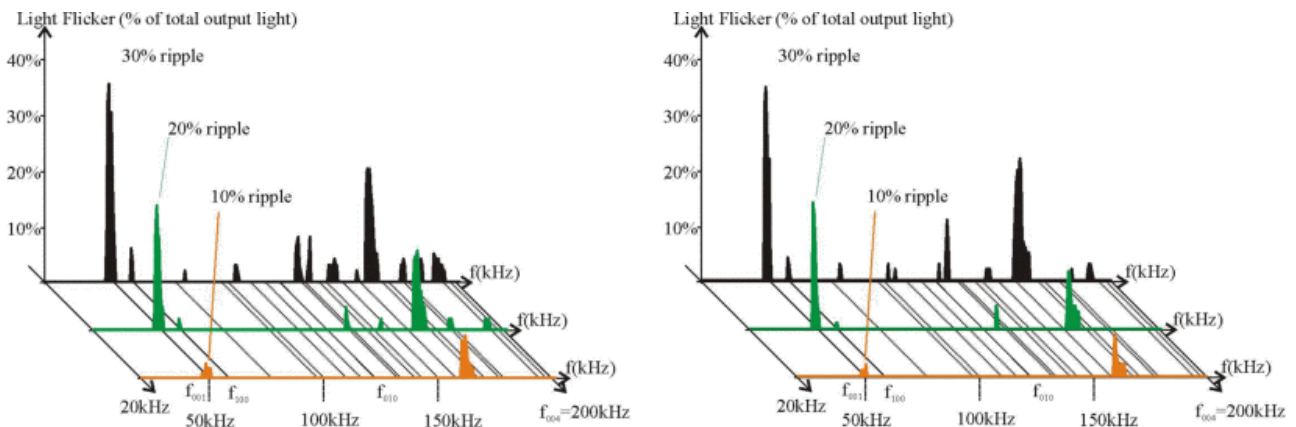


Fig. 2-24 The supply system for the tested lamps [10]

To simulate the low-frequency square wave ballast, a DC voltage source followed by a resistive ballast and a full-bridge inverter were used. A variable HF sinusoidal voltage source is connected in series with the DC source in order to control the high frequency (HF) ripple amplitude.



(c) Two Osram HCI-T 35W/WDL



(d) Two Philips CDM-T 35W/830

Fig. 2-25 Light flicker at AR situations [10]

In Fig. 2-25, the black lines are the theoretical AR frequencies in the tested lamps. Vertical axis represents the lamp light flicker due to the occurrence of AR. The results showed that AR frequency bands are enlarged, and the light flicker gets more serious as the rise of the voltage ripple from 10% to 30%. Therefore, for the LFSW ballast, controlling the voltage ripple can adjust AR levels in HID lamps. This method is as same as the previous one, presented in the paper [14].

2.4.2.3 Optogalvanic method

Using optogalvanic effect (OGE) to excite or detect AR in an HPS lamp was introduced [15]. The laser system with an Ar^+ pump laser and a tunable dye laser was used to excite AR modes. The laser beam was chopped with a mechanical chopper. The chopper frequency is near the AR frequency. The changes due to the laser were measured via a blocking capacitor with a lock-in amplifier. The results show that the laser excitation of AR depends strongly on the axial position of the laser beam and that the laser excitation at a nodal point of the acoustic standing wave is not possible. This method can detect AR effects before the occurrence of visible instability. However, this method is not applicable to more complex acoustic modes.

2.4.3 Sound spectrum

The sound spectrum was detected in a 300W high-pressure mercury lamp by Schäfer and others [64] [16]. In this case, the lamp was operated in an anechoic room of about 0.5 m³ volume and supplied by power amplifiers with a sinusoidal waveform without DC offset. The sound was picked up by a capacitor microphone and the pre-amplified microphone output signal was subsequently processed by a spectrum analyzer.

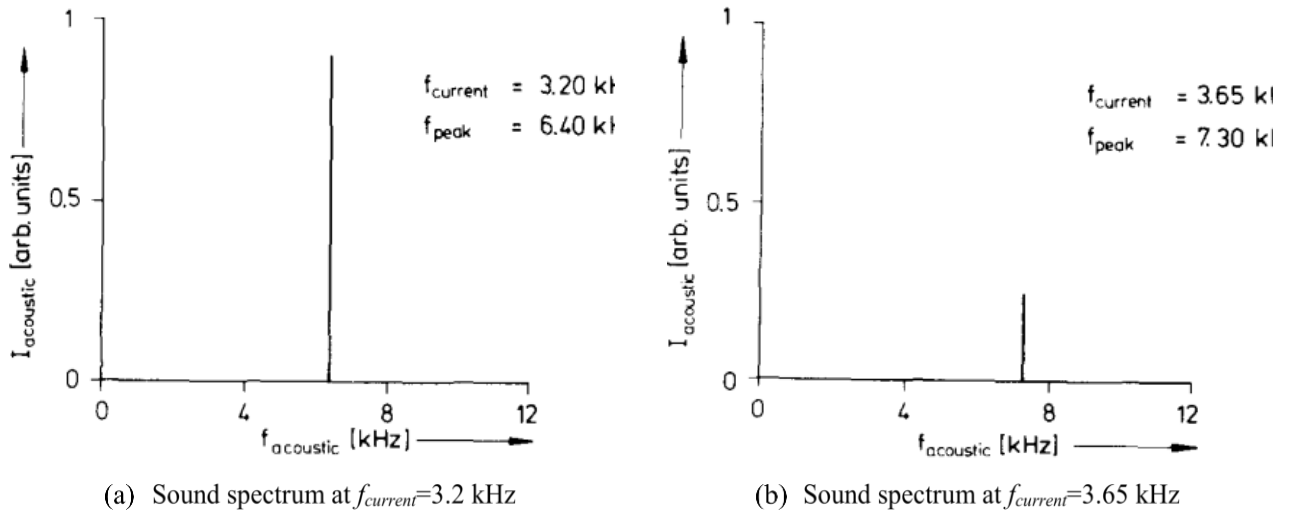


Fig. 2-26 Sound spectra of the 300-W mercury lamp at two different lamp current frequencies.

Fig. 2-26 illustrates sound spectra at two different values of the current frequency. A strong peak of the sound amplitude is found at the power frequency $f_{\text{peak}} = 2f_{\text{current}}$. The results also show that the sound amplitude depends strongly on the applied current frequency. The acoustic amplitude as a function of the current frequency is shown Fig. 2-27.

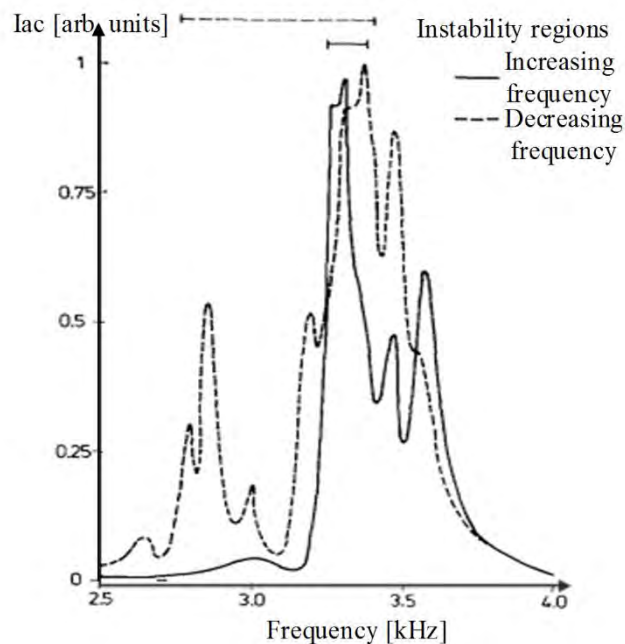


Fig. 2-27 Acoustic amplitude as a function of the lamp current frequency [64]

In Fig. 2-27, at about 3.2 kHz the sound amplitude reaches a maximum, corresponding to the fundamental longitudinal frequency. In addition, a strong hysteresis is found between increasing and decreasing frequency. This is because that the time-dependent arc temperature profiles are different in increasing and decreasing frequency. The results show that the sound emission occurs without the appearance of visual arc instabilities as well at some certain frequencies. This is an accurate method to detect AR, but the sound spectra is easily disturbed by outside noise.

2.4.4 Temperature variations

Schäfer and others [64] also measured arc temperature profiles at various axial positions in AR and no AR frequency bands in order to investigate variations of the plasma parameters due to the occurrence of the fundamental AR. The deformations of temperature profiles subjected to acoustic disturbances were observed as early as 1964. Fig. 2-28 (b) shows the resulting axial dependence of the axis temperature. The axial coordinate $z=0$ mm corresponds to the position of the lower electrode, while the upper electrode is located at $z=40$ mm (see Fig. 2-28 (a)).

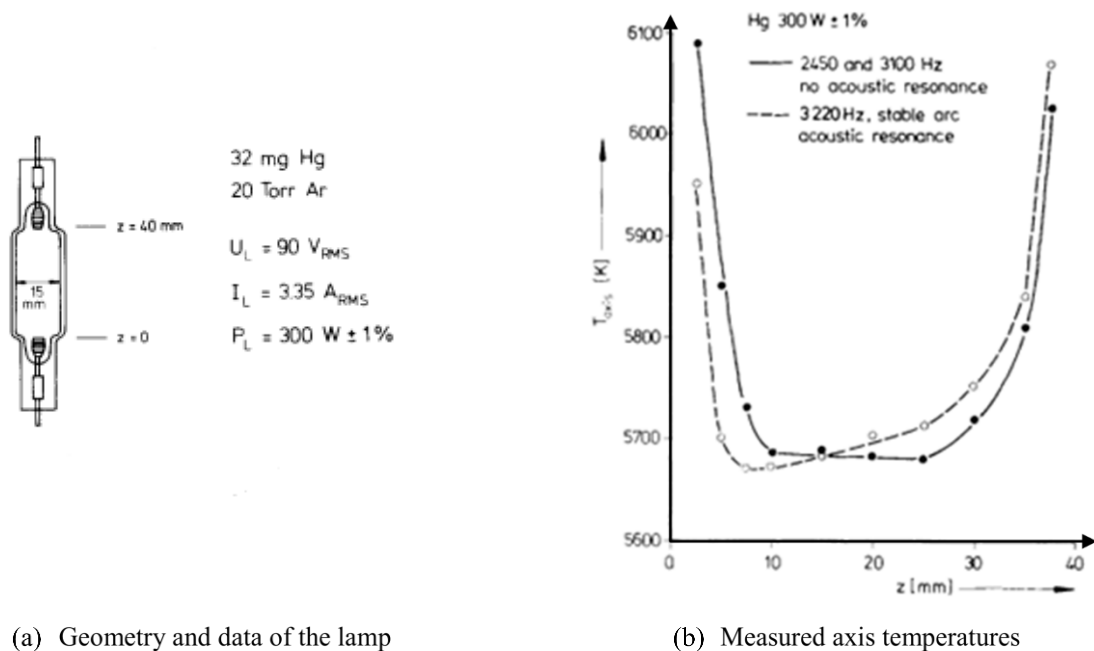


Fig. 2-28 Lamp model and comparison of the measured axis temperatures with and without AR [64]

As can be seen from Fig. 2-28 (b), the axis temperature is almost constant in the middle of the arc and increases towards the electrodes when AR is not present. At AR situation (dashed curve), the axis temperature changes greatly. The axis temperature decreases below $z=15$ mm to the lower electrode, whereas an increase of about 50 K is found above $z=15$ mm. The changes of axis temperature also accompanied by changes in the radial arc temperature profiles.

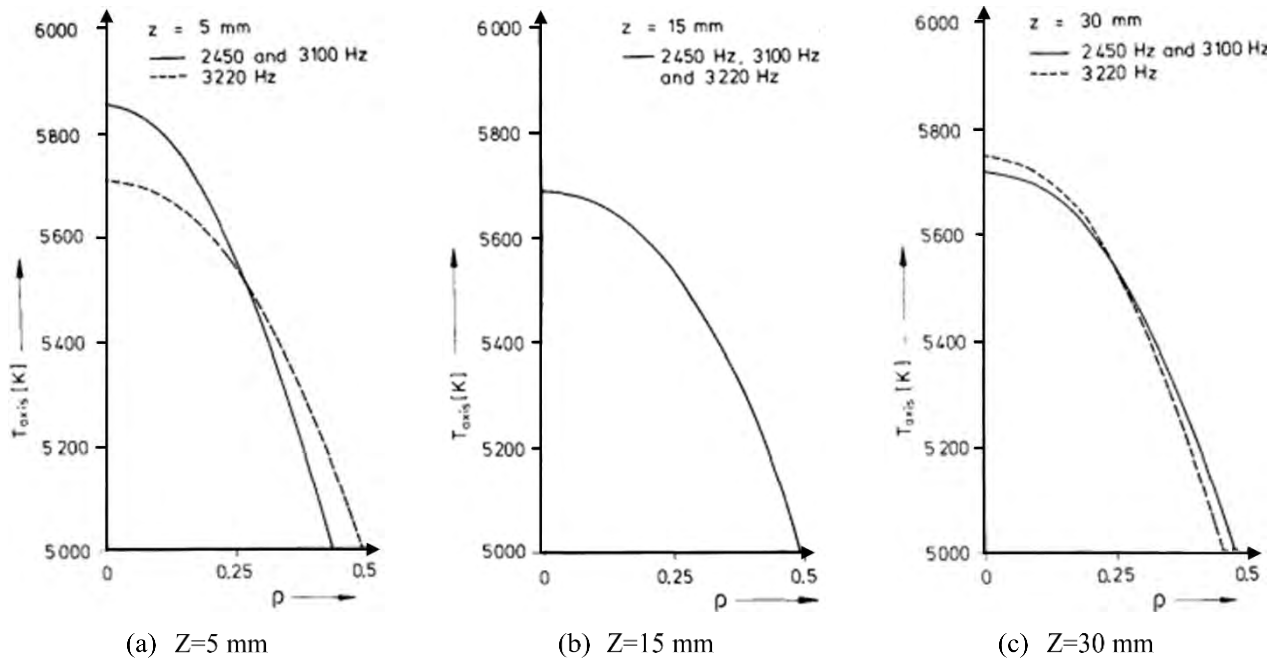


Fig. 2-29 Radial arc temperature profiles in different part at with and without AR situation [64]

In Fig. 2-29 (a), the decrease of the axis temperature in the lower part ($z=5$ mm) causes big changes in the temperature of radial profile. Fig. 2-29 (b) show that the temperature profiles are equal in the middle section of the lamp at $z=15$ mm. There is a slight constriction of the arc temperature profile (Fig. 2-29 (c)).

Owing to the changes of the arc temperature profiles in the radial position in the presence of AR, the heat flux to the wall of the arc tube will change as well. To investigate this, Schäfer and others [64] measured the variations of the wall temperature distribution of the arc tube using an infrared pyrometry $\lambda \approx 5 \mu\text{m}$. Wall temperature profiles were detected at a constant azimuthal position on the cylindrical arc tube in AR and no AR situations, as shown in Fig. 2-30.

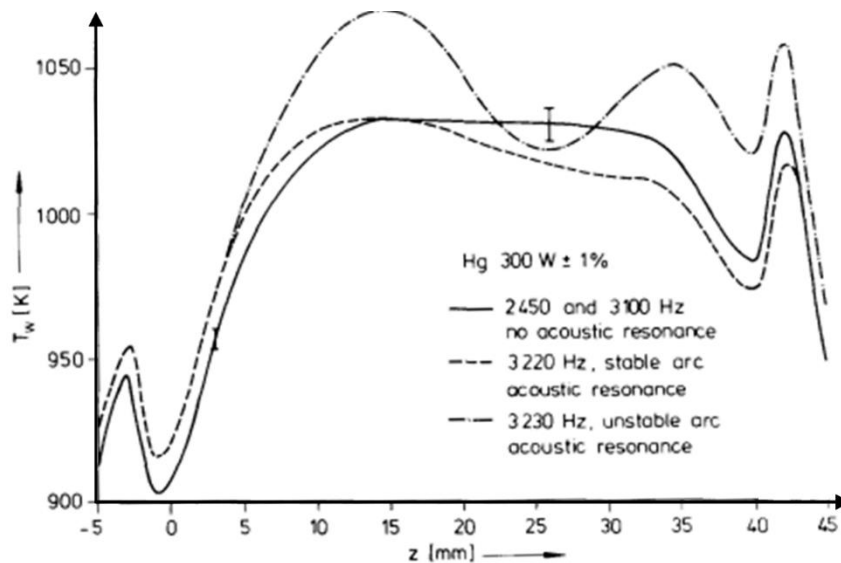


Fig. 2-30 Axial wall temperature distribution in AR and no AR situation [64]

Compared to the no AR situation, great variations of wall temperature are observed in the middle of the arc tube, especially for unstable arc AR situation. In addition to this, wall temperature increases 20 K in the low part of the arc tube.

This method has a good ability to classify AR, but it is not easy to fulfill. Another issue is measuring the temperature profiles cannot implement in real detection.

2.4.5 Comparisons between different acoustic resonance detection methods

TABLE 2-4 Comparisons between different acoustic resonance detection methods

Methods		Pros	Cons
Electrical	Observed variations of electrical parameters [3]	Good sensitivity	Subjective
	Low-frequency fluctuation	Real-time detection	Bad sensitivity, non-linear and requires threshold voltage
	Changing trend of electrical parameters [12]	Simple	Bad sensitivity and subjective
	Harmonic detection of current FFT [13]	Simple	Requires computation
Optical	Arc images [3]	Good sensitivity, independent of the aging of lamps	High cost, fast camera, requires digital image processing
	Arc motion [14]	Good sensitivity, independent of the aging of lamps	High cost and high computational load (Digital image processing)
	Arc flicker [14], [10]	Good sensitivity, independent of the aging of lamps	Requires tight optical coupling between lamp and sensor
	Optogalvanic [15]	observed AR before visual effects	Only lab method
Physical	Sound emission [64], [16]	observed AR before visual effects	Shielded outside noise, and lab method
	Temperature variation [64]	Good sensitivity	Only lab method

Different AR detection methods have been reviewed, TABLE 2-4 shows advantages and disadvantages of each of them. By analyzing these detection methods, we found some issues. Firstly, most of methods are not suitable to apply into real-time detection and there are no objective approaches to classify AR severity. Secondly, the methods based on envelope detection of electrical variables suffers from non-linearity, noise sensitivity, and threshold issues.

In the first phase of this research, a linear demodulator appeared as a good candidate in order to detect AR occurrence from a monitoring of the electrical parameters. This lead us to develop specific circuits implementing this functionality. The conception details and results will be fully explained in chapter 3 and 4. The demodulated signal must be further analyzed by statistical methods in order to classify between no R and AR situations. This permitted to define some objective metric.

During the assessment phase, it was also found that standard photometric and colorimetric parameters presented variations during AR occurrence through modifications of the light spectrum. Although known and reported in the literature, these variations were never used as a tool to detect AR. In fact, when MH lamps work in the normal situation, the elements inside of the arc tube keep chemical balances. No light spectral variations are observed in the arc tube. However, AR can shift these balances, resulting in significant light spectral variations. Therefore, we propose some statistical methods to analyze how AR influence on these variations. The detailed information of light spectral variations will be presented in chapter 4 as well.

2.5 Methods for acoustic resonance avoidance

AR can bring potential risks for lamps or ballasts. It is essential to avoid the occurrence of AR phenomenon through some control mechanism. The methods of AR avoidance use two degrees of freedom: either control the frequency, either control the harmonic energy.

2.5.1 Changing lamp related parameters (*AR-free frequency*)

AR eigenfrequencies of HID lamps can be calculated by solving the simplified wave equation. The bands between those frequencies are supposed AR-free. There are some parameters determine the eigenfrequency of the lamp as follow:

A. Lamp geometry

The first important factor for the lamp is the geometry of the arc tube. Its modification can reduce the potential power of AR and shift AR frequencies. AR is more likely to be excited in spherical arc tube or tubes with spherical end than flattened or narrow and cylindrical arc tubes. As presented in the paper [17], increasing the radius of spherical arc tubes can increase AR frequency bands and AR can be more easily excited. The cylindrical arc tube with the aspect ratio of IL: ID about 1:1 (Inner Length to Inner Diameter) can result in maximizing the lowest AR frequency.

B. Type of gas filling

According to Eq. 2-11, the sound velocity affect AR frequencies. The sound velocity is directly related to the types of gas fillings and gas thermodynamic state variables such pressure, temperature, and gas density. Consequently, changing the temperature and gas density can directly change AR frequencies.

C. Burning position

The burning position of the lamp determines the temperature inside the arc tube. AR frequencies are different in vertical and horizontal position.

D. Gas pressure

The gas pressure affects AR frequencies. Increasing the gas pressure decreases the damping coefficient accounting for AR. This means that the rise of the gas pressure of the arc tube can increase the sensitivity of AR and the threshold of AR energy is reduced. The damping coefficient of AR increases with increasing viscosity. On the other hand, absorption of acoustic energy due to the viscosity of the medium leads to generating of acoustic streaming. Viscosity not only suppresses the motion of the fluid but also is the source of the driving force in generating acoustic streaming by converting the acoustic energy into the momentum.

E. Density of atoms

AR phenomenon can be affected by the density of mercury atoms inside the arc tube of MH lamps. As presented in the paper [18], increasing the mercury atom density can increase the lamp sensitivity to the higher frequency component. This means that AR is more likely to occur as mercury pressure increases.

In conclusion, lamp related factors affect the AR phenomenon, but it is impossible to avoid AR just by changing lamps' parameters. In addition, the lamps' colorimetric parameters such as color rendering index, color temperature, lamps' lifetime are affected by changing the lamps' related parameters.

2.5.2 Operation supply of ballast

2.5.2.1 DC-type ballast

AR can be explained that the periodic power input brings gas-pressure fluctuations in the arc tube of lamps. DC power source cannot cause the periodic power input. Thus, ballasts supplied by DC power source do not have AR problem. Nevertheless, DC-type ballasts can cause electrophoresis [19], destroy electrodes and reduce the lifetime of lamps.

2.5.2.2 Low-frequency square wave electronic ballast

The most common method for AR avoidance is to supply lamps with a low-frequency square wave [20]. The nominal values of the supply range between 100 Hz and 400 Hz. The principle of low-frequency square wave supply for AR elimination is that to operate the lamps well below the minimum AR frequencies.

2.5.2.3 Extra-high frequency electronic ballast

HID lamps are driven by extra-high frequency (greater than several hundred Hz or 1 MHz) which is above the AR frequency range. Theoretically speaking, there are infinite numbers of resonance modes. Resonances at higher frequency bands are close to each other or almost continuous. This means that there are no AR-free frequencies at higher frequency regions. However, two factors affect AR-free frequencies as follows:

- 1) the importance of the AR mode decreases by increasing the resonance frequency;
- 2) the damping effect increases with frequency.

Therefore, there is not enough energy to excite AR at extra-high frequency regions. As presented in the paper [17], 700 kHz is chosen to avoid AR for 35 W MH lamps. However, the extra high-frequency regions also depend on a variety of factors, one of which is the dimensions of the lamp and thus varies from one lamp to another lamp. Electromagnetic-interference (EMI) and switch losses of ballasts increase at extra-high frequency regions as well.

2.5.3 Spread power spectrum

As mentioned in section 2.5.1, choosing a specific AR-free frequency cannot avoid AR totally. AR frequencies depend on the lamp power, manufacturer, arc tube shape and the aging of the lamp. As reviewed literatures, frequency modulation [21], amplitude modulation, injection of fundamental and the third harmonic [22], and injection of several adjacent frequency signals [23] were used to avoid AR. The basic ideas of these approaches are to lower the excitation energy below the threshold energy at the eigenfrequency of the lamp. In this section, we mainly analyze the frequency modulation and the injection adjacent frequency signals to eliminate AR.

2.5.3.1 Frequency modulation

J. Correa presented frequency modulation technique to avoid AR in HID lamps [21]. Frequency modulation can spread the power spectrum of the lamp and lower the eigenfrequency energy below the threshold energy in order to avoid AR. The spectral amplitude effect caused by modulation index is shown in Fig. 2-31.

For a modulated frequency signal, the modulation index is defined as the peak frequency deviation divided by the frequency of the modulated signal:

$$m = \frac{\Delta f}{f_m} \quad (2-19)$$

where m is the modulation index, Δf is the deviation frequency and f_m is the modulating frequency.

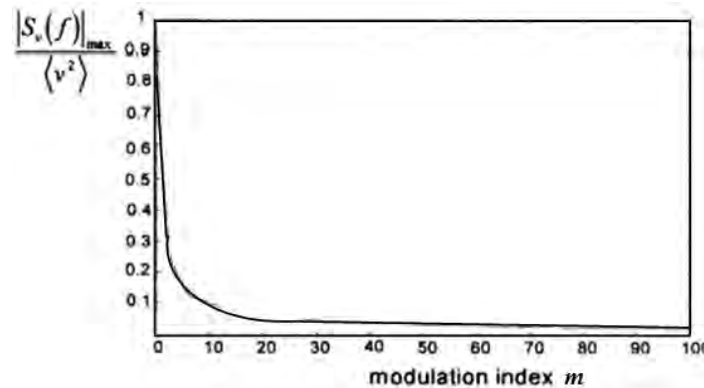


Fig. 2-31 Normalized maximum term vs. the modulation index (power spectrum density $S_v(f)$) [21]

In Fig. 2-31, when the modulation index $m > 10$, the spectral components decrease significantly. J. Correa proposed the frequency modulation technique to eliminate AR by injecting periodic signals into the driving signals of inverter of the ballast. Fig. 2-32 illustrates the ballast for tested lamps. Periodic signals with different modulation index values: 10, 20, 50, and 200 were used to determine their effect on AR elimination. HPS, MH and HPM lamps were tested in their experiment. TABLE 2-5 shows obtained results for tested HID lamps in the worst AR situation.

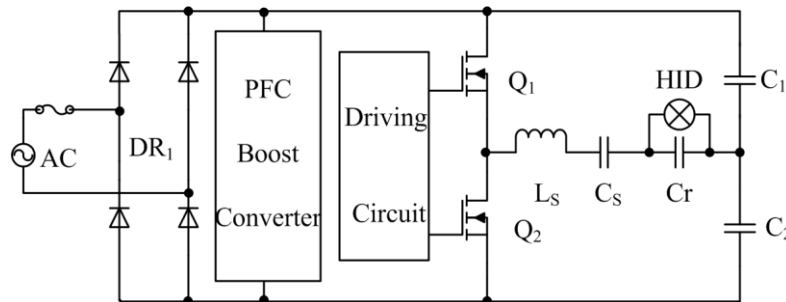


Fig. 2-32 Electronic ballast for testes lamps [21]

TABLE 2-5 Obtained results for tested HID lamps [21]

Lamp	Modulation index	Modulation signal
HQITS-150 W (MH lamp)	25	Sinusoidal (Triangular)
MHNTD-70 W (MH lamp)	10	Triangular
LU-70 W/52 (HPS lamp)	50	Triangular
H38JA-100 W (HPM lamp)	150	Sinusoidal

According to the results, the frequency modulation technique with periodic sinusoidal and triangular signals injection can eliminate AR phenomena. However, the technique needs to choose different modulation index for different kinds of HID lamps for AR avoidance.

2.5.3.2 Injecting adjacent frequency

Several adjacent frequencies of sinusoidal signals were injected to avoid AR in an HPS lamp, presented by Chhun and others [23]. The principle of injection several adjacent frequencies confined within the frequency bandwidth of the ballast defined by the characteristic of LCC resonant circuit which was the same as Fig. 2-32. The harmonics can cause AR if their amplitude exceeds the threshold values at corresponding frequencies. Injection of adjacent frequencies can restrict certain harmonics. Because the increase of injected signals allows a better dispersion of power harmonics and the number of harmonics can be controlled.

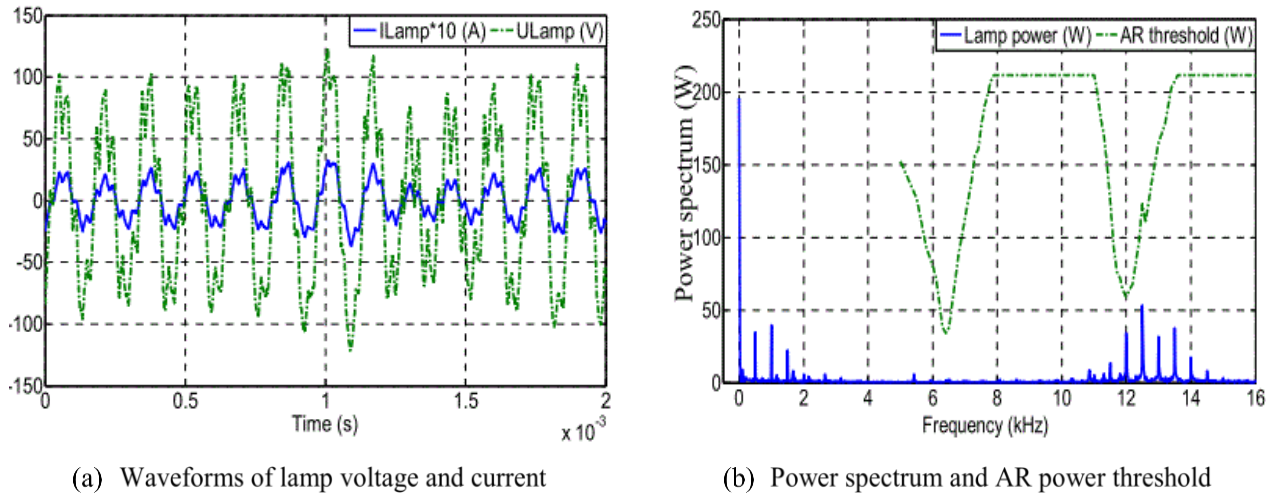


Fig. 2-33 Experimental results after injecting 5 adjacent frequencies [23]

Injecting adjacent frequencies can avoid AR well, whereas this method has higher crest factor. As can be seen from Fig. 2-33 (a), after injecting some adjacent frequencies, there are some distortions in the lamp voltage and current. In addition, the lamp power spectrum is lower than the AR power threshold in Fig. 2-33 (b). That is why this method can be used to eliminate AR in HPS lamps.

2.5.4 Comparisons of acoustic resonance avoidance methods

We highlight the main advantages and disadvantages of the review methods, as summarized in TABLE 2-6. The results show that changing lamps' related parameters just shift AR frequencies, and cannot avoid AR totally. DC supply ballasts can avoid AR, but cause electrophoresis. Low-frequency square wave electronic ballast can avoid AR, but with complicated structure. Extra-high frequency ballasts can eliminate AR, but cause electromagnetic interference and increase switches losses. Frequency modulation and injection of adjacent frequencies can spread the lamp power spectrum and lower the energy of the power for AR avoidance. Both approaches have drawbacks, but those cons can be controlled.

In our experiment, an improved frequency modulation is used to avoid AR in MH lamps. Low-frequency 300-500 Hz periodic signals are injected into the PWM signals of half-bridge inverter of our high frequency electronic ballast. This method can be implemented by integrated circuits. We also can use a function generator to produce low-frequency periodic signals such as square wave, triangular wave, and sinusoidal wave and then add modulated signals to the driving signals of inverter. The results show these methods can avoid AR in different HPS lamps and MH lamps, but we did not continue to study AR avoidance methods. On one hand, this thesis focuses on AR detection methods. On the other hand, the author did this kind of study during in Master degree.

TABLE 2-6 Comparisons between different acoustic resonance avoidance methods

Methods		Pros	Cons
AR-free frequencies (Changing lamp related parameter) [18]		Simple structure of ballasts	Low reliability to avoid AR
Operation supply of ballast	DC-type ballast [19]	Simple	Cause electrophoresis
	Low-frequency square wave ballast [20]	Operation frequencies below AR frequencies	Complicated structure of ballasts
	Extra-high frequency ballast [17]	Simple structure of ballast	Electromagnetic-interference and switches losses
Spreading power spectrum	Frequency modulation [21]	Lowering the harmonic energy	Need to change modulation index according to lamps
	Injection of adjacent frequencies [23]	Lowering the harmonic energy	Causes current and voltage distortion

2.6 Advantages of acoustic resonance

As presented in many literatures, AR cause light flicker, light fluctuations, damages in electrodes and reduce lamps' lifetime, even destroying lamps. AR also can bring some benefits.

2.6.1 Arc straightening

As reported in [23], when HID lamps operate at horizontal position resulting to upward bowing of the discharge because of buoyancy force in the arc tube. This effect is not desirable when the lamp optics need a straight line, for example, automotive lamps and projecting lamps. Upward bowing results in a significant temperature difference between the upper side and the down side of the arc tube's wall that are called hot spot and cold spot. Extra heating of hot spot can shorten the lifetime of lamps, especially for quartz lamps. The lamp efficacy is also reduced due to upward bowing of the discharge. An advantage of AR operation is arc straightening. Some acoustic modes can push the discharge downward and maintain the discharge in a straight position between two electrodes. Arc straightening results in a more isothermal temperature of the arc tube. The temperature difference between the hot spot and cold spot can be reduced due to arc straightening. The lamp efficacy increases because of more gas atoms. In addition, arc straightening reduces the maximum wall temperature up to 200 °C, which in turn increases the lamp efficacy [23].

2.6.2 Color mixing for HID lamps operated vertically

Some of MH lamps have long cylindrical ceramic arc tube for high light efficiency. However, when this kind of MH lamps operates in horizontal or vertical position, they have different color appearance. For instance, different color bands along the arc tube of MH lamps are observed in a vertical position. This is because of non-homogenous distribution of filling elements inside arc tube which is called color segregation. The top part of the discharge appears greenish while the bottom looks pinkish. The reason is that the density of thallium and mercury atoms dominates at top of the discharge and emissions of metal salts are found at the bottom of the discharge. In order to avoid such color segregation, a second longitudinal acoustic mode is built [25], [26], because the longitudinal acoustic mode can move metal salts axially due to acoustic streaming.

2.6.3 *Strength test of arc tube and outer bulb*

HID lamps must have enough strength of arc tube and outer bulb to avoid lamps destruction. The strength test of the arc tube and outer bulb is an important part of work for HID lamps because of safety issues. When AR occurs in lamps, overheating of arc tube results in extreme thermal stress that can cause lamp explosion. For this case, the acoustic mode can be applied to test whether or not the arc tube has a strong strength.

2.7 Conclusions

In this chapter, AR phenomena are put forward first, the theoretical AR frequencies are analyzed, and an example of AR frequency calculation in our tested MH lamp is given. AR phenomena bring various problems to lamps or ballasts. The manifestations of AR phenomena are various and dynamic. Researchers propose different detection methods to detect AR, such as observing the voltage, current, and power of the lamp, and detecting light flicker spectral variations, sound emission, temperature variations, and even optogalvanic effects. We showed that none of them is simple and robust enough.

In addition, how to avoid AR is the first essential problem that should be considered for ballasts or lamps designers. Some methods based on related lamp parameters are proposed to eliminate AR. However, these kinds of methods cannot solve totally the AR phenomena. Different power waveforms have been tested to supply the discharge as well. Spreading the power spectrum of the lamps can reduce the harmonic power to a level lower than the threshold power in order to avoid AR. Nevertheless, it can also bring some advantages like arc straightening, color mixing for lamp operated vertically or horizontally, strength test for arc tube and bulb.

References

- [1] Sylvain Epron, "Etudes et effets des oscillations acoustiques dans les lampes à décharge haute pression", thèse doctorat en génie électrique en 1999, université Paul Sabatier, Toulouse, France.
- [2] H. L. Witting, "Acoustic resonances in cylindrical high-pressure arc discharges," *Journal of Applied Physics*, 1978, vol. 49, no 5, p. 2680-2683.
- [3] H. Peng, S. Ratanapanachote, P. Enjeti, L. Laskai, I. Pitel, "Evaluation of acoustic resonance in metal halide (MH) lamps and an approach to detect its occurrence," *IEEE Industry Applications Conference 1997*, 32nd IAS Annual Meeting, Oct. 1997, Volume: 3, Page(s): 2276 – 2283.
- [4] J. C. Anton et al., "Acoustic resonance band detection workbench for HID lamps," *Conference Record of the 2004 IEEE Industry Applications Conference*, 2004. 39th IAS Annual Meeting., 2004, pp. 667.
- [5] R. Schäfer, H. P. Stormberg, "Investigations on the fundamental longitudinal acoustic resonance of high pressure discharge lamps," *Journal of Applied Physics*, 1982, vol. 53, no 5, p. 3476-3480.
- [6] Wei Yan, Y. K. E. Ho and S. Y. R. Hui, "Stability study and control methods for small-wattage high-intensity-discharge (HID) lamps," in *IEEE Transactions on Industry Applications*, vol. 37, no. 5, pp. 1522-1530, Sep/Oct 2001.
- [7] M Schulz, U Ingard, "Acoustic kink instability in an argon discharge," *Physics of Fluids*, 1967, vol. 10, no 5, p. 1031-1036.
- [8] R. Ruscassie, J. B. Rouffet, S. Bhosle, G. Zissis and C. Glaize, "Defining acoustic resonances in dimmed HID lamps using a finite element model," *14th Industry Applications Conference*, vol. 3, pp. 1588-1592, Oct. 2005.
- [9] L. Chhun, P. Maussion, S. Bhosle, G. Zissis, "Characterization of acoustic resonance in a high-pressure sodium lamp," *IEEE Trans. Industry Applications*, vol. 4, no. 2, pp. 1071-1076, Dec. 2010.

- [10] M. A. Dalla Costa, J. M. ALONSO, E. López, J. Garcia and J. Ribas, "Acoustic resonance characterization of low-wattage metal-halide lamps under low-frequency square-waveform operation," *IEEE Transactions on Power electronics*, 2007, vol. 22, no 3, p.735-743.
- [11] C. S. Moo, C. K. Huang, C. Y. Yang, "Acoustic-Resonance-Free High-Frequency Electronic Ballast for Metal Halide Lamps," *IEEE Trans. Industrial Electronics*, vol. 55, no. 10, pp. 3653-3660, Apr. 2008
- [12] L. Chhun, P. Maussion, S. Bhosle and G. Zissis, "Interpolation modelling of acoustic resonance in high pressure sodium lamp," 34th Annual Conference of IEEE Industrial Electronics, Orlando, FL, 2008, pp. 1974-1979.
- [13] Y. Jiang, M. S. Shen, H. L. Z. M. Qian, "An adaptive acoustic resonance free electronic ballast for HID lamps," in *Proc. IEEE IAS Annual Meeting*, vol. 2, pp. 1020-1024, Oct. 2003.
- [14] J. Schwieger, M. Wolff, B. Baumann, F. Manders, J. Suijker, "Characterization of Discharge Arc Flicker in High-Intensity Discharge Lamps," in *IEEE Trans. on Industry Applications*, May-June 2015, vol. 51, no. 3, pp. 2544-2547.
- [15] M. J. Jongerius, A. J. M. Ras, Q. H. F. Vrethen, "Optogalvanic detection of acoustic resonances in a high-pressure sodium discharge," *Journal of applied physics*, 1984, vol. 55, no 7, pp. 2685-2692.
- [16] H. P. Stormberg, R. Schäfer, "Excitation of acoustic instabilities in discharge lamps with pulsed supply voltage," *Lighting Research & Technology* 15, no. 3 (1983): 127-132.
- [17] W. Yan, Y. K. E. Ho and S. Y. R. Hui, "Investigation on methods of eliminating acoustic resonance in small wattage high-intensity-discharge (HID) lamps," *IEEE Industry Applications Conference 2000, 35th IAS Annual Meeting and World Conference on Industrial Applications of Electrical Energy*, 2000, vol.5, pp. 3399-3406.
- [18] S. Wada, A. Okada, and S. Morii, "Study of HID lamps with reduced acoustic resonances," *Journal of the Illuminating Engineering Society*, 1987, vol. 16, no 1, p. 162-175.
- [19] F. Goodenough, "Novel DC-DC Converter Keeps Power Constant," *Electronic Design*, 1996, pp: 51-62.
- [20] H. L. Cheng, C. A. Cheng, Y. N. Chang and K. M. Tsai, "Analysis and implementation of an integrated electronic ballast for high-intensity-discharge lamps featuring high-power factor," in *IET Power Electronics*, vol. 6, no. 5, pp. 1010-1018, May 2013.
- [21] J. Correa, M. Ponce, J. Arau, M. Sanchez, J. M. Alonso, "Evaluation of frequency modulation techniques to avoid acoustic resonances in electronic ballast for HID lamps: analysis and methodology," in *Proc. IEEE Power Electronics*, Oct. 2004, vol.10, pp. 245-250.
- [22] L. M. F. Morais, P. F. Donoso-Garcia, S. I. Seleme, P. C. Cortizo and F. N. A. Silva, "Acoustic Resonance Rejection via Voltage Modulation Method for HPS Lamps," *IEEE International Symposium on Industrial Electronics*, pp. 2996-3001, Jun. 2007.
- [23] L. Chhun, P. Maussion, S. Bhosle, G. Zissis and O. Durrieu, "Injection of adjacent frequency signals for acoustic resonance avoidance in HPS lamp," 35th Annual Conference of IEEE Industrial Electronics, 2009, pp. 3537-3544.
- [24] G. R. Allen, J. M. Allison, J. M. Davenport and R. L. Hansler, "Acoustic resonance operation of xenon-metal halide lamps," U.S. Patent No 5 121 034, 9 Jun. 1992.
- [25] Shen, Eric. "Method for coloring mixing of hid lamps operated at VHF frequencies using duty cycle modulation," U.S. Patent No. 6 498 441, 24 Dec. 2002.
- [26] Kramer, Jerry M. "Reduction of vertical segregation in a discharge lamp," U.S. Patent No. 6 184 633, 6 Feb. 2001.

**Chapter 3 Online Acoustic Resonance Detection
and Electrical Modeling of Lamp Voltage
in Metal Halide Lamps**

3.1 Introduction

Several AR detections methods were reviewed in chapter 2. We concluded that almost no approaches can be applied at low cost on the field. The aim of this chapter is to introduce an approach based on a linear AM demodulator permitting a much simpler real-time envelope extraction method for AR detection. Combined to numerical processing, this approach enabled us to build an objective way to classify AR levels so as to deepen further our understanding of AR phenomena.

Our own characterization framework will be fully analyzed. To this end, the circuits of our high-frequency electronic ballast are described. A simplified model will permit to obtain its transfer function. This ballast also generates the required 3-5 kV voltage pulses for the glow-to-arc transition and warmup phase required by MH lamps. The protection against those high voltages pulses is part of the design methodology.

In a first research phase, a generic apparatus permitted to evaluate the sensitivities of various electrical variables with respect to the presence of AR. The conclusion was that the most sensitive approach consisted in evaluating the voltage envelope through synchronous detection, which implies multiplying the lamp voltage waveform by the generator waveform and low-pass filtering the resulting variable. The measurement setup and results will be described in chapter 4.

A multiplier circuit is used to implement the same kind of function in order to perform the detection with a simpler and low-cost device associated to the electronic ballast. This is the topic of section 3.4.4. This circuit is further simplified using a single rectifier as presented in section 3.4.5.

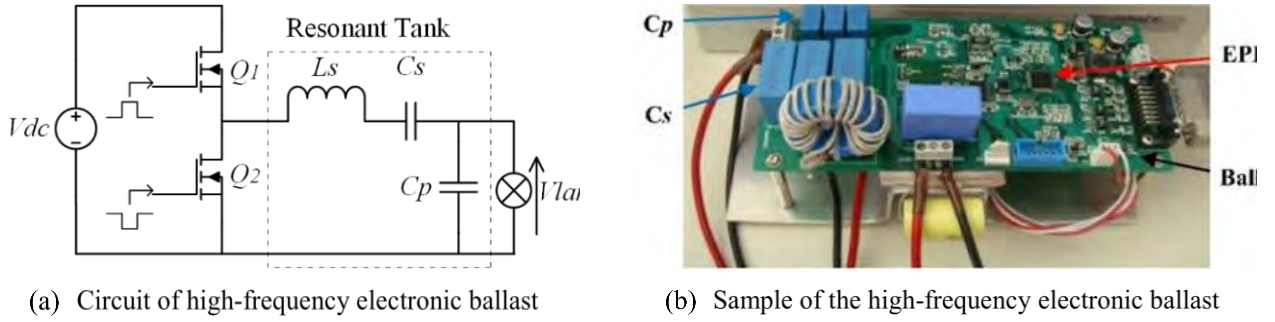
In addition, the characterizations of the voltage envelope in the presence of AR are analyzed. The periodic and stochastic components of the signals are extracted from on the voltage envelope. Based on the results obtained by the proposed rectifier detection circuit, the electrical modelings of the lamp voltage in the presence of different AR phenomena are built in PSIM software. AR characterizations will be concluded at the end of this chapter.

3.2 Circuit of the high-frequency electronic ballast

A typical setup for the high-frequency electronic ballast consists of an electromagnetic interference (EMI) filter, an AC-DC rectifier containing four diodes, a boost converter for improving the power factor, a half-bridge inverter and the igniter. This classical architecture is used because of benefits such as high efficiency, small size, light weight, and long lifetime [2].

3.2.1 Main circuit

The high-frequency electronic ballast is supplied by an *LCC* half-bridge inverter as described in Fig. 3-1. The ballast consists of the *DC* supply V_{dc} , two switches Q_1 and Q_2 , the coupling capacitor C_s , the resonant inductor L_s , the resonant capacitor C_p and lamps. The *LCC* resonant circuit can generate the high voltage required to strike the arc and maintains a stable arc after ignition [3].


 Fig. 3-1 Circuit of the high frequency electronic ballast ($L_s=1.8\text{mH}$, $C_s=300\text{nF}$ and $C_p=15\text{nF}$)

The simplified circuit of the high-frequency electronic ballast by using fundamental approximation is shown in Fig. 3-2. The lamp is assumed to behave prior to ignition as an open-circuit with infinite resistance, and as a high resistance during ignition. After the ignition, the lamp I-V characteristic is modeled as a simple resistance.

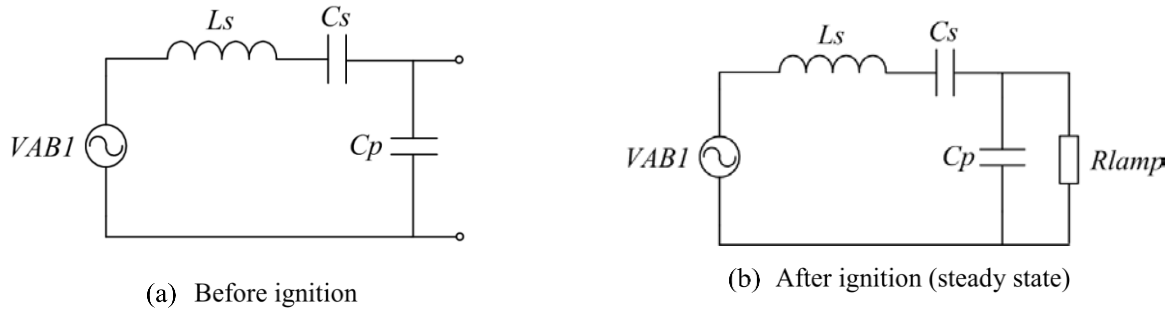


Fig. 3-2 Simplified equivalent circuit using fundamental approximation

In Fig. 3-2 (b), the shunt current in C_p can be neglected in the steady state, so the lamp power is described as:

$$P_{lamp} = \frac{V_{AB1}^2 R_{lamp}}{\left[\left(\omega_s L_s - \frac{1}{\omega_s C_s} \right) + R_{lamp} \right]^2} = \frac{2V_{dc}^2 R_{lamp}}{\pi^2 \left[\left(2\pi f L_s - \frac{1}{2\pi f C_s} \right) + R_{lamp} \right]^2} \quad (3-1)$$

where $\omega_s = 2\pi f$, f is the lamp current frequency; V_{dc} is the dc-link voltage; R_{lamp} is the equivalent resistance of the MH lamp.

Hence, according to Eq. 3-1, the lamp power can be adjusted by V_{dc} or the lamp current frequency f .

3.2.2 Ignition methods

Light is generated by creating an arc between the two electrodes located inside the arc tube. To start an MH lamp, a high voltage pulse is applied to the lamp's electrodes to ionize the gas and create plasma before current can flow [4]. When the lamp is ignited, the applied voltage must satisfy two conditions:

- 1) Sufficient voltage amplitude;
- 2) Appropriate rise and width time of the voltage pulse.

There are two kinds of circuits used to start HID lamps. One applies a transformer to generate the high pulse voltage. The other one is used a resonant LC or LCC circuit to generate a high voltage pulse at high frequency. In our experiment, the resonant LCC circuit is chosen to start the lamps, as shown in Fig. 3-1.

3.2.2.1 Lamp ignited by a transformer

As presented in the paper [5], a transformer with a solid-state device (SIDAC) was used to generate high amplitude pulse to start MH lamps, as shown in Fig. 3-3.

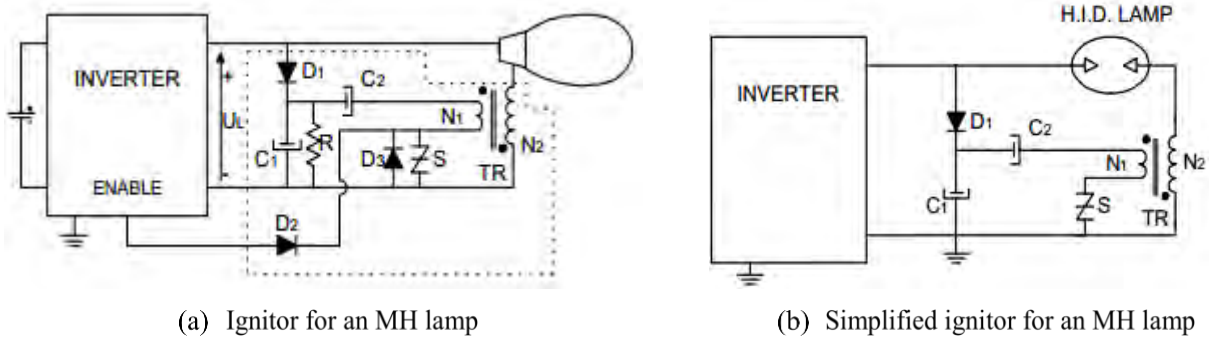


Fig. 3-3 Transformer ignitor for an MH lamp [5]

In Fig. 3-3, when the voltage in the lamp reaches a threshold value, the device S generates a pulse that is transferred to the lamp by a small transformer in series with the lamp. If the circuit is designed properly, the pulse has enough energy as to ionize the gas in the discharge tube, thus starting the lamp

3.2.2.2 LCC circuit with frequency sweeping ignition for metal halide lamps in our experiment

Researchers already proved that an HID lamp operated at high frequency can be considered as a pure resistance [6]. During the lamp ignition, the lamp resistance is estimated about 100 k Ω . Nevertheless, after lamp ignition, the lamp resistance reduces to tens of ohms. The discharge lamps are ignited as a conducting plasma appears inside the lamp bulb.

In order to ignite the MH lamps safely, LCC circuit with frequency sweeping is applied in our experiment.

The transfer function of LCC circuit in Fig. 3-2 (b) also can be expressed as follow:

$$\frac{V_{lamp}}{V_{AB1}} = \frac{\frac{1}{L_s C_p} S}{S^3 + \frac{1}{R_{lamp} C_p} S^2 + \frac{C_p + C_s}{L_s C_s C_p} S + \frac{1}{R_{lamp} L_s C_s C_p}} \quad (3-2)$$

According to Eq.3-2, the Bode diagram of our circuit is shown in Fig. 3-4. In our case, the lamp resistance is estimated about 100 k Ω during the lamp ignition, and 50 Ω at the steady state. In addition, in order to start the lamps safely, a frequency sweeping is proposed, and the operation sequence is illustrated in Fig. 3-5.

In Fig. 3-5, f_{st} is the starting frequency, f_{ig} is the ignition frequency, and f_{nom} is the nominal frequency of the lamps. U_{st} , U_{ig} , and U_{nom} are the corresponding voltages at those frequencies. It is very important to choose the starting frequency in MH lamps. If the starting operation frequency is equal to the resonant of the LCC circuit proper, the high voltage pulse may destroy the electronic ballast.

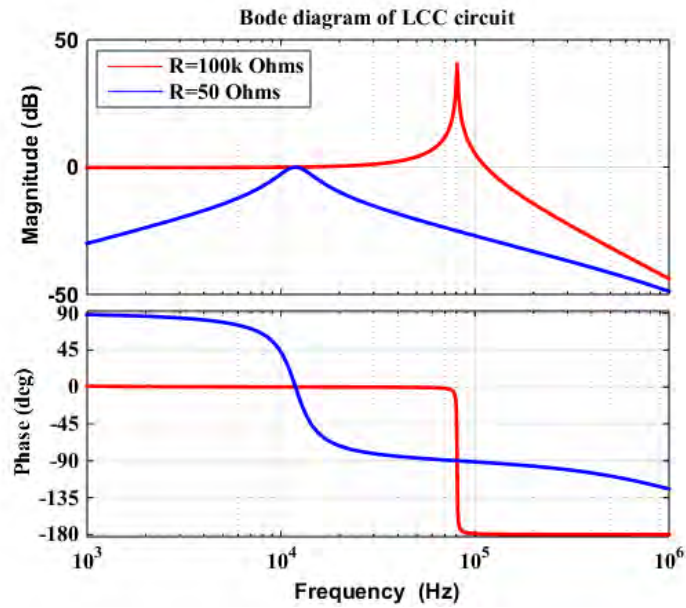


Fig. 3-4 Bode diagram of LCC circuit ($L_s=1.8\text{mh}$, $C_s=100\text{nf}$, $C_p=2.2\text{nf}$)

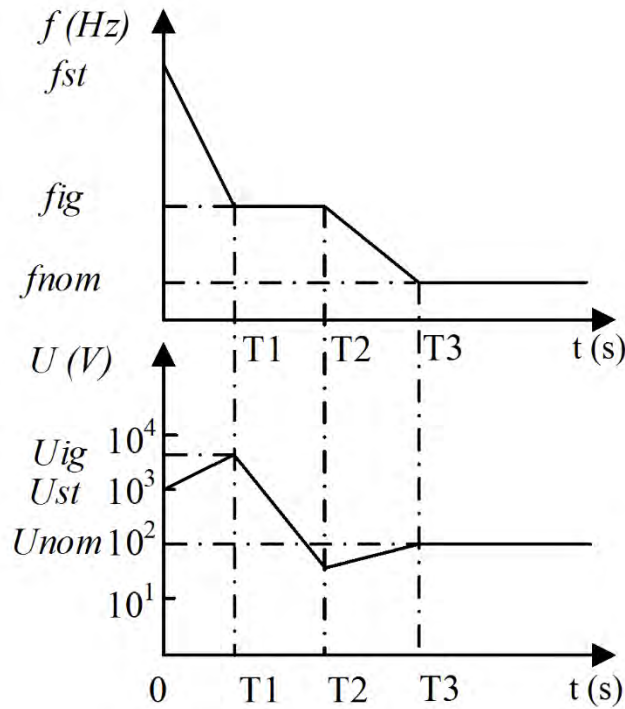


Fig. 3-5 Operation sequences in MH lamps

The starting frequency can be chosen higher than the resonance frequency. As can be seen from Fig. 3-4, at the resonance frequency, the gain is high. Then, we use the backward frequency sweeping. When the sweeping frequency is decreased to f_{ig} which is near the resonance frequency, the voltage reaches several thousand volts and the lamp can be ignited. After the lamp ignition, the lamp resistance decreases quickly, reaching tens ohms and the lamp changes to steady state.

3.3 Experimental set-up at Laplace N7

The experimental set-up at “Laboratoire Plasma et Conversion d’énergie (Laplace)” in the “Enseeiht (N7) site is shown in Fig. 3-6. The high-frequency electronic ballast that we used is presented in Fig. 3-1. A function generator (Yokogawa FN120) is used to generate two signals: the first one is the driving signals of the electronic ballast and the second one is the frequency-sweeping signal. A power source (Kikusui PCR 500M) is applied to supply our electronic ballast. A digital power meter (Yokogawa WT210) is used to measure the input current, voltage, power and power factor of the system. Arc images of MH lamps are captured by a digital camera (Nikon D3300). A digital Oscilloscope Tektronix TDS 2024 or Wavesurfer 3024 is used to measure the current, voltage and power of MH lamps. In addition, in order to detect and characterize AR phenomena, two kinds of online envelope circuits are proposed.

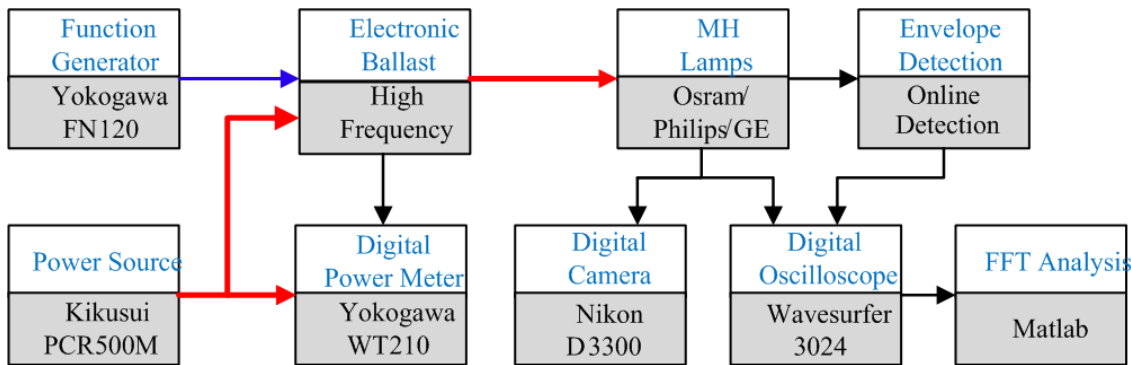


Fig. 3-6 Experimental set-up of the online AR detection

3.4 Online envelope detection for acoustic resonance

By reviewing literatures in chapter 2, there are no simple online detection methods that can be applied to real-time AR detection. On the other hand, when AR occurs in the lamps, the lamp voltage waveform is similar to the double side amplitude modulation. Based on those two reasons, two simple online envelope detection methods are proposed in this chapter.

Low frequencies of discharge arc flicker and arc fluctuations are observed in the arc tube of MH lamps, due to the excitation of AR. The reason of the low-frequency flicker or fluctuations in the presence of AR can be identified as acoustic streaming effects [1]. Those low-frequency movements on plasma arc result in fluctuations of the lamp voltage envelope.

3.4.1 Principle of envelope detection

The aim of the envelope detection is to recover the information signal of the amplitude modulation signal.

Amplitude modulation signal can be described as:

$$y(t) = (1 + m(t))c(t) = (1 + m(t))\cos \omega_c t \quad (3-3)$$

where $0 < \text{abs}(m(t)) \ll 1$ is the modulating signal, $1 + m(t)$ is the modulated (slowly time-varying with respect to the carrier) envelope of the signal, and $c(t)$ is the carrier. The information signal can be recovered by extracting the envelope of the amplitude modulated signal. Fig. 3-7 illustrates a signal and its envelope.

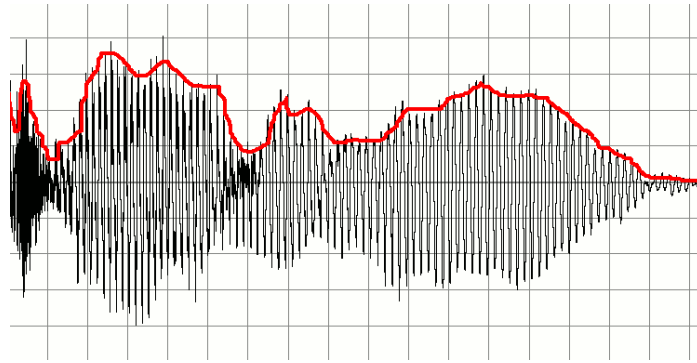


Fig. 3-7 A signal and its envelope marked in red [7]

An envelope detector is an electronic circuit that takes a high-frequency signal as input and provides an output that is the envelope of the original signal. Envelope detection methods can be categorized into two types: synchronous and asynchronous envelope detections. Fig. 3-8 shows the simplest envelope detector that was used by most portable radios for amplitude modulation radio signals reception.

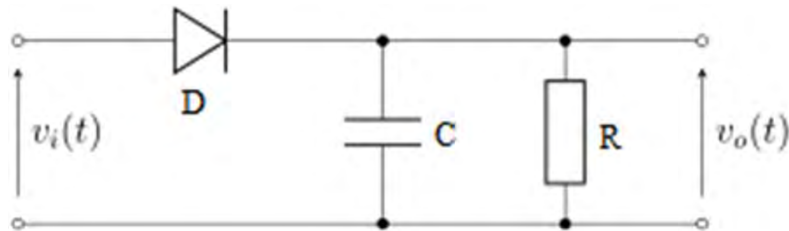


Fig. 3-8 A simple envelope detector [7]

In Fig. 3-8, a simple envelope detector consists of a diode D in series with a parallel combination of the resistor R and capacitor C . When the voltage across the diode D is greater than the threshold voltage, the capacitor is charged towards the peak values. When the voltage starts decreasing, D enters blocking state and the capacitor can only discharge via its shunt resistor R . With this circuit, there is a trade-off: if the RC time constant is too high, the waveform becomes a damped exponential when the envelope decreases quickly, leading to signal distortion. If the time constant is short, a portion of the carrier reaches the circuit output.

3.4.1.1 Synchronous envelope detection (Multiplier circuit)

The typical synchronous envelope detection is a multiplier detector. In the synchronous envelope detection, the incoming signal is multiplied by a locally generated carrier, and the resulting signal is passed through a low pass filter. In particular, the product of the incoming signal with the locally generated carrier yields,

$$\begin{aligned} [1 + m(t)] \cos^2 \omega_c t &= [1 + m(t)] \cdot \frac{1}{2} (1 + \cos 2\omega_c t) \\ &\rightarrow \frac{1}{2} [1 + m(t)] + \frac{1}{2} [1 + m(t)] \cos 2\omega_c t \end{aligned}$$

where $\omega_c = 2\pi f_c$ is the angular frequency of the carrier signal.

The spectral component of the first term is that of the baseband signal, and the spectrum of the second term is twice of the carrier frequency. Therefore, only the baseband signal remains at the output of the low-pass filter.

Fig. 3-9 illustrates a synchronous envelope detector. There are two requirements in a synchronous envelope detector. The first one is that the carrier frequency of the received input signal must be regenerated within the envelope detector to provide the local oscillator's signal. The other one is that the local oscillator output must be in-phase with the input signal. Its main advantage with respect to the previous one is a better linearity.

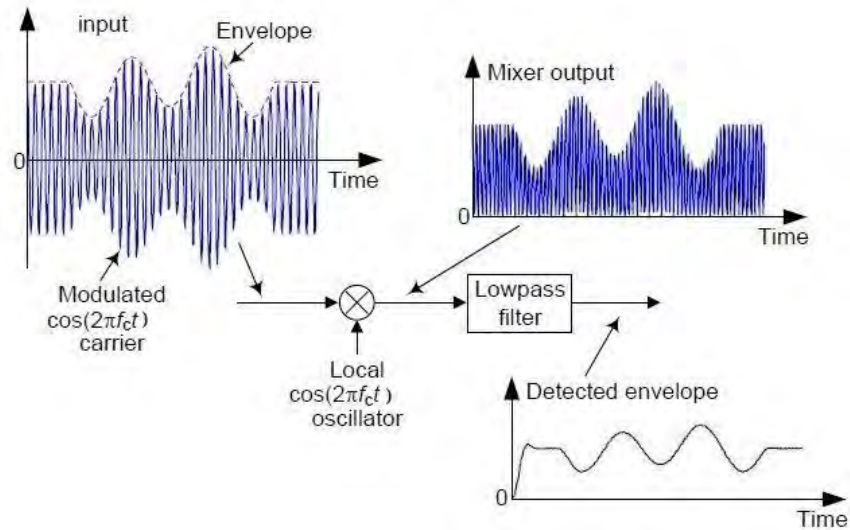


Fig. 3-9 Synchronous full-wave envelope detector [8]

3.4.1.2 Asynchronous full-wave envelope detection (Rectifier circuit)

An asynchronous envelope detector is a kind of envelope detector without the reference signal. Fig. 3-10 shows the schematic of the asynchronous envelope detector. The input frequency of the low pass filter is $2f_c$ Hz. Therefore, the harmonic is more thoroughly attenuated by the low pass filter. There is a slight difference in the noise transfer function of this circuit with respect to the previous one. During the carrier zero crossing, the noise itself is rectified, leading potentially to a small offset.

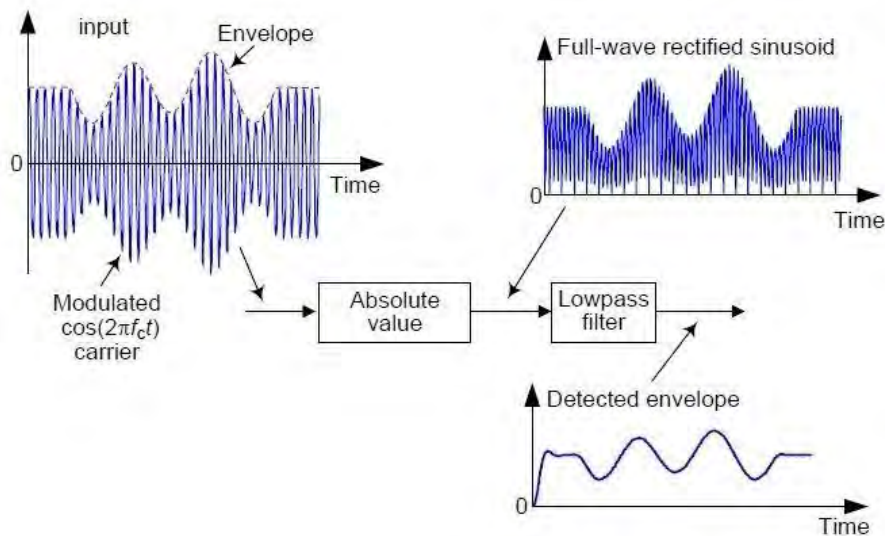
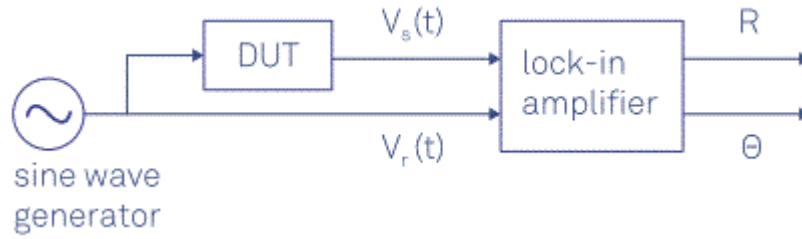


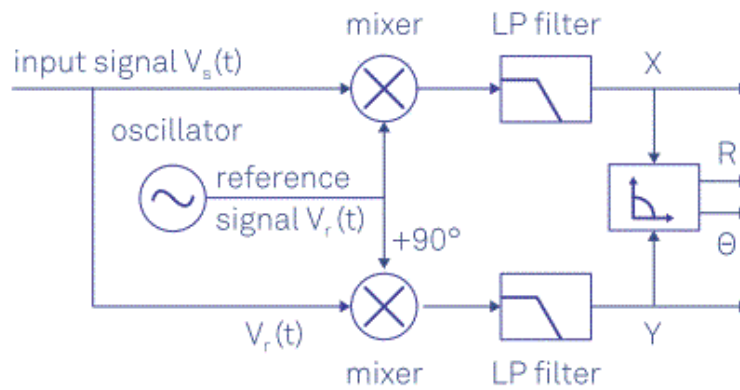
Fig. 3-10 Asynchronous full-wave envelope detector [8]

3.4.1.3 Synchronous complex envelope detection (Lock-in amplifier)

A lock-in amplifier is a type of synchronous complex envelope detector that can extract a signal with a known carrier waveform from an extremely noisy environment. The lock-in amplifier performs a multiplication of its input with a reference signal, also called heterodyne or homodyne detection, and then an adjustable low-pass filter is applied to obtain the final results. Fig. 3-11 shows the detection principle of a lock-in amplifier.



(a) Diagram of a typical lock-in amplifier measurement



(b) Schematic of a lock-in amplifier

Fig. 3-11 Detection principle of a lock-in amplifier [9]

In Fig. 3-11 (a), in a typical measurement, the device under test (DUT) is stimulated by a sinusoidal signal. The input signal $V_s(t)$ and the reference signal $V_r(t)$ are used by the lock-in amplifier to determine the amplitude R and θ . In Fig. 3-11 (b), the input signal is split and separately multiplied by the reference signal and 90° phase shifted with respect to the reference signal. The outputs of the mixer then pass low pass filters, resulting in two outputs in-phase X and in-quadrature component Y . The relationship between the amplitude R and the phase θ can be derived from X and Y , as presented in Eq.3-4.

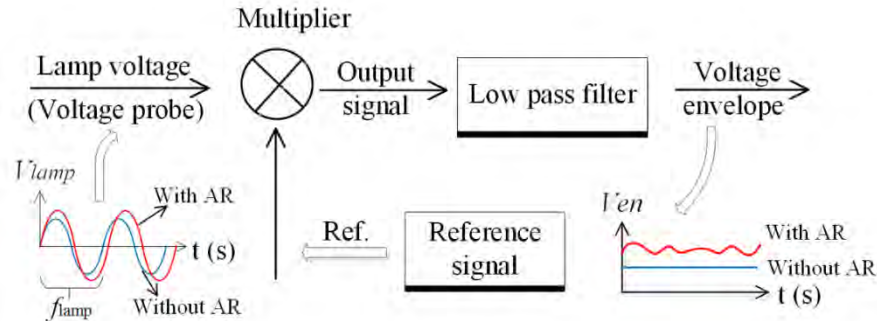
$$\begin{aligned} R &= \sqrt{X^2 + Y^2} \\ \theta &= \arctan(Y, X) \end{aligned} \quad (3-4)$$

3.4.2 Principle of synchronous voltage envelope detection

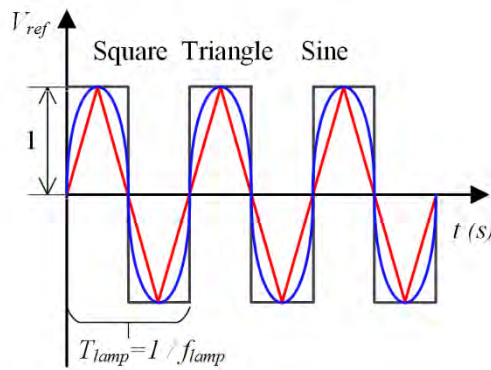
For lamps, three kinds of signals: lamp voltage, current, and power [10], can be used as the inputs of an envelope detector. In our experiment, the lamp voltage is chosen as the input of the envelope detector. On one hand, the lamp voltage variations are more pronounced than current and power when AR occurs in HID lamps. On the other hand, current needs to be sampled by a current sensing resistor or current transformer which is expensive. Consequently, the voltage envelope is retained in our experiment.

Fig. 3-12 presents the envelope detection principle in the experiment. There are two input signals in the multiplier, one is the lamp voltage that comes from the differential probe, and the other one is the reference signal.

The reference signal can be the driving signal of the electronic ballast itself or different kinds signals but must be in-phase with the lamp voltage. The maximum amplitude of the input signal of the lock-in amplifier (SR830) or the multiplier is 1 V. Thus, a differential probe whose attenuation ratio gain is 1/200 or 1/20 is used. Finally, a low-pass filter is used to get low-frequency fluctuations of the lamp voltage envelope.



(a) Diagram of voltage envelope detection



(b) Reference signals

Fig. 3-12 Principle of voltage envelope detection

3.4.2.1 Mathematical model of amplitude modulation for synchronous envelope detection

In Fig. 3-12 (b), three kinds of signals: square wave, triangle wave, and sinusoidal wave, can be used as the references signals of the synchronous envelope detection.

a) Square wave as the reference signal

The lamp voltage in the presence of AR can be expressed as follows:

$$V_{lamp} = (1 + m(t)) \cdot c(t) = (1 + m(t)) \cos \omega t \quad (3-5)$$

where $m(t)$ is the acoustic signal and the carrier signal is $c(t) = \cos \omega t$.

When the reference signal is a symmetric square wave signal. According to the Fourier series, a 50% duty-cycle square wave consists of odd order harmonic sine waves with a fundamental at the same frequency as the square wave.

Fourier series of the square wave is given by Eq.3-6,

$$V_{ref} = \frac{4A}{\pi} \sum_{n=1}^{\infty} \frac{\sin(2n-1)\omega t}{2n-1} \quad (3-6)$$

where A is the peak amplitude of the square wave.

The output of the multiplier can be written as:

$$y(t) = V_{lamp} \cdot V_{ref} \quad (3-7)$$

when $A=1$, which can be rewritten as

$$y(t) = \frac{2}{\pi} + \frac{2}{\pi} m(t) - \frac{2}{\pi} (1 + m(t)) \cos 2\omega t + \frac{2}{\pi} (1 + m(t)) \sum_{n=1}^{\infty} \frac{1}{2(2n+1)} [\cos 2n\omega t - \cos 2(n+1)\omega t] \quad (3-8)$$

b) Triangle wave as the reference signal

Fourier series of the triangle wave

$$V_{ref2} = \frac{8}{\pi^2} A \sum_{n=1}^{\infty} (-1)^{n-1} \frac{1}{(2n-1)^2} \sin(2n-1)\omega t \quad (3-9)$$

Similarly, when $A=1$,

$$y_2(t) = \frac{4}{\pi^2} + \frac{4}{\pi^2} m(t) - \frac{4}{\pi^2} (1 + m(t)) \cos 2\omega t + \frac{4}{\pi^2} (1 + m(t)) \sum_{n=1}^{\infty} (-1)^n \frac{1}{(2n+1)^2} [\cos 2n\omega t - \cos 2(n+1)\omega t] \quad (3-10)$$

c) Sine wave as the reference signal

Fourier series of sine wave

$$V_{ref3} = A \sin \omega t \quad (3-11)$$

Similarly, when $A=1$

$$y_3(t) = \frac{1}{2} + \frac{1}{2} m(t) - \frac{1}{2} (1 + m(t)) \cos 2\omega t \quad (3-12)$$

As can be seen from Eq. 3-8, Eq. 3-10 and Eq.3-12, after the lamp voltage and the reference signal passing the synchronous envelope detector, the output signals of the mixer contain *DC* component, acoustic signal component $m(t)$, and upper even harmonic components. Both Eq. 3-8 and Eq. 3-10 contain the upper even harmonics. However, in Eq.3-10, the even harmonics decrease as $1/(2n+1)^2$ instead of $1/(2n+1)$ in equation Eq.3-8. In Eq.3-12, the output signal just contains the second harmonics. The low-frequency acoustic signal $m(t)$ can be recovered by a low-pass filter. Therefore, after the lamp voltage passing the low-pass filter $m(t)$ contains the minimum harmonics when the reference signal is the sine wave.

A low-pass filter is a filter that passes signals with a frequency lower than a certain cutoff frequency and attenuates signals with frequencies higher than this cutoff frequency. The amount of attenuation for each frequency depends on the filter design.

3.4.3 Implemented methods

In our experiment, both synchronous and asynchronous envelope methods are applied to detect the lamp voltage envelope. The synchronous real envelope detection is implemented by a multiplier circuit, which will be presented in section 3.4.4. The asynchronous full-wave envelope is achieved by a simple rectifier consisting an amplifier and several resistors and capacitors, and it will be presented in section 3.4.5. The synchronous complex envelope detection is implemented by a lock-in amplifier and it will be presented in chapter 4.

3.4.4 Multiplier envelope detection for acoustic resonance

3.4.4.1 Schematic of detection circuit and test bench

The schematic of the multiplier AR detection is shown in Fig. 3-13. Fig. 3-14 illustrates our test bench and the multiplier circuit. The multiplier circuit is based on an AD633 that is a functionally complete, four-quadrant and analog multiplier. It includes high impedance, differential X , and Y inputs, and a high impedance summing input Z . The low impedance output voltage is a nominal 10 V full scale provided by a buried Zener diode. W is the output that can be expressed as follows in Eq. 3-13:

$$W = \frac{(X_1 - X_2)(Y_1 - Y_2)}{10} + Z \quad (3-13)$$

X_1 is the input signal V_{lamp} and Y_1 is the reference signal V_{ref} which comes from the controller or a phase locked loop (PLL). X_2 and Y_2 are connected to the ground. Z can be used to adjust the offset of the output signal. The amplitude of the reference signal in the multiplier circuit is 1 V. A differential probe which attenuation ratio is 1/20 is used in this experiment. The operating frequency of the ballast is from several kHz up to several ten kHz. Low-frequency 5-20 Hz voltage fluctuations appear in the lamp voltage [11]. The aim of this multiplier envelope detection is to extract these low-frequency voltage envelopes. Therefore, a low-pass filter is used to recover them. The cutoff frequency of this low-pass filter should be higher than 20 Hz and lower than 50 Hz in order to extract these low-frequency signals and avoid the AC 50 Hz line signal.

In our experiment, a simple RC filter is used, and the cutoff frequency f_c is 34 Hz, which is determined by the time constant ($R_1=1$ k Ω and $C_4=4.7$ u F) described as follows:

$$f_c = 1 / 2\pi R_1 C_4 \quad (3-14)$$

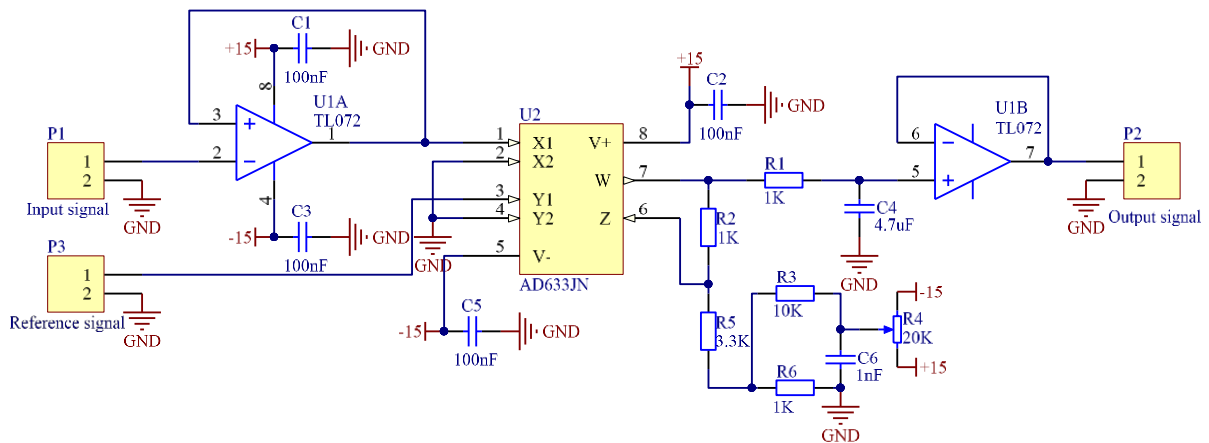
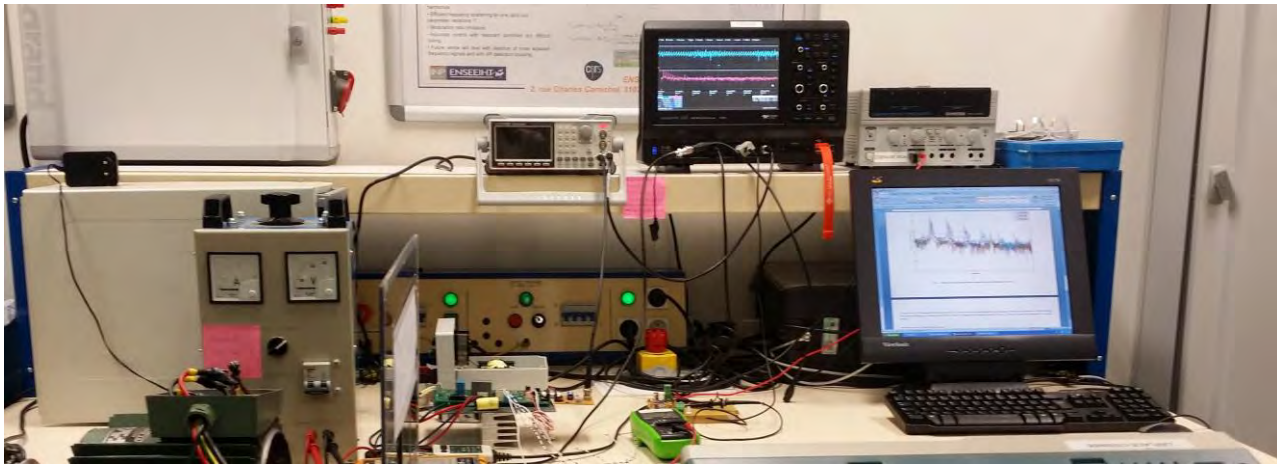
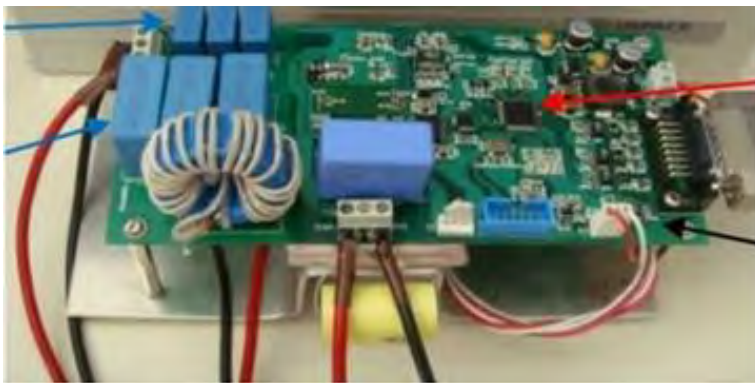


Fig. 3-13 Schematic of multiplier detection circuit



(a) Our test bench



(b) Electronic ballast



(c) Multiplier detect circuit

Fig. 3-14 Experimental bench

3.4.4.2 AR real-time detection with the proposed multiplier circuit

AR intensities can be classified into several levels, according to observed arc fluctuations. In the previous paper [12], before the lamp extinguished, three intensities levels were evaluated by eyes, such as AR-free, slight AR, and serious AR. In our experiment, AR levels will be classified according to the peak value of the voltage envelope. The aim of this experiment is to evaluate the sensitivity of the proposed detection circuit. Therefore, the AR-free and slight AR levels are detected in different manufacturers' MH lamps. Meanwhile, an example detection is given when AR is at the serious level.

Fig. 3-15 shows the lamp voltage and voltage envelope variations at AR-free and serious AR situations in a GE MH lamp. Fig. 3-16, Fig. 3-17 and Fig. 3-18 show the arc shape and the relevant voltage envelope variations in AR-free and slight AR situations in GE, Osram, and Philips MH lamps. ($V_{en-peak}$ means the peak value of voltage envelope).

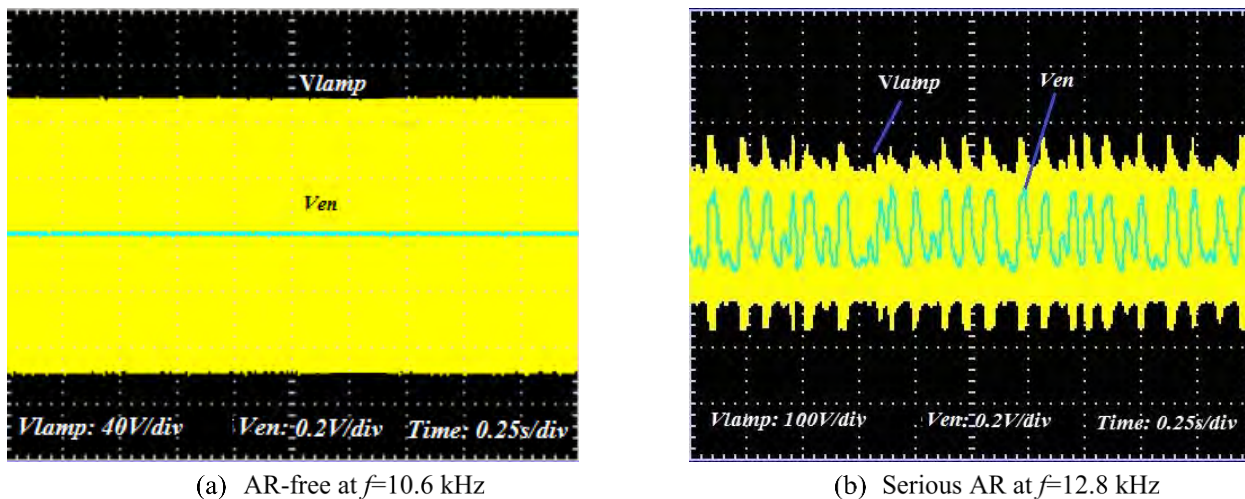


Fig. 3-15 Lamp voltage (V_{lamp} : Yellow) and lamp voltage envelope (V_{en} : Blue) in the GE MH lamp (Constant Color CMH)

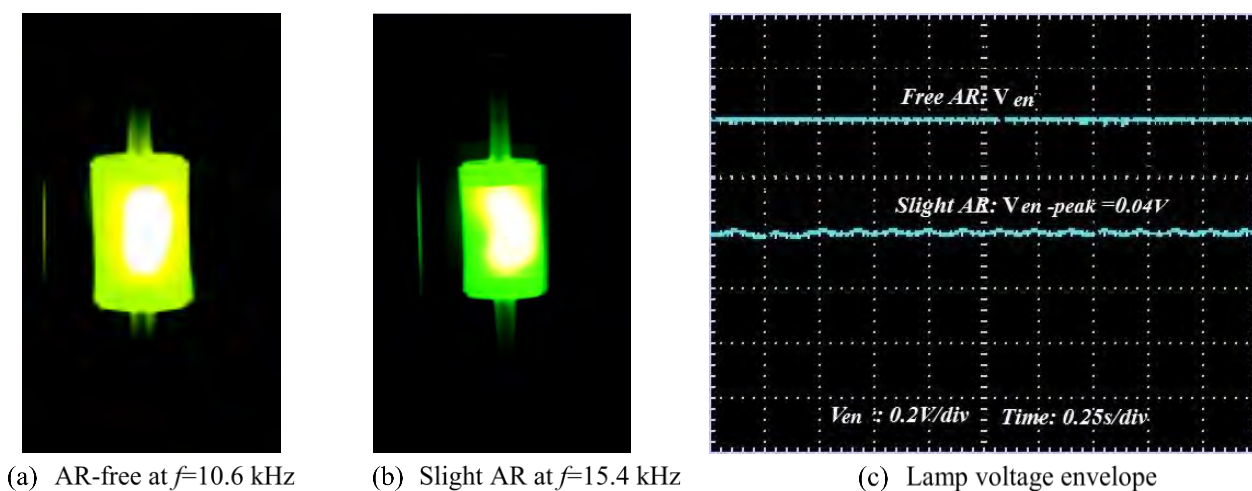


Fig. 3-16 Arc images and lamp voltage envelope (V_{en}) in the GE Constant Color MH lamp

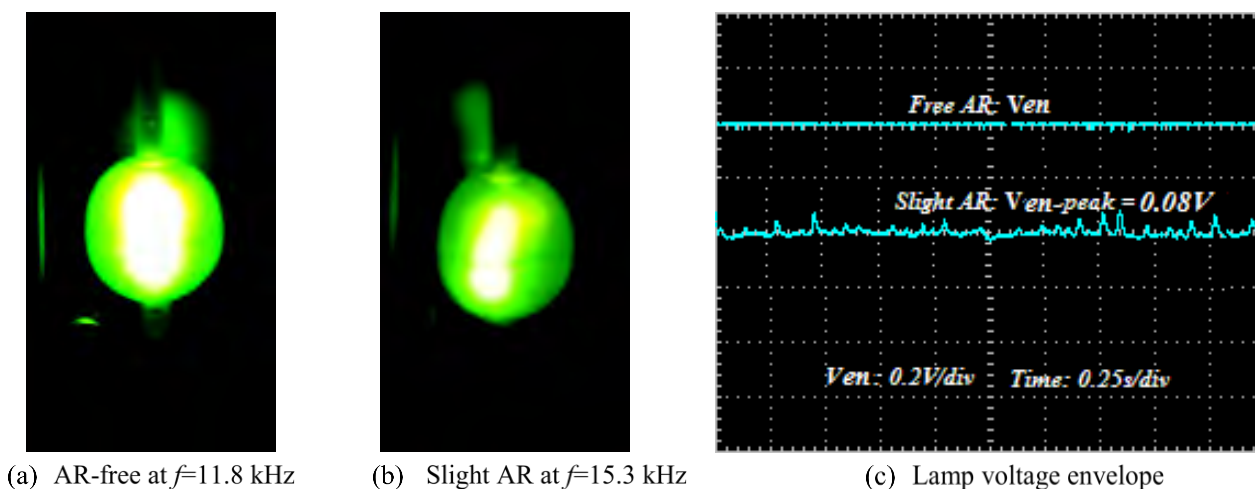


Fig. 3-17 Arc images and lamp voltage envelope (V_{en}) in the Osram Powerball HCI-TT MH lamp

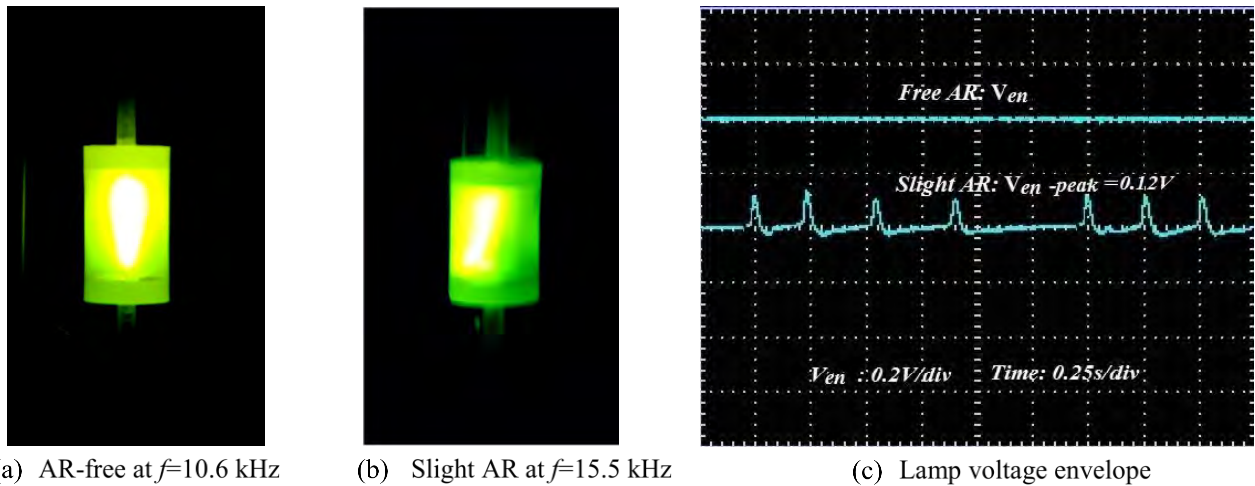


Fig. 3-18 Arc images and lamp voltage envelope (V_{en}) in the Philips Master CityWhite CDO-TT MH lamp

In this experiment, the oscilloscope is in AC mode for measuring the fluctuations of the lamp voltage only. This means the DC components of the lamp voltage is removed. As can be seen from Fig. 3-15, in the no AR situation at $f=10.6$ kHz, the lamp voltage V_{lamp} is constant, and thus the voltage envelope V_{en} is flat and no peak value are observed. In the AR situation, low-fluctuations are observed at $f=12.8$ kHz and the peak of the voltage envelope $V_{en-peak}$ is about 0.3 V. This result shows that whatever in the no AR or AR case, our detection circuit can follow the lamp voltage envelope correctly.

In Fig. 3-16, the arc is straight and there is no light flicker in the AR-free case at $f=10.6$ kHz in the GE MH lamp. Meanwhile, no voltage envelope variations are observed. However, the arc bends a little, voltage envelope variations are detected, and low-frequency fluctuations are observed from the lamp arc, even if the AR level is slight at $f=15.4$ kHz. Furthermore, the common phenomenon is found in Osram and Philips MH lamps as well, as shown in Fig. 3-17 and Fig. 3-18. No deformations of the arc are observed, and the voltage envelope are constant at AR-free situation. The arcs bend, and the relevant voltage envelope variations are observed in the presence of AR. The experimental results show our detection circuit can distinguish AR-free and slight AR cases.

As can be seen from Fig. 3-16, Fig. 3-17, and Fig. 3-18, at slight AR level, the peak values of the lamp voltage envelope $V_{en-peak}$ are 0.04 V, 0.08 V, and 0.12 V respectively, and all these values are below 0.2 V. At the same time, no serious light flickers are observed from the lamp arc and the lamps are not extinguished. In these cases, we regard the lamps are at slight AR levels. In Fig. 3-15, $V_{en-peak}$ is about 0.3 V, and meanwhile, the serious light flickers are observed and just several seconds later, the lamps will be extinguished. These cases can be regarded as serious AR levels. Otherwise, if the peak value of voltage envelope $V_{en-peak}$ is less than 100 times of 0.2 V and no light flickers are observed, which can be regarded as the AR-free case. Therefore, we propose a new criterion to classify different AR levels according to the peak value of voltage envelope $V_{en-peak}$ and the observations of light flicker. TABLE 3-1 shows our criterion for classify different levels.

TABLE 3-1 Criterion of different AR levels

AR-free level	Slight AR	Serious AR
$V_{en-peak} \leq 2 \text{ mV}$	$2 \text{ mV} < V_{en-peak} \leq 200 \text{ mV}$	$V_{en-peak} > 200 \text{ mV}$

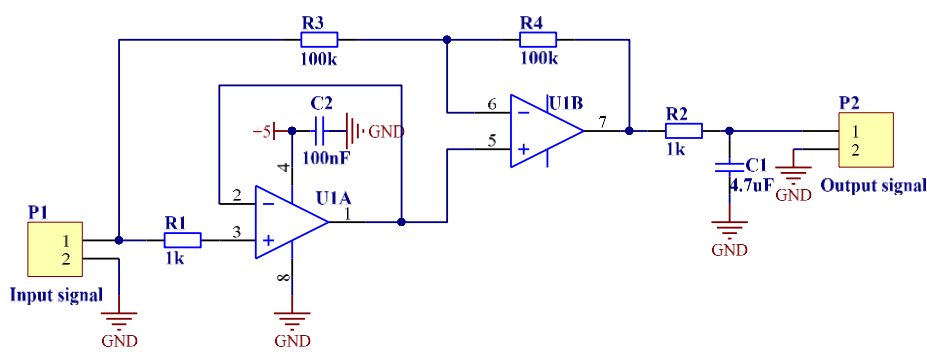
Comparing our results with the results in the literatures [12], [13], our circuit can detect the peak value of the lamp voltage envelope reaching to 0.04 V, whereas their circuits just can detect 0.2 V, 0.5 V respectively. This

means the sensitivity of our circuit is several to ten times to their circuits. Thus, the voltage envelope detection with a multiplier has been proven to be a high-sensitivity method to detect AR phenomena in MH lamps. The proposed online circuit cannot only trace the voltage envelope but also have a higher sensitivity than others to distinguish the AR-free level from the slight AR level. The more serious AR, the much greater voltage envelope variations are detected. This real-time detection is achieved and could be embedded into ballast board, leading to characterize AR phenomena quite easily.

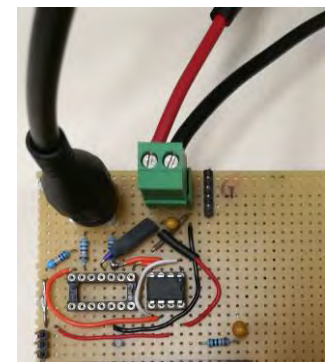
3.4.5 Rectifier envelope detection for acoustic resonance

3.4.5.1 Schematic of detection circuit

As we presented in section 3.4.1, an asynchronous full-wave envelope detection is a simple and straightforward method to extract the envelope of the signal. Based on this principle, a simple rectifier circuit is designed, and the schematic of this circuit is shown in Fig. 3-19.



(a) Schematic of the rectifier



(b) Rectifier circuit

Fig. 3-19 AR detection with rectifier circuit

In Fig. 3-19, *UI* is the operational amplifier AD804. When the input signal is negative, the *UIA* output is clamped at ground level while the *UIB* works as an inverter and thus the output signal is equal to the negative input. When the input signal is positive, the *UIA* works as a voltage follower and the output is equal to the input. The low-pass *RC* filter that is as same the multiplier envelope detection is used to extract low-frequency fluctuations of the lamp voltage envelope. This filter is composed of resistor R_2 and capacitor C_1 , and the cutoff frequency is 34 Hz as well.

3.4.5.2 AR Real-time detection with proposed rectifier circuit

In this experiment, two 150W Osram MH lamps were tested. In this kind of lamps, AR phenomenon is very intensive and always causes lamp extinction. As presented in the paper [14], AR level increases with the rise of the operating power in HID lamps. In order to make the lamp work at a stable operating point and avoid lamp extinction and explosion, the lamp operating power is lower than the nominal power. Fig. 3-20 illustrates the arc shapes in the AR and no AR situations.

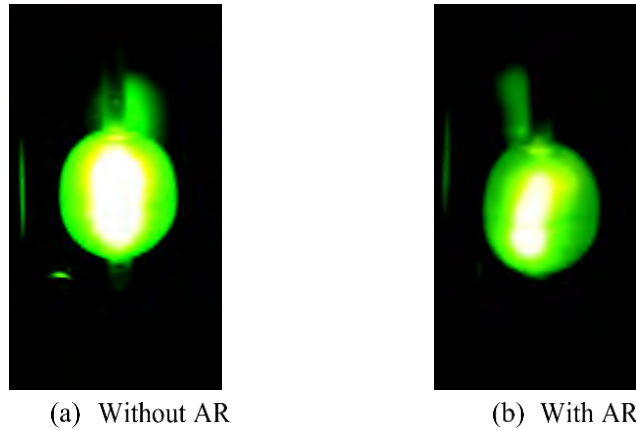
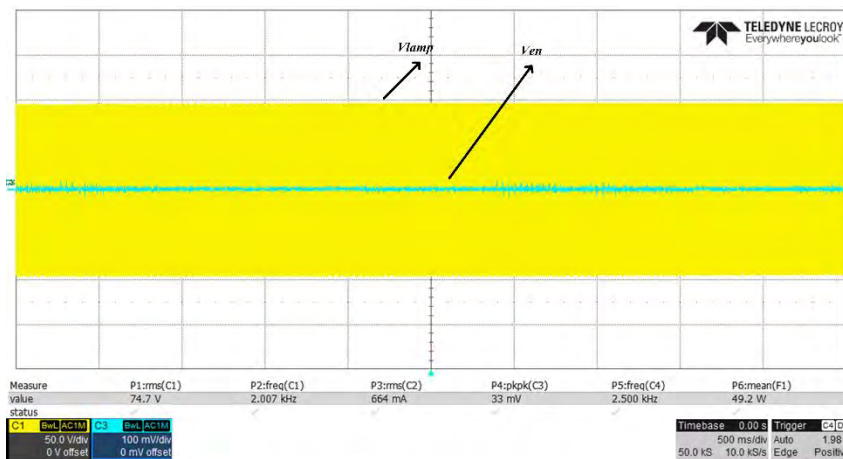


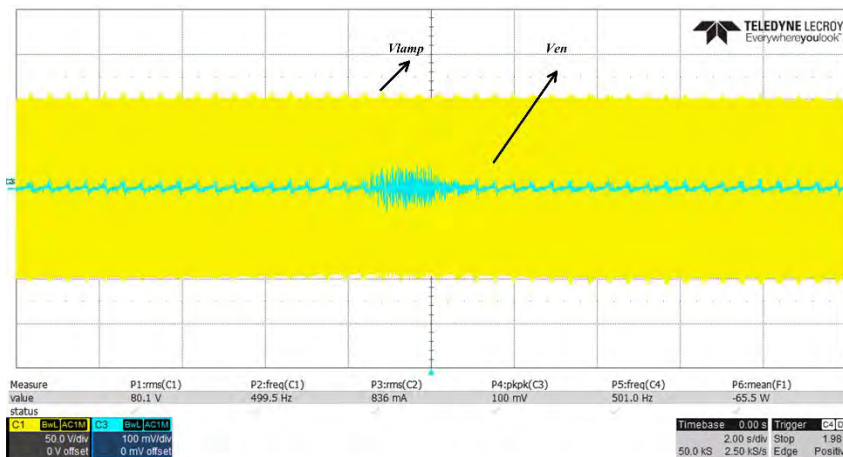
Fig. 3-20 Lamp arc shape in the Osram Powerball HCI-TT MH lamp

When MH lamps work at the no AR situation, there is no flicker and the lamp arcs are straight. The arc image of MH lamps at the normal situation is shown in Fig. 3-20 (a). Conversely, the arcs bend and the light flashes due to the AR phenomenon. Arc discharge deformations can be clearly observed in Fig. 3-20 (b).

Fig. 3-21 illustrates the lamp voltage (yellow) and the voltage envelope (blue) in no AR and AR situations. The lamp voltage envelopes (blue) are detected by the proposed rectifier circuit.



(a) In the no AR ($f=18.0$ kHz and $P_{lamp}=64$ W)



(b) Periodic AR signal ($f=17.1$ kHz and $P_{lamp}=65$ W)

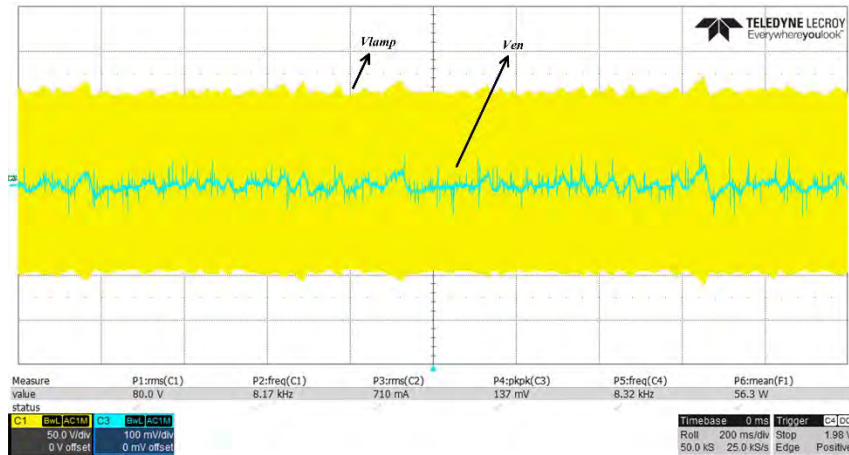

 (c) Stochastic AR signal ($f=16.9$ kHz and $P_{lamp}=65$ W)

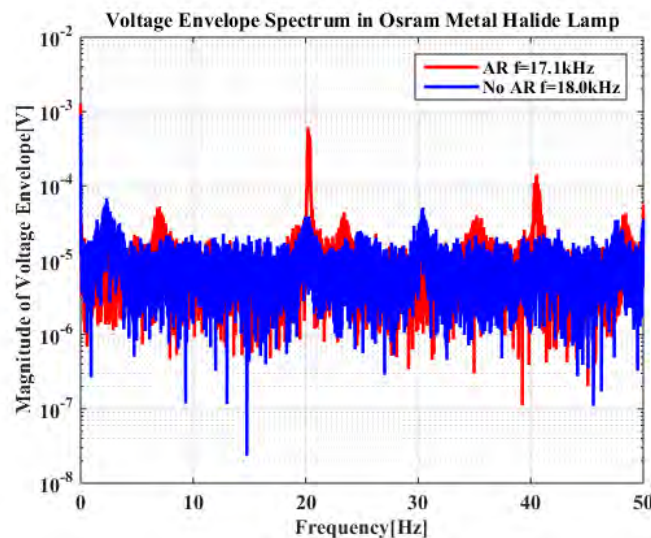
Fig. 3-21 Lamp voltage and voltage envelope in AR and no AR situations in the Osram MH lamp (Yellow: lamp voltage, blue: voltage envelope)

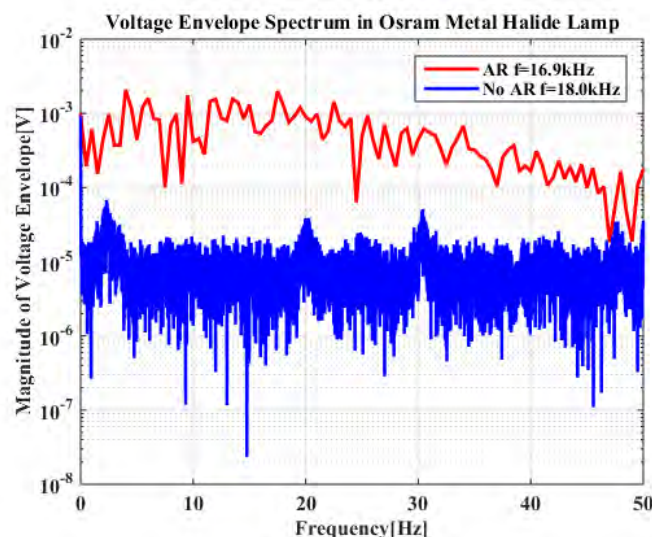
In Fig. 3-21, the proposed rectifier circuit can follow the lamp voltage envelope correctly whatever in the AR situation or no AR situation. In Fig. 3-21 (a), in no AR situation, the lamp voltage is constant, and the lamp voltage envelope is constant as well. In Fig. 3-21 (b), when AR occurs at $f=17.1$ kHz, low-frequency periodic variations are observed in the lamp voltage and the proposed rectifier circuit follows this periodic voltage envelope too. In Fig. 3-21 (c), at $f=16.9$ kHz with AR, the rectifier circuit also follows the stochastic variations of the lamp voltage.

To conclude, the designed circuit can detect the lamp voltage variation, follow the lamp voltage envelope, and distinguish AR and AR-free cases effectively.

3.4.5.3 Characterizations of voltage envelope

As presented in section 3.4.5.2, periodic and stochastic signals are detected in the voltage envelope by our rectifier circuit. In order to verify those conclusions, fast Fourier transform (FFT) is used to analyze the voltage envelopes shown in Fig. 3-21. Fig. 3-22 illustrates the results of FFT analysis of voltage envelopes, where original differences in the behavior of the lamp voltage envelope can be verified: periodic and stochastic.


 (a) FFT analysis of the periodic voltage envelope with AR ($\Delta f=0.01$ Hz) in Fig. 3-21 (b)



(b) FFT analysis of the stochastic voltage envelope with AR ($\Delta f=0.5$ Hz) in Fig. 3-21 (c)

Fig. 3-22 FFT analysis of voltage envelopes in the Osram MH lamp

In Fig. 3-22 (a), the fundamental frequency of the voltage envelope is 20 Hz, when AR occurs at $f=17.1$ kHz in the Osram MH lamp. This means that low-frequency fluctuations appear in the lamp voltage and these fluctuations are 20 Hz periodic signals. In Fig. 3-22 (b), the lamp voltage envelope is a stochastic signal in the presence of AR at $f=16.9$ kHz. Additionally, during the low-frequency domain (0-50 Hz), the amplitude of the voltage envelope in the AR case is much higher than the amplitude in the no AR case, about 100 times. FFT analysis of the voltage envelope shows that AR can cause the periodic or stochastic signal in the lamp voltage envelope. In addition, by observing the arc motion, we also find that the periodic voltage envelope and the stochastic voltage envelope are corresponding to the periodic arc flicker and the stochastic voltage envelope respectively. When the stochastic voltage envelope is detected, the AR phenomenon is more serious, and the lamp is easier to extinguish. Our experimental results are consistent with the results presented by J. Schwieger and others [1]. In their paper [1], the periodic arc flicker and the stochastic arc flicker were detected by a photodiode. They also concluded that these low-frequency fluctuations are most likely caused by temperature changes in the arc tube.

3.5 Electrical modeling of lamp voltage in presence of acoustic resonance

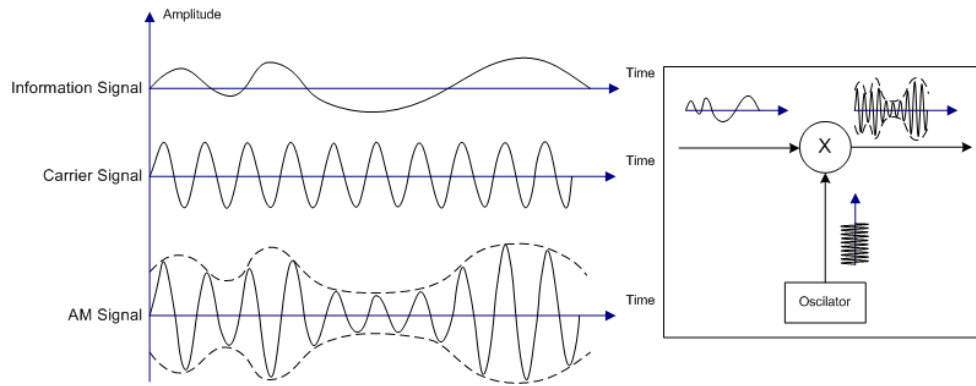
According to the experimental results in Fig. 3-21, the voltage waveform in the presence of AR is similar to the signal with amplitude modulation. Based on this fact, electrical modelings of the lamp voltage are built in PSIM software. By reviewing previous literatures, this approach was never encountered. Such modelings can be used by ballast circuit designers and engineers to explore solutions in simulation for AR avoidance.

3.5.1 Principle of lamp voltage modeling

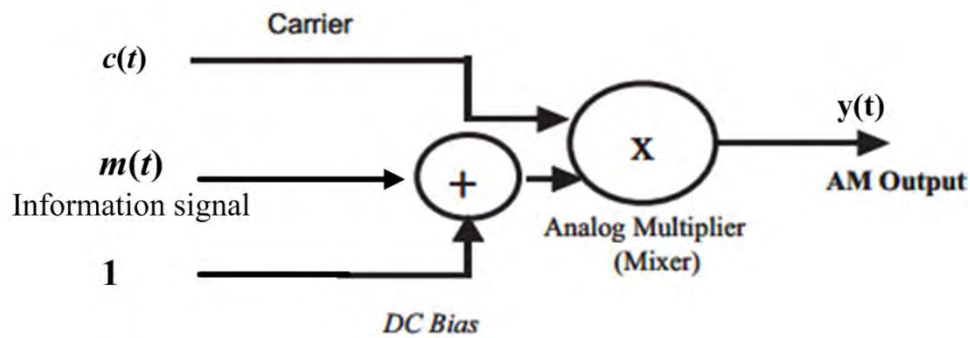
3.5.1.1 Amplitude modulation

Amplitude modulation is the amplitude of high frequency carrier wave is changed in accordance with the intensity of the information signal [15]. In amplitude modulation, only the amplitude of the carrier wave is

changed in accordance with the intensity of the signal. However, the frequency of the modulated wave remains the same i.e. carrier frequency. Fig. 3-23 shows the principle of amplitude modulation.



(a) Illustration of amplitude modulation [16]



(b) Block diagram of AM modulation [15]

Fig. 3-23 Principle of amplitude modulation

In Fig. 3-23 (b), $c(t)$ is the carrier signal and $m(t)$ is the information signal. When the carrier $c(t)$ is multiplied by the positive quantity $(1+m(t))$, the result $y(t)$ is:

$$y(t) = (1 + m(t)) \cdot c(t) \quad (3-15)$$

3.5.2 Electrical modelings of acoustic signals and acoustic resonance detection

Our simulation is based on the principle of amplitude modulation. Hence, the lamp voltage with AR occurrence can be expressed by Eq. 3-16:

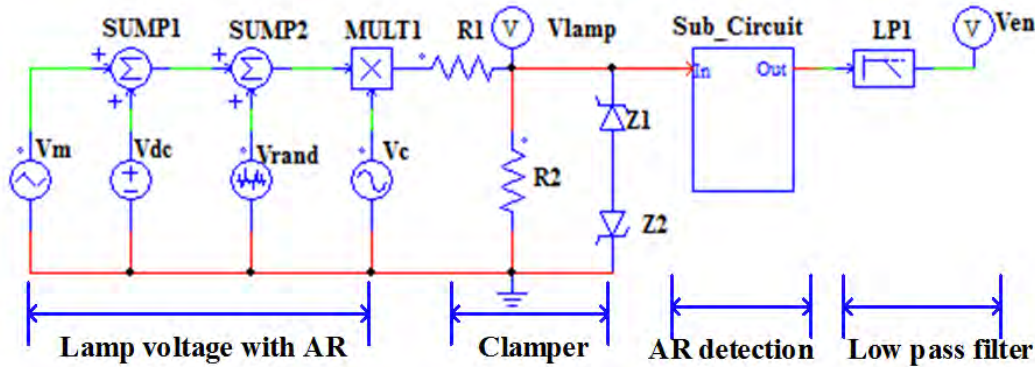
$$V_{lamp} = (V_m + V_{dc} + V_{rand}) \cdot \frac{R_2}{R_1 + R_2} V_C \quad (3-16)$$

V_m , V_{dc} , V_{rand} , and V_c represent the information signal, positive quantity, environmental noise, carrier signal respectively. Our simulations are built in PSIM according to Eq. 3-16.

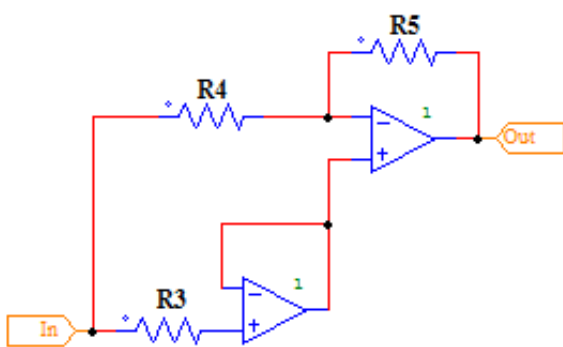
As explained in section 3.4.5, the periodic and stochastic information signals are detected in the lamp voltage. This means that two kinds of information signals modulate the lamp voltage. Here, two kinds of lamp voltage modeling are built as well. In [10], there are low-frequency fluctuations of current or voltage with AR occurrence in the MH lamps. In [18], a periodic or stochastic flicker is observed, when AR occurs in the MH lamps. These findings are consistent with our experimental results in Fig. 3-21. Thus, the periodic and stochastic fluctuations of the lamp voltage are simulated in Fig. 3-24 and Fig. 3-25 respectively.

3.5.2.1 Periodic acoustic signal with acoustic resonance

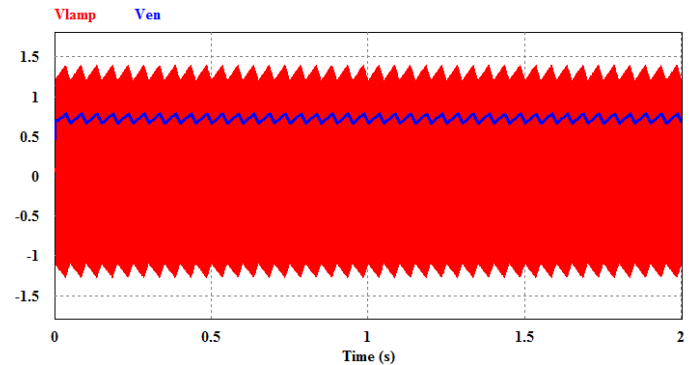
The periodic or stochastic signal is the information signal in the lamp voltage. In our simulation, different modelings are built by setting the parameters of V_m . Fig. 3-24 show the modeling of the lamp voltage with periodic acoustic signal.



(a) Lamp voltage modeling with periodic AR and AR detection



(b) AR detection circuit (Sub circuit in Fig. 3-24 (a))



(c) Simulated lamp voltage and voltage envelope (periodic AR)

Fig. 3-24 Modeling of lamp voltage with an example of periodic AR and AR detection

In Fig. 3-24 (a), the lamp voltage modeling is composed of four main parts: the lamp voltage with AR, the voltage divider and clamper, the AR detection and the low-pass filter. The voltage divider is used to protect the AR detection circuit during the lamp ignition. The clamper is used to limit the input voltage of the operational amplifier and the interference caused by noise fluctuations. The aim of the low-pass filter is to get low-frequency variations in the voltage envelope.

The amplitude and the frequency of V_m depend on AR intensity and which kinds of signals are observed in the lamp voltage envelope in the AR situation. V_{dc} is added in order to ensure that the $(V_m + V_{dc})$ is positive. V_{rand} is used to simulate the random noise from outside environment. The amplitude and the frequency of V_c depend on the operating state of the lamp. In the simulation, all of those parameters are set based on the experimental results in Fig. 3-21 (b). In Fig. 3-21 (b), the operating frequency of the lamp voltage is 17.1 kHz, and the RMS value of the lamp voltage is 80 V. According to the results in Fig. 3-22, the frequency of the periodic voltage envelope is 20 Hz. The parameter of the environmental noise V_{rand} is estimated. TABLE 3-2 illustrates the parameter setting in the simulation.

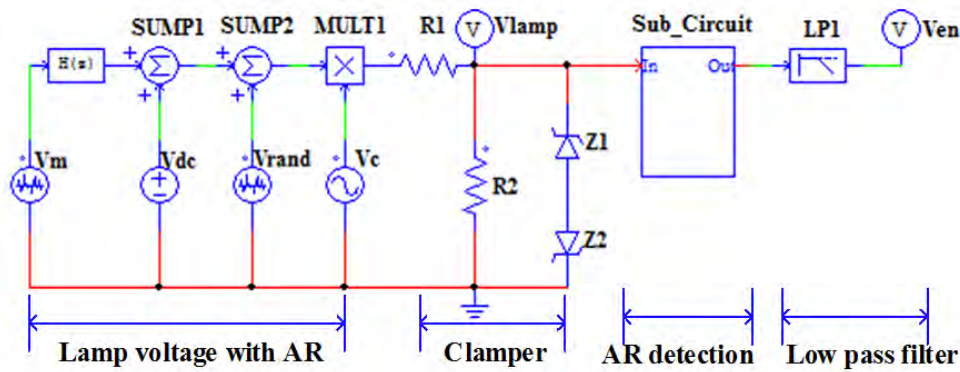
TABLE 3-2 Parameter setting of the lamp voltage with periodic modulation

Parameters	Source type	Frequency (Hz)	Peak amplitude (V)
V_m	Swath-wave source	20	0.1
V_{dc}	DC source	0	1
V_{rand}	Random voltage source	0	0.1
V_c	Sinusoidal voltage source	17100	113

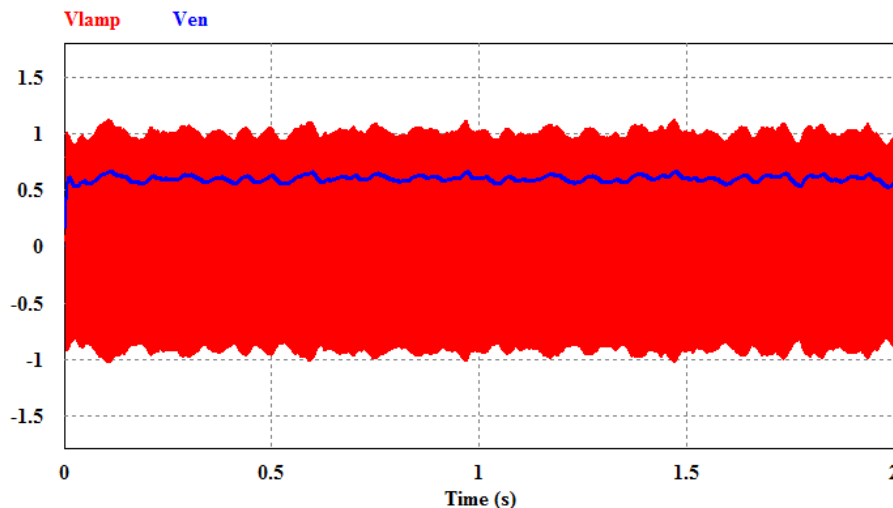
According to the results in Fig. 3-24 (c), the simulated lamp voltage with periodic acoustic signal is similar to the real lamp voltage in Fig. 3-21. In the simulation, the lamp voltage is divided by the voltage divider R_1 and R_2 . Therefore, the value of the simulated lamp voltage and the real lamp voltage are not exactly the same. In addition, the simulation results show that the rectifier circuit follow the lamp voltage envelope effectively.

3.5.2.2 Stochastic acoustic signal with acoustic resonance

Fig. 3-25 shows the modeling of the lamp voltage with stochastic acoustic signal. The AR detection circuit is as same as in Fig. 3-24 (b).



(a) Lamp voltage modeling with stochastic AR and AR detection



(b) Simulated lamp voltage and voltage envelope (stochastic AR) with second-order filter

Fig. 3-25 Modeling of the lamp voltage with an example of stochastic AR signal and AR detection

The modeling of the lamp voltage with stochastic AR signal is similar to the previous modeling. The difference between these two is that an autoregressive filter is added to fit the real AR signal in Fig. 3-25 (a). Other parameters are the same to the modeling in Fig. 3-24.

The purpose of this filter is to simulate a “random-walk” like behavior. Hence, the second order filter can be described as follows:

$$H(z) = \frac{1}{(1 - az^{-1})^2} \quad (3-17)$$

where q is the unit delay.

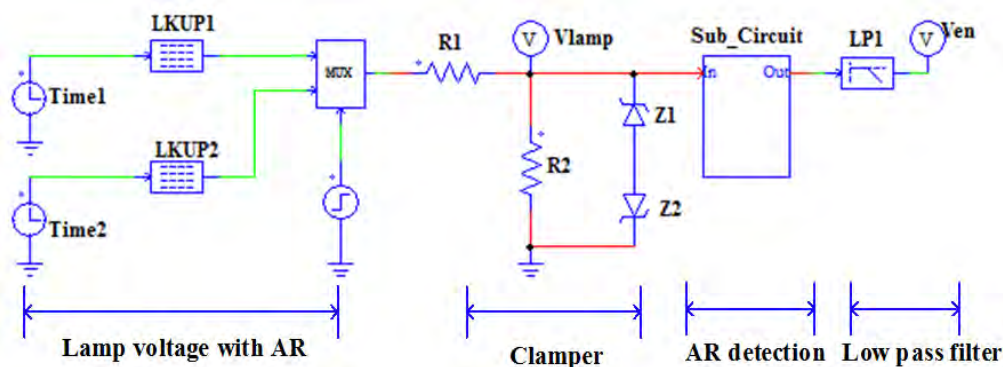
The second order filter is introduced in order to shape the noise auto-correlation function. By using a pole with multiplicity two, linear displacements can be observed on short-time intervals while on the average the perturbing signal is zero-mean. The duration of the linear phase is inversely proportional to the closeness of the pole to the -1 point.

According to the simulation results in Fig. 3-25 (b), the lamp voltage with a stochastic signal envelope can be simulated in our modeling. The simulated lamp voltage is similar to the real lamp voltage in Fig. 3-21 (c).

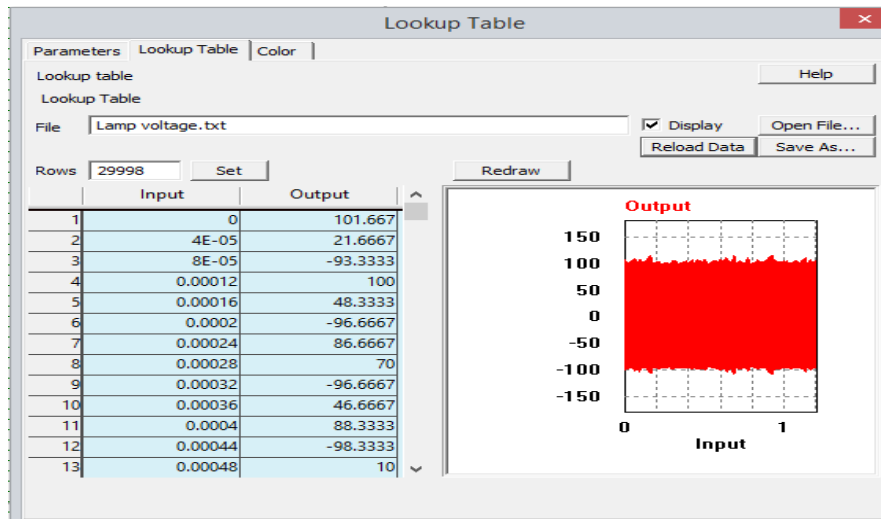
To conclude, our modelings are close to the real lamp voltage with AR occurrence. Simulation results also show that the rectifier detection circuit can follow the lamp voltage envelope effectively.

3.6 Lookup table of lamp voltage in the presence of acoustic resonance

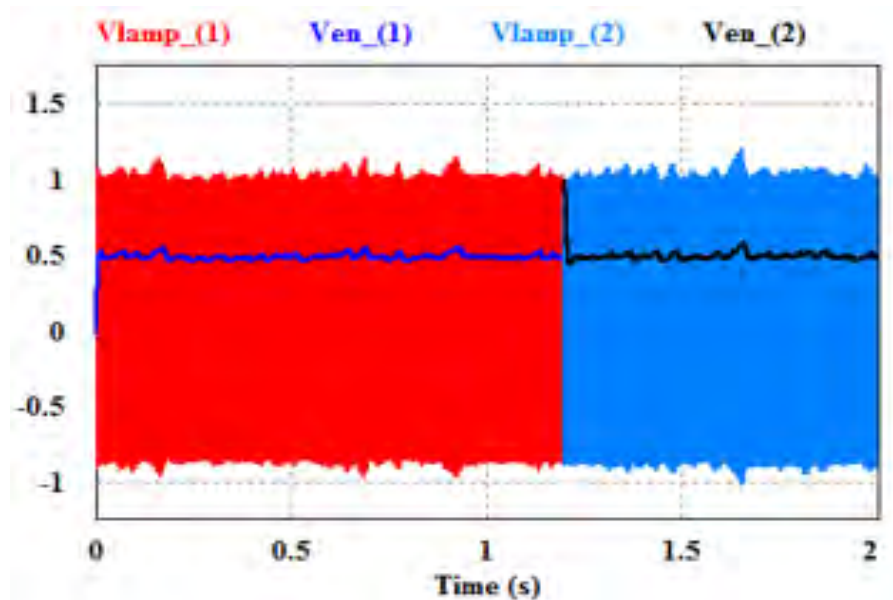
In order to simulate accurately the AR phenomenon, a real lamp voltage in the presence of AR is injected into a look-up table. The schematic is composed of four parts, the lookup table of lamp voltage, clamper, AR detection and low-pass filter, as shown in Fig. 3-26. The lookup table in PSIM just can be loaded limited data (maximum 30000 points). In order to simulate large time slots, two lookup tables are used to import the data of real lamp voltage from experimental results. Firstly, data of LKUP1 are imported and then data of LKUP2 are imported. These two intervals of simulation results are merged into Fig. 3-26 (c). In this simulation, the data of the lamp voltage with a stochastic acoustic signal are imported.



(a) Schematic of lamp voltage simulation and detection circuit using a look-up table



(b) The real data of lamp voltage in Fig. 3-21 (b)



(c) Lamp voltage and voltage envelope simulation

Fig. 3-26 Lookup table of lamp voltage and voltage envelope detection with AR

The AR detection circuit in Fig. 3-26 is the rectifier circuit presented. As can be seen from Fig. 3-26 (c), the lookup table can load the real lamp voltage and the designed detection circuit can follow the real voltage envelope well. To conclude, importing the real lamp voltage in the simulation can help designer search real-time control methods for ballast circuits and verify AR detection and avoidance methods just by simulations.

3.7 Summary of acoustic resonance characterizations

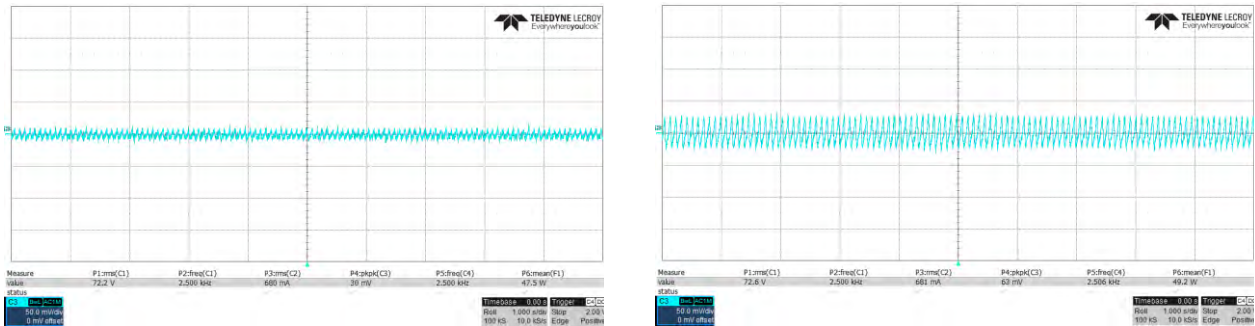
As presented in many literatures, AR causes the lamp arc fluctuation, arc rotation, arc bending, lamp extinction and in the worst case, lamp explosion. AR also can change electrical parameters of lamps, resulting in the lamp voltage increasing and the lamp current decreasing. In this section, AR characterizations are summarized as follows:

- 1) AR causes low-frequency fluctuations on the lamp voltage envelope. These low-frequency fluctuations can be periodic or stochastic fluctuations;

Which kinds of voltage envelope fluctuations appear on the lamp voltage depends on AR eigenfrequencies. In MH lamps, AR frequencies can be longitudinal, radial and axial fundamental frequencies or combinations of these three fundamental frequencies of the arc tube. Different AR frequencies cause different AR phenomena.

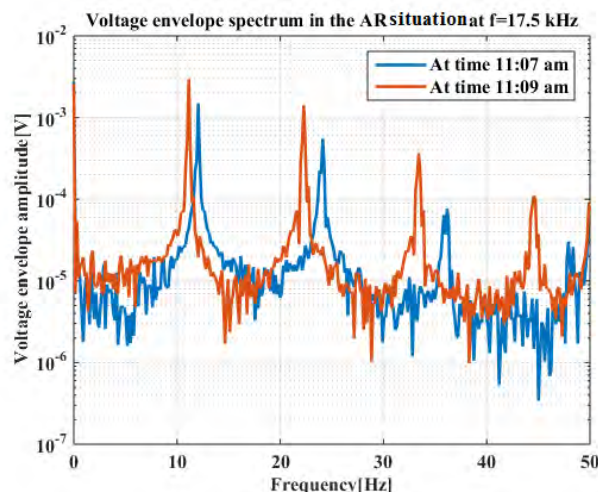
- 2) AR phenomenon is a dynamic process;

AR phenomenon is different at different AR eigenfrequencies. At the same frequencies, the AR phenomenon may change over time. Fig. 3-27 shows the lamp voltage envelope in the AR situation at $f=17.5$ kHz with different observed time.



(a) Voltage envelope at time 11:07 am

(b) Voltage envelope at time 11:09 am



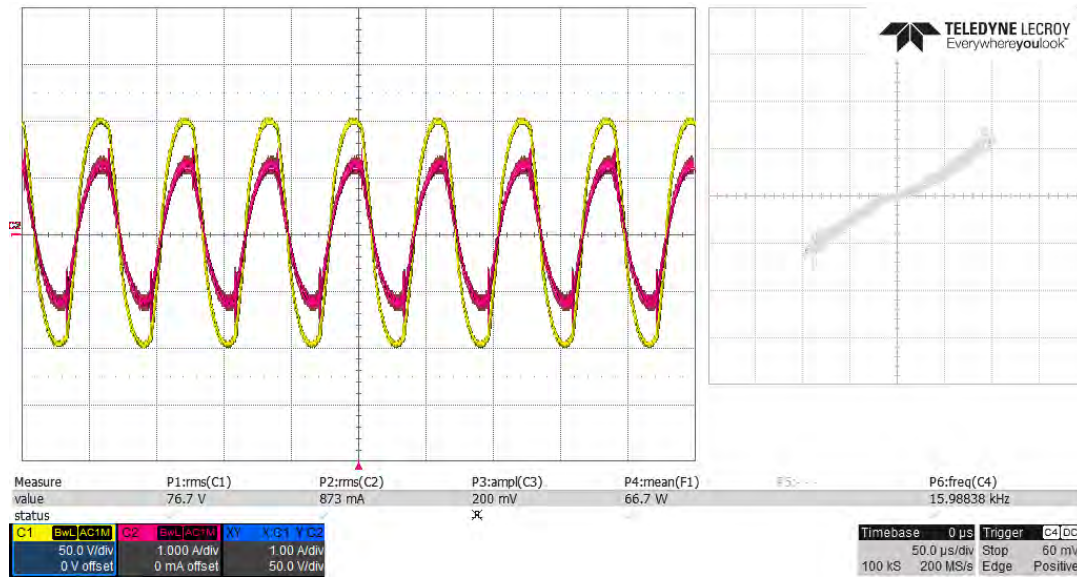
(c) Voltage envelope spectrum in the AR situation at time 11:07 am and 11:09 am

Fig. 3-27 Voltage envelope in the AR situation ($f=17.5$ kHz) at different observed time

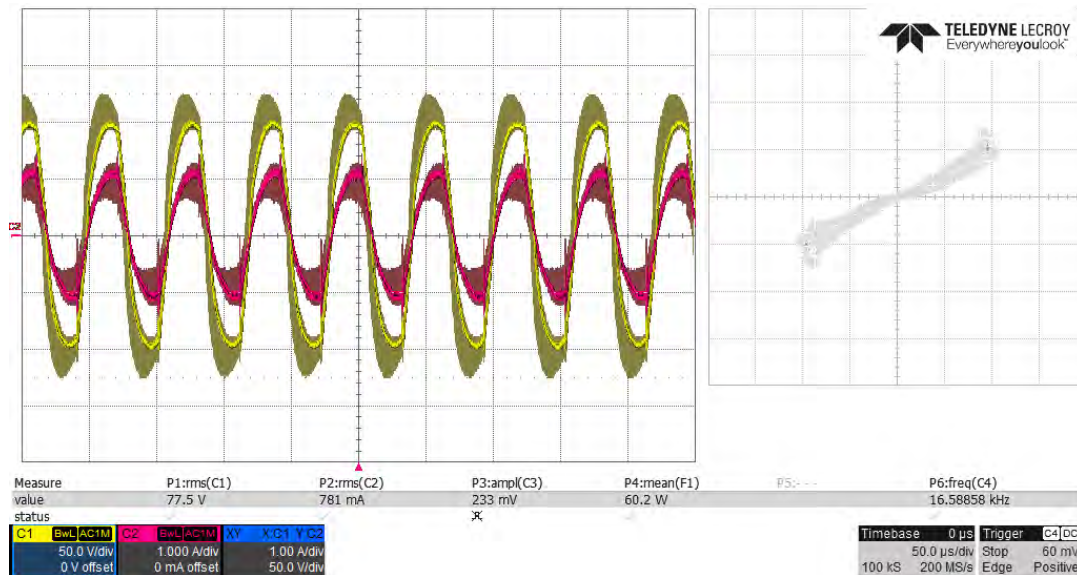
In Fig. 3-27, periodic voltage envelopes are detected in the lamp voltage. The lamp works in the AR situation at same frequency $f=17.5$ kHz. However, with time changing, the frequency of the voltage envelope changes from 12 Hz at 11:07 am to 11 Hz at 11:09 am, and the amplitude of the voltage envelope increases as well. This experimental result shows that the AR phenomenon is a dynamic process, and the manifestation and intensity of AR change over time.

- 3) Non-linear of I-V curve increase with AR occurrence.

Fig. 3-28 illustrates the waveforms of the lamp voltage and current, and I-V curves in no AR and AR situations.



(a) $f=16.0$ kHz without AR (Yellow: voltage, red: current)



(b) $f=16.7$ kHz with AR (Yellow: voltage, red: current)

Fig. 3-28 Voltage, current waveforms and I-V curve in the Osram MH lamp

In Fig. 3-28, these waveforms are obtained by the “persistence function” of the oscilloscope. With this function, several sampled waveforms are displayed on the same screen. By inspecting such waveforms, in the no AR situation, the voltage and current waveforms almost do not have fluctuations and I-V curve is close to linear. In the AR situation, obvious fluctuations are observed on the voltage and current waveforms. The non-linear characteristic of I-V curve increases. It could be concluded that AR changes the discharge state of plasma.

3.8 Conclusions

Two simple online envelope detection methods such as the multiplier and rectifier circuit are proposed, in order to quantify the real-time AR phenomena in MH lamps. A new criterion classifying AR levels is therefore

defined, based on the peak value of voltage envelope by our multiplier detection circuit. A threshold of 200 millivolts seems to be the border between no AR and slight AR levels related to observable arc motion.

In addition, periodic and stochastic voltage envelopes are detected by the proposed rectifier circuit in the AR situation. The experimental results also show that the rectifier can detect the voltage envelope effectively. Based on the amplitude modulation of the lamp voltage, the electrical modeling of the lamp voltage in the presence of AR are built as well. The simulation results show that the simulated modeling of the lamp voltage is close to the real lamp voltage.

The multiplier and rectifier circuits are online envelope detection, which could be embedded into the ballast board. This way, real-time control could be achieved, leading to the use of MH lamps at higher frequencies with AR avoidance. The electrical modeling of the lamp voltage could help the ballast circuit designer to search some solutions for AR detection and avoidance just by doing simulations.

References

- [1] J. Schwieger, M. Wolff, B. Baumann, F. Manders, J. Suijker, "Characterization of Discharge Arc Flicker in High-Intensity Discharge Lamps," in *IEEE Trans. on Industry Applications*, vol. 51, no. 3, pp. 2544-2547, May-June 2015.
- [2] F. F. Tao, "Advanced High-Frequency Electronic Ballasting Techniques for Gas Discharge Lamps," Ph.D. thesis, Virginia Tech, 2001.
- [3] J. M. Alonso, C. Blanco, E. Lopez, A. J. Calleja, M. Rico, "Analysis, design, and optimization of the LCC resonant inverter as a high-intensity discharge lamp ballast," in *IEEE Trans. Power Electronics*, vol.13, no.3, pp.573-585, May 1998.
- [4] <http://reefkeeping.com/issues/2007-03/sj/index.php>
- [5] J. Garcia-Garcia et al., "Using solid-state over-voltage protection devices for high intensity discharge lamps ignition," *Conference Record of the 2002 IEEE Industry Applications Conference*, Pittsburgh, USA, vol. 120, pp. 363-368, Dec. 2002.
- [6] J. C. Anton, F. Ferrero, A. Martin, N. Bordel, G. Zissis, S. Bhosle, "Acoustic Resonance Effects in High Pressure Sodium Lamps," *2007 IEEE Industry Applications Annual Meeting*, New Orleans, LA, 2007, pp. 479-483.
- [7] https://en.wikipedia.org/wiki/Envelope_detector
- [8] <https://www.dsprelated.com/showarticle/938.php>
- [9] <https://www.zhinst.com/applications/principles-of-lock-in-detection>
- [10] C. H. Yao, C. S. Moo, H. W. Chen, M. J. Soong, "Detection of acoustic resonance in metal halide lamps," in *Proc. IEEE International Symposium on*, vol. 2, pp. 881-885, Jun. 2001.
- [11] J. Zhou, L. Ma and Z. Qian, "A novel method for testing acoustic resonance of HID lamps," *Applied Power Electronics Conference and Exposition*, Dallas, TX, vol. 1, pp. 480-485, Mar. 1999.
- [12] C. S. Moo, C. K. Huang, Y. N. Hsiao, "High-frequency electronic ballast with auto-tracking control for metal halide lamps," in *Proc. IEEE IAS Annual Meeting*, vol. 2, pp. 1025-1029, Oct. 2003.
- [13] C. S. Moo, C. K. Huang, C. Y. Yang, "Acoustic-Resonance-Free High-Frequency Electronic Ballast for Metal Halide Lamps," *IEEE Trans. Industrial Electronics*, vol.55, no.10, pp.3653-3660, Apr. 2008.
- [14] J. Correa, M. Ponce, J. Arau, M. Sanchez, J. M. Alonso, "Evaluation of frequency modulation techniques to avoid acoustic resonances in electronic ballast for HID lamps: analysis and methodology," in *Proc. IEEE Power Electronics*, vol.10, pp.245-250, 17-22 Oct. 2004.
- [15] J. Héctor, C. Sturm, and J. Pontes, "Radio systems engineering: A tutorial approach," Springer, 2014.
- [16] https://upload.wikimedia.org/wikipedia/commons/8/8d/Illustration_of_Amplitude_Modulation.png

- [17] Y. Jiang, M. S. Shen, H. L. Z. M. Qian, "An adaptive acoustic resonance free electronic ballast for HID lamps," in Proc. IEEE IAS Annual Meeting, vol. 2, pp. 1020-1024, Oct. 2003.
- [18] J. Schwieger, M. Wolff, B. Baumann, F. Manders, J. Suijker, "Characterization of Discharge Arc Flicker in High-Intensity Discharge Lamps," in IEEE Trans. on Industry Applications, vol. 51, no. 3, pp. 2544-2547, May-June 2015

**Chapter 4 Statistical Method
for Acoustic Resonance Characterization
in Metal Halide Lamps**

4.1 Introduction

Two kinds of online envelope detection methods: multiplier and rectifier detection circuits were introduced in chapter 3. The results showed that the voltage envelope detection is a robust method to detect AR. To this end, we applied a lock-in amplifier which is a laboratory device used to measure and characterize the lamp voltage fluctuations as explained in this chapter. Statistical criteria based on the standard deviation (STD) of the voltage envelope are proposed to assess AR presence and classify its severity. The average lamp power and AR level are controlled by adjusting the input DC voltage and the lamp operating frequency of the high-frequency electronic ballast. The proposed criteria enabling to classify AR *versus* no AR cases use a two-dimensional plane plot, a boxplot, a histogram or an analysis of variance.

To corroborate those criteria, the light spectral variation detection is presented as well. In MH lamps, the plasma contains chemical radicals produced from argon, mercury and metal salts. The mixture of the radiations produced by these elements results in the required spectral irradiance and colorimetric parameters. In a normal situation, all the elements keep their chemical balance inside the arc tube. However, when AR occurs in the MH lamp, AR can shift this balance and cause some variations of the spectrum and colorimetric parameters; we will refer collectively to them as spectral variations. The spectral irradiance and colorimetric parameters are measured by a spectrophotometer. The STD and the relative standard deviation (RSD) of the spectral irradiance and colorimetric parameters are calculated to evaluate their variations as well.

Finally, the correlation between the voltage envelope detection and spectral variation detection is analyzed. Both the voltage envelope and spectral parameters contain low-frequency fluctuations in the AR situation. However, using a lock-in amplifier or a spectrophotometer for AR detection can only be performed in a laboratory, as the commercial devices are difficult and expensive to apply to real-world. In order to verify our designed online detection circuits, we compare different detection methods and evaluate advantages and disadvantage of each of them.

4.2 Experimental set-up at Laplace UPS

As presented in section 4.1, two kinds of AR detection methods, the voltage envelope and spectral variation detection will be proposed in this chapter. Therefore, the measurement parts of the experimental set-up are composed of electrical and spectral variation detection. Fig.4-1 shows the schematic of our experimental set-up.

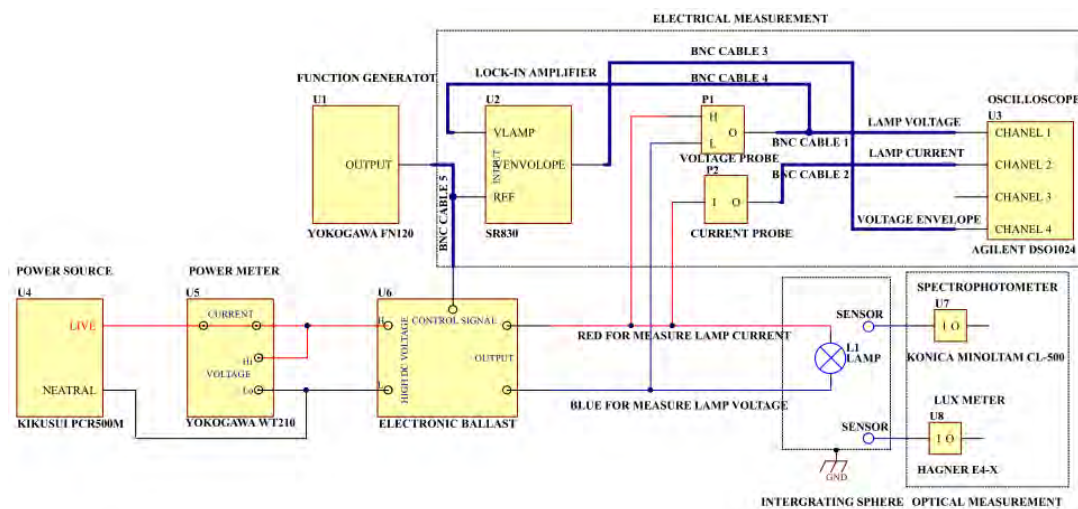


Fig.4-1 Schematic of the experimental set-up

The experimental set-up is composed of several blocks: a power source, a power meter, an electronic ballast, an MH lamp, an integrating sphere, and the electrical and optical measurement devices. The aims of the measurement parts are to monitor the operation status and detect AR phenomena in the lamp.

The power source is supplied by a power supply (Kikusui PCR500M). The input current, voltage, power and power factor of the electronic ballast are measured by a power meter (Yokogawa WT210). A function generator (Yokogawa FN120) is used to supply the driving signal of the ballast. The lamp current and voltage are measured by a current probe (LEM PR30) and a differential probe (Langlois ISOL601) respectively. A digital oscilloscope (Agilent DSO1024) displays the lamp voltage, current, and power. A lock-in amplifier (SR830) is used to measure the voltage envelope in order to detect AR.

Additionally, an integrating sphere is used to evaluate the generated light parameters. The integrating sphere consists of a hollow spherical cavity with a diffuse white reflective coating inside, with small holes for entrance and exit ports, as shown in Fig.4-2. The integrating sphere is designed to spatially integrate radiant flux in order to measure optical radiation. The spectral irradiance and colorimetric parameters are measured by a spectrophotometer (Konica Minolta CL-500A).

To implement the measurement automatically, the devices are connected to a computer via GPIB bus or USB lines. LabVIEW software is used to control the program and carry out automatically the whole process of the acquisition, storage, and monitoring.



Fig.4-2 Integrating sphere [1]

4.3 Statistical characterization of acoustic resonance using commercial devices

In chapter 3, the principle of the voltage envelope detection has been introduced. Also, the obtained results already proved that the voltage envelope detection is a simple and robust method to detect AR. In this chapter, the lock-in amplifier SR830 is used as the reference approach to measure the voltage envelope. To study AR phenomenon further, several statistical methods are used to analyze the voltage envelope characterization. The used lock-in amplifier is manufactured by Stanford Research System.

4.3.1 Data acquisition of voltage envelope and spectral variations

4.3.1.1 LabVIEW program in our experiment

Laboratory virtual instrument engineering workbench (LabVIEW) is used for data acquisition and instrument control. Fig.4-3 illustrates the main user interface window of the LabVIEW program.

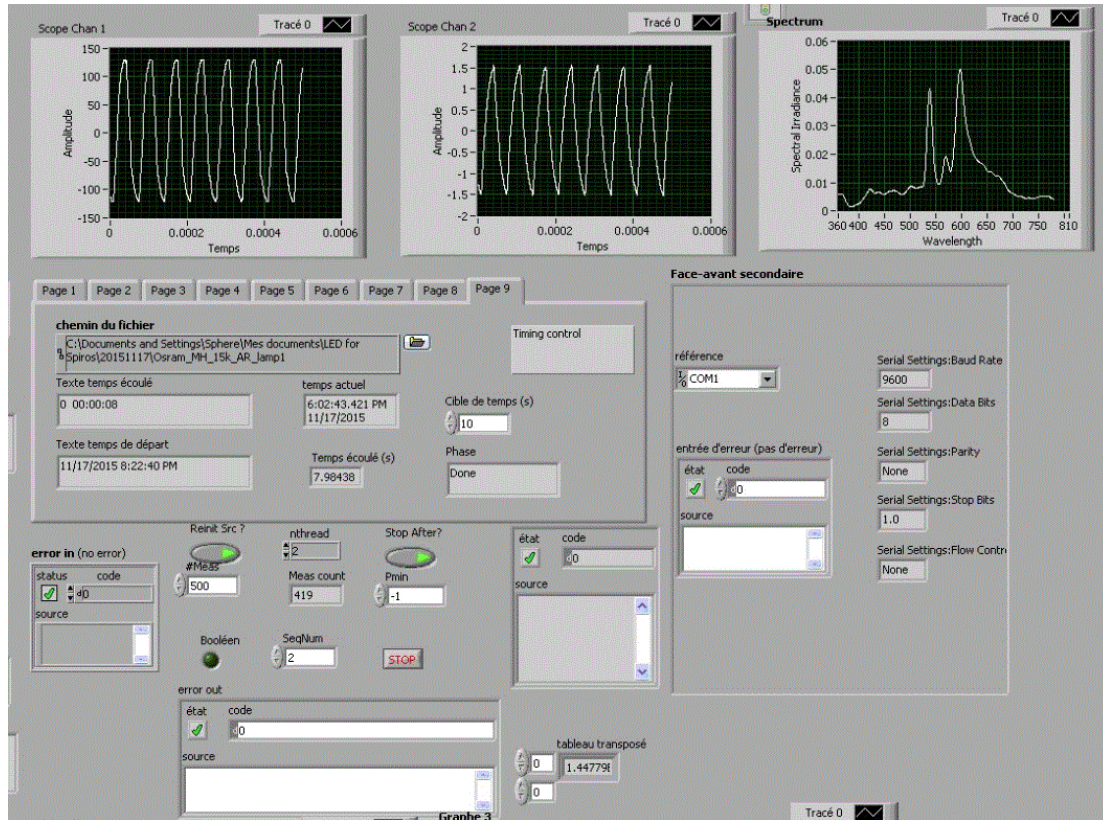


Fig.4-3 Control and acquisition window of LabVIEW program in our experiment

This framework is a system-design platform and development environment for a visual programming language from National Instruments and it can apply to most operating systems e.g. Microsoft Windows, various version of UNIX, Linux and macOS [2].

In Fig.4-3, the control procedure is managed in a tabbed environment to reduce visual clutter.

- 1) Page 1: control the power source Kikusui PCR500M;
- 2) Page 2: control the power meter Yokogawa WT210;
- 3) Page 3: control the multi-meter Agilent HP 34401A to measure the light level;
- 4) Page 4: control the spectrophotometer Konica Minolta CL-500A to measure the spectral irradiance and colorimetric parameters;
- 5) Page 5: control the digital oscilloscope Agilent DSO1024 to measure the lamp current, voltage and power;
- 6) Page 6: control the microphone to record sound emission of the lamp;
- 7) Page 7: control the driving signal of the ballast supplied by the function generator Yokogawa FN120;
- 8) Page 8: control the lock-in amplifier SR830 to measure the voltage envelope;
- 9) Page 9: global timing and acquisition control.

Using this program, all the devices are controlled, and data are collected and saved automatically. We propose three kinds of AR detection methods: light spectral variation detection, voltage envelope detection, and sound emission detection. In this last solution, a microphone is used to detect sound emission in the presence of AR. Nevertheless, external noises are detected as well as it is difficult to extract weak sound emission from noise signals. Then, this approach was not developed further, and we do not discuss this method in the thesis.

4.3.1.2 Data acquisition of voltage envelope

LabVIEW implements the supervision program in our experiment, as presented in Fig.4-3. The principle of the voltage envelope acquisition is shown in Fig.4-4. Between two measurement points, the time interval is 24 seconds, which means that new data are obtained every 24 seconds after lamp ignition. A supplemental warm-up of 10 min is allowed to the lamp reach a stable regime in order to obtain reliable data. Fifty-one measurement points over a time window of 20 min are then recorded in no AR or AR cases.

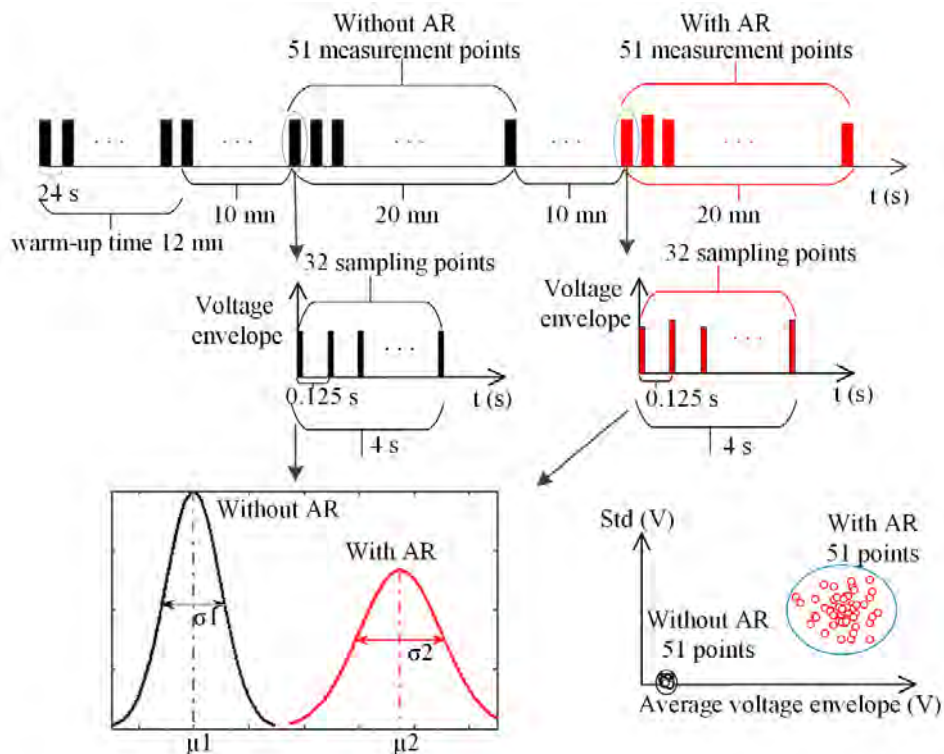


Fig.4-4 Principle of the voltage envelope acquisition in lock-in amplifier

The voltage envelope is evaluated by the lock-in amplifier with a sample rate of 8 Hz within 4 seconds (32 samples). The short-time average value and standard deviation are computed on those 32 samples. Those two variables are then plotted in the 2D plane. Additionally, in each situation (without AR and with AR) and for each manufacturer's lamp, two close operating frequencies are chosen within a range of 100 Hz.

4.3.1.3 Data acquisition of spectral variations (spectral irradiance and colorimetric parameters)

The experimental procedure for measuring the spectral irradiance and colorimetric parameters is the same as the one used for voltage envelope measurement. For spectral variation detection, spectral irradiance and colorimetric parameters are measured by the spectrophotometer (Konica Minolta CL-500A) within 24 seconds at each measurement.

This spectrophotometer can measure chromaticity coordinates, CRI and color temperature of lamps. In addition, the spectral irradiance waveform and peak wavelength can also be checked. The spectral irradiance can

be measured at a 1-nm pitch from 360 to 780 nm. The exposure time of the spectrophotometer is 0.2 seconds in our experiment.

a) How does the spectrophotometer work?

A spectrophotometer is a device that measures the amount of photons over some time window (the intensity of light or spectral irradiance). Fig.4-5 shows the structure of a charge coupled device (CCD spectrophotometer).

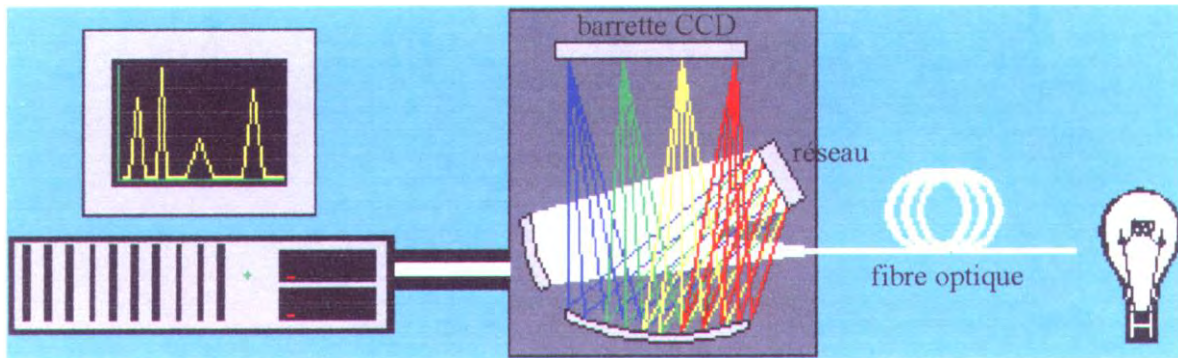


Fig.4-5 Structure of a CCD spectrophotometer [3]

An optical fiber transmits a straight beam of light (photons) to a mirror set in order to widen the beam. This beam then hit a grating whose goal is to separate the photons according to their wavelengths. The photons reach a CCD array permitting to translate the photon count into intensities. The CCD is a silicon-based multichannel array detector of UV, visible and near-infra light. CCD detectors are typically linear or area arrays of thousands or millions of individual detector elements (also known as pixels). Upon reading by a controller or a computer, this count is converted into per-wavelength light intensity. Further numerical processing permits to extract photometric and colorimetric properties.

4.3.1.4 Spectral variations and detection principle

The light-emitting material in polycrystalline alumina (PCA) bulb of MH lamps is filled with several metal halide salts, while the buffer gas and the starting rare gas are formed from mercury and argon respectively. Gas discharge works through excitation of the metal halide salts and the mercury is excited by the current flow. The mixture of the visible radiation of the different elements results in the designed spectral irradiance and CCT, CRI and chromaticity coordinates for MH lamps. Fig.4-6 illustrates the tasks in an MH lamp and TABLE 4-1 lists the elements in this lamp.

In the normal situation, these elements keep chemical balance. However, the phenomenon of AR can shift the chemical balance inside arc tube, affecting the spectral irradiance and colorimetric parameters such as CCT, CRI and chromaticity coordinates. In this thesis, spectral variations are used both for the variations of the spectral irradiance and colorimetric parameters. To analyze how AR phenomenon influences spectral variations, we measured the spectral irradiance and CRI, CCT, and chromaticity coordinates in AR and no AR situations for several manufacturers' MH lamps.

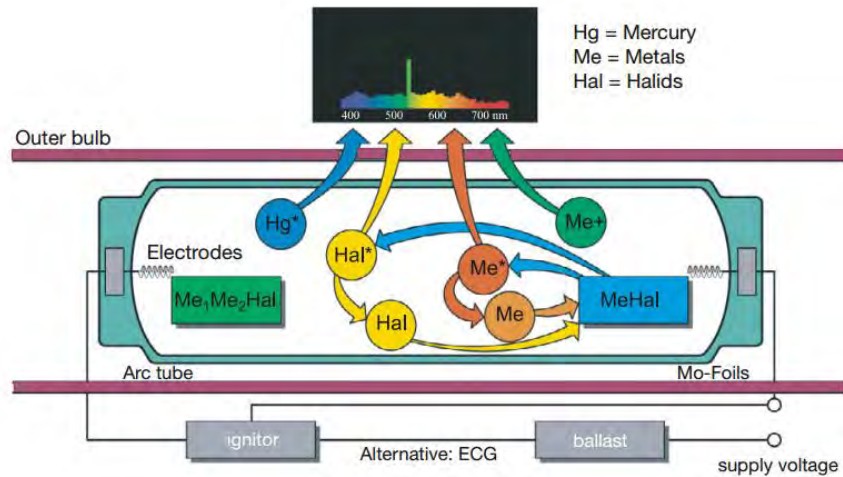


Fig.4-6 Tasks of metal halide salts in an MH lamp [4]

TABLE 4-1 Elements in an MH lamp

Type	Composition
Light-emitting materials	Dysprosium iodide (DyI3), thulium iodide (TmI3), holmium iodide (HoI3), thallium iodide (TlI), sodium iodide (NaI)
Buffer gas	Mercury
Starting rare gas	Argon

4.3.2 Statistical analysis of voltage envelope detection

In our experiment, three kinds of 150 W MH lamps are tested such as: Osram (Powerball HCI-TT), GE (Constant Color CMH), and Philips (Master City White CDO-TT). The tested Osram and GE MH lamps have been aged 100 hours. The tested Philips MH lamps have been aged 8 000 hours in order to observe aging effects.

In this section, several statistical methods, such as 2-D plane plot, boxplot, histogram, analysis of variance, are proposed to analyze voltage envelope characterizations.

4.3.2.1 Two-dimensional plane of voltage envelope standard deviation versus average voltage envelope

A. Results in the Osram MH lamp

In the Osram MH lamp, $f=15.2$ kHz and $f=15.3$ kHz are inside an AR-frequency band, while $f=11.7$ kHz and $f=11.8$ kHz are in an AR-free frequency band.

To analyze voltage envelope characterizations, it is worth considering the 2D plane of the standard deviation of the voltage envelope *versus* the average voltage envelope. Fig.4-7 illustrates those values obtained with the Osram MH lamp at different operating powers. TABLE 4-2 lists the corresponding electrical parameters.

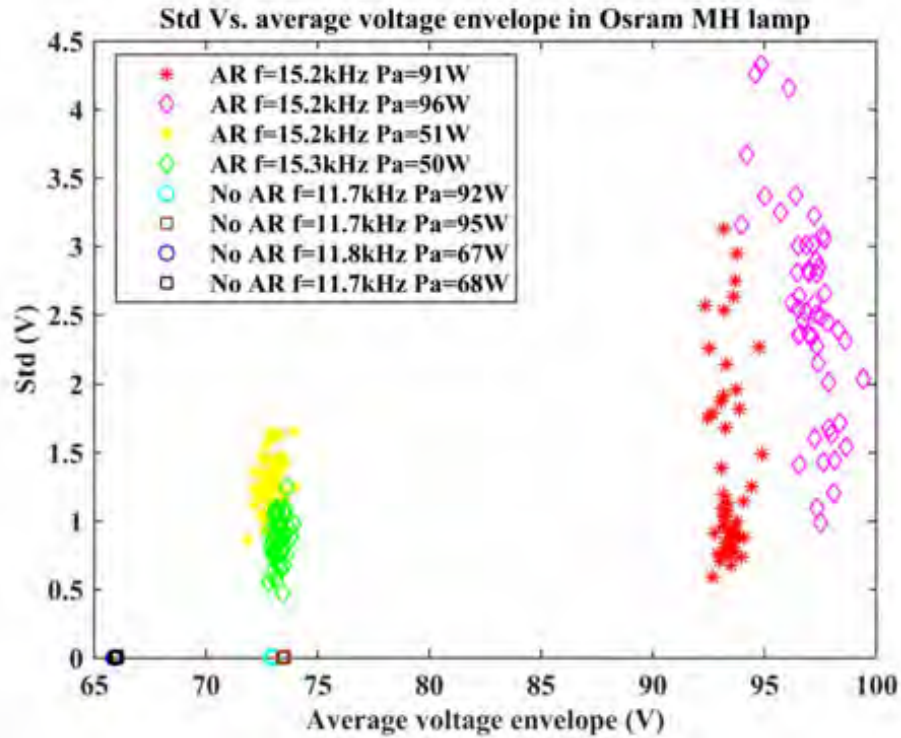


Fig.4-7 Voltage envelope standard deviation vs. average voltage envelope in the Osram MH lamp

TABLE 4-2 Electrical parameters in the Osram MH lamp at different power in Fig.4-7

Operation state	V_{dc} (V)	f (kHz)	Long-term average active power (W)	Average voltage (V)		STD (V)
				Min-max	Min-max	
AR	370	15.2	91	92.0~96.0		0.5~3.0
	380	15.2	96	94.0~100.0		0.7~4.5
AR	270	15.2	51	72.0~74.0		0.8~1.8
	270	15.3	50	72.9~74.0		0.4~1.4
No AR	300	11.7	92	73.0		1.1e-3~1.1e-2
	310	11.7	95	74.0		1.3e-3~1.3e-2
No AR	270	11.8	67	65.8		1.1e-3~7.7e-3
	270	11.7	68	66.0		1.1 e-3~1.4e-2

As can be observed from Fig.4-7, in AR cases at $f=15.2$ kHz and $f=15.3$ kHz, the standard deviation of voltage envelope fluctuates a lot whatever the lamp operating power (vertical axis). The horizontal axis reveals that average voltage envelopes also exhibit some fluctuations during the 20-min observation window. However, in the no AR case, the situation is quite different. The points form a dense cloud. The short-time RMS values voltage envelopes are nearly constant during the 20-min interval and their short-time standard deviations are close to zero. It is thus easy to spot the differences graphically between the AR and no AR cases in the 2D plane. Results show that the occurrence of the AR phenomenon influences significantly the lamp voltage envelopes.

B. Results in the GE MH lamp

In the GE 150W Constant Color MH lamp, $f=15.5$ kHz and $f=15.6$ kHz are inside an AR frequency band while AR-free frequency band contains $f=10.7$ kHz and $f=10.6$ kHz. Fig.4-8 shows the voltage envelope standard deviation *versus* the average voltage envelope. TABLE 4-3 lists the electrical parameters of the lamp.

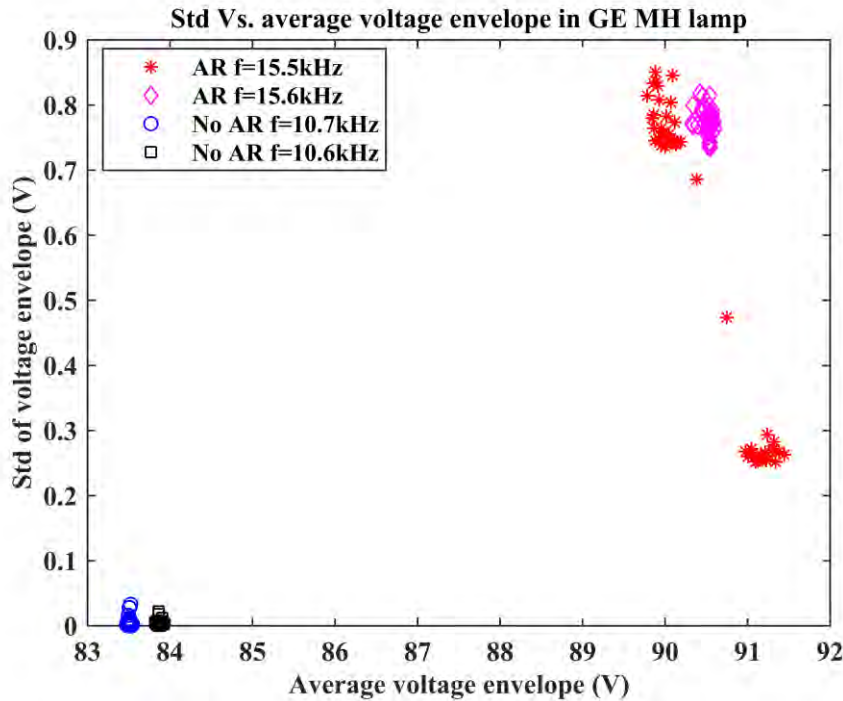


Fig.4-8 Voltage envelope standard deviation vs. average voltage envelope in GE MH lamp

The clustering patterns observed in Fig.4-8 are similar to the previous case. In the no AR situation, both the X and Y axis dispersions are quite limited. Standard deviations of voltage envelopes range between around one mV up to a few tens of mV. However, in the AR situation, data are much scattered, and their standard deviations are quite different from zero. The RMS voltage envelopes randomly change between 90.0 V and 91.5 V. The minimum of their standard deviations is at least 0.2 V. Furthermore, at 15.5 kHz, data are visually clustered in two parts. This implies that the associated AR phenomenon randomly switches between two distinct modes as illustrated in the next section.

TABLE 4-3 Electrical Parameters in GE MH Lamp in Fig.4-8

Operation state	V_{dc} (V)	f (kHz)	Long-term average active power (W)	Average voltage (V)	STD (V)
				Min-max	Min-max
AR	270	15.5	56	90.0~91.5	0.2~0.9
	270	15.6	54	90.0~91.0	0.7~0.9
No AR	270	10.7	99	83.5	$1.1e-3 \sim 3.3e-2$
	270	10.6	101	83.8	$1.1e-3 \sim 2.2e-2$

C. Results in the Philips MH lamp

In the Philips MH lamp, $f=12.5$ kHz and $f=12.4$ kHz are inside an AR-frequency band while $f=10.5$ kHz and $f=10.4$ kHz are in an AR-free frequency band. Fig.4-9 illustrates the standard deviation of the voltage envelope *versus* the average voltage envelope at these frequencies. TABLE 4-4 lists the corresponding electrical parameters of the lamp.

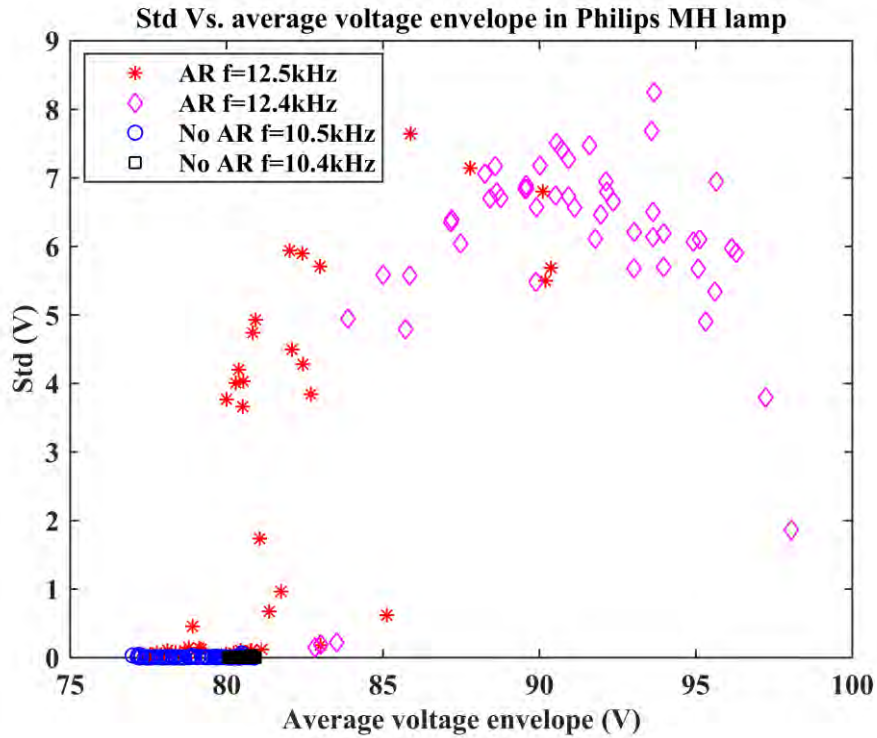


Fig.4-9 Voltage envelope standard deviation vs. average voltage envelope in Philips MH lamp

TABLE 4-4 Electrical Parameters in Philips MH Lamp in Fig.4-9

Operation state	V_{dc} (V)	f (kHz)	Long-term	RMS voltage (V)	STD (V)
			average active power (W)	Min—max	Min—max
AR	270	12.5	58	77.0~90.0	0.8~8.0
	270	12.4	64	85.0~97.0	4.0~9.0
No AR	270	10.5	102	78.0~80.0	$2.0e-3$ ~ $6.2e-2$
	270	10.4	104	80.0~81.0	$2.3e-3$ ~ $3.1e-2$

According to Fig.4-9, when AR occurs in the Philips MH lamp, average voltage envelopes (X-axis) change between 77.0 V and 90.0 V at $f=12.5$ kHz and between 82.0 V and 97.0 V at $f=12.4$ kHz. The standard deviations of the voltage envelope (Y-axis) span a range overlapping the values in the no-AR case. In the no AR situation, average voltage envelopes are stable within a 1 V interval. Their short-term standard deviations are limited to around 60 mV.

4.3.2.2 Boxplot of voltage envelope and voltage envelope waveform

The boxplot is a standardized way of depicting the distribution of data based on a set of order statistics (the median, the first, and the third quartiles). Outliers are observations that fall below the lower fence (LF) or above the upper fence (UF). The boxplot displays variations in samples of a statistical population without making any assumptions about the underlying statistical distribution. The spacing between the different parts of the box indicates the degree of dispersion and skewness of data [5]. Fig.4-10 shows the characteristics of boxplot.

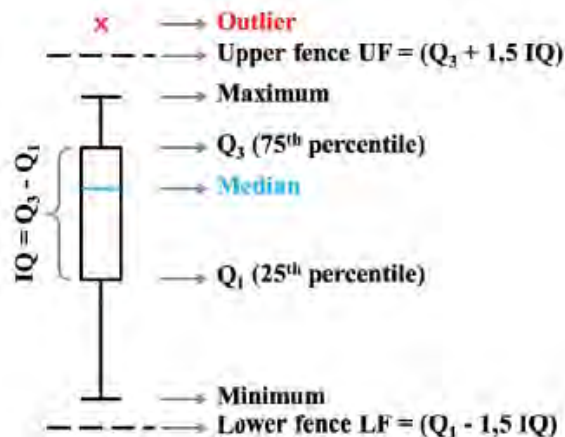


Fig.4-10 Characteristics of boxplot [6]

A. Results in the Osram MH lamp

To probe further, Fig.4-11 illustrates the boxplot of the previously used data. In particular, if the boxplots of two groups of data have no overlap, those two groups can be considered as significantly different.

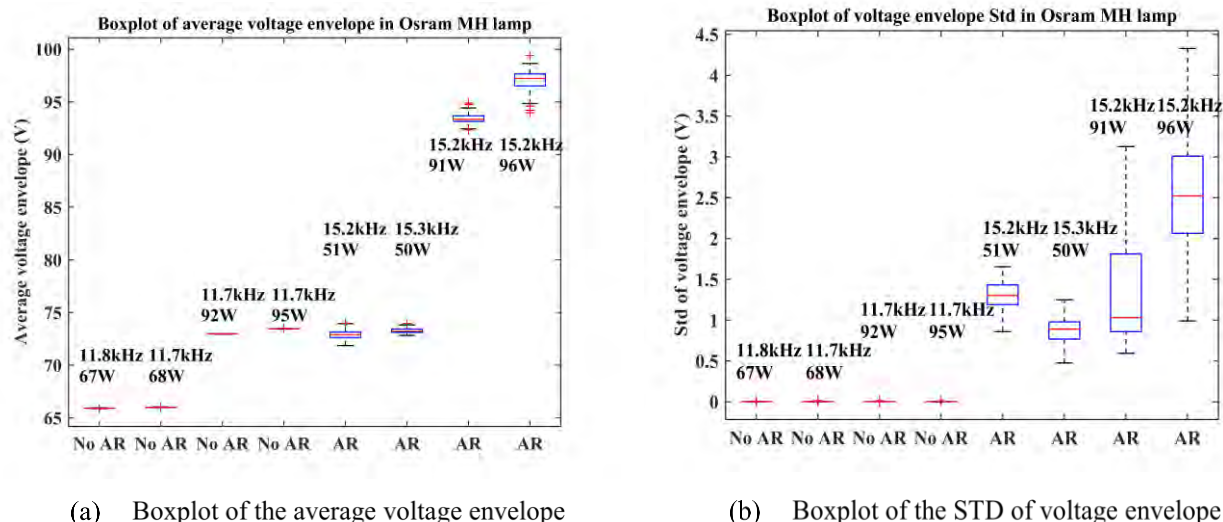
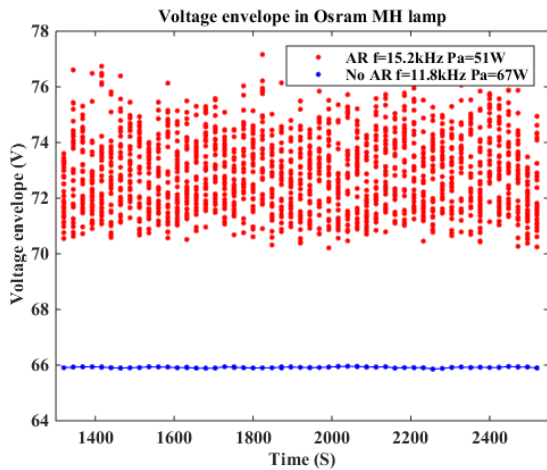


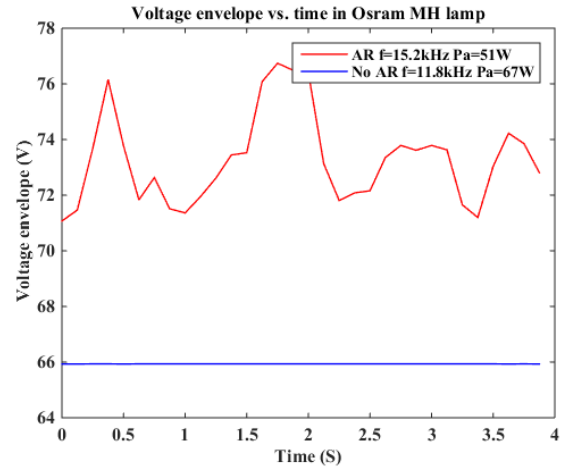
Fig.4-11 Boxplot of the voltage envelope in Osram MH lamp

The results contained in Fig.4-11 confirm the observations performed in the 2-D plane of Fig.4-7, but in a clearer way. In the no AR cases, all the boxplot of the short-term standard deviation overlaps around zero, while in the AR cases there is a partial overlap, with a range going between 0.5 V and 4.5 V. The boxplot of the short-term average value reveals e.g. that the combination of no AR @11.7 kHz, 92 Watts cannot be distinguished from AR @15.2 kHz, 51 Watts.

Fig.4-7 represents the changes of the STD and mean of the voltage envelope within 20 min (51 measurements, 51*32 points) at each operating frequency. Fig.4-11 describes the time-resolved dispersions of these data within 20 min. By applying a low-pass filter on data, the long-time trend is computed. Fig.4-12 illustrates one example of the voltage envelope waveforms in AR and no AR cases.



(a) Voltage envelope at $f=15.2$ kHz and $f=11.8$ kHz



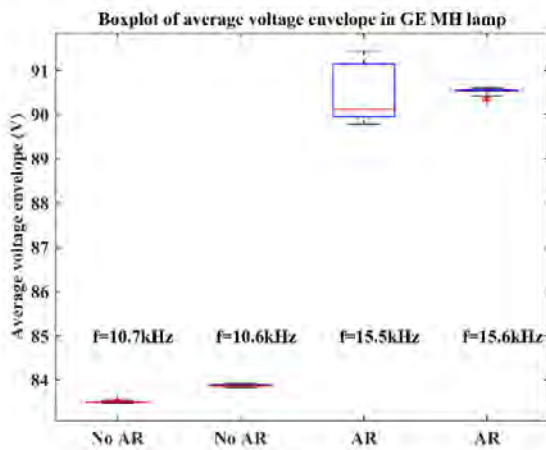
(b) Voltage envelope at $f=15.2$ kHz and $f=11.8$ kHz within 4 seconds

Fig.4-12 Voltage envelope waveform in Osram MH lamp at lower operating power

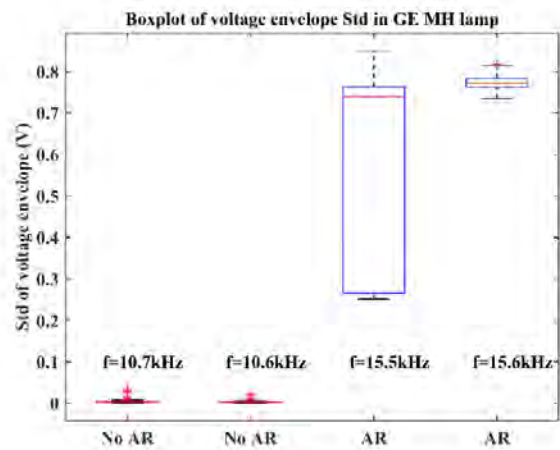
Fig.4-12 (a) shows the changes of voltage envelopes change within 20 min (51 measurements, 51*32 points). Fig.4-12 (b) illustrates how the voltage envelope changes within 4 seconds (32 points). Distinctive differences are observed: the voltage envelope waveform has some fluctuations at 15.2 kHz in AR case and the waveform is constant at 11.8 kHz in no AR case whatever in the long-time or short-time observation window.

B. Results in the GE MH lamp

Similarly, Fig.4-13 illustrates the boxplot of Fig.4-8 data in the GE MH lamp.



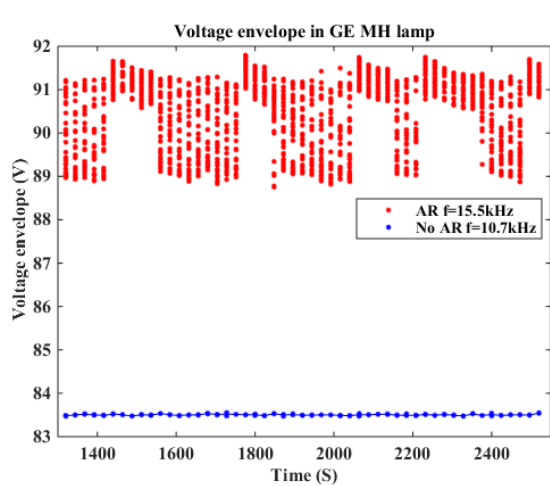
(a) Boxplot of the average voltage envelope



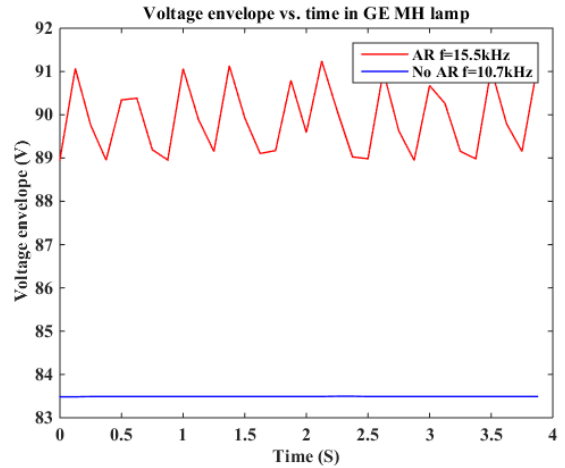
(b) Boxplot of the STD of voltage envelope

Fig.4-13 Boxplot of the voltage envelope in the GE MH lamp

The observed patterns are similar to the results obtained in the Osram lamp. In the no AR situation, RMS values change significantly with operating frequency as there is no overlap between the associated boxplots. Their standard deviations, except for a few isolated points, overlap within a range whose upper value is 8 mV. In the AR situation, the lower value of the 95 % confidence interval is around 250 mV. By splitting data at 15.5 kHz with a low threshold of 0.3 V and an upper threshold of 0.7 V, boxplots reveal the existence of two separated, non-overlapping clusters. The lower one contains around 60 % of the samples.



(a) Voltage envelope at $f=15.5$ kHz and $f=10.7$ kHz



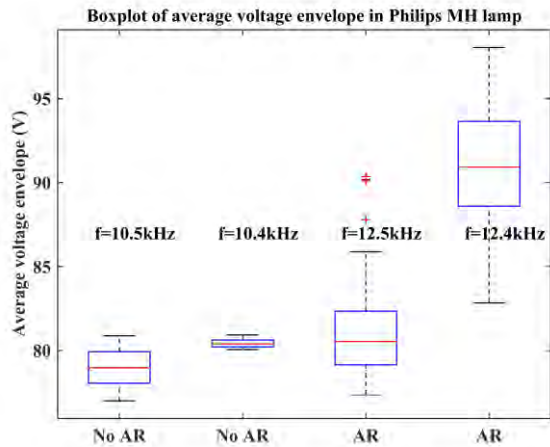
(b) Voltage envelope at $f=15.5$ kHz and $f=10.7$ kHz within 4 seconds

Fig.4-14 Voltage envelope waveform in GE MH lamp

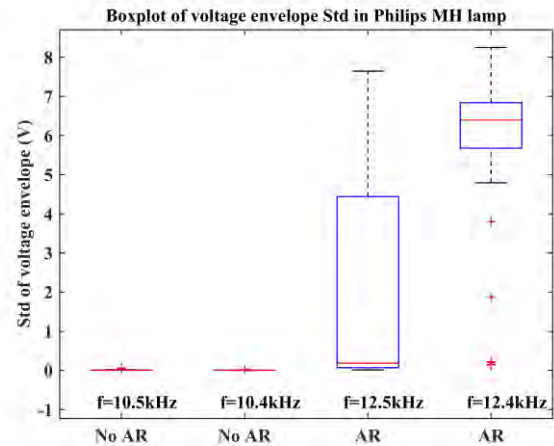
The reason that the data is separated into two parts at $f=15.5$ kHz in Fig.4-8 can be found in Fig.4-14 (a). That is because the voltage envelope always fluctuates from high level to low level. Thus, in the 2-D plane at the same frequency, the data is separated two clouds.

C. Results in the Philips MH lamp

Likewise, Fig.4-15 shows the boxplot of the voltage envelope in the Philips MH lamp.



(a) Boxplot of the average voltage envelope



(b) Boxplot of the STD of voltage envelope

Fig.4-15 Boxplot of the voltage envelope in the Philips MH lamp

The boxplot of the average voltage envelope illustrated in Fig.4-15 (a) reveals that the groups of data are overlapping. In consequence, this criterion alone cannot classify between AR and no AR situations. The boxplot of their standard deviations in Fig.4-15 (b), exhibits an apparent overlap of the two situations as well.

The reasons behind this overlap can be inferred from Fig.4-16. This figure also contains a short-term voltage envelope waveform. Three phenomena can be observed:

- 1) Even in the no AR situation, jumps with an amplitude of around 5 V are detected in Fig.4-16 (a);

- 2) In the AR situation, oscillations between stable and noisy operating points occurred randomly. Stable, AR-free periods are intermixed with AR periods, all the parameters being kept constant in Fig.4-16 (a);
- 3) The same oscillating behavior is also observed on a short-time observation window as shown in Fig.4-16 (b), where the stable period is two seconds in the AR situation.

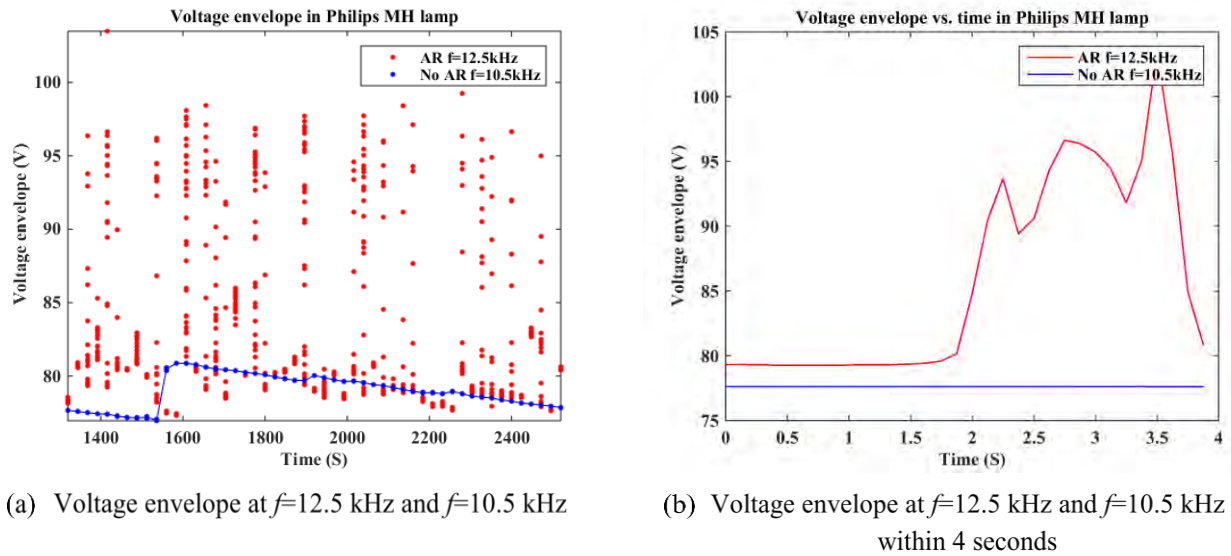


Fig.4-16 Voltage envelope waveform in the Philips MH lamp

These results show the apparent discrepancies between this lamp and two other lamps. The analysis should be refined one-step further, splitting the signal between stable and noisy periods. Furthermore, this oscillation between stable and unstable modes in the AR situation may be an indicator of the lamp lifetime.

4.3.2.3 Histogram of voltage envelope

A. Results in the Osram MH lamp

A histogram is a graphical representation of the numerical data distribution [7]. It is similar to a bar chart, but the histogram groups numbers into ranges [8]. Fig.4-17 shows histograms of the voltage envelope in the Osram MH lamp in AR and no AR cases.

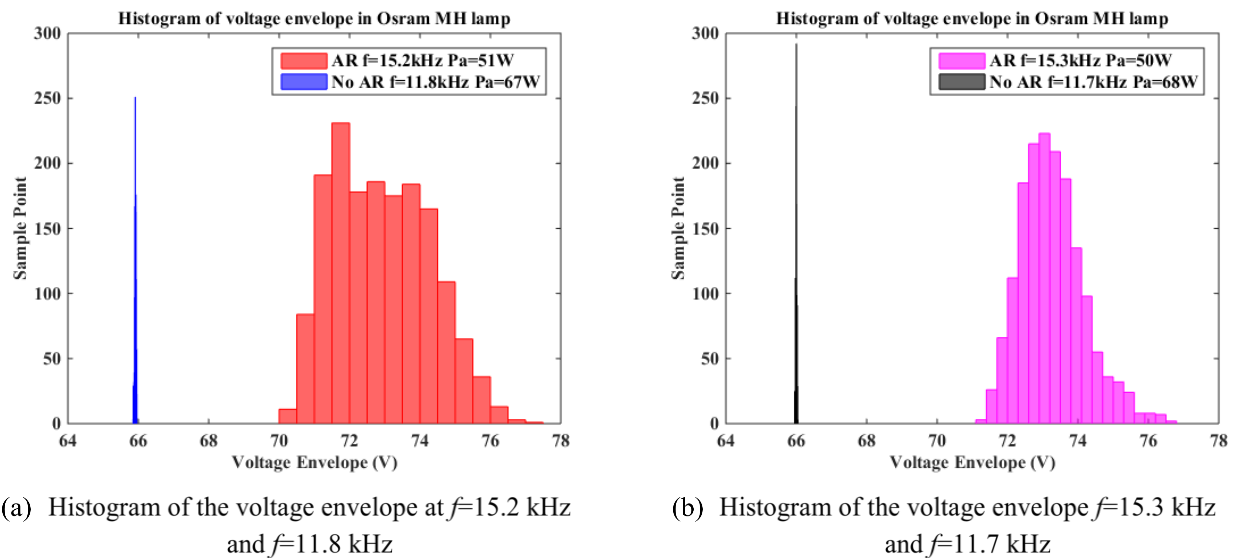
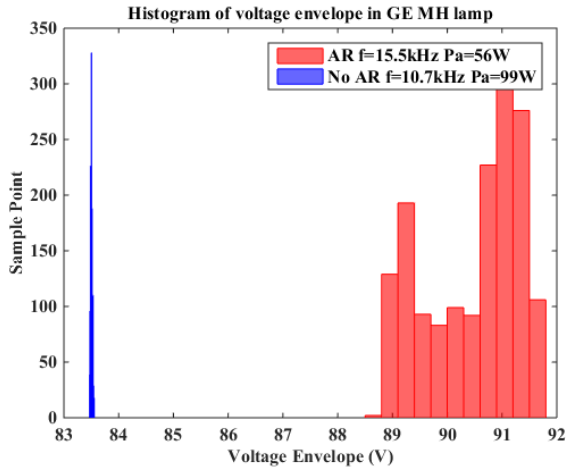


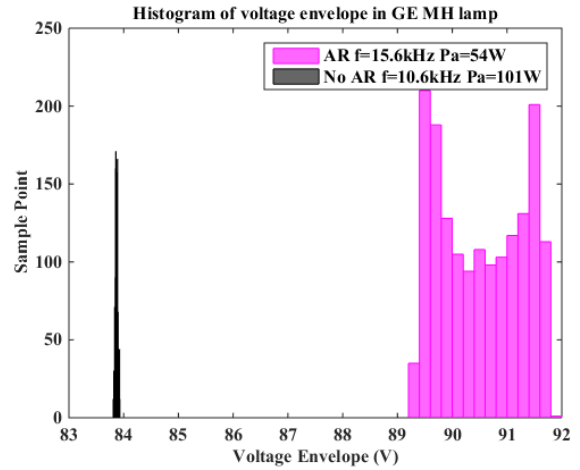
Fig.4-17 Histogram of the voltage envelope in the Osram MH lamp

These figures show the data distribution of the voltage envelope during 20-minute observation (51 measurements). In the AR situation at $f=15.2$ kHz and $f=15.3$ kHz, the ranges of the voltage envelope are wide. In the absence of AR at $f=11.8$ kHz and $f=11.7$ kHz, the ranges of the voltage envelope are narrow.

B. Results in the GE MH lamp



(a) Histogram of voltage envelope at $f=15.5$ kHz and $f=10.7$ kHz

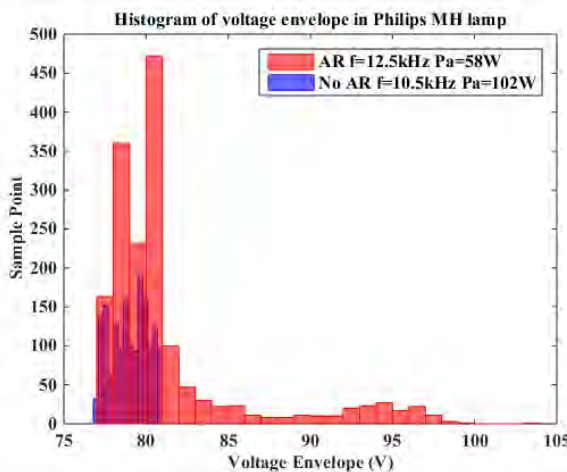


(b) Histogram of voltage envelope at $f=15.6$ kHz and $f=10.6$ kHz

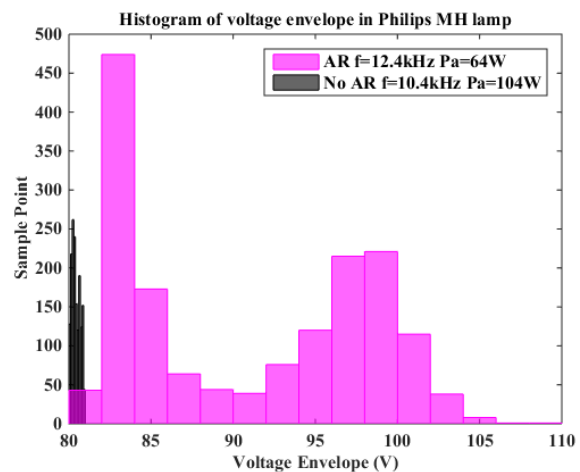
Fig.4-18 Histogram of the voltage envelope in the GE MH lamp

The histogram is a representation to show the difference between no AR and AR situations. In Fig.4-18, in the no AR situation, the variations of voltage envelope are small, about 200 mV. In the AR situation, the variations of voltage envelope are much bigger, about 4 V. The results are similar to the Osram MH lamp.

C. Results in the Philips MH lamp



(a) Histogram of voltage envelope at $f=12.5$ kHz and $f=10.5$ kHz



(b) Histogram of voltage envelope at $f=12.4$ kHz and $f=10.4$ kHz

Fig.4-19 Histogram of the voltage envelope in Philips MH lamp

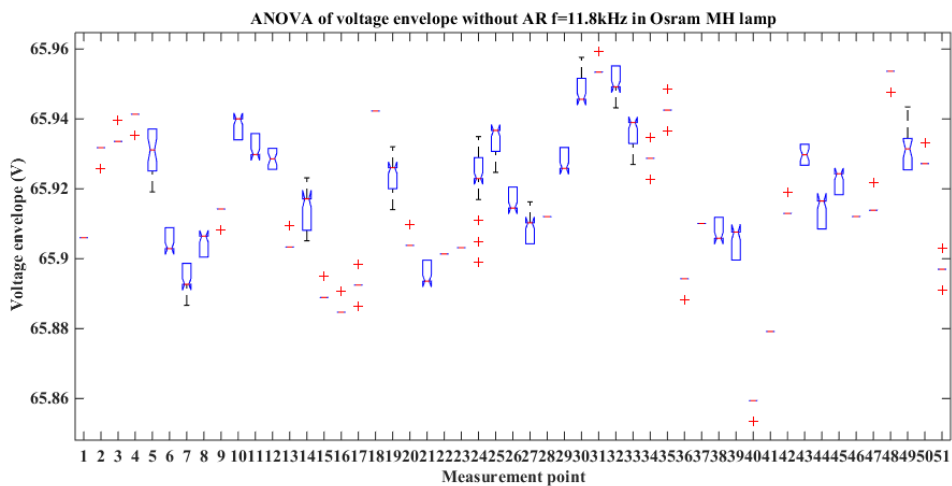
In case of AR at $f=12.5$ kHz and $f=12.4$ kHz, the histogram looks like a bimodal distribution. The outcomes of two processes with different distributions are combined in one set of data. This is because that there are oscillations between stable and unstable modes in the AR situations.

4.3.2.4 Analysis of variance of voltage envelope

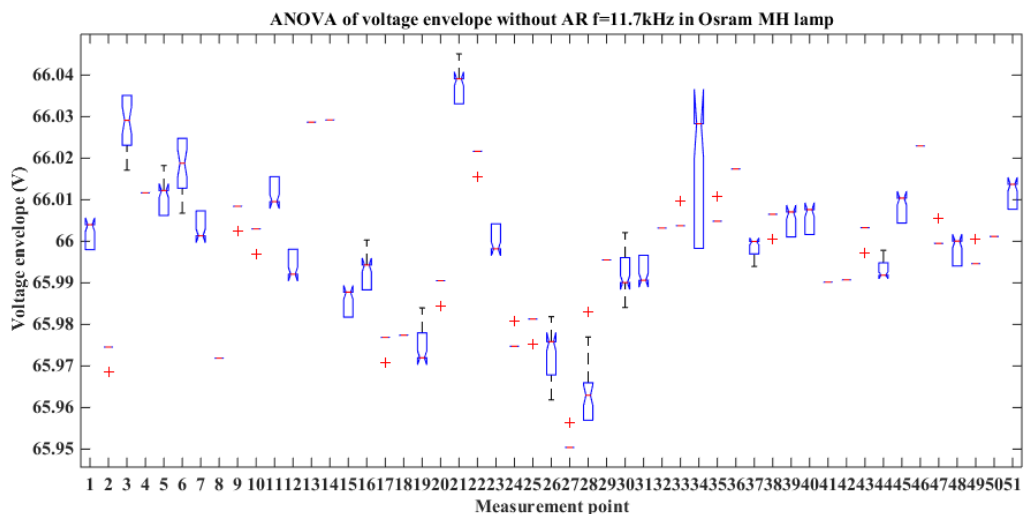
The boxplots and histograms of the voltage envelope describe the entire data of the voltage envelope during 51 measurements within 20 min. It is impossible to see how the data change at each measurement. Thus, it is worth to use the ANOVA (analysis of variance) to analyze the voltage envelope at each measurement.

A. Results in the Osram MH lamp

ANOVA is a procedure for determining whether variation in the response variable arises within or among different population groups [9]. ANOVA returns boxplots of the observations by the groups. Boxplots provide a visual comparison of the group location parameters. Fig.4-20 illustrates the ANOVA of the voltage envelope in the Osram MH lamp.



(a) In the no AR situation ($@f=11.8\text{ kHz}$, $\text{Pa}=67\text{ W}$)



(b) In the no AR situation ($@f=11.7\text{ kHz}$, $\text{Pa}=68\text{ W}$)

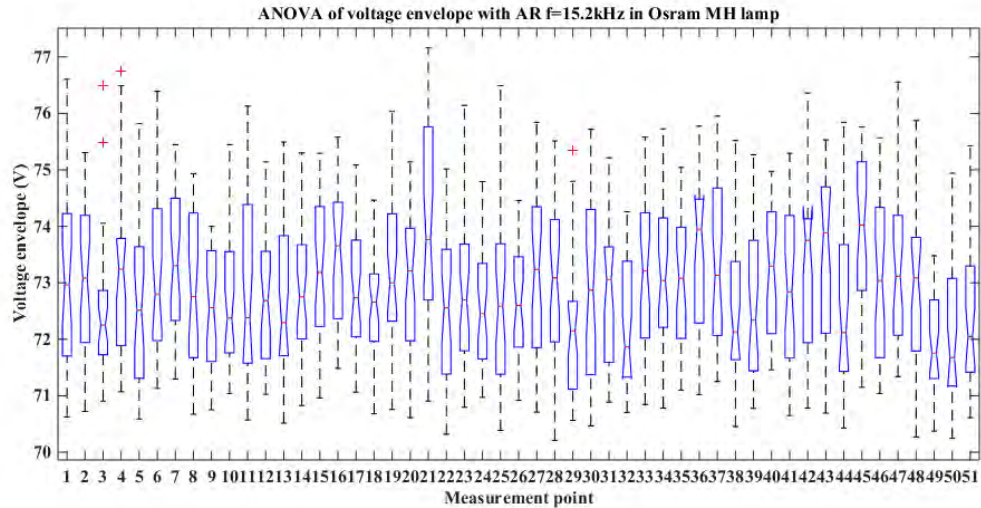
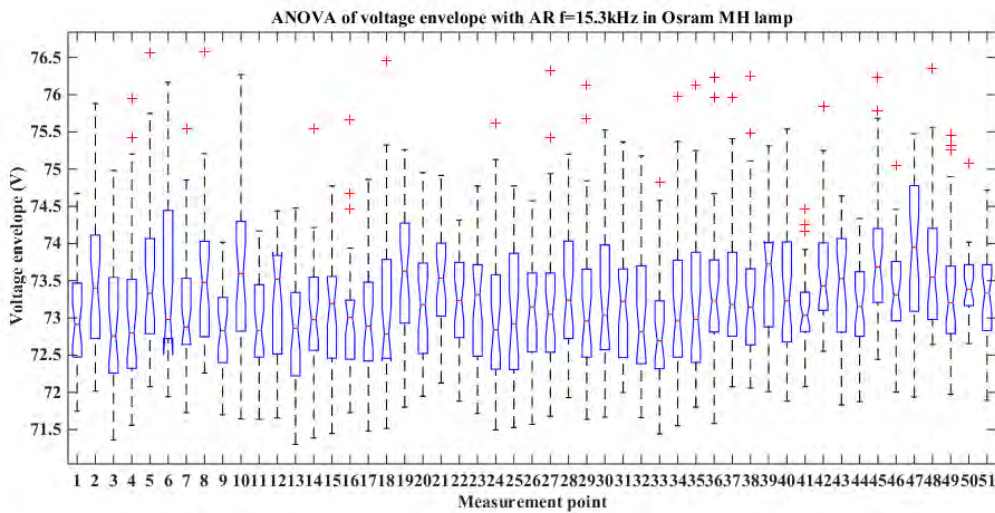
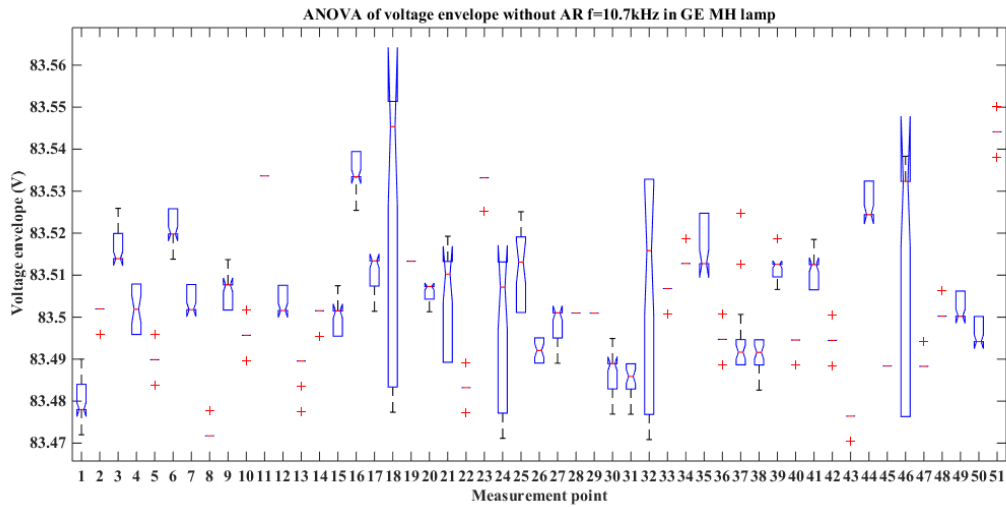
(c) In the AR situation ($@f=15.2$ kHz, $Pa=51$ W)(d) In the AR situation ($@f=15.3$ kHz, $Pa=50$ W)

Fig.4-20 ANOVA of the voltage envelope in the Osram MH lamp

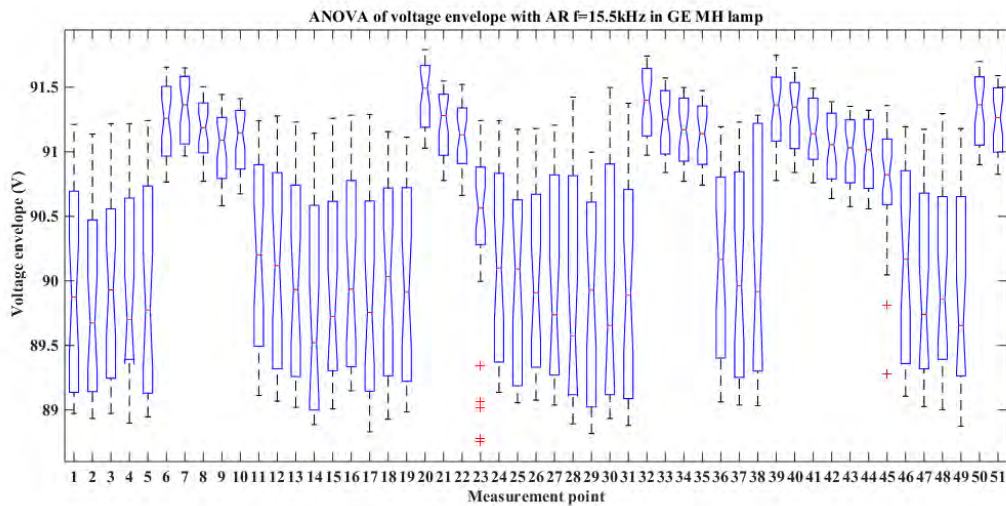
In Fig.4-20 (a) and (b), the range of each box is narrow at each measurement, and the variations of voltage envelopes are about 20 or 30 mV in no AR cases. In addition, one, two or three different values are observed during 32 samples (4 seconds) at each measurement. This because that these variations are caused by the quantification noise that cannot be avoided. In Fig.4-20 (c) and (d), in case of AR, the range of the box is much larger at each measurement and the variations of voltage envelopes are about 10 or 100 times than the values in the no AR situation. Those variations are produced by signal noises (Acoustic resonance). Furthermore, 31 or 32 different values are observed during 32 samples at each measurement.

In conclusion, Fig.4-20 not only shows how the data change in a short-time observation window within 4 seconds, but also present the data changing in a long-time observation window within 20 min (51 measurements). ANOVA of the voltage envelope demonstrates the significant differences between no AR and AR cases and can distinguish these two situations well.

B. Results in the GE MH lamp



(a) In the no AR situation ($@f=10.7$ kHz, $Pa=99$ W)

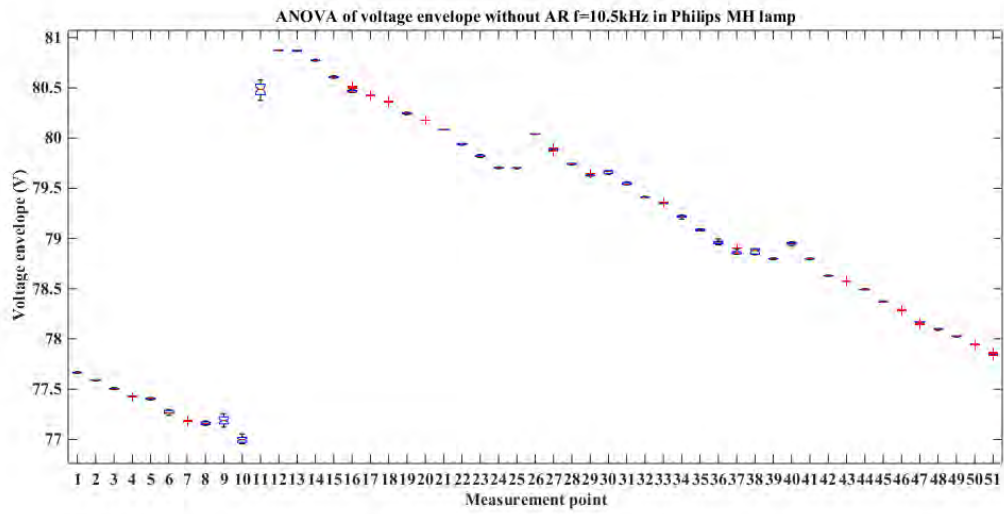


(b) In the AR situation ($@f=15.5$ kHz, $Pa=56$ W)

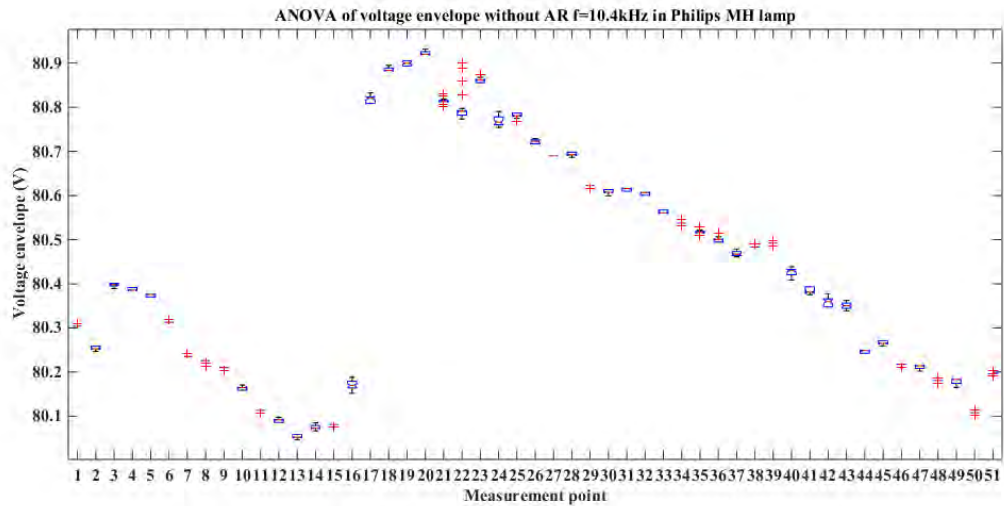
Fig.4-21 ANOVA of the voltage envelope AR in the GE MH lamp

In Fig.4-21 (a), voltage envelopes have one, two or three different values at each measurement in the no AR case. In Fig.4-21 (b), in the AR situation, 31 or 32 different values of the voltage envelope are found during 32 samples at each measurement. These results of this lamp are similar to the Osram lamp presented in Fig.4-20. In addition, voltage envelopes have high level values at some measurement points and low-level values at other measurement points in Fig.4-21 (b). This means that the operation states of the lamp change from one to another mode. This also can explain why the data at $f=15.5$ kHz are separated into two parts in Fig.4-8.

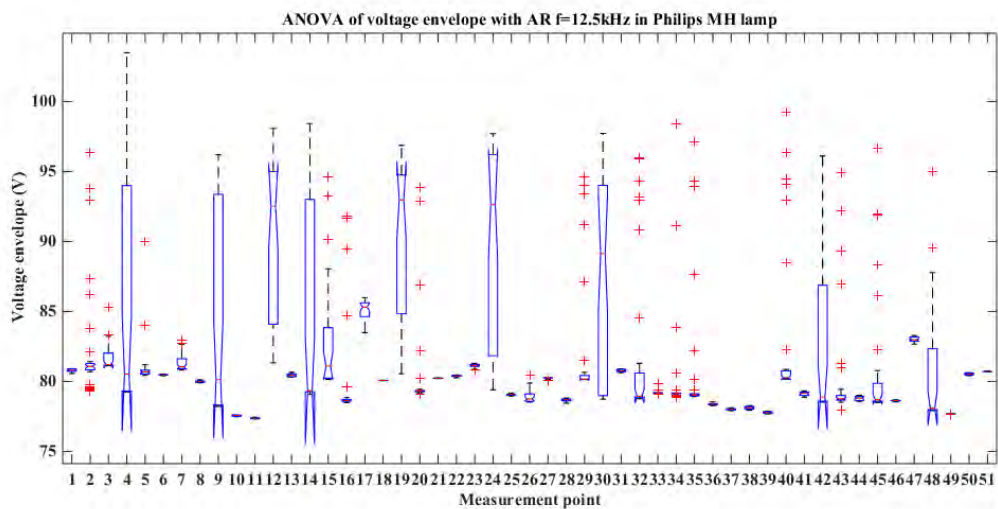
C. Results in the Philips MH lamp



(a) In the no AR situation ($@f=10.5\text{ kHz}$, $P_a=102\text{ W}$)



(b) In the no AR situation ($@f=10.5\text{ kHz}$, $P_a=104\text{ W}$)



(c) In the AR situation ($@f=12.5\text{ kHz}$, $P_a=58\text{ W}$)

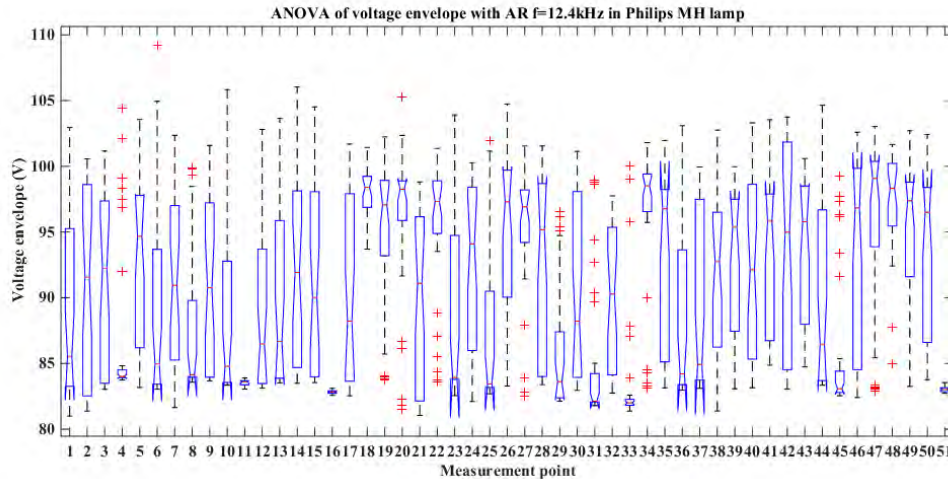
(d) In the AR situation ($@f=12.4$ kHz, $P_a=64$ W)

Fig.4-22 ANOVA of voltage envelope in the Philips MH lamp

In Fig.4-22 (a) and (b), there are some voltage jumps in the no AR situation at $f=10.5$ kHz and $f=10.4$ kHz. In Fig.4-22 (c) and (d), at some certain measurements, voltage envelopes are stable and then get unstable again at $f=12.5$ kHz and $f=12.4$ kHz in case of AR. These phenomena just are observed in the aged Philips MH lamp. These characterizations could be evaluated the lifetime of MH lamps.

One explanation is that elements inside the lamp arc tube significantly changed over time. Their concentration gets lower and the chemical equilibria have drifted, leading to other plasma modes. Another explanation is that there is a buildup of traps at the glass interface, resulting in a sudden capture and release of elements.

4.3.2.5 Results Inter-comparison

Based on the fact that there seems no scientific agreement over the definition of AR level, we propose an objective definition classifying the AR phenomenon according to the voltage envelope standard deviation. TABLE 4-5 compares this value at different AR levels in different MH lamps. It can be inferred from those observations that:

- 1) The no-AR case corresponds to a stable voltage envelope; the associated standard deviation magnitude is in the range from 10 to 100 mV. The produced light does not exhibit flicker.
- 2) The most extreme AR situation that was applied without destroying the lamp corresponds to observable flicker and arc bending. In those cases, the associated short-time standard deviation, on observation window of 4 seconds peaks are at least at 2 V.
- 3) Between the no-AR and the most extreme AR cases are intermediate cases: arc bending can be detected but the light variation stays low. Those situations correspond to a minimum of standard deviation always greater than 200 mV, but never greater than 2 V.

Sometimes, it was observed that the lamp voltage envelope switched quickly between two stable values. This is why it is important to perform the standard deviation computation on short timescales and monitor it on wider observation windows. As commented previously, the RMS value alone is not sufficient to detect AR as different combinations of DC power supply and operating frequencies may result in values that are not significantly different.

To summarize, in AR case, the standard deviation of the voltage RMS value and its fluctuations are several orders of magnitudes greater than in the no AR case. The proposed new criterion, therefore, can provide in real-time a quantitative evaluation of the AR presence and severity level.

TABLE 4-5 Voltage envelope standard deviations in different MH lamps

Lamp and operation situation	STD (V)				
	No AR f (kHz)		AR levels	AR levels f (kHz)	
Osram (at lower power)	1.1e-3~7.7e-3	11.8		Slight	0.8~1.8
	1.1 e-3~1.4e-2	11.7	0.4~1.4		15.3
GE	1.1e-3~3.3e-2	10.7	Slight	0.2~0.9	15.5
	1.1e-3~2.2e-2	10.6		0.7~0.9	15.6
Philips	2.0e-3~6.2e-2	10.5	Serious	0.8~8.0	12.5
	2.3e-3~3.1e-2	10.4		4.0~9.0	12.5
Osram (at higher power)	1.1e-3~1.1e-2	11.8	Serious	0.5~3.0	15.2
	1.3e-3~1.3e-2	11.7		0.7~4.5	15.3

4.3.2.6 Conclusions of voltage envelope using statistical analysis methods

- 1) Statistical methods have shown that voltage envelope variations exhibit significantly different patterns in response to AR levels. A new criterion classifying AR levels is therefore defined, based upon the level of the voltage envelope standard deviation. A threshold of 200 mV seems to be the border between no AR and slight AR coupled to the observable optical phenomenon.
- 2) Voltage envelope jumps in the absence of AR and some oscillation patterns in case of AR only appear in aged lamps, which leading to the possibility to use these characterizations as a health-monitoring tool of the lamp lifetime.
- 3) In section 4.3.3, different statistical methods are used to analyze the voltage envelope characterization. The characterization of each analysis method can be concluded in TABLE 4-6.

TABLE 4-6 Characterizations of different analysis methods for AR detection

Analysis method	Detection characterization	Type
2D plane	Mean and STD need to be analyzed together	Long-time analysis
Boxplot	No coverage between AR and NO-AR cases	
Histogram	Not exploited	
ANOVA	Low computation power	Short-time + long-time analysis
Voltage envelope waveform	Detect switches between stable and unstable states in aged lamps	

The 2D plane, boxplot, and histogram describe the changes or the distribution of the voltage envelope within 20 min (51 measurements, 51*32 points). These methods are the long-time analysis. The ANOVA and the voltage envelope waveform represent changes or the distribution of the voltage envelope within 4 seconds (32 samples) and 20 min. These two approaches are the short-time and long-time analysis.

To conclude, in the AR situation, there are both a short-term signature and a long-term signature. This means that AR phenomenon is an ergodic process.

4.3.3 Statistical analysis of spectral variation detection

In our experiment, voltage envelope of the lamps is measured by the lock-in amplifier SR830 and, spectral variations are measured by the spectrophotometer CL-500. These two kinds of measurements are performed at the same time. The operating frequencies of lamps are the same as the previous experiment.

4.3.3.1 Standard deviation and relative standard deviation in the spectral irradiance

Spectral irradiance is measured by the spectrophotometer. In this thesis, a normalized spectral irradiance is recommended to quantify the behavior of the lamp in the different situations. This is because that normalization is targeting to compare different data. The normalized spectral irradiance is equal to real value / RMS value.

A. Results in Osram MH lamp (aged 100 hours)

As presented in section 4.3.2, in the Osram MH lamp, $f=15.2$ kHz and $f=15.3$ kHz are inside an AR-frequency band, and $f=11.7$ kHz and $f=11.8$ kHz are in an AR-free frequency band. Fig.4-23 and Fig.4-24 show the spectral irradiance of the Osram MH lamp operated at different power in no AR and AR situations.

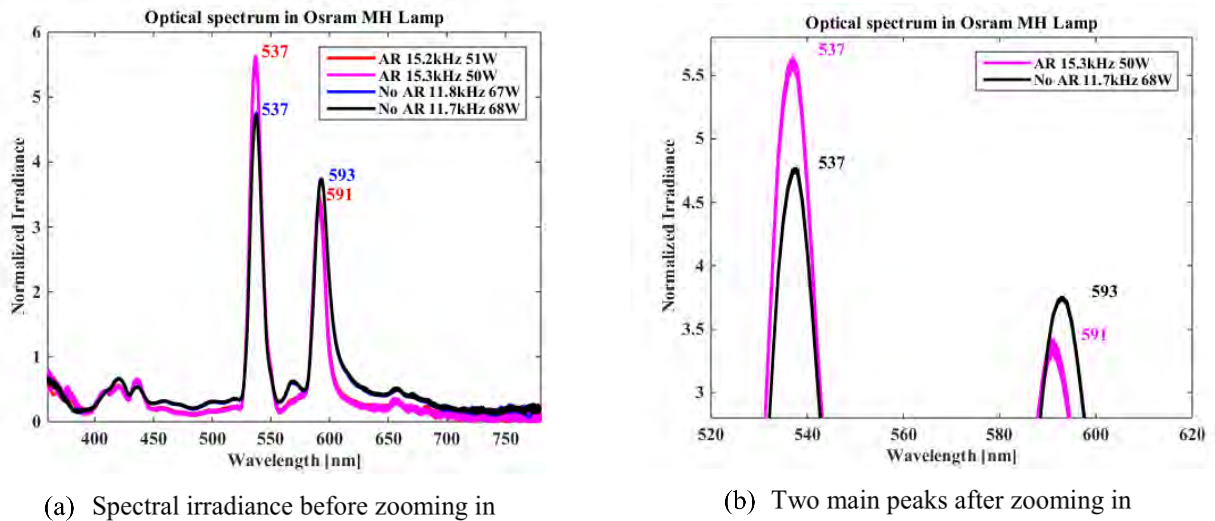


Fig.4-23 Spectral irradiance of the Osram MH lamp operated at lower power

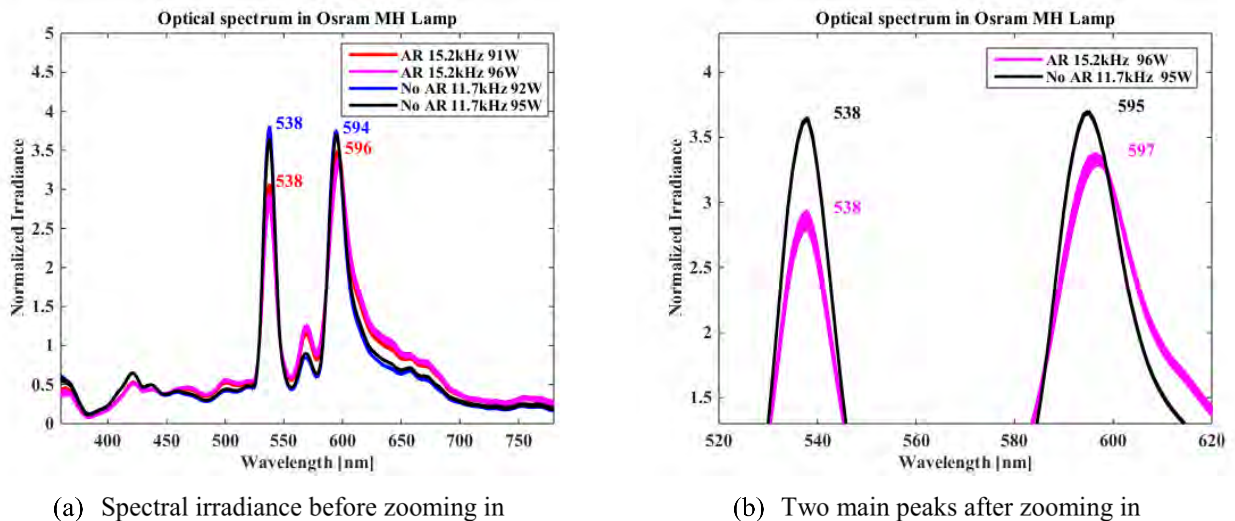


Fig.4-24 Spectral irradiance in the Osram MH lamp operated at higher power

The spectral irradiance of the lamp contains information on how the optical energy or power is distributed over different wavelength. As can be seen from Fig.4-23 and Fig.4-24, there are two main peaks in the spectrum of the lamp between 360-780 nm. The ratio between the first peak and the second peak is different in AR and no AR situations. In the AR situation, this ratio increases significantly. We also observe that the variations at two

main peaks are different during the 20-minute observing window in AR and no AR situations. After zooming in the spectrum, these variations can be seen more clearly.

The standard deviation (STD) and the relative standard deviation (RSD) are calculated in order to analyze the variations of the spectral irradiance at the two main peaks and classify between AR and no AR cases. RSD also called the coefficient of variation (CV) is a standardized measure of dispersion of a probability distribution. It is defined as the ratio of the STD to mean value and often expressed as a percentage. RSD is used to compare data sets with different units or widely different means. Thus, The STDs and RSDs of the spectral irradiance at two main peaks are presented in TABLE 4-7. P1 and P2 respectively represent the first and the second peak in the spectral irradiance.

TABLE 4-7 Variations of the spectral irradiance in the Osram MH lamp

Operation situation & Operation frequency		Peaks in spectrum (Mean, ± 2 *STD) RSD	
AR	$f=15.2$ kHz Pa=91 W	P1 = (0.0431 \pm 4.0e-4) P2 = (0.0494 \pm 3.2e-4)	RSD1=0.47% RSD1=0.31%
	$f=15.2$ kHz Pa=96 W	P1 = (0.0429 \pm 7.0e-4) P2 = (0.0495 \pm 6.4e-4)	RSD1=0.82% RSD2=0.64%
	$f=15.2$ kHz Pa=51 W	P1 = (0.0232 \pm 5.8e-4) P2 = (0.0139 \pm 7.4e-4)	RSD1=1.27% RSD1=2.65%
	$f=15.3$ kHz Pa=50 W	P1 = (0.0230 \pm 6.6e-4) P2 = (0.0136 \pm 6.4e-4)	RSD1=1.44% RSD2=2.37%
No AR	$f=11.7$ kHz Pa=92 W	P1 = (0.0582 \pm 8.0e-5) P2 = (0.0566 \pm 6.2e-5)	RSD1=0.068% RSD2=0.055%
	$f=11.7$ kHz Pa=95 W	P1 = (0.0586 \pm 9.6e-5) P2 = (0.0580 \pm 1.0e-4)	RSD1=0.083% RSD2= 0.089%
	$f=11.8$ kHz Pa=67 W	P1 = (0.0322 \pm 4.0e-5) P2 = (0.0260 \pm 5.8e-5)	RSD1=0.064% RSD2=0.11%
	$f=11.7$ kHz Pa=68 W	P1 = (0.0322 \pm 4.0e-5) P2 = (0.0260 \pm 5.2e-5)	RSD1=0.061% RSD2= 0.098%

In TABLE 4-7, the STD and RSD at two main peaks are much greater in the AR situation whatever the lamp operates at lower power or higher power. In no AR situation, the STD and RSD are almost equal to the reference itself (the lowest STD and RSD). In the AR situation, the STD and RSD are at least 5 or 6 times of the reference STD and RSD. Especially, when the lamp works at lower power, the STD and RSD are more than 10 or 20 times of the reference STD and RSD. For example, the STD and RSD (@15.2 kHz, Pa=51 W) at the first peak are 15 or 20 times of the reference STD and RSD.

In order to classify AR and no AR situations, Fisher's exact test is proposed here. The Fisher's exact test computes the probability to observe an indicator with a value "worse" than the one observed due to noise only. If we reject the hypothesis that the difference is explained by noise only, this result is also the probability of being

wrong in taking the decision. As a practical rule, values lower than 5 % are considered as significant, and values below 0.5% are very significant. For instance, when compared in the no AR situations (@11.7 kHz, 92 W and @11.7 kHz, 95 W), the p-value is equal to 0.1. This means that these two situations are not significantly different. If we compare peaks of the spectrum in the no AR situation (@11.7 kHz, 92 W) with no AR situation (@15.2 kHz, Pa=91 W), and the p-value is equal to 0. This means that these two situations are totally different.

B. Results in the GE MH lamp (aged 100 hours)

In the GE MH lamp, $f=15.5$ kHz and $f=15.6$ kHz are inside an AR frequency band while AR-free frequency band contains $f=10.7$ kHz and $f=10.6$ kHz. Fig.4-25 shows the spectral irradiance of the GE MH lamp in no AR and AR situations.

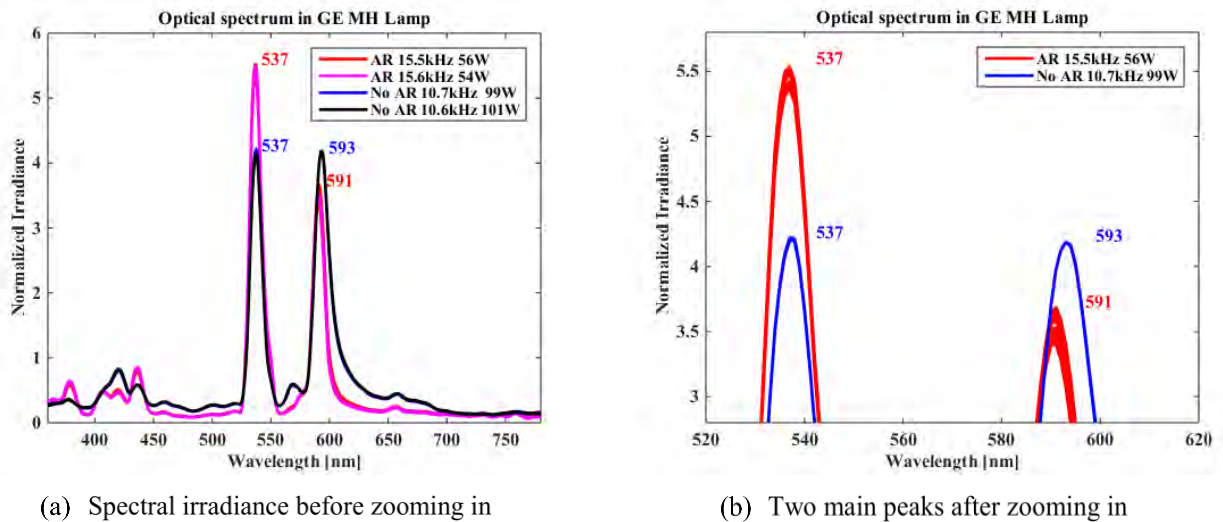


Fig.4-25 Spectral irradiance in GE MH lamp

In Fig.4-25 (a), the first peak P1 and the second peak P2 appear at 537 nm 593 nm respectively @ 15.5 kHz, 56 W in the AR situation. In the no AR situation @ 10.7 kHz, 99 W, the first peak P1, and the second peak P2 appear at 537 nm 591 nm respectively. There are no obvious differences of wavelength in AR and no AR situation. The maximum irradiance at which wavelength depends on the elements in the arc tube and the lamp operating power. In Fig.4-25 (b), the variations of the irradiance are apparent different at two main peaks in no AR and AR situations. This means that AR influences on the spectrum of the lamp. The STD and RSD of the irradiance at two peaks are shown in TABLE 4-8.

TABLE 4-8 Variations of spectral irradiance in GE MH lamp

Operation situation & Operation frequency		Peaks in spectrum (Mean, ± 2 *STD) RSD	
AR	$f=15.5$ kHz Pa=56 W	P1 = (0.0576 \pm 1.1e-3) P2 = (0.0377 \pm 1.9e-3)	RSD1=0.92% RSD1=2.54%
	$f=15.6$ kHz Pa=54 W	P1 = (0.0567 \pm 7.2e-4) P2 = (0.0363 \pm 3.4e-4)	RSD1=0.64% RSD2=0.48%
No AR	$f=10.7$ kHz Pa=99 W	P1 = (0.1081 \pm 1.5e-4) P2 = (0.1093 \pm 7.2e-5)	RSD1=0.072% RSD2=0.033%
	$f=10.6$ kHz Pa=101 W	P1= (0.1058 \pm 2.2e-4) P2 = (0.1114 \pm 8.0e-5)	RSD1=0.10% RSD2= 0.036%

According to TABLE 4-8, in the no AR situation, the STD of P1 at $f=10.6$ kHz is about 1.5 times of the reference STD ($7.5e-5$), and the RSD of P1 is around 1.4 times of the reference RSD (0.072%). The STD of P2 at $f=10.6$ kHz is about 1.1 times of its reference ($3.6e-5$) and the RSD of P2 at $f=10.6$ kHz is around 1.1 times of its reference (0.033%).

In the AR situation, the STD and RSD of P1 at $f=15.5$ kHz is about 5 and 9 times of the reference STD ($7.5e-5$) and RSD (0.072%) individually. In addition, the STD and RSD of P2 at this frequency are about 5 and 15 times of the reference STD ($3.6e-5$) and RSD (0.033%).

In summary, in absence of AR, the STD and RSD of P1 and P2 are less than 2 times of their reference values. On the other hand, in the presence of AR, the STD and RSD of P1 and P2 are at least 5 times of their reference values. There are more variations of the spectrum at two main peaks in case of AR. These results are similar to the Osram MH lamp.

C. Results in old Philips MH lamp (aged 8000 hours)

In the Philips lamp, $f=12.5$ kHz and $f=12.4$ kHz are inside an AR-frequency band while $f=10.5$ kHz and $f=10.4$ kHz are in an AR-free frequency band. Fig.4-26 shows the spectral irradiance of the GE MH lamp in no AR and AR situations.

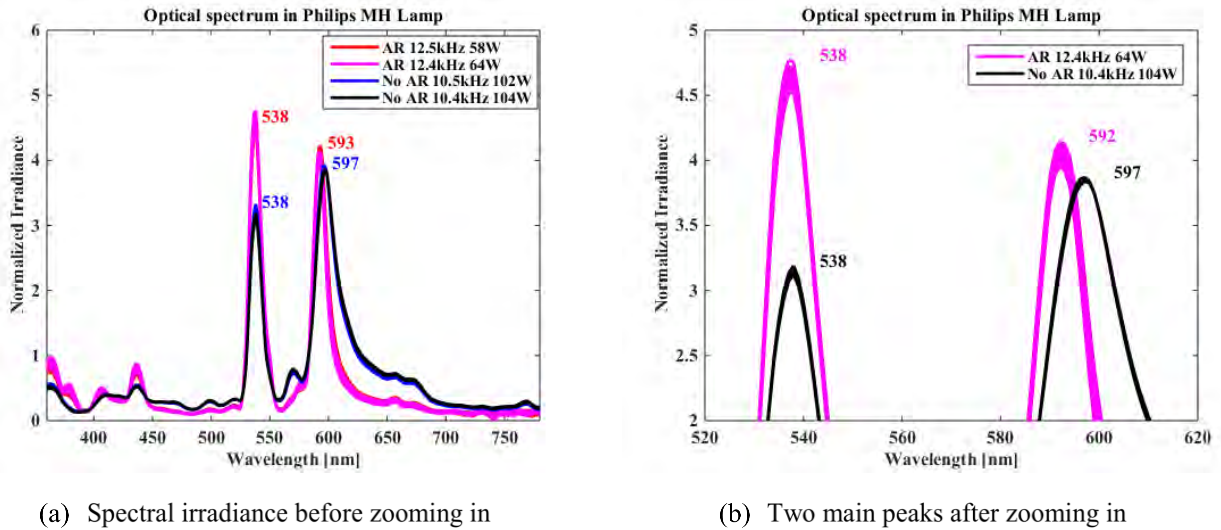


Fig.4-26 Spectral radiance in Philips MH lamp

Similar results are found in the Philips MH lamp. In the presence of AR ($f=12.4$ kHz), the variations of the irradiance at 538 nm are much greater than the variations in absence of AR ($f=10.4$ kHz) in the observing window of 20 min (51 measurements). Likewise, the variations of the irradiance at 592 nm (AR) are bigger than the variations at 597 nm (no AR). TABLE 4-9 shows the variations of the spectrum at two main peaks in the Philips MH lamp.

Similarly, the STD and RSD at two main peaks in the no AR situation are larger than the values in the no AR situation. However, some differences also are found in the aged Philips MH lamp. Comparing the results in aged Philips lamp with the previous two new lamps, we find that a few variations exist in the aged lamp, even in the no AR situations. Additionally, the STD and RSD of the irradiance in the presence of AR are much greater than the values in the absence of AR. This means that variations of the spectrum are more evident in aged lamps.

TABLE 4-9 Variations of spectral irradiance in the Philips MH lamp

Operation situation & Operation frequency		Peaks in spectrum (Mean, $\pm 2*STD$) RSD
AR	$f=12.5$ kHz $P_a=58$ W	P1 = (0.0549 \pm 1.1e-2) RSD1=10.2% P2 = (0.0500 \pm 9.8e-3) RSD1=9.75%
	$f=12.4$ kHz $P_a=64$ W	P1 = (0.0467 \pm 1.6e-2) RSD1=17.5% P2 = (0.0411 \pm 1.4e-2) RSD2=17.4%
No AR	$f=10.5$ kHz $P_a=102$ W	P1 = (0.0688 \pm 2.4e-3) RSD1=1.71% P2 = (0.0831 \pm 2.0e-3) RSD2=1.18%
	$f=10.4$ kHz $P_a=104$ W	P1= (0.0665 \pm 8.2e-4) RSD1=0.62% P2 = (0.0817 \pm 7.0e-4) RSD2=0.43%

4.3.3.2 Boxplot, standard deviation and relative standard deviation of colorimetric parameters

A. Results in the Osram MH lamp

As presented in section 4.3.2, in the Osram MH lamp, $f=15.2$ kHz and $f=15.3$ kHz are inside an AR-frequency band, and $f=11.7$ kHz and $f=11.8$ kHz are in an AR-free frequency band. Fig.4-27 shows chromaticity coordinate of MH lamps in no AR and AR situations at different operating powers.

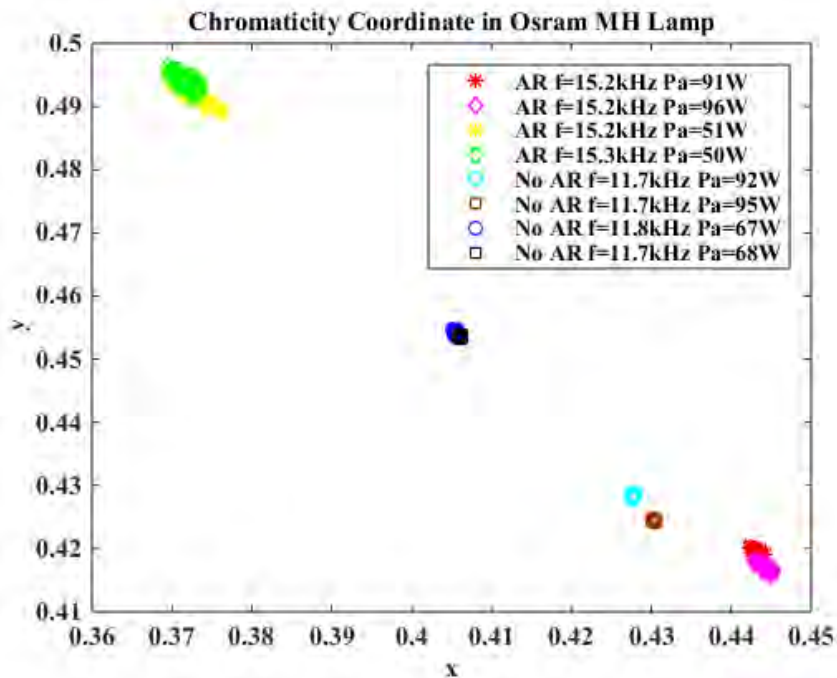


Fig.4-27 Chromaticity coordinate in the Osram MH lamp

In Fig.4-27, chromaticity coordinates are constant whatever the coordinate x or y during a long-time (20 min) observation window in the no AR situation at different operating power. However, in the AR situation, these coordinates fluctuate a lot (horizontal axis vertical axis) and the variations of coordinates x and y look like two clouds @15.2 kHz, 51 W and @15.3 kHz, 50 W. From the figure, we may observe that:

- 1) The cloud centers are roughly aligned on a line with slope 40° ;
- 2) The main factor is the power, while the driving frequency seems to have much lower influence;
- 3) Increasing the power displace the points towards higher x values, lower y values;
- 4) The presence of AR induces both a shift and a widening of the cloud;
- 5) Variance in the AR at high power is not significantly lower than the variance in the AR at low power.

As presented in section 4.3.2, boxplot is a tool to show quantiles and the spread of a random variable. To analyze the variations of colorimetric parameters between AR and no AR situations further, Fig.4-28 shows the boxplot of the previously used data. Additionally, Fig.4-29 (a) and (b) illustrate the boxplots CCT and Ra as well.

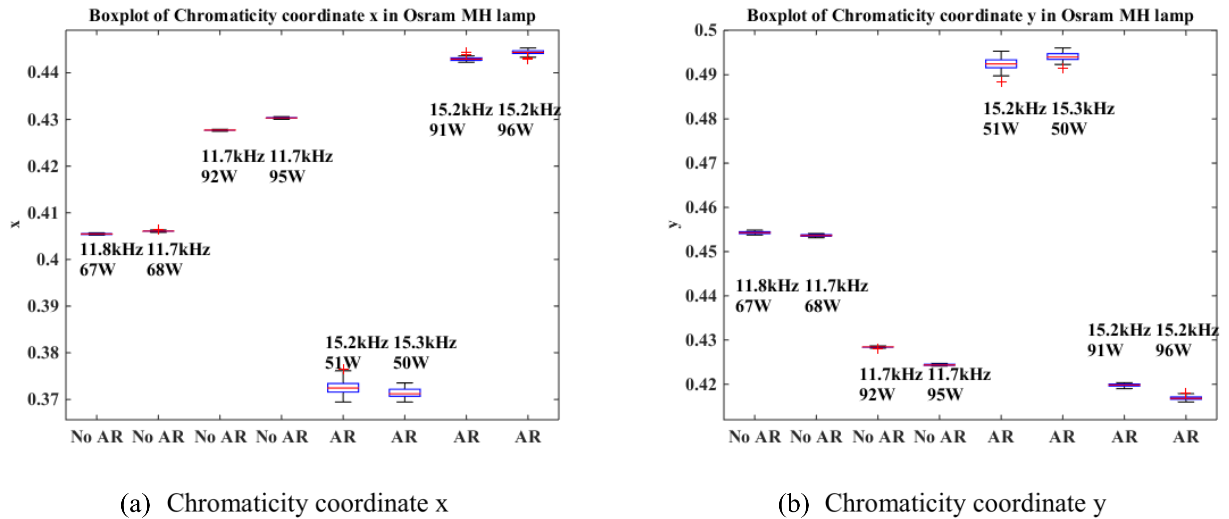


Fig.4-28 Boxplot of chromaticity coordinates x and y in the Osram MH lamp

In Fig.4-28 (a), (b), the data range as indicated from the boxes is greater at $f=15.2$ kHz and $f=15.3$ kHz in case of AR. Greater range as indicated by boxplots means chromaticity coordinates have greater dispersion. This means that the phenomenon of AR influences chromaticity coordinates of the lamp. In no AR situation, at $f=11.8$ kHz and $f=11.7$ kHz, the data are stable and the variation range of boxes in the boxplot is smaller.

In addition, Fig.4-29 shows the boxplot of chroma $C_{u'v'}$ and CCT in the Osram MH lamp. Chroma $C_{u'v'}$ is the colorfulness of an area judged as a proportion of the brightness of a similarly illuminated area that appears white or highly transmitting. $C_{u'v'}$ can be calculated from the CIE 1916 chromaticity coordinates u' and v' . The CIE 1976 chromaticity diagram is a projective transformation of the CIE 1931 x, y chromaticity diagram.

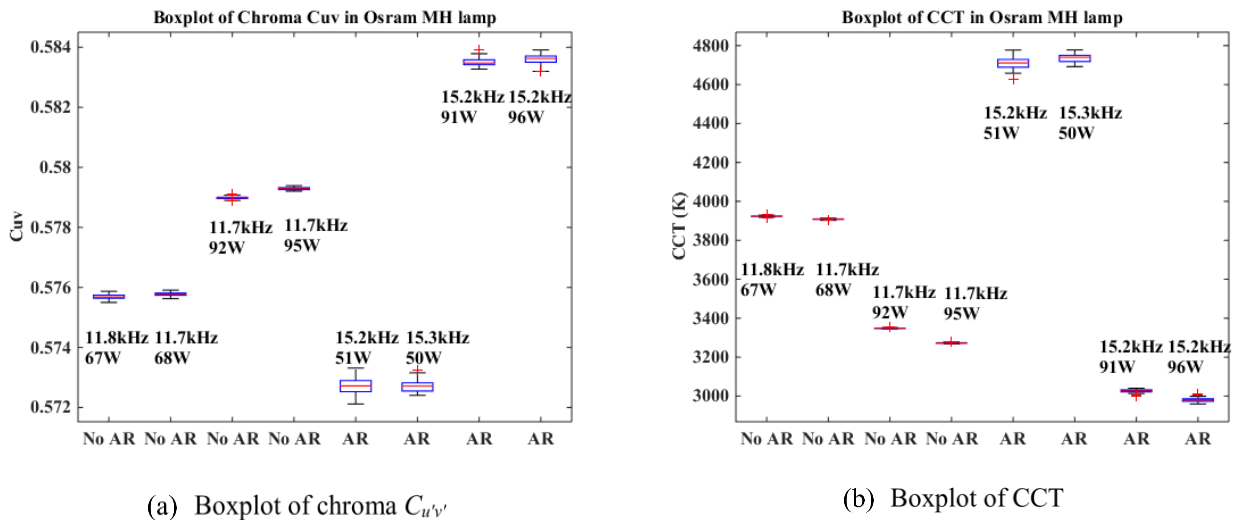


Fig.4-29 Boxplot of chroma $C_{u'v'}$ and CCT in the Osram MH lamp

In Fig.4-29 (a), the boxplot of chroma $C_{u'v'}$ shows the similar characterizations to chromaticity coordinates of Fig.4-28. In the AR situation, the dispersions of chroma $C_{u'v'}$ are greater than dispersions in the no AR situation. Additionally, the difference between no AR and AR situations is more evident in the boxplots of chroma $C_{u'v'}$.

In Fig.4-29 (b), in the AR situation @15.2 kHz, 51 W and @15.3 kHz, 50 W, Max-Min of CCT is about 150 K, In the no AR situation @11.8 kHz, 67 W and @11.7 kHz, 50 W, Max to Min of CCT is just about 10 K. The variations of CCT in the AR situation are still greater than variations in the no AR situation.

In order to evaluate the variations of colorimetric parameters, the STD and the RSD are calculated as well, as shown in TABLE 4-10.

TABLE 4-10 Variations of colorimetric parameters in the Osram MH lamp

Operation situation & operating frequency		Variations of colorimetric parameters (Mean \pm 2*STD) RSD			
		x	y	$C_{u'v'}$	CCT
AR	$f=15.2$ kHz Pa=91 W	(0.4430 \pm 7.8e-4) 0.089%	(0.4198 \pm 6.4e-4) 0.077%	(0.5835 \pm 2.6e-4) 0.022%	3025 \pm 16) 0.27%
	$f=15.2$ kHz Pa=96W	(0.4444 \pm 1.1e-3) 0.13%	(0.4196 \pm 9.4e-4) 0.11%	(0.5836 \pm 3.4e-4) 0.029%	(2981 \pm 24) 0.40%
	$f=15.2$ kHz Pa=51 W	(0.3725 \pm 3.0e-3) 0.39%	(0.4924 \pm 2.8e-3) 0.29%	(0.5727 \pm 5.2e-4) 0.045%	(4709 \pm 62) 0.66%
	$f=15.3$ kHz Pa=50 W	(0.3715 \pm 2.0e-3) 0.27%	(0.4941 \pm 2.0e-3) 0.20%	(0.5727 \pm 4.0e-4) 0.036%	(4735 \pm 42) 0.45%
No AR	$f=11.7$ kHz Pa=92 W	(0.4277 \pm 2.0e-4) 0.024%	(0.4284 \pm 2.5e-4) 0.029%	(0.5790 \pm 9.2e-5) 0.0079%	(3348 \pm 4) 0.062%
	$f=11.7$ kHz Pa=95 W	(0.4303 \pm 2.2e-4) 0.026%	(0.4244 \pm 3.4e-4) 0.039%	(0.5793 \pm 8.8e-5) 0.0076%	(3272 \pm 5) 0.083%
	$f=11.8$ kHz Pa=67 W	(0.4055 \pm 2.6e-4) 0.033%	(0.4543 \pm 6.0e-4) 0.065%	(0.5757 \pm 1.6e-4) 0.014%	(3924 \pm 5) 0.069%
	$f=11.7$ kHz Pa=68 W	(0.4061 \pm 2.4e-4) 0.029%	(0.4536 \pm 4.6e-4) 0.051%	(0.5758 \pm 1.2e-4) 0.011%	(3908 \pm 5) 0.064%

Comparing Fig.4-27 with TABLE 4-10, we can find that greater dispersions of chromaticity coordinates x, y in the figure and the higher RSD in the table in the AR case. In TABLE 4-10, the STDs and RSDs of chromaticity coordinates x, y, $C_{u'v'}$, and CCT in the AR situation are greater than the values in the no AR case.

AR phenomenon gets more serious with the lamp operating power increasing [10] and unstable visual effects of the lamp arc get more evident. The variations of lamp electrical parameters such as current, voltage and power also get more unstable. Nevertheless, variations of colorimetric parameters do not increase as the rise of lamp operating power. In contrast, the variations of colorimetric parameters are more evident when the lamp operates at lower power.

By comparing the STDs and RSDs in AR and no AR situations, we conclude as follows:

- 1) In the absence of AR, the STDs and RSDs of colorimetric parameters: chromaticity coordinates x and y, $C_{u'v'}$, and CCT are always about equal to the reference (the lowest STD and RSD in the no AR situation).

- 2) In the presence of AR, the STDs and RSD of colorimetric parameters are at least 3 times of the reference (the lowest STD and RSD in the no AR situation) at the significance level 0.05.

B. Results in the GE MH lamp

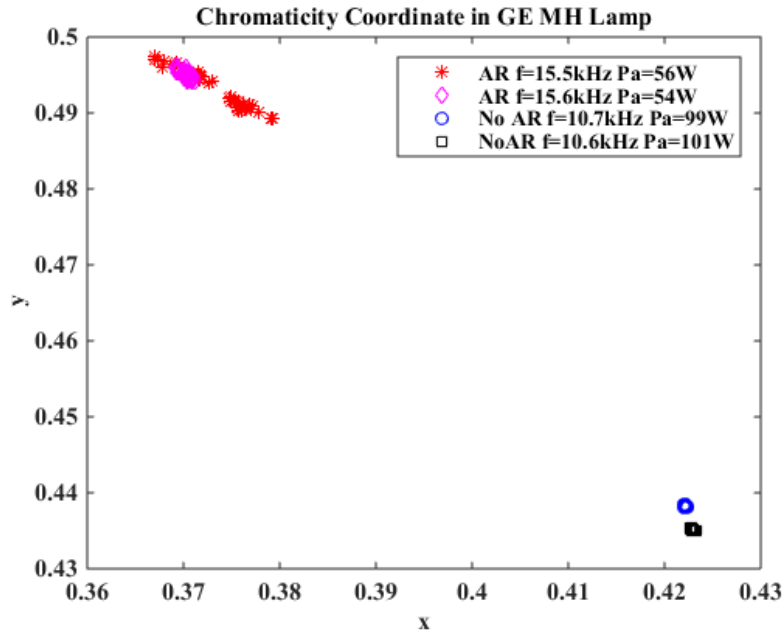


Fig.4-30 Chromaticity coordinate in the GE MH lamp

In Fig.4-30, in the AR situation, low-frequency fluctuations are observed in the chromaticity coordinates and at $f=15.5$ kHz, these fluctuations are more evident than fluctuations in the no AR situation. In the no AR situation, all chromaticity coordinates are constant, and they keep the same points at each operating frequency $f=10.7$ kHz and $f=10.6$ kHz. These results are similar to the obtained results in the Osram MH lamp.

Same statistical analysis methods are implemented in the GE MH lamp. Therefore, Fig.4-31 and Fig.4-32 show the boxplots of chromaticity coordinates, C_{uv} , and CCT respectively.

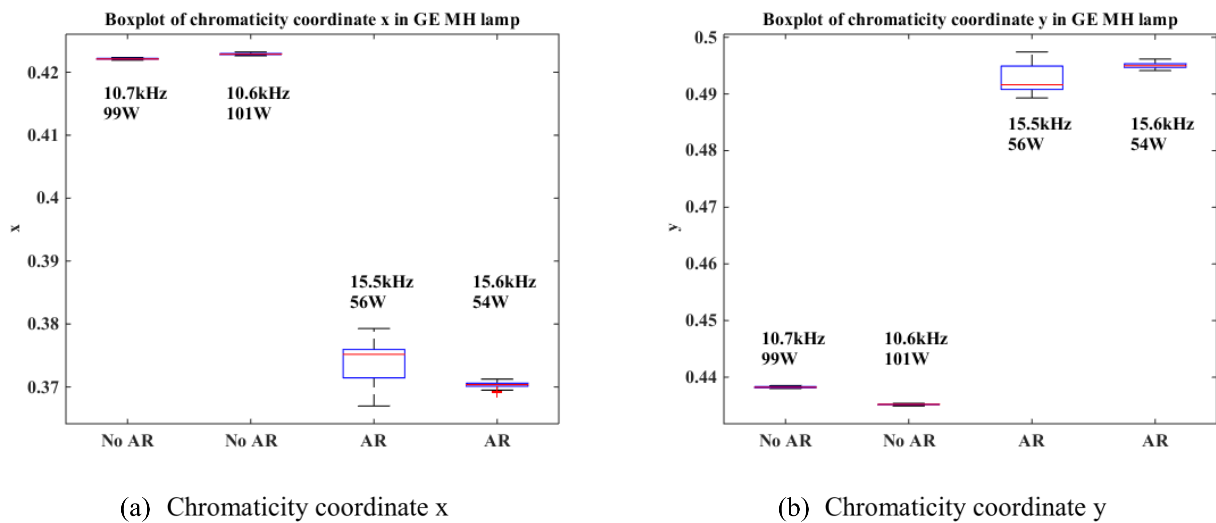


Fig.4-31 Boxplots of chromaticity coordinate in GE MH lamp

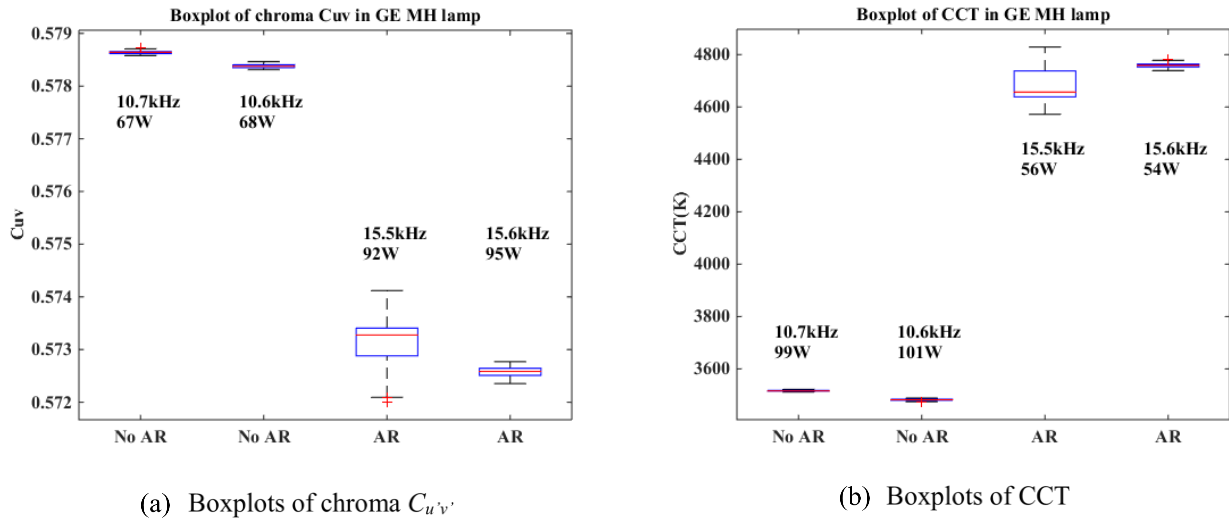


Fig.4-32 Boxplots of $C_{u'v'}$ and CCT in the GE MH lamp

Fig.4-31 (a) and (b) confirm the obtained results in Fig.4-30. In Fig.4-31, the Max-Min of boxplots is about equal to the interquartile range (IQR) in the absence of AR @10.7 kHz, 67 W and @10.6 kHz, 68 W. In the presence of AR @15.5 kHz, 92 W, in the boxplot of chromaticity coordinate x, Max-Min is about 0.002, and IQR is about 0.001. The data are dispersed. The boxplots of $C_{u'v'}$ and CCT in Fig.4-32 show the similar characterizations to Fig.4-31 as well.

TABLE 4-11 illustrates the STDs and RSDs of colorimetric parameters in the GE MH lamp.

TABLE 4-11 Variations of colorimetric parameters in the GE MH lamp

Operation situation & Operation frequency		Variations of colorimetric parameters (Mean, $\pm 2*STD$)			
		RSD			
		x	y	$C_{u'v'}$	CCT
AR	$f=15.5$ kHz	$(0.3736 \pm 6.4e-3)$ 0.87%	$(0.4929 \pm 4.8e-3)$ 0.49%	$(0.5731 \pm 1.0e-3)$ 0.087%	(4689 ± 138) 1.46%
	$f=15.6$ kHz	$(0.3703 \pm 1.0e-3)$ 0.14%	$(0.4950 \pm 9.8e-4)$ 0.10%	$(0.5726 \pm 2.0e-4)$ 0.016%	(4760 ± 22) 0.23%
No AR	$f=10.7$ kHz	$(0.4221 \pm 2.0e-4)$ 0.024%	$(0.4382 \pm 2.5e-4)$ 0.029%	$(0.5786 \pm 6.0e-5)$ 0.0052%	(3516 ± 5) 0.071%
	$f=10.6$ kHz	$(0.4229 \pm 2.8e-4)$ 0.033%	$(0.4352 \pm 2.4e-4)$ 0.028%	$(0.5784 \pm 7.4e-5)$ 0.0063%	(3482 ± 6) 0.092%

As can be seen in TABLE 4-11, the STDs and RSDs of chromaticity coordinates in the AR situation are at least 4 times of the reference (the lowest STD and RSD in the no AR situation). In the absence of AR, their STDs and RSDs are about equal to the reference. This means that the variations of chromaticity coordinates in the AR

situation are much higher than the variations in the no AR situation. Other colorimetric parameters such as C_{uv} and CCT confirm these variations as well. The STD and RSD of colorimetric parameters could be as an indicator to evaluate the severity of AR phenomena.

C. Results in the Philips MH lamp

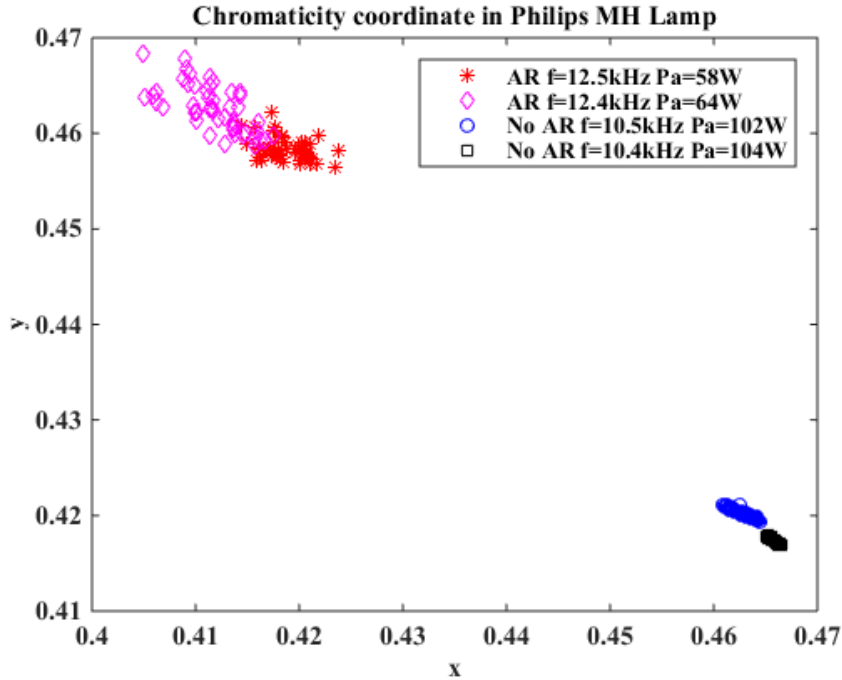
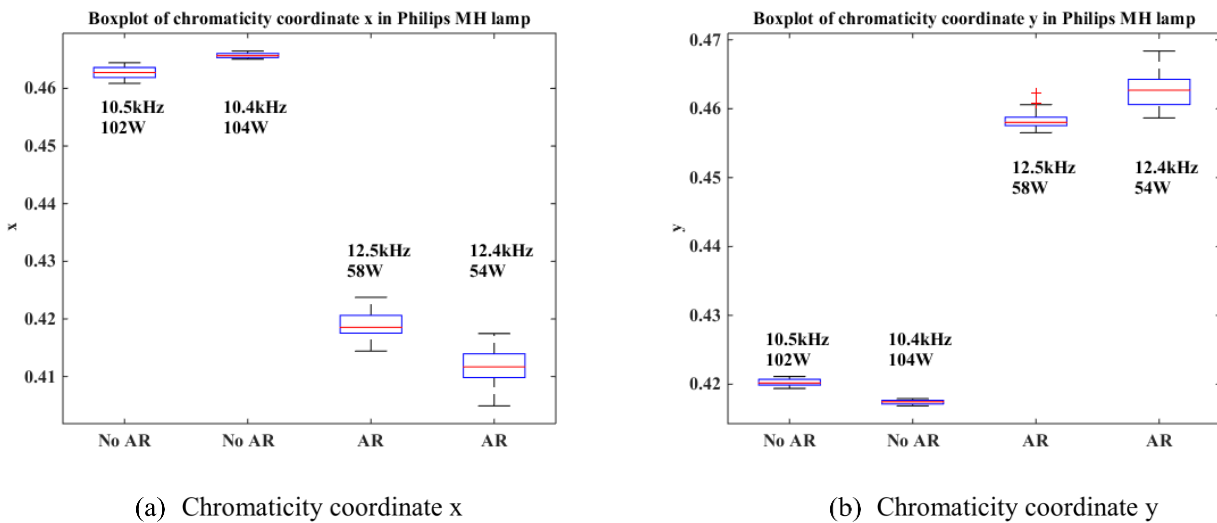


Fig.4-33 Chromaticity coordinate in Philips MH lamp

Fig.4-33 illustrates chromaticity coordinates in the aged Philips MH lamp. Evident fluctuations are observed in the AR situation at $f=12.5$ kHz and $f=12.4$ kHz. In the no AR situation, small fluctuations are observed as well, even after the low-time drift data are corrected. This is different to the results in two other new lamps. In new Osram and GE MH lamps, chromaticity coordinates are almost constant, and no variations are observed.



(a) Chromaticity coordinate x

(b) Chromaticity coordinate y

Fig.4-34 Chromaticity coordinate in Philips MH lamp

The boxplots of chromaticity coordinates in Fig.4-34 confirm the results in Fig.4-33. Greater variations of chromaticity coordinate in the AR situation and smaller variations in the no AR situation for aged MH lamps.

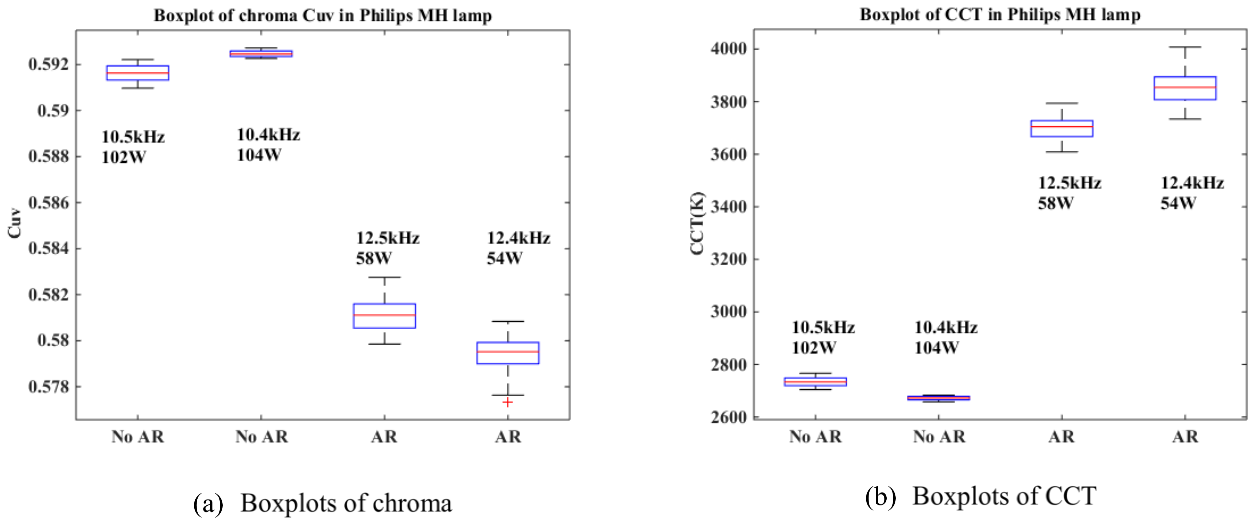


Fig.4-35 Boxplots of chroma C_{uv} and CCT in the Philips MH lamp

Fig.4-35 (a) and (b) show the boxplots chroma C_{uv} and CCT respectively. Although different boxplots are presented, but similar results are obtained. AR causes obvious variations of C_{uv} and CCT for aged MH lamps. On the other hand, some variations of C_{uv} and CCT are observed even in the no AR situation for aged MH lamps.

TABLE 4-12 Variations of colorimetric parameters in the Philips MH lamp

Operation situation & Operation frequency		Variations of colorimetric parameters (Mean, $\pm 2*$ STD) RSD			
		x	y	C_{uv}	CCT
AR	$f=12.5$ kHz	$(0.4188 \pm 4.2e-3)$ 0.51%	$(0.4583 \pm 2.4e-3)$ 0.26%	$(0.5810 \pm 1.4e-3)$ 0.12%	(3702 ± 82) 1.10%
	$f=12.4$ kHz	$(0.4117 \pm 6.4e-3)$ 0.77%	$(0.4627 \pm 4.8e-3)$ 0.53%	$(0.5794 \pm 1.7e-3)$ 0.15%	(3853 ± 134) 1.74%
No AR	$f=10.5$ kHz	$(0.4627 \pm 2.0e-3)$ 0.23%	$(0.4203 \pm 9.4e-4)$ 0.11%	$(0.5916 \pm 7.4e-4)$ 0.063%	(2735 ± 36) 0.65%
	$f=10.4$ kHz	$(0.4657 \pm 8.0e-4)$ 0.086%	$(0.4174 \pm 6.2e-4)$ 0.074%	$(0.5925 \pm 2.6e-4)$ 0.023%	(2672 ± 15) 0.29%

TABLE 4-12 confirms the results in Fig.4-33, Fig.4-34 and Fig.4-35 further. Greater variations are observed in the figure, and higher STDs and RSDs are in the table. Comparing the results in aged Philips MH lamp with the results in the Osram and GE MH lamps, some differences are observed. In the new MH lamps, there are almost no spectral variations in the no AR situation. In aged MH lamps, even in the no AR situation, spectral

variations are observed. This means that the spectral irradiance and colorimetric parameters get unstable in aged MH lamps. On the other hand, greater spectral variations are observed in the AR situations. All the lamps present similar results. This means that AR significantly influences the spectral irradiance and colorimetric parameters.

4.3.3.3 Comparisons between spectral variation detection methods

In order to evaluate the spectral variation detection method, TABLE 4-13 shows the advantages and disadvantages of this method.

TABLE 4-13 Disadvantages and advantages of spectral variation detection

Type	Spectral irradiance	Colorimetric parameters			
		CIE 1931 chromaticity coordinate		CIE 1976 chroma	CCT
		x	y	$C_{uv'}$	
Sensitivity to AR	High	High	High	High	High
Ability to discriminate AR	Very good	Very good	Good	Good	Good
Discriminate close frequency	Low	Require statistical analysis	Require statistical analysis	Require statistical analysis	Require statistical analysis
Sensitivity to noise	High	High	High	High	High
Cost	High	Low	Low	Low	Low

As can be seen from this table, the spectral irradiance, chromaticity coordinate, CCT have high sensitivity to AR phenomenon. They are enabled to discriminate no AR and AR cases. However, the spectral irradiance and colorimetric parameters are not enabled to distinguish close frequencies. Moreover, spectral irradiance and colorimetric parameters are sensitive to noise signals. These parameters are easily influenced by environmental factors such as temperature, humidity and so on. From the economical factor speaking, detecting the spectral irradiance is a high-cost method to fulfill.

4.4 Correlation between voltage envelope detection and light spectral variation detection

According to the detection results using the commercial devices, we concluded that both voltage envelope detection and light spectral variation detection could distinguish AR well, and found the correlation between these two detection methods as well. The obtained experimental results in the previous sections show that different kinds of MH lamps have similar characterizations in AR and no AR situations. Therefore, the following section only presents the correlation between voltage envelope detection and light spectral variation detection in the Osram MH lamp.

4.4.1 Standard deviation of voltage envelope versus colorimetric parameters

Fig.4-36 and Fig.4-37 demonstrate the relationship between these two kinds of detection methods in the Osram MH lamp. As presented in section 4.3.1, the data acquisition system of the voltage envelope is the same to chromaticity coordinates. These two kinds of data are sampled simultaneously. At each operating power, 51

measurements are recorded. The voltage envelopes are sampled by the lock-in amplifier SR830. Chromaticity coordinates are sampled by the spectrophotometer CL-500.

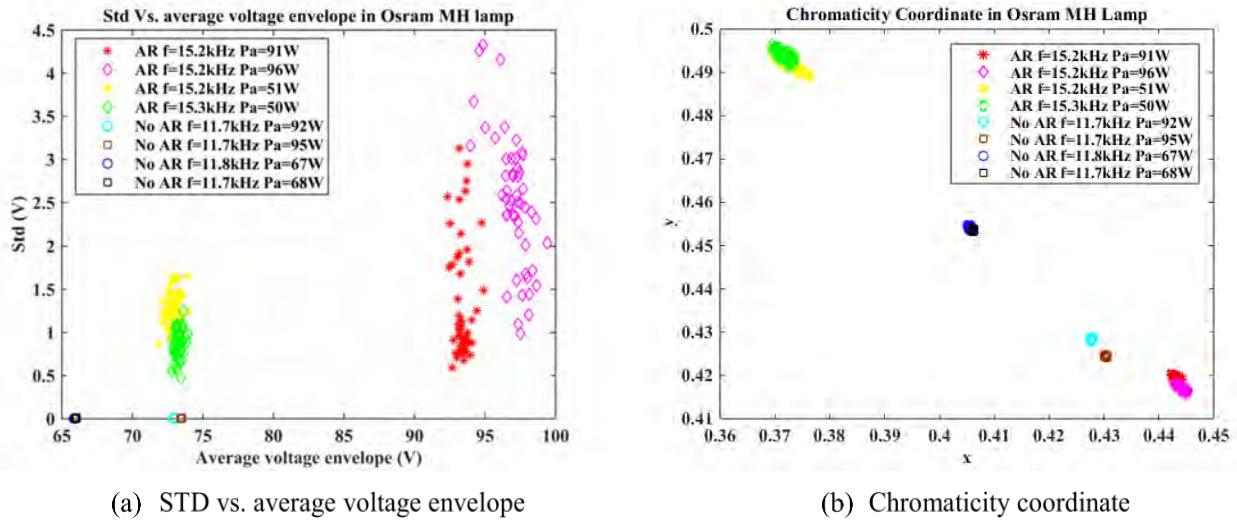


Fig.4-36 Comparison between voltage envelope detection and spectral variations detection

As can be seen from Fig.4-36, the distribution of these data presents some striking similarities between the 2D plane of voltage envelope and chromaticity coordinates. In Fig.4-36 (a), the data are scattered, and the STDs of voltage envelopes change a lot in the presence of AR. Meanwhile, chromaticity coordinates are dispersed as well in Fig.4-36 (b). Conversely, in the no AR situation, when the data are constant in the 2D plane, chromaticity coordinates are constant too.

Another 2D plane of the STD of voltage envelope *versus* colorimetric parameters is illustrated in Fig.4-37, in order to analyze the relationship between these two kinds of detection methods.

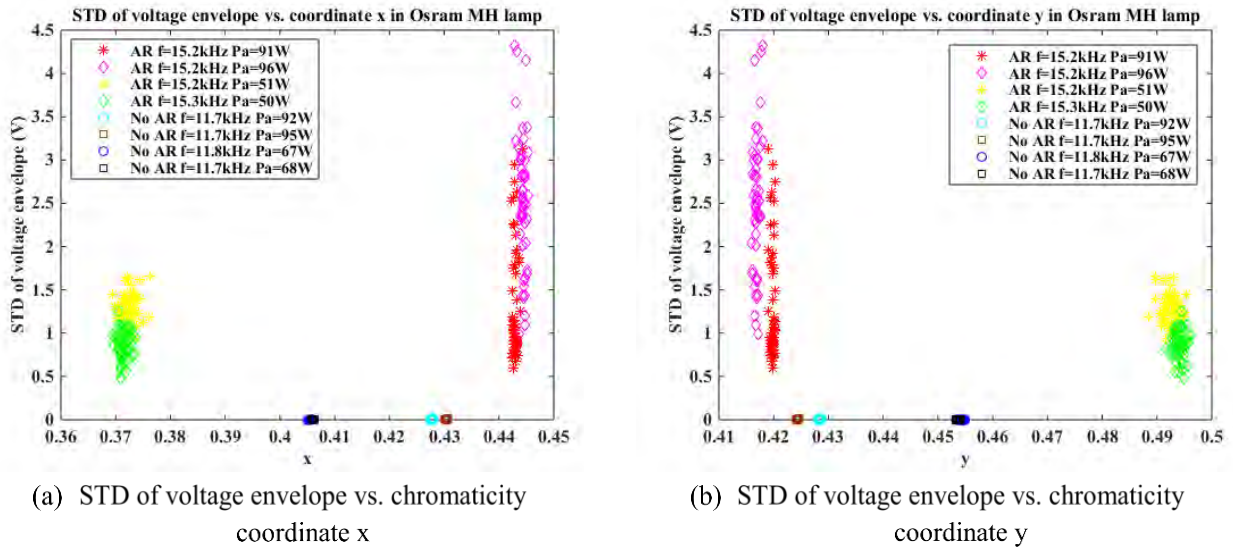


Fig.4-37 Correlation between voltage envelope detection and spectral variation detection in the Osram MH lamp

In Fig.4-37, the STDs of voltage envelope are almost zero and chromaticity coordinates x and y are constant in the no AR situation. On the other hand, the data are significantly different, and the STDs of voltage always

changes a lot. Meanwhile, there are greater variations of chromaticity coordinates in the presence of AR. Therefore, AR and no AR cases can be totally separated from our proposed 2D plane.

The 2D plane of the average voltage envelope *versus* chromaticity coordinates is also proposed here, as presented in Fig.4-38. Voltage and chromaticity coordinate have different units. Data are normalized, and the normalized value is equal to the real value divided by the maximum value.

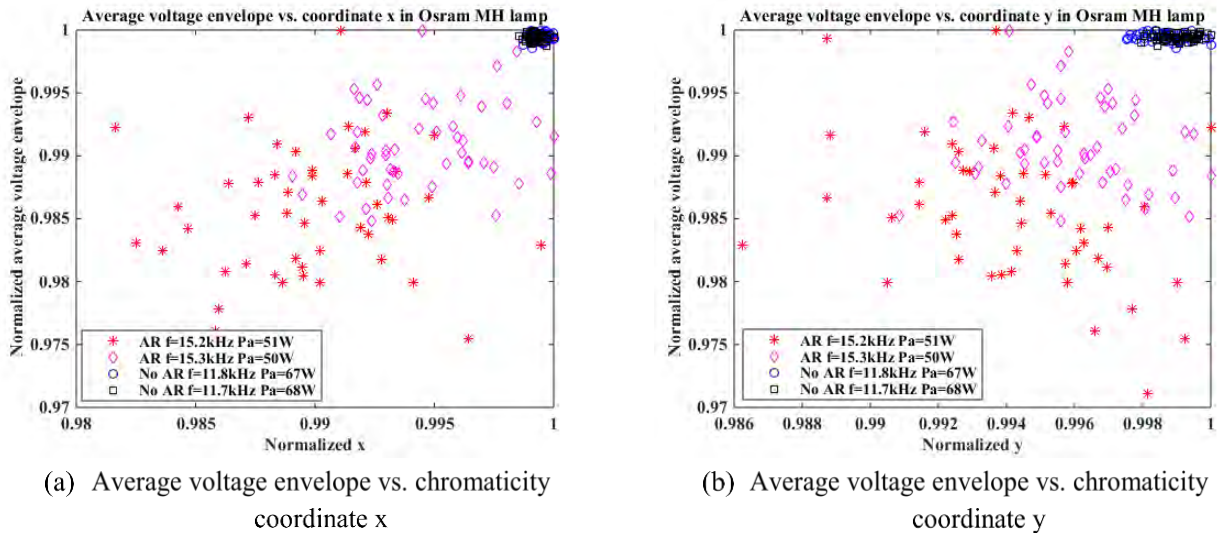


Fig.4-38 Correlation between voltage envelope detection and spectral variation detection in the Osram MH lamp

In Fig.4-38, both average voltage envelopes (y-axis) and chromaticity coordinates (x-axis) have greater variations in case of AR. In the no AR situation, these data are much more constant.

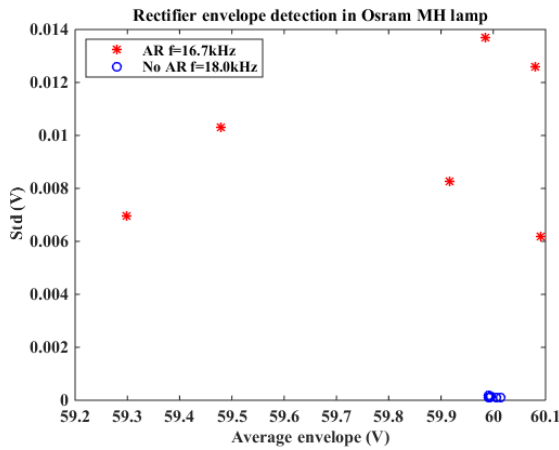
In conclusion, AR not only causes fluctuations in the lamp voltage, but also causes some fluctuations in the colorimetric parameters. AR significantly influences the performance of the lamps.

4.5 Validations of our online detection methods with respect to the lock-in amplifier

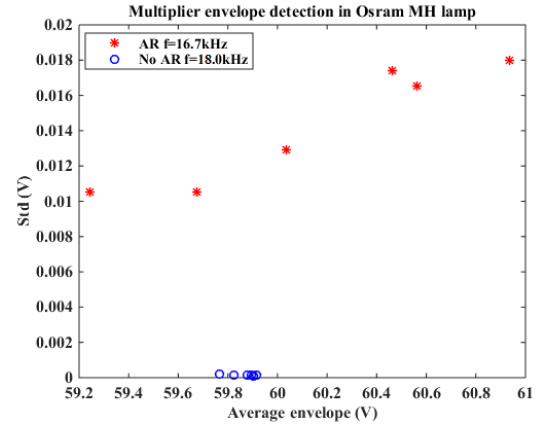
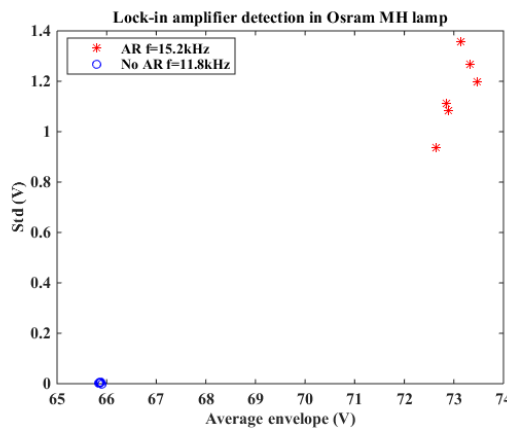
In chapter 3, two kinds of online envelope detection methods were proposed. In this chapter, a lock-in amplifier is used to obtain the voltage envelope and statistical methods are used to analyze AR characterizations. In this section, it will be verified that our online detection methods have the similar performances to those using the lock-in amplifier.

4.5.1 Experimental result comparisons between different detection methods

To verify our online envelope detection methods, have the similar function to those using the commercial lock-in amplifier, the results of different envelope detection methods are compared here. Fig.4-39 illustrates comparisons of different envelope detection results.



(a) Online detection using the rectifier circuit

(b) Online detection using the multiplier circuit
(Reference with DC offset)

(c) Voltage envelope detection using a lock-in amplifier

Fig.4-39 Comparisons of different envelope detection results

According to Fig.4-39, the 2-D plane of STD of voltage envelope *versus* average envelope is able to separate AR and no AR situations, although different envelope detection methods have been used for AR detection. In addition, all these figures show that in the AR situation, the STDs of voltage envelope change a lot. The data are constant, and the STDs are close to zero in the no AR situation.

The differences among these figures are the changing ranges of STDs. This main reason is that different acquisition systems are used in the experiments.

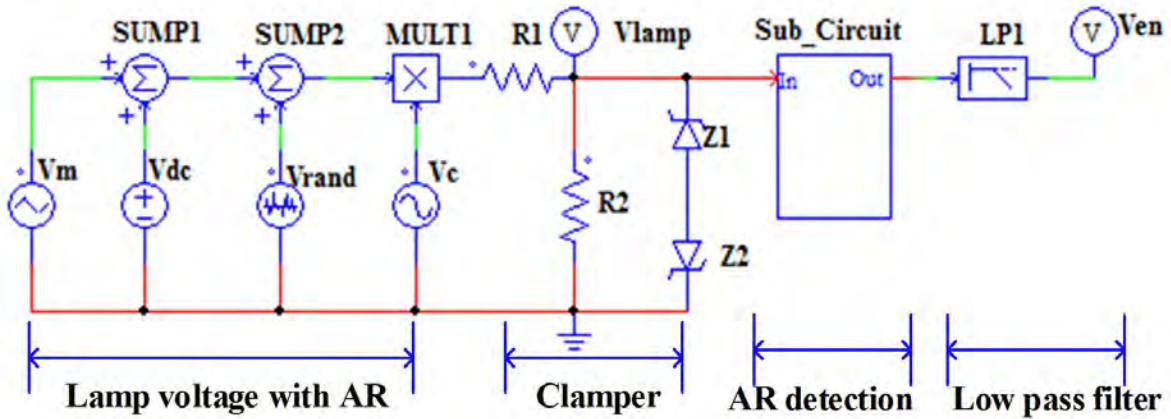
In Fig.4-39 (a) and (b), the lamp works at same situation and voltage envelopes are sampled by an oscilloscope and saved as CSV file. Then, data are separated into 6 segments in order to calculate the STDs and the averages of the voltage envelope. In Fig.4-39 (c), the voltage envelopes are sampled by a lock-in amplifier and the sample rate is 8 Hz within 4 seconds (32 data). The results show six measurements within 124 seconds.

In conclusion, we got similar 2D plane plots, even using different envelope detection methods.

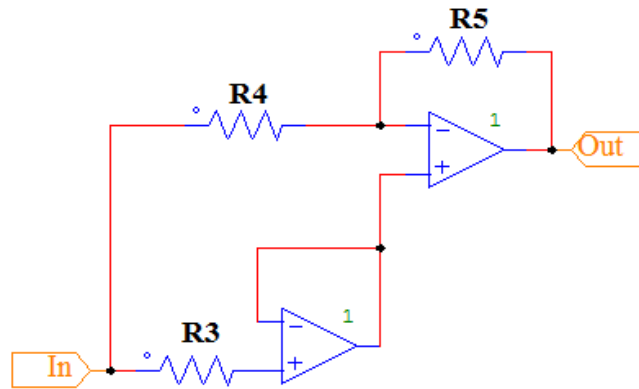
4.5.2 Simulation results between different detection methods

As presented in section 4.5.1, we got similar 2-D plane plots in our experiments by using different detection methods. However, our online detection methods and the lock-in amplifier use different acquisition systems. We cannot compare the sensitivity and the signal to noise ratio (SNR) from experimental results. Thus, in order to

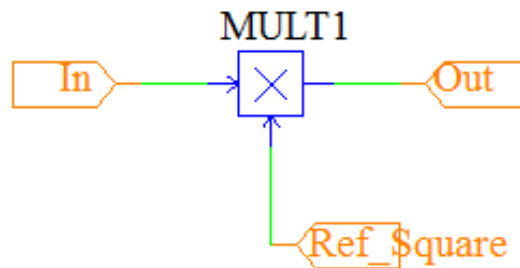
evaluate the performances of different detection methods, we also implement some simulations in PSIM software. Fig.4-40 shows the schematic of different AR detection methods.



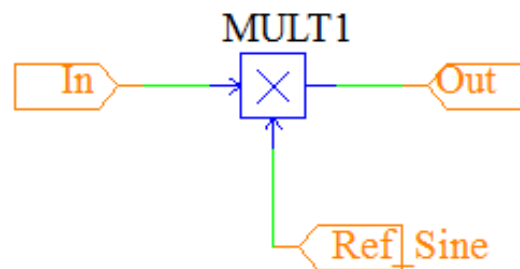
(a) Schematic of main circuit for AR detection



(b) Rectifier circuit for AR detection



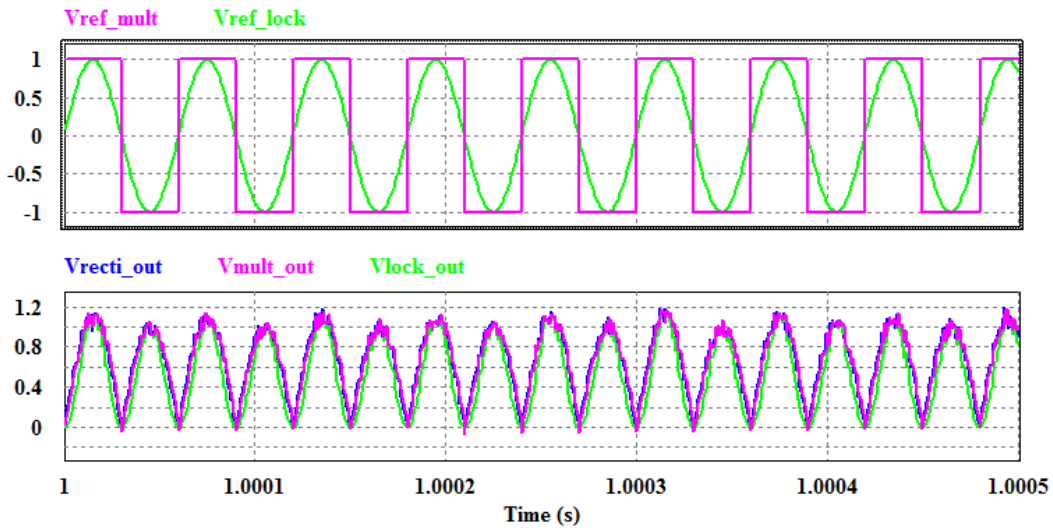
(c) Multiplier circuit for AR detection



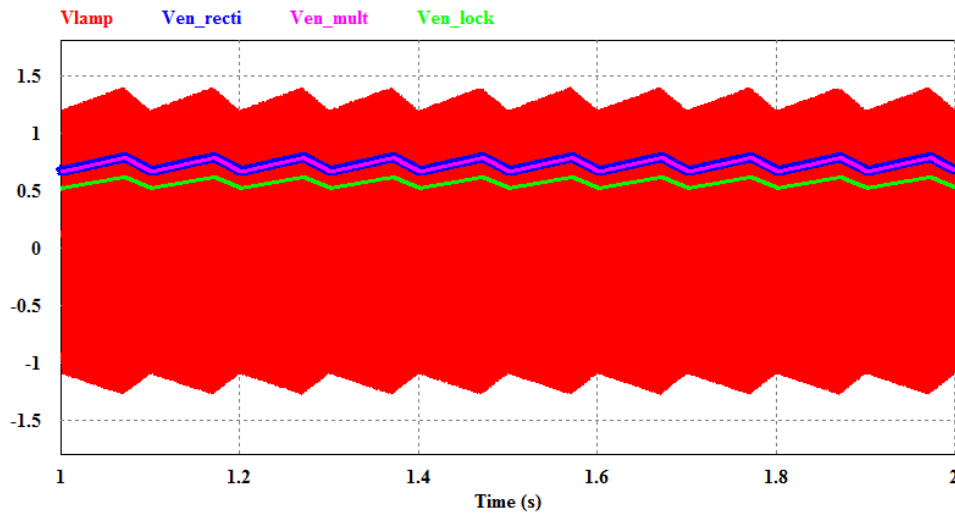
(d) Lock-in amplifier for AR detection

Fig.4-40 Schematic of different AR detection methods

In Fig.4-40, a periodic signal 10 Hz is simulated appearing on the lamp voltage envelope. V_{rand} simulates the environmental noise. The lamp operating frequency is set to 16.7 kHz which is an AR frequency. The principle of the multiplier circuit Fig.4-40 (a) is similar to the lock-in amplifier Fig.4-40 (b). Both of them are the synchronous envelope detection. The difference between them is the reference signals. In real AR detection, the reference signal of the multiplier is a square waveform and the DC offset can be changed. The reference of the lock-in amplifier is always a symmetric sine wave and its DC offset cannot be changed. In order to evaluate how the DC offset of the reference signal influences the performance of the multiplier circuit, the reference signals with different offset are considered as well. Fig.4-41 shows simulation results of different AR detection methods.

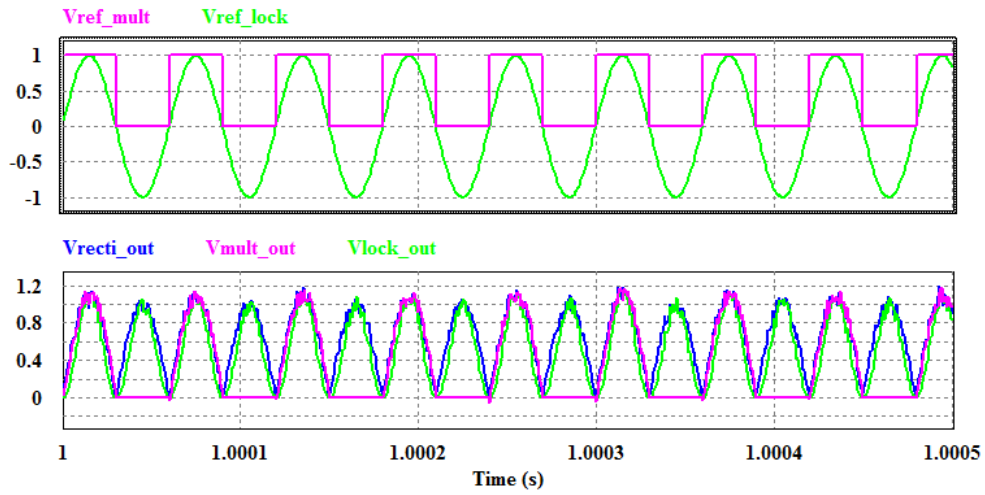


(a1) Reference signals and the output of AR detection circuits before the low-pass filter

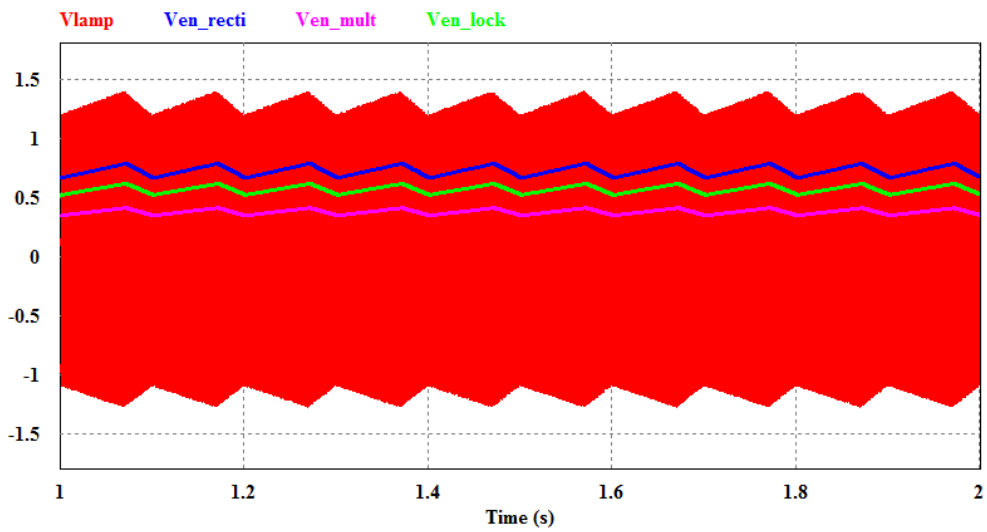


(a2) Lamp voltage and voltage envelope with different detection circuits

(a) when the multiplier is full-wave rectification

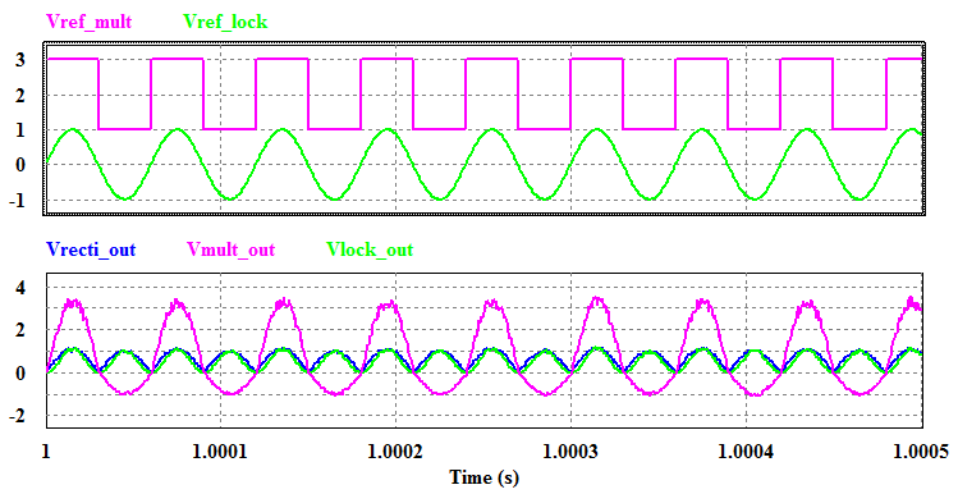


(b1) Reference signals and the output of AR detection circuits before the low-pass filter

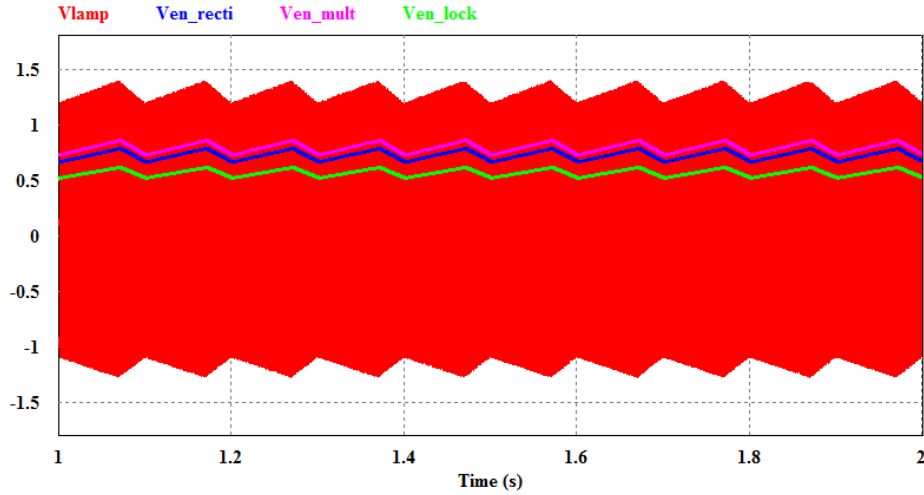


(b2) Lamp voltage and voltage envelope with different detection circuits

(b) When the multiplier is half-wave rectification without DC offset



(c1) Reference signals and the output of AR detection circuits before the low-pass filter



(c2) Lamp voltage and voltage envelope with different detection circuits

(c) when the multiplier is half-wave rectification with DC offset

Fig.4-41 Simulation results of different AR detection methods and reference signals for multiplier and the lock-in

In Fig.4-41, V_{en_recti} , V_{en_mult} , and V_{en_lock} are the voltage envelope by using the rectifier, the multiplier and lock-in amplifier detection methods. V_{ref_multi} is the reference for the multiplier circuit and V_{ref_lock} is the reference for the lock-in amplifier.

The simulation results show that these three detection circuits can follow the lamp voltage envelop quite well. AR can be detected by envelope detection methods. Whatever how the DC offset of the reference signal in the multiplier circuit, the voltage envelope can be always detected. However, the DC offset of the reference signal influences the sensitivity and SNR of the multiplier circuit. TABLE 4-14 shows the performances of different envelope detection methods.

Signal-to-noise ratio (SNR or S/N) is a measure used in science and engineering that compares the level of a desired signal to the level of background noise [11]. SNR can be described as follow:

$$SNR = 20 \log_{10} \left(\frac{A_{signal}}{A_{noise}} \right) \quad (4-1)$$

where A_{signal} and A_{noise} are the amplitudes of the signal and noise are measured in V or A.

Another definition of SNR is as the reciprocal of the coefficient of variation, i.e., the ratio of mean to standard deviation of a signal [12]:

$$SNR = \frac{\mu}{\sigma} \quad (4-2)$$

where μ is the signal mean, and σ is the standard deviation of the noise.

In this thesis, the circuit sensitivity is equal to peak-peak value of voltage envelope in the detection circuit divided by the peak-peak value of original lamp voltage envelope.

TABLE 4-14 Performance of different AR detection methods

Methods	Sensitivity	SNR	STD	RSD=STD/Mean
Rectifier detection	0.60	13	0.0345	8%
Multiplier detection (full-wave rectification)	0.60	13	0.0344	8%
Multiplier detection (half-wave rectification without DC offset)	0.32	7	0.0181	14%
Multiplier detection (half-wave rectification with DC offset)	0.98	14	0.0378	7%
Lock-in amplifier detection	0.50	10	0.0271	10%

As can be seen from TABLE 4-14, the multiplier detection circuit can have better performance or lower performance which depends on the DC offset of the reference signal. This means that the DC offset of the multiplier circuit influences the detection results. The rectifier detection circuit presents better sensitivity and higher SNR than the lock-in amplifier.

In simulation, the rectifier is a perfect circuit. In real detection, the rectifier circuit may have switching glitch problem. Fig.4-42 illustrates the output signal of the rectifier circuit in our experiment.

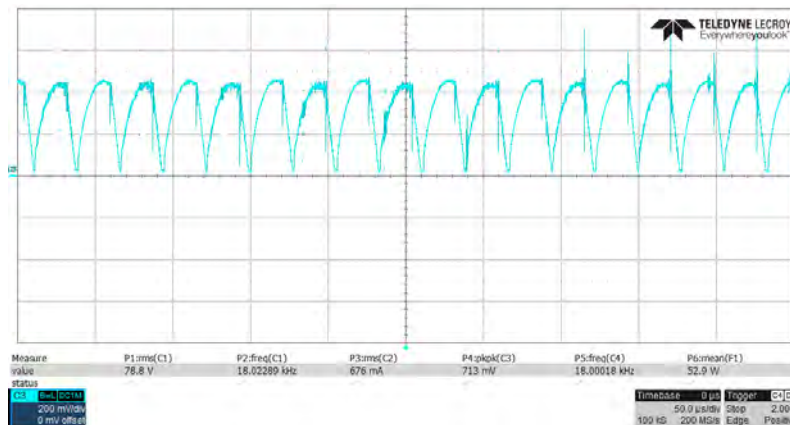


Fig.4-42 Output signal of the rectifier circuit in our experiment

In Fig.4-42, the glitch time is very short and much less than the period time of the lamp voltage. This glitch time does not influence the detection results.

In conclusion, our proposed online detection methods achieve an equivalent sensitivity and SNR to the lock-in amplifier. They are easy to apply to the real AR detection with much lower cost as well.

4.5.3 Comparison between voltage envelope detection and spectral variation detection

Different detection methods are compared, and their characteristics shown in TABLE 4-15.

According the results in TABLE 4-15, both spectral variation detection and voltage envelope detection have a very good ability to classify AR. Although the variations of the spectral irradiance and colorimetric parameters

can distinguish AR, this method is sensitive to noise and the spectrophotometer we used is expensive as well. Thus, the spectral variation detection is just a lab method, and it is not suitable to the real AR detection.

Furthermore, it is easy to detect AR phenomena by using envelope detection methods with a multiplier, a rectifier or a lock-in amplifier. The proposed multiplier and rectifier detection have a very good ability to classify AR. More importantly, our online detection circuits can be embedded into ballast boards and implement the real-time detection with much lower cost.

TABLE 4-15 Characteristics of our detection methods

	Spectral variation detection		Voltage envelope detection		
	Spectral irradiance	Colorimetric parameters	Multiplier	Rectifier	Lock-in amplifier
Sensitivity to AR	High	High	High	High	High
Ability to classify AR	Very good	Very good	Very good	Very good	Very good
Discriminate close frequency	Require statistical analysis	Require statistical analysis	Low	Low	Low
Sensitivity to noise	High	High	Low	Low	Low
Cost	High	Low	Low	Low	High
Method type	Lab method		Online detection		Lab method

4.6 Conclusions

Two kinds of lab methods (envelope detection with a lock-in amplifier and spectral variation detection with a spectrophotometer) have been presented for AR detection in this chapter. In order to analyze AR characterizations and classify AR, the 2-D plane plots, the boxplots, the histograms and the ANOVA plots of the voltage envelope are proposed. The results show that statistical methods are powerful to separate AR and no AR cases. The voltage envelope variations exhibit significantly different patterns in response to AR levels. A new criterion classifying AR levels is therefore defined, based upon the level of the voltage envelope standard deviation. Furthermore, some oscillation patterns only appeared in aged lamps, resulting in using this method as a health monitoring tool of the lamp lifetime.

Statistical analyses are used to characterize light spectral variations as well. STDs and RSDs of the spectral irradiance and colorimetric parameters are calculated to analyze these variations. The results show that STDs and RSDs of spectral variations are about equal to the reference STD and RSD in the no AR situation. In the presence of AR, the STDs and RSDs are several times of the reference STD and RSD. The spectral variation detection can classify AR. However, this approach cannot be applied to a real-time detection.

To conclude, AR phenomena have both short-term signatures and long-term signatures, and significantly influence the performance of the lamps. Thus, online detection methods are essential to the ballast board in order to monitor the lamp directly, leading to the use of MH lamps at higher frequencies with AR avoidance.

References

- [1] https://en.wikipedia.org/wiki/Integrating_sphere
- [2] “Application Design Patterns: State Machines,” National Instruments whitepapers. 8 September 2011.
- [3] Michel Negre, Cours « Photométrie », M1 ISCID Institut Supérieur Couleur Image Design, Université Toulouse 1.
- [4] <https://www.scribd.com/document/94153378/Metal-Halide-Lamps-Instructions-for-the-Use-and-Application>
- [5] M. Hubert, E. Vandervieren (2008), “An adjusted boxplot for skewed distributions,” *Computational Statistics and Data Analysis*, 52 (12): 5186–5201.
- [6] F. Salameh, A. Picot, M. Chabert, E. Leconte, A. Ruiz-Gazen and P. Maussion, “Variable importance assessment in lifespan models of insulation materials: A comparative study,” 2015 IEEE 10th International Symposium on Diagnostics for Electrical Machines, 2015, pp. 198-204.
- [7] <https://en.wikipedia.org/wiki/Histogram>
- [8] Pearson, Karl. “Contributions to the mathematical theory of evolution,” *Philosophical Transactions of the Royal Society of London*, A 185 (1894): 71-110.
- [9] A. Gelman, “Analysis of variance? Why it is more important than ever,” *The Annals of Statistics*, 2005, Vol. 33, pp. 1–53.
- [10] J. C. Anton et al., “Acoustic resonance band detection workbench for HID lamps,” *Conference Record of the 2004 IEEE Industry Applications Conference*, 2004. 39th IAS Annual Meeting, 2004, pp. 667.
- [11] C. J. Billings, K. L. Tremblay, G. C. Stecker, W. M. Tolin, “Human evoked cortical activity to signal-to-noise ratio and absolute signal level,” *Hear Res*, 2009, Vol. 254, pp: 15–24.
- [12] J. T. Bushberg, et al., *The Essential Physics of Medical Imaging*, (2e). Philadelphia: Lippincott Williams & Wilkins, 2006, pp. 280.

General Conclusion and Perspectives

Conclusions

As the electrical consumption of lighting is still growing possibly leading to a world energy crisis, searching high-efficiency lamps and corresponding high-efficiency power supplies are vital for energy savings.

MH lamps are one kind of the most efficiency lamps in the HID lamp family. Because of their excellent luminous efficacy (up to 150 lm/W) and higher color-rendering index (90), they are widely used in supermarket, shops, highway roads and stadiums. High-frequency electronic ballasts are regarded as one kind of high-efficiency power supplies for MH lamps. However, AR phenomena occur in the high-frequency domain (>1 kHz). AR not only causes some visual effects such as light flicker, arc motion, arc rotation, arc bending, lamp extinction and in the worst case, lamp explosion. AR, this problematic phenomenon may damage the lamps or ballasts, or bring risks to the end-users. The objective of this thesis was to search some innovative solutions for AR characterization and real-time detection in order to solve this AR problem.

To better understand this phenomenon, we simulated in MATLAB the pressure distributions in one of our tested lamps at three fundamental frequencies. According to simulation results, we found that the pressure distribution is diverse at different acoustic frequency modes and may cause diverse AR phenomena and damage lamps. In addition, by reviewing the literature of AR detection methods, we concluded that almost no one is simple and robust enough.

According to the conclusions of this theoretical approach, we proposed two simple online envelope detection methods: multiplier detection and rectifier circuit in order to quantify the real-time AR phenomena in MH lamps, as developed in chapter 3. In order to evaluate the sensitivity of the designed multiplier circuit, no AR and slight AR cases were detected in several manufacturers' MH lamps. The results showed that our designed multiplier circuit can distinguish no AR case from slight AR case, and have a good sensitivity to different AR levels. Besides, periodic and stochastic voltage envelopes are detected in MH lamps by our proposed rectifier circuit. The experimental results also showed that the rectifier circuit can follow the voltage envelope effectively whatever the kind of AR phenomena. Based on AM modulation on the lamp voltage in the presence of AR, the electrical modelings of the lamp voltage were built in PSIM software. We found that our simulated lamp voltage modelings are close to the real lamp voltage. These electrical modelings could help ballast designer to find some AR detection and avoidance methods.

Two envelope detection methods are proposed as real-time detection. Their simplicity allows them to be easily embeddable into the ballast board in order to control and to avoid AR phenomena.

Two kinds of lab methods are presented and compared in chapter 4. For reference purposes, the lamp voltage envelopes were measured by a lock-in amplifier. Statistical post-process was applied in order to test the significance of parameter changes between stable and AR mode. The 2-D plane plot, the boxplot, the histogram and the ANOVA plot of the voltage envelope were proposed to analyze and detect AR. The 2D plane, boxplot, and histogram describe the changes or the distribution of the voltage envelope within 20 mins, which are the long-time analysis. The ANOVA and the voltage envelope waveform represent changes or the distribution of the voltage envelope within 4 seconds and 20 mins, which are the short-time and long-time analysis. The results show that statistical methods are able to discriminate AR occurrences. AR significantly influences the lamp voltage envelope variance. An objective criterion classifying different AR levels is defined based on the level of the voltage envelope relative standard deviation as well. Furthermore, by analyzing the voltage envelope, some oscillations only appeared in aged lamps. Therefore, this method can be used as a health monitoring tool of the lamp lifetime.

In addition, the light spectral variations such as the spectral irradiance and chromaticity coordinates, CCT were evaluated by a spectrophotometer. These original results showed that AR phenomena significantly influence the light spectral variations. In the no AR situation, the STDs and RSDs of spectral variations are about equal to the reference STD and RSD. In the presence of AR, the STDs and RSDs are several times of the reference STD and RSD. The light spectral variation detection can classify AR from no AR case evaluation. However, this approach cannot be applied to a real-time detection because of the high cost of the measurement process and the need for tight optical coupling between the source and the detector.

By analyzing the fluctuations of the voltage envelope and colorimetric parameters, we also found that light spectral variations and voltage envelope variations are correlated. Low-frequency fluctuations were observed simultaneously both in the voltage envelope and colorimetric parameters.

To conclude, AR phenomenon has both short-term signatures and long-term signatures. Therefore, online detection methods are essential to the ballast board in order to monitor the lamp directly, leading to the use of MH lamps at higher frequencies with AR avoidance. AR not only causes fluctuations in the lamp voltage but also causes some fluctuations in the colorimetric parameters. AR significantly influences the performance of the lamps.

Perspectives

Based on those findings, we recommend optimizing the high-frequency electronic ballast systems and improving the measurement process of colorimetric parameters.

Laboratory and theoretical perspectives:

- 1) Optimize the online detection methods; for instance, by integrating the online detection methods and A-D converter to sample the voltage envelope;
- 2) Use the same sampling systems, compare the sensitivity and SNR with different envelope detection methods;
- 3) Use higher sampling speed spectrophotometer to measure the spectral irradiance and colorimetric parameters;
- 4) Use high sensitivity photodiode to get the fluctuations frequency of colorimetric parameters in the presence of AR.

Industrial perspectives:

- 1) Use statistical methods of lamp voltage envelopes or lamp voltage envelopes to monitor the health of HID lamps and predict their lifetime;
- 2) Optimize our high-frequency electronic ballast, integrate our online detection and avoidance methods together and embed them into a single smart ballast board;
- 3) Finally, achieve energy savings.

Annexes

List of Figures

Fig. 1-1	Electromagnetic spectrum [22]	8
Fig. 1-2 [24]	Brightness relative sensitivity of human eyes under photopic and scotopic vision conditions [23] 9	
Fig. 1-3	Parameters for defining the luminance [26].....	10
Fig. 1-4	Standard color-matching functions and CIE 1931 chromaticity diagram [28]	12
Fig. 1-5	CIE 19761 chromaticity diagram [30]	13
Fig. 1-6	Blackbody temperature [31]	14
Fig. 1-7	Spectral irradiance for different light sources [32] (The axis of solar irradiance (on the right) and the axis of artificial light sources (on the left)).....	15
Fig. 1-8	Families of artificial light sources [33].....	16
Fig. 1-9	Luminous efficiency of various lamps [33]	16
Fig. 1-10	Incandescent lamp [34] [35]	17
Fig. 1-11	The general V-I characteristics of self-sustained discharges [37]	18
Fig. 1-12	Fluorescent lamps [38] [39].....	19
Fig. 1-13	The basic structure and operation principle of a fluorescent lamp [41].....	19
Fig. 1-14	High pressure mercury lamp [43]	20
Fig. 1-15	High pressure sodium lamp [45].....	20
Fig. 1-16	Metal halide lamps [46] [47] [48].....	21
Fig. 1-17	Structure of the electrodeless lamp [51]	21
Fig. 1-18	Structure of the LED [52]	22
Fig. 1-19	OLEDs [53]	23
Fig. 1-20	The impedance of discharge lamp [57] [58]	24
Fig. 1-21	Magnetic ballast and waveforms of the lamp current and voltage [59].....	25
Fig. 1-22	Low-frequency square wave electronic ballast.....	26
Fig. 1-23	High-frequency electronic ballast.....	27
Fig. 1-24	Arc distortions in an HPS lamp [66].....	28
Fig. 1-25	Arc distortion in an MH lamps [67].....	29
Fig. 1-26	Convection velocity including the influence of the acoustic streaming in an HPS lamp and corresponding to the frequency equal to 10.8 kHz (the streamlines correspond to the velocity) [8]	30
Fig. 1-27	The flux velocity in an HID lamp [75]	30
Fig. 1-28	Acoustic streaming velocity field (velocity in m/s) [67]	31
Fig. 1-29 consortium)	High pressure sodium lamp versus metal halide lamp (Taken by GEL UK for NumeLiTe 32	
Fig. 2-1	Plasma arc with AR in an HPS lamp [64].....	41
Fig. 2-2	Plasma arc with acoustic resonance in MH lamps (Taken in Laplace laboratory)	42
Fig. 2-3	Acoustic modes in a cylindrical cavity [64]	44

Fig. 2-4	Pressure variations at the fundamental longitudinal mode (0 0 1) $f=11.79$ kHz.....	47
Fig. 2-5	Pressure variations at the fundamental azimuth mode (1 0 0) $f=24.42$ kHz.....	48
Fig. 2-6	Pressure variations at the fundamental radial mode (0 1 0) $f=50.82$ kHz.....	49
Fig. 2-7	Acoustic resonance excitation circuit [9].....	50
Fig. 2-8	Typical lamp voltage waveform [10].....	50
Fig. 2-9	Power threshold of acoustic resonance in a 150W HPS lamp [9]	51
Fig. 2-10	Variations of the threshold power, current, harmonic power, voltage, equivalent resistance in a 150 W HPS lamp [9]	51
Fig. 2-11	Different AR detection methods.....	52
Fig. 2-12	AR detection circuit [11]	53
Fig. 2-13	Lamp voltage waveforms and their voltage envelopes [11]	54
Fig. 2-14	Sinusoidal supply for an HPS lamp [12].....	54
Fig. 2-15	Lamp voltage and current in no AR and AR situations in an HPS lamp [12]	54
Fig. 2-16	Variations of electrical parameters and AR windows Vs. the supplying frequency [12]	55
Fig. 2-17	Proposed circuit for MH lamps [13]	55
Fig. 2-18	Current detector for AR detection [13].....	55
Fig. 2-19	Arc images acquisition system [3].....	56
Fig. 2-20	AR map in a 70 W HPS lamp [3]	57
Fig. 2-21	Light intensity distribution at an excitation frequency 41.0 kHz [14].....	58
Fig. 2-22	Results of arc motion frequency and arc flicker frequency in an HID lamp [14].....	58
Fig. 2-23	Flicker as function of excitation frequency and modulation depth [14].....	59
Fig. 2-24	The supply system for the tested lamps [10]	59
Fig. 2-25	Light flicker at AR situations [10].....	60
Fig. 2-26	Sound spectra of the 300-W mercury lamp at two different lamp current frequencies.	61
Fig. 2-27	Acoustic amplitude as a function of the lamp current frequency [64].....	61
Fig. 2-28	Lamp model and comparison of the measured axis temperatures with and without AR [64].....	62
Fig. 2-29	Radial arc temperature profiles in different part at with and without AR situation [64]	63
Fig. 2-30	Axial wall temperature distribution in AR and no AR situation [64].....	63
Fig. 2-31	Normalized maximum term vs. the modulation index (power spectrum density $S_v(f)$) [21].....	67
Fig. 2-32	Electronic ballast for testes lamps [21].....	67
Fig. 2-33	Experimental results after injecting 5 adjacent frequencies [23].....	68
Fig. 3-1	Circuit of the high frequency electronic ballast ($L_s=1.8$ mH, $C_s=300$ nF and $C_p=15$ nF)	76
Fig. 3-2	Simplified equivalent circuit using fundamental approximation.....	76
Fig. 3-3	Transformer ignitor for an MH lamp [5]	77
Fig. 3-4	Bode diagram of LCC circuit ($L_s=1.8$ mh, $C_s=100$ nf, $C_p=2.2$ nf).....	78
Fig. 3-5	Operation sequences in MH lamps	78
Fig. 3-6	Experimental set-up of the online AR detection.....	79

List of Figures

Fig. 3-7	A signal and its envelope marked in red [7]	80
Fig. 3-8	A simple envelope detector [7]	80
Fig. 3-9	Synchronous full-wave envelope detector [8]	81
Fig. 3-10	Asynchronous full-wave envelope detector [8]	81
Fig. 3-11	Detection principle of a lock-in amplifier [9]	82
Fig. 3-12	Principle of voltage envelope detection	83
Fig. 3-13	Multiplier circuit for AR detection	85
Fig. 3-14	Lamp voltage (V_{lamp} : Yellow) and lamp voltage envelope (V_{en} : Blue) in the GE MH lamp (Constant Color CMH) 87	
Fig. 3-15	Arc images and lamp voltage envelope (V_{en}) in the GE Constant Color MH lamp	87
Fig. 3-16	Arc images and lamp voltage envelope (V_{en}) in the Osram Powerball HCI-TT MH lamp MH lamp 87	
Fig. 3-17	Arc images and lamp voltage envelope (V_{en}) in the Philips Master CityWhite CDO-TT MH lamp 88	
Fig. 3-18	Schematic of the rectifier circuit for AR detection	89
Fig. 3-19	Lamp arc shape in the Osram Powerball HCI-TT MH lamp	90
Fig. 3-20	Lamp voltage and voltage envelope in AR and no AR situations in the Osram MH lamp (Yellow: lamp voltage, blue: voltage envelope)	91
Fig. 3-21	FFT analysis of voltage envelopes in the Osram MH lamp	92
Fig. 3-22	Principle of amplitude modulation	93
Fig. 3-23	Modeling of lamp voltage with an example of periodic AR and AR detection	94
Fig. 3-24	Modeling of the lamp voltage with an example of stochastic AR signal and AR detection	95
Fig. 3-25	Lookup table of lamp voltage and voltage envelope detection with AR	97
Fig. 3-26	Voltage envelope in the AR situation ($f=17.5$ kHz) at different observed time	98
Fig. 3-27	Voltage, current waveforms and I-V curve in the Osram MH lamp	99
Fig.4-1	Schematic of the experimental set-up	105
Fig.4-2	Integrating sphere [1]	106
Fig.4-3	Control and acquisition window of LabVIEW program in our experiment	107
Fig.4-4	Principle of the voltage envelope acquisition in lock-in amplifier	108
Fig.4-5	Structure of a CCD spectrophotometer [3]	109
Fig.4-6	Tasks of metal halide salts in an MH lamp [4]	110
Fig.4-7	Voltage envelope standard deviation vs. average voltage envelope in the Osram MH lamp	111
Fig.4-8	Voltage envelope standard deviation vs. average voltage envelope in GE MH lamp	112
Fig.4-9	Voltage envelope standard deviation vs. average voltage envelope in Philips MH lamp	113
Fig.4-10	Characteristics of boxplot [6]	114
Fig.4-11	Boxplot of the voltage envelope in Osram MH lamp	114
Fig.4-12	Voltage envelope waveform in Osram MH lamp at lower operating power	115
Fig.4-13	Boxplot of the voltage envelope in the GE MH lamp	115

Fig.4-14	Voltage envelope waveform in GE MH lamp	116
Fig.4-15	Boxplot of the voltage envelope in the Philips MH lamp.....	116
Fig.4-16	Voltage envelope waveform in the Philips MH lamp.....	117
Fig.4-17	Histogram of the voltage envelope in the Osram MH lamp	117
Fig.4-18	Histogram of the voltage envelope in the GE MH lamp.....	118
Fig.4-19	Histogram of the voltage envelope in Philips MH lamp.....	118
Fig.4-20	ANOVA of the voltage envelope in the Osram MH lamp.....	120
Fig.4-21	ANOVA of the voltage envelope AR in the GE MH lamp	121
Fig.4-22	ANOVA of voltage envelope in the Philips MH lamp	123
Fig.4-23	Spectral irradiance of the Osram MH lamp operated at lower power	125
Fig.4-24	Spectral irradiance in the Osram MH lamp operated at higher power.....	125
Fig.4-25	Spectral irradiance in GE MH lamp.....	127
Fig.4-26	Spectral irradiance in Philips MH lamp.....	129
Fig.4-27	Chromaticity coordinate in the Osram MH lamp	130
Fig.4-28	Boxplot of chromaticity coordinates x and y in the Osram MH lamp.....	131
Fig.4-29	Boxplot of chroma $C_{u'v'}$ and CCT in the Osram MH lamp	131
Fig.4-30	Chromaticity coordinate in the GE MH lamp.....	133
Fig.4-31	Boxplots of chromaticity coordinate in GE MH lamp.....	133
Fig.4-32	Boxplots of $C_{u'v'}$ and CCT in the GE MH lamp.....	134
Fig.4-33	Chromaticity coordinate in Philips MH lamp.....	135
Fig.4-34	Chromaticity coordinate in Philips MH lamp.....	135
Fig.4-35	Boxplots of chroma $C_{u'v'}$ and CCT in the Philips MH lamp.....	136
Fig.4-36	Comparison between voltage envelope detection and spectral variations detection	138
Fig.4-37 lamp	Correlation between voltage envelope detection and spectral variation detection in the Osram MH 138	
Fig.4-38 lamp	Correlation between voltage envelope detection and spectral variation detection in the Osram MH 139	
Fig.4-39	Comparisons of different envelope detection results.....	140
Fig.4-40	Schematic of different AR detection methods.....	141
Fig.4-41 lock-in	Simulation results of different AR detection methods and reference signals for multiplier and the 144	
Fig.4-42	Output signal of the rectifier circuit in our experiment	145

List of Tables

TABLE 1-1	EM radiation with respect to wavelength.....	8
TABLE 1-2	Average color rendering index Ra of different light source.....	15
TABLE 1-3	Comparisons of different lamps [54].....	23
TABLE 1-4	Electromagnetic ballast versus electronic ballast.....	28
TABLE 1-5	Low-frequency square wave versus high-frequency electronic ballast.....	33
TABLE 2-1	AR theoretical frequencies for 150 W Philips/GE MH lamps.....	45
TABLE 2-2	AR theoretical frequencies vs. AR experimental frequencies in our tested MH lamps.....	46
TABLE 2-3	The fluctuations of electrical parameters in a GE MH lamp [3].....	53
TABLE 2-4	Comparisons between different acoustic resonance detection methods.....	64
TABLE 2-5	Obtained results for tested HID lamps [21].....	67
TABLE 2-6	Comparisons between different acoustic resonance detection methods.....	69
TABLE 3-1	Criterion of different AR levels.....	88
TABLE 3-2	Parameter setting of the lamp voltage with periodic modulation.....	95
TABLE 4-1	Elements in an MH lamp.....	110
TABLE 4-2	Electrical parameters in the Osram MH lamp at different power in Fig. 4-7.....	111
TABLE 4-3	Electrical Parameters in GE MH Lamp in Fig. 4-8.....	112
TABLE 4-4	Electrical Parameters in Philips MH Lamp in Fig. 4-9.....	113
TABLE 4-5	Voltage envelope standard deviations in different MH lamps.....	124
TABLE 4-6	Characterizations of different analysis methods for AR detection.....	124
TABLE 4-7	Variations of the spectral irradiance in the Osram MH lamp.....	126
TABLE 4-8	Variations of spectral irradiance in GE MH lamp.....	128
TABLE 4-9	Variations of spectral irradiance in the Philips MH lamp.....	129
TABLE 4-10	Variations of colorimetric parameters in the Osram MH lamp.....	132
TABLE 4-11	Variations of colorimetric parameters in the GE MH lamp.....	134
TABLE 4-12	Variations of colorimetric parameters in the Philips MH lamp.....	136
TABLE 4-13	Disadvantages and advantages of spectral variation detection.....	137
TABLE 4-14	Performance of different AR detection methods.....	145
TABLE 4-15	Characteristics of our detection methods.....	146

List of Publications

International Journals

- 1) F. Lei, P. Dupuis, O. Durrieu, G. Zissis and P. Maussion, "Acoustic Resonance Detection Using Statistical Methods of Voltage Envelope Characterization in Metal Halide Lamps," *in IEEE Transactions on Industry Applications*, vol. 53, no. 6, pp. 88-96, Nov. 2017.
- 2) F. Lei, P. Dupuis, O. Durrieu, G. Zissis and P. Maussion, "A Simple High-Sensitivity Acoustic Resonance Detection Method for Metal Halide Lamps," *The Journal of Light and Visual Environment (JLVE)*, vol. 41, pp. 1-6, Aug. 2017.

International Conferences:

- 1) F. Lei, P. Dupuis, O. Durrieu, G. Zissis and P. Maussion, "Modeling and characterization of acoustic resonance in metal halide lamps," *IEEE ELECTRIMACS*, Toulouse, France, Jul. 2017.
- 2) F. Lei, P. Dupuis, O. Durrieu, G. Zissis and P. Maussion, "Acoustic resonance detection using statistical methods of voltage envelope characterization in metal halide lamps," *in Proc. IEEE Industry Application Society Annual Meeting*, pp. 1-7, Oct. 2016.
- 3) F. Lei, P. Dupuis, G. Zissis and P. Maussion, "Spectral variations of metal halide lamps during acoustic resonance," *2016 IEEE International Conference on Plasma Science (ICOPS)*, pp. 1-1, Jun. 2016.
- 4) F. Lei, P. Dupuis, O. Durrieu, G. Zissis and P. Maussion, "A Simple High-Sensitivity Acoustic Resonance Detection Method for Metal Halide Lamps," *15th International Symposium on the Science and Technology of Lighting*, Kyoto, Japan, May. 2016.